Molecular characterisation and functional assessment of FGFR3 mutations in cancer

Nádia Sofia de Carvalho Lima

A thesis submitted for the degree of Doctor of Philosophy

The Institute of Cancer Research
University of London

Declaration

I, Nádia Sofia de Carvalho Lima, confirm that the work presented in this thesis is my own. Where information has been derived from other sources, I confirm that this has been clearly indicated in the thesis.

Abstract

Genetic alterations such as mutations in the Fibroblast Growth Factor Receptors (FGFRs) family play important roles in the development and progression of several cancer types. How these mutations affect protein function within the cell and drive tumour growth is still unknown. Despite the development of selective inhibitors for FGFR, the majority are still being evaluated in clinical trials where their efficacy in patients is not always achieved and disease recurrence often affects responders. This project seeks to understand the receptor mechanisms and downstream molecular rewiring in tumour cells that sustain cell survival signalling through FGFR3. I have generated NIH-3T3 cellular models expressing FGFR3 cancer-associated mutants for molecular characterisation. A set of mutants were analysed for their baseline activation levels using a multiplex assay and for their downstream signalling dependencies using a targeted small molecule inhibitor screen. I have identified that FGFR3 cancer-associated alterations display increased Src phosphorylation when compared to the WT FGFR3. Paradoxically, cell lines expressing the FGFR3 S249C mutation and the FGFR3-TACC3 fusion protein were found to be resistant to Src inhibitors such as dasatinib. Interestingly, profiling these cells indicate that effective durable therapy requires the blockade of multiple downstream effectors to overcome resistance signalling pathways in the presence of FGFR inhibitor monotherapy. These include the simultaneous blockade of Erk and Src, by respectively utilising the FGFR inhibitor BGJ398 and the Src inhibitor dasatinib. Similarly, human bladder cancer cells harbouring the endogenous FGFR3 mutations R248C (639V) and Y375C (MGHU3) along with the FGFR3-TACC3 fusion (RT112M) were also found to achieve an effective and durable response with the same combination therapy. Mechanistic work in an extended panel of extracellular domain cysteine mutants in NIH-3T3 cells demonstrated that the substitution of the cysteine residue forms spontaneous dimers that promote growth under anchorage-independent conditions, a described hallmark of cancer. Moreover, results show that FGFR cysteine mutations are likely to be a useful biomarker to select for patients who will benefit from FGFR and Src inhibitors combination therapy.

Acknowledgements

Firstly, I would like to thank my supervisor, Dr. Paul Huang, for giving me the opportunity to work in his lab, and for his support, dedication and invaluable guidance throughout the project.

I would also like to thank all members of the Molecular and Systems Oncology lab, past and present, for their advice, help and companionship. In particular, I thank the brilliant and hard-working undergraduate student Eliza, who I had the opportunity to supervise and was a valuable contribution for this project. I also thank Prof. Matilda Katan from UCL for providing some of the cell lines used for this project.

Outside the lab, I thank my friends Juliana and Margarida. Obrigada pelo vosso suporte e verdadeira amizade durante esta etapa.

Above all, I thank Jonathan for his encouragement and love, without which I could not have done this.

Mãe e pai, muito obrigada pelo vosso apoio durante esta difícil jornada. E mãe, sei o quão paciente foste e ainda que longe os teus conselhos e ouvido atento foram fundamentais para eu chegar ao final.

Table of Contents

List of Figures

List of Tables

List of Abbreviations

aa	Amino acid
Abl	ABL proto-oncogene, non-receptor tyrosine kinase
Akt	Akt serine/threonine kinase 1
ALK	Anaplastic lymphoma kinase
ALL	Acute lymphoblastic leukemia
ATP	Adenosine triphosphate
BCA	Bicinchoninic acid
BET	Bromodomain and extra-terminal
BRD	Bromodomain containing
CBL	Cbl proto-oncogene E3 ubiquitin protein ligase
c-fos	Fos proto-oncogene, AP-1 transcription factor subunit
CI	Combination index
CML	Chronic myelogenous leukaemia
CML	Chronic myeloid leukemia
COSMIC	Catalogue of Somatic Mutations in Cancer
CSF1	Colony stimulating factor 1
C-terminus	Carboxy-terminus
CTG	CellTitre-Glo
DMSO	Dimethyl sulphoxide
ECM	Extracellular matrix
EGFR	Epidermal growth factor receptor subfamily
EML4	Echinoderm microtubule-associated protein-like 4
ePKs	Eukaryotic protein kinases
Eps8	Receptor kinase substrate 8
ErbB	Epidermal growth factor receptor family
Erk	Extracellular signal-regulated kinase
EV	Empty vector
EZH2	Enhancer of zeste homolog 2
FAK	Focal adhesion kinase

FBS	Fetal bovine serum
FDA	US food and drug administration
FGF	Fibroblast growth factor
FGFR	Fibroblast growth factor receptor
FGFR5	FGFR-like protein
FIIN	FGFR irreversible inhibitors
FIP1L1	Factor Interacting with PAPOLA And CPSF1
FLT	Fms related tyrosine kinase
FRS2	FGFR substrate 2
GAB1	GRB2-associated binding protein 1
GAB1	GRB2-associated binding protein 1
GSK3	Glycogen synthase kinase 3
Her2	Human epidermal growth factor receptor 2
HS	Heparin sulphate
IC_{50}	Half maximal inhibitory concentration
Ig	Immunoglobulin
IGF1R	Insulin-like growth factor 1 receptor
IgG1	Immunoglobulin G1
JAK	Janus kinase
JM	Juxtamembrane
JNK	Jun N-terminal kinase
KD	Kinase domain
KIT	KIT proto-oncogene, receptor tyrosine kinase
LC	Loading control
mAbs	Monoclonal antibodies
MAPK	Mitogen-activated protein kinase
MEF	Mouse embryonic fibroblast
MEK	Mitogen-activated protein kinase
MET	Hepatocyte growth factor receptor
MKP	MAPK phosphatases

MM	Multiple myeloma
MMSET	Multiple myeloma SET domain
mTOR	Mammalian target of rapamycin
MW	Molecular weight
NFkB	Nuclear factor kappa B
NSCLC	Non-small cell lung cancer
N-terminus	Amino-terminus
p	Phospho
PAGE	Polyacrylamide gel electrophoresis
PBS	Phosphate buffered saline
PCR	Polymerase chain reaction
PDGFR	Platelet-derived growth factor receptor
PEI	Polyethylenimine
PI3K	Phosphoinositide 3-kinases
PIK3CA	PI3K catalytic subunit
PKC	Protein kinase C
PLCγ	Protein phospholipase Cγ
PTB	Phosphotyrosine-binding
PTEN	Phosphatase and tensin homolog
RAF	Raf proto-oncogene serine/threonine-protein kinase
RAS	Proto-oncogene GTPase
Rb	Retinoblastoma-associated protein
RET	RET proto-oncogene, tyrosine-protein kinase receptor Ret
RSK2	p90 ribosomal protein S6 kinase 2
RT	Room temperature
RTK	Receptor tyrosine kinases
RTKi	RTK inhibitors
SCC	Squamous cell cancer
SDM	Site directed mutagenesis
SDS	Sodium dodecyl sulphate

SEF	Similar expression to fgf genes
SFK	Src family kinase
SH2/3	Src homology-2/3
SHP2	Protein tyrosine phosphatase 2
SOS	Son of sevenless
SPRY	Sprouty homolog
SqNSCLC	Squamous non-small cell lung cancer
Src	Src proto-oncogene, non-receptor tyrosine kinase
STAT	Signal transducer and activator of transcription
t	Total
TACC3	Transforming acidic coiled-coil-containing protein 3
TBS-T	Tris-buffered saline solution with 0.01 % (v/v) tween
TK	Tyrosine kinase
TKIs	Tyrosine kinase inhibitors
TM	Transmembrane
TrkA	Tropomyosin receptor kinase A
UCL	University College of London
VEGFR	Vascular endothelial growth factor receptor
WT	Wild-type

Chapter 1

Introduction

1.1 - Overview of Receptor Tyrosine Kinases (RTKs)

The eukaryotic protein kinases (ePKs) account for one of the largest superfamilies of homologous proteins, constituting 1.7% of the entire human genome (Manning et al., 2002). Protein kinases mediate most of the signal transduction processes within eukaryotic cells. They are enzymes that catalyse the transfer of phosphate groups to protein substrates in a reversible reaction. By doing so, they control and regulate a vast amount of intracellular processes such as metabolism, transcription, cell cycle, apoptosis and differentiation as well as intercellular communication for maintenance of homeostasis and physiological regulation (Manning et al., 2002). Despite a variety of protein sequences, structures, substrate specificity and mode of regulation, ePKs share structural features in the catalytic kinase domain (KD) (Steven K. Hanks, 1995). These conserved amino acids and motifs in the KD have been used to group closely related enzymes into phylogenetic trees, which are found to reflect similar structures, modes of regulation and catalytic functions. The ability to predict the structure and function of a protein from its amino acid sequence simplifies the study of this superfamily and allows their categorisation. Generically, ePKs can be divided into two main subfamilies: protein-serine/threonine kinases and protein-tyrosine kinases, depending on their target phosphorylation site (Steven K. Hanks, 1995). Although the tyrosine kinases are less divergent as a group, they can be further subdivided into two classes: receptor tyrosine kinases (RTKs) and non-receptor tyrosine kinases, depending on the presence or absence of a transmembrane (TM)-spanning region, respectively (Hanks, 1991). While non-receptor tyrosine kinases are found in the cytosol, nucleus and inner surface of the cell membrane, RTKs are TM proteins that possess an extracellular ligand-binding domain, a single-helix TM domain and an intracellular catalytic tyrosine KD (Hanks, 1991; Krause and Etten, 2005).

RTKs are a highly conserved family in evolution from *Caenorhabditis elegans* to *Homo sapiens*, which supports their importance in multicellular organisms (Hanks, 1991).

The human genome encodes for 58 RTKs that can be divided into 20 closely related subfamilies based on their molecular architecture (Figure 1.1) (Lemmon

and Schlessinger, 2010). RTK subfamilies include amongst others, fibroblast growth factor receptor (FGFR), epidermal growth factor receptor subfamily (EGFR/ErbB), vascular endothelial growth factor receptor (VEGFR), platelet-derived growth factor receptor (PDGFR), erythropoietin-producing human hepatocellular receptor (Eph/Ephrin) and MET proto-oncogene (Regad, 2015). In the inactive state, the majority of RTKs are expressed as monomers at the cell surface, with the exception of the Ins RTK subfamily where the insulin receptor (InsR) and the Insulin-Like Growth Factor 1 Receptor (IGF1R) exist as disulphide-linked dimers.

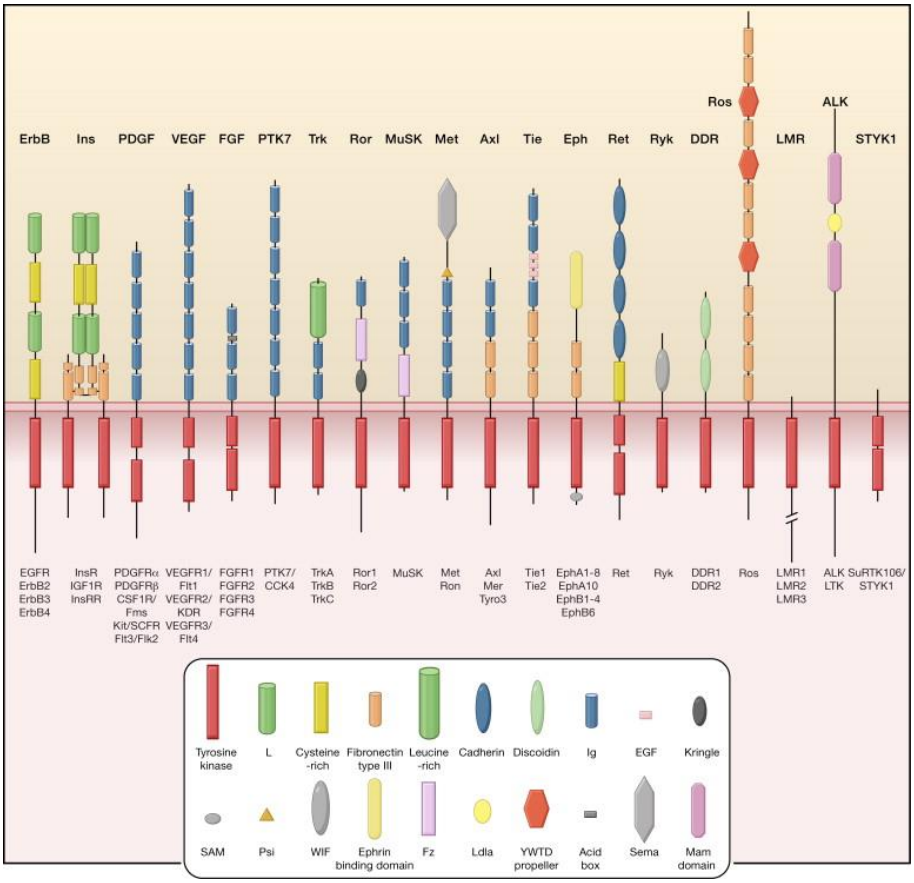

Figure 1.1 – Human tyrosine kinase family. The 58 human RTKs categorised into 20 RTK subfamilies are here schematically represented according to their structural organisation. The intracellular KD of each subfamily is well conserved in comparison to the extracellular domain which differs between subfamilies. Figure adapted with permission from Elsevier, (Lemmon and Schlessinger, 2010).

RTKs are characterised by the presence of a glycosylated amino(N)-terminus extracellular domain rich in disulphide bonds. This domain is composed by immunoglobulin (Ig)-like domains enriched for cysteine, leucine, fibronectin type

III and other domains depending on the RTK subfamily (Lemmon and Schlessinger, 2010). These different domains define the specificity and selective recognition of growth factor ligands. The binding of a receptor-specific growth factor to the extracellular region of RTKs induces receptor dimerisation and/or oligomerisation, except for Ins RTK that already exists as an inactive dimer. The single α-helix TM domain of RTKs plays a key role in the formation and stabilisation of this dimer. It has been proposed that in the lipid environment of the cell membrane, receptors exist as non-covalent oligomers making it possible for RTKs to pre-dimerise before ligand binding (Arkin, 2002). When a ligand binds to the receptor, conformational changes facilitate intracellular proximity of both cytoplasmic tyrosine KDs of each monomer allowing its activation through trans-autophosphorylation (Hubbard and Till, 2000). RTK activation generally requires the activation of the KD and the formation of phosphorylated binding sites for docking of proteins responsible for signal transduction. The intracellular domain is composed of the juxtamembrane (JM) region (just after the TM helix), followed by the tyrosine KD and the carboxy(C)-terminus region. The intracellular JM region and the C-terminus regions vary in length between RTKs, whereas the KD is well conserved across RTKs (Ségaliny et al., 2015). The KD is formed by 12 subdomains forming two lobes connected by the kinase insert domain which is the ATP-pocket site (Figure 1.2) (Hanks, 2003). The first lobe is formed by β-sheets and one α-helix and are known for orienting and stabilising ATP to the binding pocket site (Hubbard and Till, 2000). The second lobe formed by α-helices helps in the chelation of ATP by Mg^{2+}. The second lobe of the KD also includes an activation loop containing between one and three tyrosine residues, depending on the RTK (Hubbard and Till, 2000). Tyrosine phosphorylation in the activation loop by ATP, changes its orientation resulting in an open conformation of the KD, which is essential for creating the active kinase and stabilising the active conformation (Ségaliny et al., 2015). With the KD “open” in both chains of the dimer, each KD is then able to catalyse the transfer of phosphate groups from ATP to other tyrosines in the intracellular JM, kinase insert and C-terminus regions of the opposite receptor chain, generating docking sites for adaptor or scaffolding proteins with specific modular domains. These include proteins that contain Src homology-2 (SH2), phosphotyrosine-binding (PTB) or pleckstrin homology (PH) domains (Volinsky and Kholodenko, 2013). Some of these

proteins contain enzymatic activity themselves, such as Src proto-oncogene (Src) and protein phospholipase Cγ (PLCγ), or serve as adapter proteins that can recruit other molecules able to activate distinct signalling pathways. The number of tyrosine residues that can be phosphorylated and its distribution within the intracellular domain vary between RTKs. For example, there are 6 tyrosines prone to phosphorylation in tropomyosin receptor kinase A (TrkA) and 19 in PDGFRβ (Bradshaw et al., 2013). These differences determine the type of docking proteins that bind to the active receptor and the downstream signalling pathways that are subsequently activated. Although there are a number of shared docking proteins recruited by multiple RTKs, such as GRB2-associated binding protein 1 (GAB1), some are specific for particular RTKs, such as FGFR substrate 2 (FRS2) family that mediate FGFR and TrkA signalling, or insulin receptor substrate (IRS) family for the Ins RTKs (Lemmon and Schlessinger, 2010).

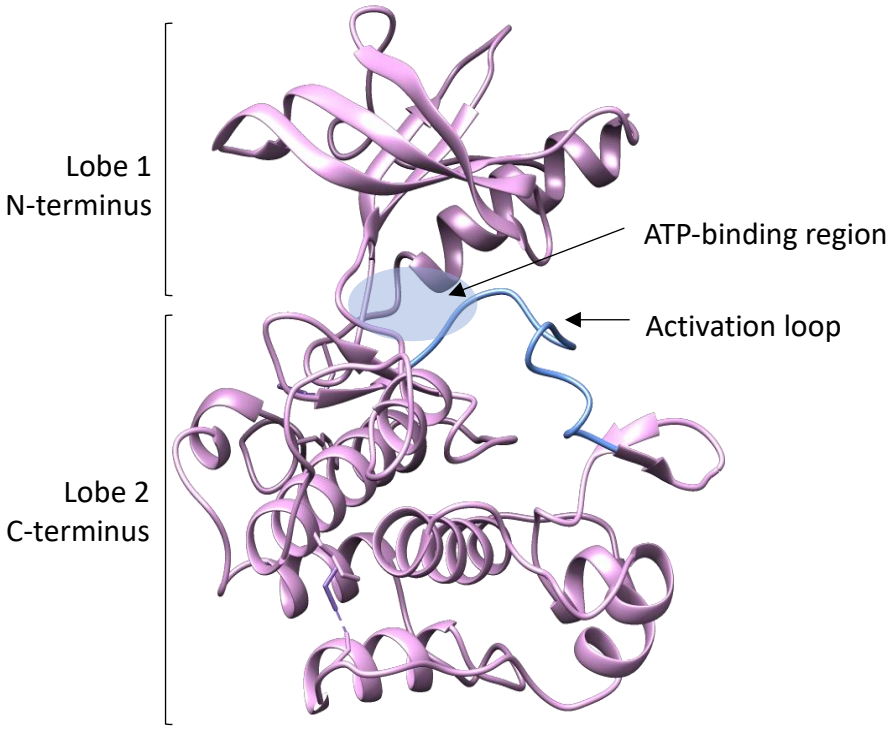

Figure 1.2 – Representation of the kinase domain organisation of RTKs. Crystal structure of the tyrosine KD of the human insulin receptor shows the structural conformation of the kinase into two lobes separated by the activation pocket region. The activation pocket binds ATP in the ATP-binding region (shown by the blue circle) and is responsible for the phosphorylation of other tyrosine residues on the KD for complete activation. The activation loop (coloured in blue) is key for the KD activation, as its phosphorylation triggers a conformational change of the domain to an open status, allowing further tyrosine kinase phosphorylation for docking of adaptor proteins mediators of different signalling pathways. [PDB: 1IRK].

RTKs can be considered the starting point for the activation of a complex network of cellular signalling cascades (Ségaliny et al., 2015). Upon RTK activation, docking proteins are phosphorylated, these then have other protein kinases as targets, which in turn phosphorylate a third protein kinase, and so on. The result is a cascade of reactions that amplifies the signal by many orders of magnitude. Such cascades are composed of well-defined signalling pathways including the mitogen-activated protein kinase (MAPK), phosphoinositide 3-kinases/Akt serine/threonine kinase 1 (PI3K/Akt), Src and signal transducer and activator of transcription (STAT) pathways (Choudhary and Mann, 2010). Once these signalling cascades reach the nucleus, they activate transcription factors that regulate the transcription of genes involved in the regulation of many cellular processes (Du and Lovly, 2018). For example, MAPK plays a role in controlling cell death, proliferation, migration and differentiation (Cargnello and Roux, 2011). PI3K/Akt pathway has a role in regulating cell survival by degrading pro-apoptotic proteins such as BCL2 associated agonist of cell death (BAD) and tumour protein 53 (p53) or inducing anti-apoptotic proteins like BCL2 apoptosis regulator (Bcl-2) (Song et al., 2005). And Src pathway is involved in cell adhesion, motility and survival and its known to activate other pathways, such as the STAT, PI3K and focal adhesion kinase (FAK) pathways (Paul A Bromann, 2004).

Given that a single protein adaptor can interact with different RTKs and that there are different pathways activated by the same RTK which sometimes overlap with other RTKs, questions have been raised about the specificity of signalling mediated by different RTKs. Although there is a defined activation cascade of signalling in distinct pathways such as MAPK that is known to sequentially activate RAS-RAF-MEK-Erk, all pathways are highly interconnected and form a complex network with RTKs as key initiation nodes (Volinsky and Kholodenko, 2013). Pathways have points of crosstalk through several protein effectors, and there are multiple feedback and feedforward loops, both positive and negative that integrate and regulate cell signalling to determine specific biological functions (Kholodenko, 2006). For example, there is evidence that PI3K and MAPK pathways communicate and interact to regulate downstream functions (Von Kriegsheim *et al.*, 2009; Michelle C. Mendoza, 2011). And there is a known crosstalk between Src and EGFR, where both can activate each other (Kim et al.,

2006). Moreover, Raf-1 proto-oncogene (RAF1) from MAPK pathway, transmits the signal to the downstream effector mitogen-activated protein kinase/Erk kinase (MEK) followed by extracellular-signal-regulated kinase (Erk). Erk in turn, can phosphorylate and also inactivate RAF1, in a positive and negative feedback loop (Dougherty et al., 2005). Other mechanisms also contribute to the negative regulation of RTK signalling. For example, E-cadherin has been shown to interact with EGFR, MET or IGF1R and decrease the receptor mobility and affinity for their ligands (Andl and Rustgi, 2005). The direct inhibition of RTKs autophosphorylation can also be achieved by protein tyrosine phosphatases (PTPs) which have been described in the regulation of several RTKs including EGFR or TrkA (Mertins et al., 2008). Additionally, signal transduction regulation can also be mediated by antagonist proteins that target effectors of downstream pathways, such as sprouty homolog (SPRY) and similar expression to fgf gene (SEF) proteins that are able to inhibit the MAPK pathway and PI3K/Akt signalling pathways (Yusoff et al., 2002). Receptor ubiquitination for internalisation and degradation within the lysosomes is also a well-studied mechanism that regulates RTK signalling (Ledda and Paratcha, 2007).

There are many components that integrate RTK regulation and signalling, making it a highly complex system, where spatiotemporal dynamics of receptor activation determines the specificity of signalling. It has been shown that the cellular response is dependent on cellular context as well as the duration and strength of signal (Kholodenko et al., 2010). For example, the same RTK can lead to cell proliferation or differentiation in different tissue contexts. MET levels have a determinant role in embryogenesis and its enhanced ectopic expression in myoblasts is buffered in most tissues avoiding development perturbation (Fan, 2015). Whereas in the limb mesenchyme, MET ectopic expression in myoblasts reduces the bioavailability of hepatocyte growth factors (HGF) resulting in myoblast migration defects leading to a disruption of morphogen gradients (Fan, 2015; Gurdon and Bourillot, 2001). In addition, the way in which RTKs use shared pathways to induce differential cellular responses has been intensively studied for MAPK pathway. Observations in rat pheochromocytoma PC-12 cells show that sustained Erk activation initiated by nerve growth factor (NGF) induced cell differentiation whereas transient Erk activation by epidermal growth factor (EGF)

induced cell proliferation (Pellegrino and Stork, 2006). Moreover, this sustained Erk activation is required to trigger accumulation of active Fos proto-oncogene (c-fos) (an immediate-early transcriptional target of Erk) and induce transcription of genes which otherwise would not been transcribed (Marshall, 1995). Although not completely understood, temporal dynamics of cell signalling activity, regulation and termination is clearly vital for cell fate.

1.1.1 - RTKs in cancer

Given the crucial role of RTKs in multiple cellular processes and the complexity of its regulation, it is not surprising to find that alterations in RTKs are associated with several pathologies (McDonell et al., 2015). Germline mutations have been described in inherited human syndromes. For instance, mutations in the FGFR family can lead to congenital bone diseases including chondrodysplasia and craniosynostosis syndromes, such as dwarfism, or deafness (Alsmadi et al., 2009; Ornitz and Itoh, 2015; Rousseau et al., 1996). Another example is mutations in ErbB3 which have been associated with lethal contractural syndrome type 2 (Narkis et al., 2007). On the other hand, somatic alterations are commonly found in malignancies, such as mutations in FGFR3 (S249C) that are found in urothelial carcinomas, which is the most common form of bladder cancer and affects 90 % of these patients (Lamont et al., 2011), or mutations in EGFR (L858R) found in non-small cell lung cancer (NSCLC) (Cappellen et al., 1999; Gazdar, 2010). Mechanisms of RTK dysregulation that encompass protein overexpression, amplification, genomic translocations and gain- or loss-of-function somatic mutations have been described in over ten RTK families as human cancers drivers (Robertson et al., 2000). In particular, genomic rearrangements can result in the formation of new RTK fusion oncoproteins (Stransky et al., 2014). Common examples are the fusion of anaplastic lymphoma kinase (ALK) RTK with a domain of partner proteins such as nucleophosmin (NPM), echinoderm microtubule-associated protein-like 4 (EML4) or striatin (STRN), found in anaplastic large cell lymphoma (ALCL), NSCLCs and thyroid cancers (Lai and Ingham, 2013; Pérot et al., 2014; Soda et al., 2007). ROS proto-oncogene 1 (ROS1) and RET proto-oncogene (RET) fusions have also been

identified in lung and thyroid cancers (Bos et al., 2013; Celestino et al., 2012). Other fusions have been described between EGFR and septin 14 (SEPT14) in glioma and FGFR3 with the transforming acidic coiled-coil-containing protein 3 (TACC3) in bladder cancer (Stransky et al., 2014). This resulting fusion of an RTK with another protein can lead to the constitutive oligomerisation of the tyrosine kinase (TK) with a domain of the partner protein and consequent kinase activation in the absence of ligand as it happens in the fusion EML4-ALK in NSCLC (Du and Lovly, 2018). The resulting fusion protein can also lack its inhibitory domain which may similarly contribute to its constitutive activation, as is the case for the fusion PDGFRα-FIP1L1, found in chronic eosinophilic leukaemia, where the breakpoint in PDGFRα is located within the inhibitory JM region, and this truncation is sufficient to constitutively activate PDGFRα (Stover et al., 2006).

Another common example of RTK dysregulation are oncogenic point mutations. These mutations are often associated with a disruption of the autoregulatory function of receptors leading to increased kinase activity in the absence of ligand (Webster et al., 1996). For example, mutations in the residue K652 of the activation loop of the KD of FGFR3 impairs the stabilisation of the inactive conformation of the receptor, leading to ligand independent constitutive activation of FGFR3. This mutation is often observed in skeletal dysplasia and different cancer types, such as bladder and multiple myeloma (MM) (Webster et al., 1996). Other mechanisms of constitutive kinase activation are observed in RET mutants such as M918T, where this variant becomes phosphorylated at a higher rate than the wild-type (WT) due to an increased ATP affinity that enables constitutive kinase phosphorylation (Plaza-Menacho et al., 2014). Point mutations or deletion mutations in RTKs have also been shown to increase the receptor affinity to its own or other ligands, leading to an increased receptor activation. An example of this mechanisms is in FGFR2 mutations found in Apert syndrome, where mutations in the extracellular domain such as S252W or P253R exhibit decreased dissociation kinetics for its ligand fibroblast growth factor (FGF)2 (Andersen et al., 1998).

Overexpression or amplification of RTKs and/or its ligands are also known to drive certain cancers (Ha et al., 2013; Rodríguez-Antona et al., 2010). Increased ligand expression can induce paracrine ligand activation whereas RTK gene

amplification can result in increased receptor expression at the cell surface (Du and Lovly, 2018; Korc and Friesel, 2009). The same can happen with RTK gene translocations brought under the control of an unrelated promoter leading to transcriptional/translational enhancement or impaired regulation mechanisms, that can enhance receptor expression (Zheng, 2013). Augmented receptor expression can cause increased ligand-receptor binding as it is the case for human epidermal growth factor receptor 2 (HER2) amplifications in breast cancer leading to downstream upregulation of oncogenic signalling (Iqbal and Iqbal, 2014). Finally, increased RTK activity can also be a result from impaired negative regulation mechanisms. For instance, when the mechanisms that control signal termination or receptor internalisation are faulty, signalling is not terminated and receptors constitutively exert their activity. An example is the down-regulation of the TK inhibitor Sprouty2 in NSCLC (Krause et al., 2005; Sutterluty et al., 2007).

Ultimately, there are multiple ways by which RTK aberrations lead to the dysregulation of the cellular downstream signalling. These alterations can upset the balance between cell-cycle, apoptosis and growth within the cell, which can trigger cellular transformation and oncogenesis (McDonell et al., 2015).

1.1.2 - RTKs as targets for cancer therapy

RTKs were initially disregarded in drug development due to the lack of evidence for a causative role in human cancers, concerns about their drug-target specificity and on- and off-target effects that compromised the risk-benefit analysis of RTKs as viable therapeutic targets (Shah et al., 2013). However, with the discovery of the non-receptor TK Bcr-Abl gene fusion as a key driver for chronic myelogenous leukaemia (CML), followed by the use of the small molecule TK inhibitor imatinib mesylate as an effective cancer therapy in CML, kinase inhibitors have since become a valuable part of the arsenal for cancer treatment (Druker et al., 1996; Salesse and Verfaillie, 2002). Treatments have rapidly evolved since the licensing of imatinib in 2001, with more than 20 different RTK inhibitors (RTKi) now approved by the US food and drug administration (FDA) and European medicines agency (EMA) for the treatment of diverse malignancies (Table 1.1) (Bhullar et al., 2018). RTKi can be divided into two categories: multi-target (or

‘dirty’) kinase inhibitors and selective kinase inhibitors. The first category are small molecules that can target a broad range of RTKs. For this reason, multi-target kinase inhibitors often display a lower bioavailability against the kinase of interest because it binds to unspecific kinases, increasing the risk of off-target effects and toxicity in patients (Shah et al., 2013; J. Zhang et al., 2009). Selective RTKi, exert their effect against very specific kinases, with minimal off-target effects. Kinase inhibitors can also be divided into three classes, type I, II and III inhibitors depending on the way they bind to the 3D conformation of the protein (Dar and Shokat, 2011). Type I inhibitors are small molecules that bind to the active conformation of a KD in the ATP pocket site, whereas type II inhibitors bind to the inactive conformation of the KD. These type I and type II inhibitors are ATP-competitors that prevent ATP from binding to the active pocket site. Type III inhibitors are allosteric inhibitors that bind to a distinct site of the protein outside of its active site. These are non-ATP competitive inhibitors where ATP binding cannot block their interaction with the enzyme (Roskoski, 2015).

Although advances in the development of kinase inhibitors have improved disease control and patient outcomes, this class of drugs is prone to the development of acquired drug resistance in patients ultimately leading to tumour relapse. Therefore, there is a need to better understand the biology and functional role of each oncogenic RTK alteration to discover better therapeutic solutions for RTK-driven cancers. There is also an urgent need to characterise the molecular consequences of targeted therapies in order to uncover potential escape mechanisms that might induce resistance and compromise the efficacy of this class of drugs.

In particular, there is a lack of in-depth knowledge of the molecular and functional effects of FGFR mutations in cancer. These challenges are exacerbated by a poor understanding of the mechanisms of response and resistance of FGFR driven-cancers to small molecule kinase inhibitors. This thesis focuses on the functional and molecular characterisation of various FGFR aberrations, in particular FGFR3 mutations, present in different cancer types including bladder cancer. In parallel, this thesis describes the evaluation of how distinct FGFR mutations might influence kinase inhibitor sensitivity and proposes new ways to maximise inhibitor response in cancer cells.

Table 1.1 – Small molecule RTK inhibitors approved for the treatment of different human cancers. Adapted from (Bhullar et al., 2018).

Inhibitor	RTK target	Cancer type	First approval (US)
Afatinib	HER2, EGFR	NSCLC	2013
Alectinib	ALK	NSCLC	2015
Axitinib	VEGFR1-3, PDGFRβ,	RCC	2012
Brigatinib	ALK	NSCLC	2017
Cabozantinib	VEGFR2, MET	HCC	2012
Ceritinib	ALK	NSCLC	2014
Crizotinib	ALK, MET	NSCLC	2011
Erdafitinib	FGFR1-4	UC	2019
Erlotinib	EGFR	NSCLC, PC	2004
Gefitinib	EGFR	NSCLC	2004
Imatinib	PDGFR, KIT	CML, ALL,	2001
Lapatinib	EGFR, HER2	BC	2007
Lenvatinib	VEGFR2-3	HCC, TC,	2015
Osimertinib	EGFR	NSCLC	2015
Pazopanib	VEGFR1-3, KIT,	RCC, STS	2009
Ponatinib	PDGFR, VEGFR,	CML, ALL	2012
Regorafenib	VEGFR1-3, RET	CC, GIST,	2012
Sorafenib	VEGFR2	RCC, HCC,	2005
Sunitinib	PDGFRβ, KIT,	GIST, RCC,	2006
Vandetanib	VEGFR2	TC	2011

RTKs abbreviations: HER (human epidermal growth factor receptor), EGFR (epidermal growth factor receptor), ALK (anaplastic lymphoma kinase), VEGFR (vascular endothelial growth factor receptor), PDGFR (platelet derived growth factor receptor), KIT (KIT Proto-Oncogene, Receptor Tyrosine Kinase), MET (hepatocyte growth factor receptor), FGFR (fibroblast growth factor receptor), RET (RET Proto-Oncogene, Tyrosine-Protein Kinase Receptor Ret).

Cancers abbreviations: NSCLC (non-small cell lung cancer), RCC (renal cell carcinoma), HCC (hepatocellular carcinoma), CC (colorectal cancer), HNC (head and neck cancer), UC (urothelial carcinoma), PC (pancreatic cancer), CML (chronic myelogenous leukaemia), ALL (acute lymphoblastic leukaemia), GIST (gastrointestinal stromal tumour), BC (breast cancer), TC (thyroid cancer), STS (soft tissue sarcoma).

1.2 - The Fibroblast Growth Factor Receptor (FGFR) family

There are four highly conserved FGFRs in this RTK subfamily, FGFR1-4, as well as a fifth member known as FGFR-like protein (FGFR5). FGFR1-4 are TM proteins activated by the binding of a variety of FGF ligands which leads to the activation of diverse downstream signalling pathways through which these receptors exert their biological functions (Ornitz et al., 1996). FGFR1-4 are involved in a broad range of important physiological events during embryonic development including organogenesis; and adult response to injury, tissue repair and regeneration (De Moerlooze et al., 2000; Kimelman and Kirschner, 1987; Wilkie, 2005). They are also key to the regulation of a number of cellular

processes such as survival, proliferation, migration, differentiation and metabolism (Beenken and Mohammadi, 2009; Carter et al., 2015; Itoh and Ornitz, 2010; Turner and Grose, 2010). While FGFR1-4 are active kinases, FGFR5 which also localises to the cell membrane and binds FGF ligands, lacks the KD and does not possess kinase activity (Wiedemann and Trueb, 2000). FGFR5 was initially thought to act as a decoy receptor, negatively regulating the other FGFR subfamily members by binding and neutralising FGF ligands, reducing cell signalling (Wiedemann and Trueb, 2000). But later studies have shown that FGFR5 plays a role in reducing cell growth, accelerating cell differentiation and inducing cell adhesion (Baertschi et al., 2007; Trueb et al., 2003; Yang et al., 2016).

1.2.1 - Fibroblast Growth Factor (FGF) Ligands

Extracellular signals are transduced by the binding of FGF ligands to the FGFRs via the extracellular domain of the receptor. This event is mediated in the presence of proteoglycan cofactors or other specific protein co-receptors. There are 22 FGF ligands in mammals that can be subdivided into seven families according to their phylogeny. These constitute 3 categories: canonical FGFs (FGF subfamily 1, 4, 7, 8 and 9), endocrine FGFs (subfamily FGF15/19) and intracellular FGFs (FGF11 subfamily) (Figure 1.3) (Ornitz and Itoh, 2015). Intracellular FGFs are non-signalling factors that function as co-factors for sodium channels and other molecules (Goldfarb et al., 2007). Canonical and endocrine FGFs constitute the secreted FGFs that signal through the FGFRs. Canonical FGFs function as autocrine or paracrine factors and play a key role in cell proliferation, differentiation and survival (Itoh and Ornitz, 2010). Endocrine FGFs are hormone-like factors that regulate the metabolism of phosphates, bile acids, carbohydrates and lipids (Beenken and Mohammadi, 2009).

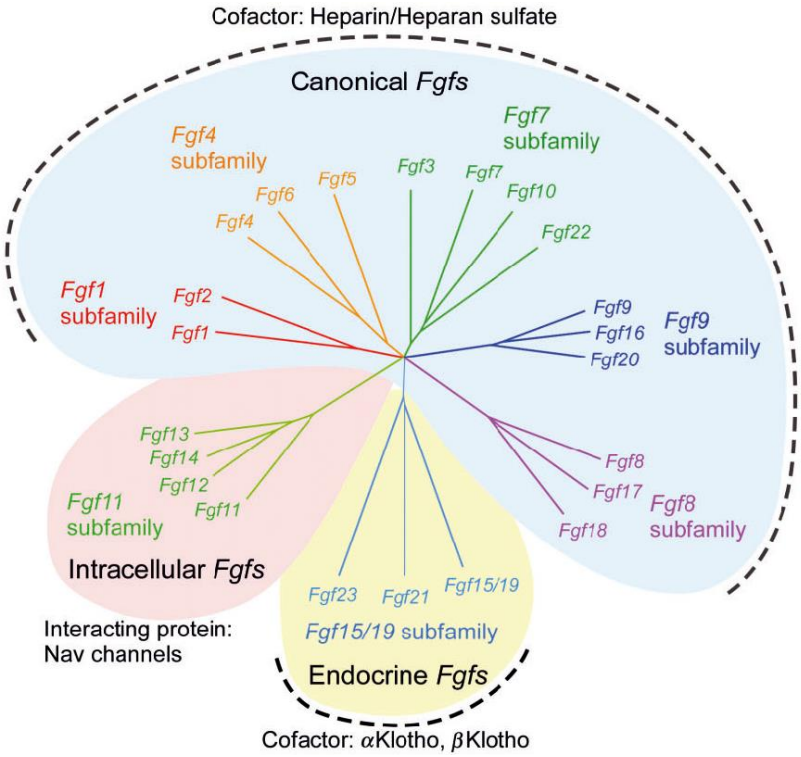

Figure 1.3 – Phylogenetic classification of the human FGF ligands. FGF ligands are here represented in a phylogenetic tree, where branch lengths are proportional to the evolutionary distance between genes. There are 22 FGF ligands subdivided into three categories. The canonical FGFs comprehend five subfamilies and require HS proteoglycan co-factor to bind and signal through FGFR. Endocrine FGFs include one subfamily and are hormone-like ligands dependent on Klotho TM proteins to signal. Intracellular FGFs are also composed by one subfamily and do not bind to FGFR, acting only as co-factors to other molecules. Free access image adapted from (Ornitz and Itoh, 2015).

FGFs range in size from 150-300 amino acids and crystallography studies show that there is a homologous core domain in all FGFs composed of around 125 amino acids (Itoh and Ornitz, 2004). The conformation of this core is conserved across canonical FGFs and is formed by 12 anti-parallel β strands (β1- β12) in a β-trefoil fold (Goetz et al., 2007). This core is also observed in endocrine FGFs which unlike canonical FGFs lack the β-11 strand, that is substituted by an α-11 helix, resulting in the adoption of an atypical trefoil appearance (Figure 1.4) (Mohammadi et al., 2005). The region outside the conserved core is composed of variable amino acid sequences that determine the selectivity of binding of distinct FGFs to different FGFR family members. After secretion, canonical FGFs are readily sequestered within the extracellular matrix (ECM) and the cellular surface by heparin sulphate (HS) proteoglycans (Turner and Grose, 2010). They

have moderate to high affinity for HS, and this binding impedes their diffusion across long distances, allowing them to act locally near the source of secretion (Goetz et al., 2007). This affinity is controlled by the HS binding site in the β1- β2 loop and β10- β12 region of FGFs. Despite similar HS binding topology, these regions vary in sequence across FGFs, which has a direct effect on the binding affinity to HS (Makarenkova et al., 2009). Differential binding to HS promotes the creation of gradients of diffusion in the ECM that contribute to differential patterning and morphogenesis in development. Moreover, HS-FGF binding prevents FGF inactivation and degradation (Gospodarowicz and Cheng, 1986; Saksela et al., 1988). To facilitate signalling, canonical FGFs are released by proteases or heparinases, which enables its binding to FGFR. This interaction of FGF and FGFR is further stabilised when a ternary complex is formed in the presence of HS (Ori, 2008). The spaciotemporal expression of HS at the cell surface as well as its length and sulphation level ultimately regulate the extent of FGF binding and signalling (Matsuo and Kimura-Yoshida, 2013; Shimokawa et al., 2011). Although HS-FGF binding seems to have an important role in cell signalling fate, there is a further degree of signalling complexity that is determined by the specificity and affinity of FGF for its receptor FGFR, which will be discussed in the next section.

In contrast to paracrine FGFs, endocrine FGFs lack the β11 strand which obstructs their interaction with HS, allowing their diffusion into the blood circulation to different organs (Harmer et al., 2004). As endocrine ligands, they act in complex with FGFR and Klotho TM proteins. Studies have shown that the Klotho proteins bind directly to FGFR monomers which increase its affinity to FGF23, therefore enhancing FGF23 binding and consequent induction of FGFR phosphorylation (Kurosu et al., 2006).

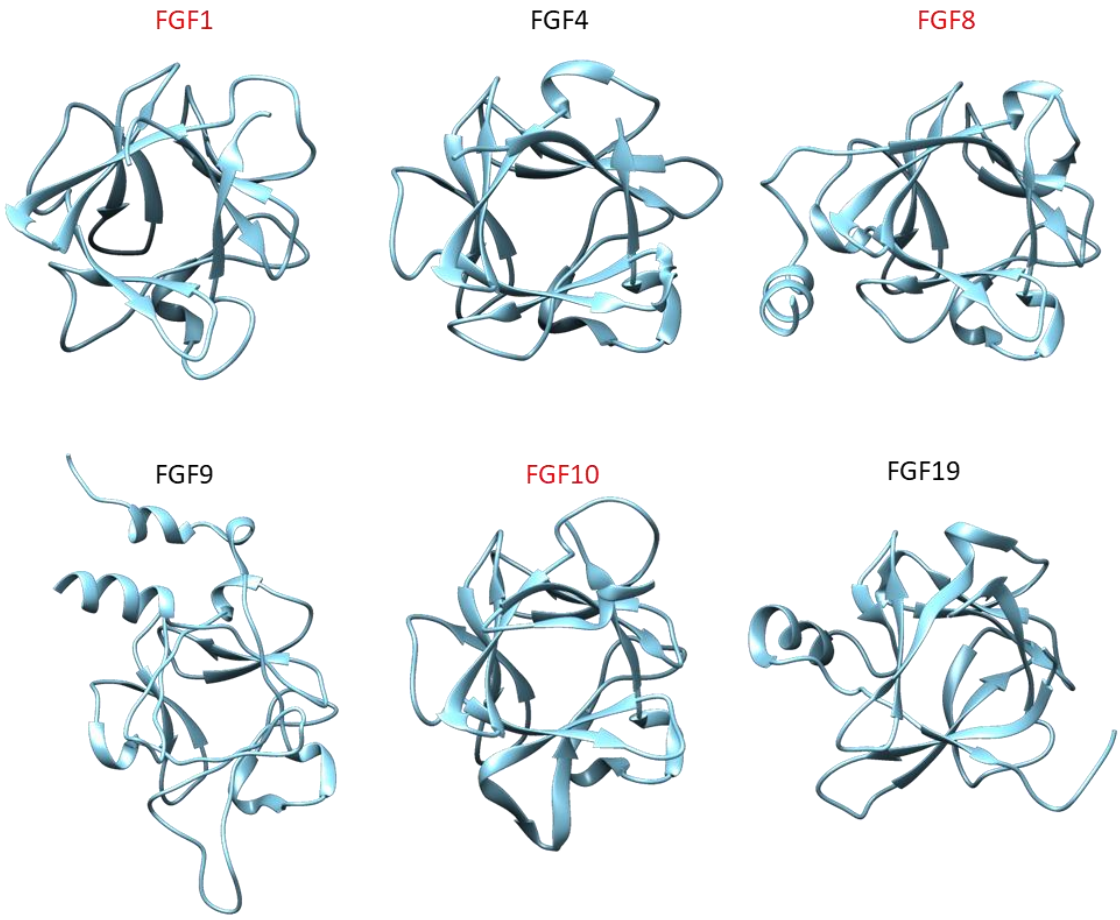

Figure 1.4 – Representative domain organisation of several FGFs. Crystal structures are here shown for each subfamily of canonical (FGF1,4,8,9,10) and endocrine (FGF19) FGFs in the same orientation. FGFs adopt a β-trefoil fold with different loop conformations, determining different specificities towards FGFR. In red are ligands whose structure was solved in complex with its receptor. FGF1 [PDB: 1EVT], FGF4 [PDB: 1IJT], FGF8 [PDB: 2FDB], FGF9 [PDB: 1IHK], FGF10 [PDB: 1NUN], FGF19 [PDB: 2P23].

1.2.2 - FGFR structure and isoforms

Similar to other RTKs, FGFRs contain an extracellular ligand-binding domain, a single TM helix domain and an intracellular compartment containing a split tyrosine KD which possesses catalytic activity (Ornitz et al., 1996). Together, these three domains of FGFR are tightly coordinated to activate essential signalling pathways (Figure 1.5).

The extracellular domain of FGFRs is composed of three Ig-like domains (Ig-I or D1, Ig-II or D2 and Ig-III or D3) separated by short linker regions (Wesche et al., 2011). Ig-I together with the acidic box, a serine-rich region between Ig-I and Ig-II, have a role in the receptor autoinhibition, competing with FGF and HS for

binding to Ig-II (Olsen et al., 2004). The Ig-II and Ig-III regions are responsible for binding FGF ligands, with the first half of Ig-II responsible for binding HS proteoglycans (Beenken and Mohammadi, 2009). Tissue specific expression of FGF ligands and receptors play a fundamental role in the specificity and selectivity of FGF-FGFR binding. Moreover, FGF ligand binding affinity and specificity of FGFR1-3 is determined by alternative splicing of the extracellular Ig-III region (Werner et al., 1991). There are two major spliced forms: when exon 8 is expressed and exon 9 is skipped, isoform IIIb of FGFR is expressed, while expression of exon 9 and skipping of exon 8 results in the expression of isoform IIIc (Figure 1.5) (Tiong et al., 2013). As outlined in Table 1.2, the two different FGFR splice isoforms present distinct ligand-binding characteristics. Moreover, these spliced forms are regulated in a tissue-specific way, such that isoform IIIb is preferably produced in the epithelium and isoform IIIc is restricted to mesenchymal lineages (Eswarakumar et al., 2005). In fact, studies have revealed that ligands secreted by epithelial tissues preferably bind and signal through mesenchymal isoform c of FGFRs, whereas FGFs secreted by mesenchymal tissues signal in the context of epithelial lineages through isoform b of FGFR, resulting in reciprocal paracrine signalling (Ornitz et al., 1996). For example, *in vitro* studies in the mouse BaF3 cell line showed that FGF7 and FGF10, both expressed by the mesenchyme, have the highest activity towards FGFR2b that is expressed in the epithelium (Ornitz et al., 1996). Similarly, FGF8 expressed by epithelial cells was shown to exclusively bind to FGFR3c and FGFR1c isoforms in the mesenchyme (Zhang et al., 2006). Crystal structures and *in silico* modelling of these complexes FGF-FGFR have provided insights into the molecular basis for this binding specificity or promiscuity. The amino acid sequence and spatial conformation of FGFs and FGFRs, along with their temporal expression patterns determine their binding affinity, and the resultant FGF-FGFR complexes initiate different intracellular signals resulting in distinct biological responses (Belov and Mohammadi, 2013).

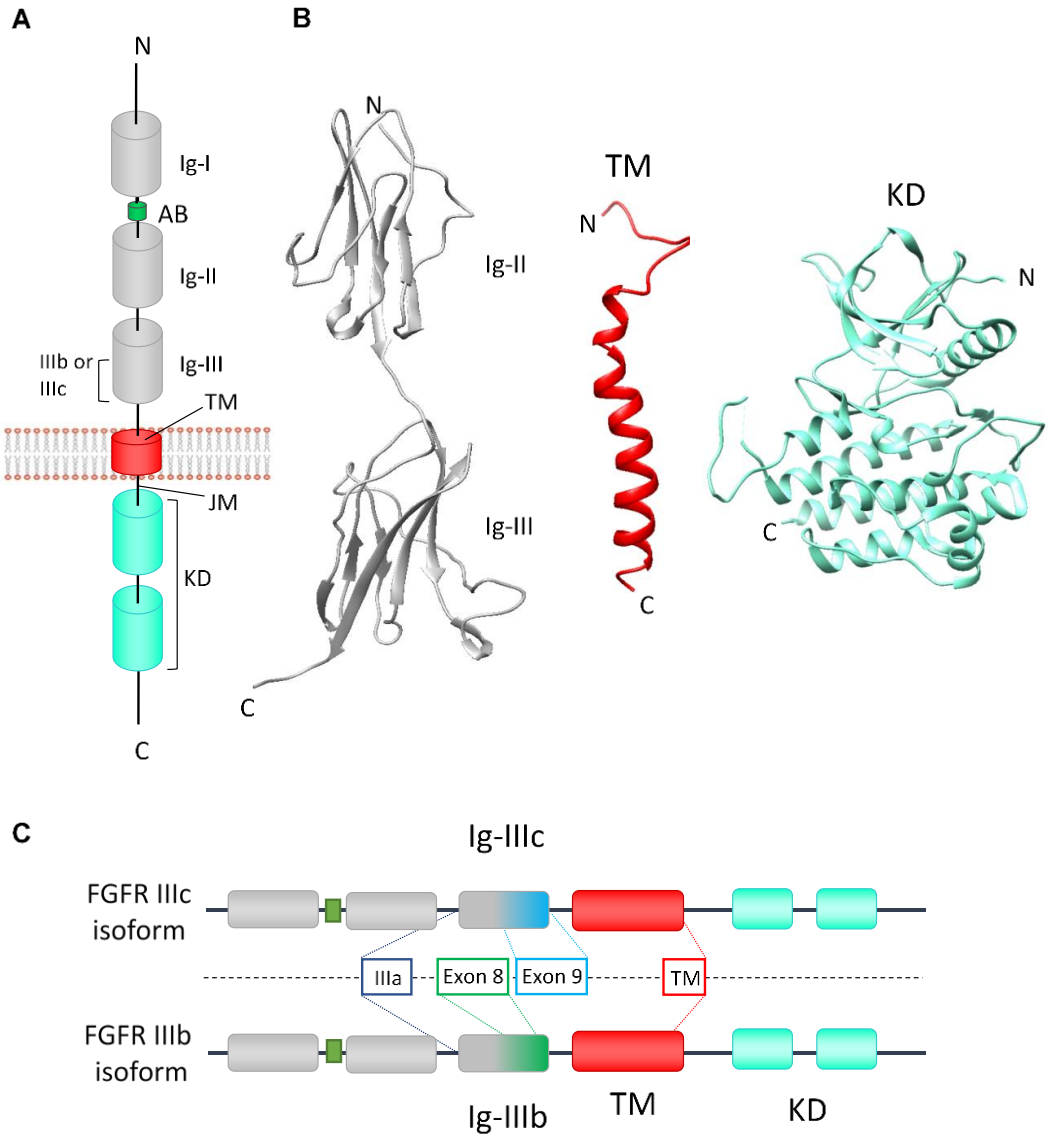

Figure 1.5 – Structural representation of FGFR and isoforms. A. Domain organisation of FGFR family common to all four FGFRs. The extracellular domain is formed by three Ig-like domains separated by short linker regions. Ig-I and the acidic box (AB) regulate the autoinhibition of FGFR. The first half of Ig-II binds HS proteoglycans, and together with Ig-III, it forms the ligand-binding pocket, with distinct properties to selectively bind different FGFs. In FGFR1-3, the second half of Ig-III is spliced to either exon IIIb or IIIc, followed by a single-pass transmembrane (TM) helix domain that links to the intracellular region. The intracellular region is formed by a juxtamembrane (JM) region and a split tyrosine kinase domain (KD) which possesses catalytic activity. **B.** Representative structure of FGFR3 as determined by crystallography. Structural models are coloured according to the different domains in A and orientation is identified by the labelling of amino-terminus (N) and carboxy-terminus (C). For FGFR3 the extracellular domain is formed by amino acids (aa) number 1 to 375, where each Ig domain is formed by β-sheets structures [PDB: 1RY7]. The single helix TM domain is formed of aa 376-396 and connects to the intracellular domain [PDB: 2LZL]. The intracellular region is composed of aa 397-806 in β-sheets and α-helixes and it includes the KD [PDB: 4K33]. **C.** FGFR1-3 ligand-binding specificity is generated by alternative splicing of Ig-III. The first half of Ig-III encodes for the invariant exon IIIa whereas the second half encodes for IIIb or IIIc depending on the exon expressed, which then splices to the exon that encodes (continuation of figure legend on following page)

(continuation of legend of Figure 1.5) the TM domain. Figure adapted with permission from Nature, (Turner and Grose, 2010).

Table 1.2 – Ligand binding specificities of FGFR isoforms. Adapted from Springer with free access, (Tiong et al., 2013).

FGFR isoform	Ligand specificity
FGFR1, IIIb	FGF-1, 2, 3, 10 and 22
FGFR1, IIIc	FGF-1, 2, 4, 5, 6, 19, 20 and 21
FGFR2, IIIb	FGF-1, 3, 4, 6, 7, 10 and 22
FGFR2, IIIc	FGF-1, 2, 4, 5, 6, 8, 9, 17, 18, 19, 21 and 23
FGFR3, IIIb	FGF-1 and 9
FGFR3, IIIc	FGF-1, 2, 4, 8, 9, 17, 18, 19, 21 and 23
FGFR4	FGF-1, 2, 4, 6, 8, 9, 16, 17, 18 and 19

1.2.3 - FGFR activation and signalling pathways

The binding of canonical FGFs to FGFR induces receptor dimerisation and activation. This interaction is quite robust, and the dimer is stabilised by a combination of bivalent ligand-receptor interactions along with additional interactions between both monomers involving the co-factor HS (Lemmon and Schlessinger, 2010). Dimerisation shifts the conformational structure of FGFR bringing the intracellular KDs into close proximity, triggering trans-autophosphorylation of each RTK in the intracellular domain, enabling FGFR activation (Chen et al., 2008; Sarabipour and Hristova, 2016).

As there are currently no full-length crystal structures of RTKs, the mechanistic role of the extracellular domain and TM domain in initiating and inducing FGFRs dimerisation for kinase activation has been extensively debated. The concept of lateral motion of RTKs through the membrane matrix and stochastic collision to facilitate dimerisation followed by kinase activation in a ligand-dependent manner was widely accepted in the 1970s (Schlessinger et al., 1978). However, recent studies indicate that FGFRs form dimers in the absence of ligand and that these dimers are phosphorylated at a basal level and stabilised by the autoinhibitory effect of the Ig-I domain (Figure 1.6) (Comps-Agrar et al., 2015; Sarabipour and Hristova, 2016). Full phosphorylation is triggered by ligand binding which induces conformational changes in the TM helices and ultimately kinase activation,

although the exact mechanisms by which this occurs is still not fully understood (Figure 1.6). Moreover, the structure of the dimer in the TM domain and the intensity of FGFR activation was shown to be dependent on the type of ligand (Sarabipour and Hristova, 2016). For FGFR1 and FGFR3, FGF1 induces TM helix-helix interactions that are stabilised by a tight packing in the central region of the TM by hydrogen-bonds, and other types of interactions such as van der Waals and electrostatic contacts, leaving the flanking charged residues on both termini sites of the TM helix unstable (Bocharov et al., 2013). This instability is thought to have a key role in the propagation of conformational changes from the ectodomain to the KD upon ligand binding. FGF2 on the other hand, induces an interaction throughout the entire TM domain resulting in a tightly compact crossed TM domain that results in higher levels of FGFR1 and FGFR3 phosphorylation compared to FGF1 ligand binding (Sarabipour and Hristova, 2016). However, this difference between the phosphorylation levels in response to FGF1 and FGF2 are not observed in FGFR2 which maintains the same phosphorylation levels in the presence or absence of these two ligands (Sarabipour and Hristova, 2016). This data provides supporting evidence that the level of FGFR activation is ligand-dependent and that different ligands might induce different phosphorylation levels and consequently distinct signalling pathways for each FGFR isoform.

In addition, the TM domain is thought to play a role in the symmetry of the KD determining its activation status (Bocharov et al., 2013). Although no work has been done directly in FGFR, studies on other RTKs such as EGFR reveals that the basal phosphorylation state of the KD adopts a symmetric configuration, whereas upon ligand binding conformational changes allow a shift of the KD to an active asymmetric orientation, allowing transphosphorylation of the adjacent KD (Bae and Schlessinger, 2010; Moosa Mohammadi et al., 1996). The hypothesis suggests that there may be two distinct FGFR dimeric structures: the unliganded symmetric inactive but basally phosphorylated structure; and the asymmetric fully phosphorylated structure where ligand binding triggers the separation of the c-terminus of the TM region to allow the intracellular KD to adopt a crossed asymmetric configuration (Bocharov et al., 2013).

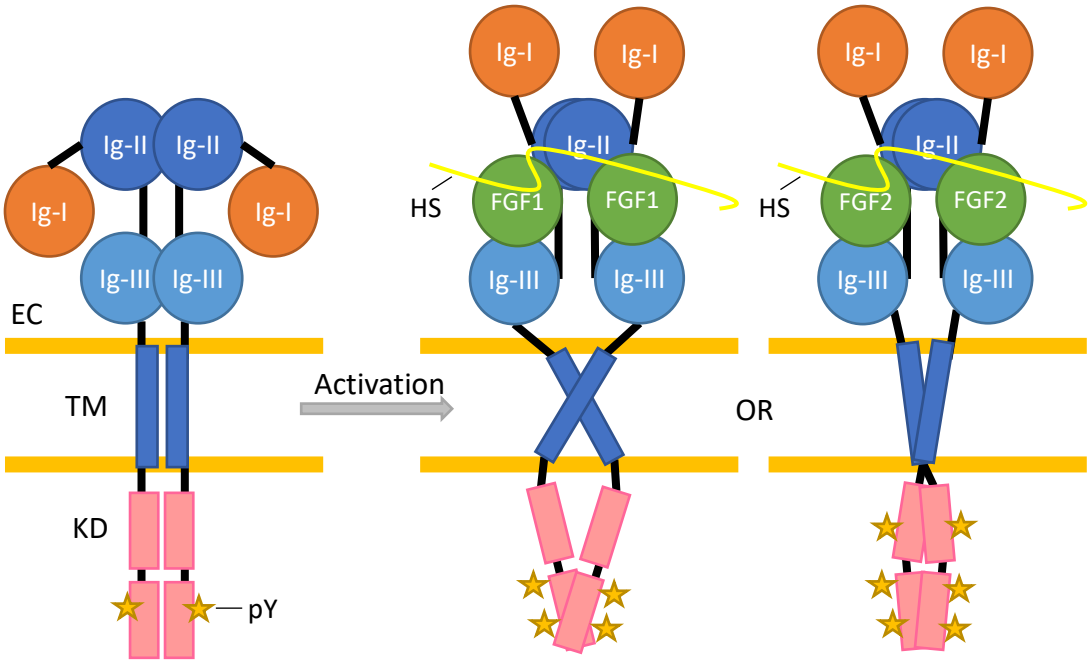

Figure 1.6 – Mechanism of FGFR dimer activation. FGFR exists as a basally phosphorylated dimer in the inactive state and ligand binding induces a conformational change in the TM domain that propagates to the intracellular domain, bringing the KD to a conformation that allows full activation of the receptor. The level of activation is ligand dependent and the conformation of the TM and KD domains is variable. FGF1 ligand is found to activate FGFR1 and FGFR3 to a lower degree than FGF2 ligand, and this activation is associated with a different structural proximity between the TM and KD domains of both monomers. *EC- extracellular; TM- transmembrane; KD- kinase domain; pY- phosphorylated tyrosine; HS- heparan sulphate.* Adapted with permission from (Bocharov et al., 2013; Sarabipour and Hristova, 2016).

The asymmetric dimer conformation of the KD allows trans-autophosphorylation of the activation loops in a reciprocal way, where one KD moiety acts as an enzyme transphosphorylating the other KD that acts as a substrate (Chen et al., 2008). Similarly to other RTKs, the split KD of FGFRs is formed by an N-terminus lobe composed by five β-sheets (β1-β5) and one α-helix (αC), and one C-terminus lobe with two β-sheets and seven α-helices. In between the two lobes lies the active site that binds ATP. This hinge region is formed by several loops with different functions allowing the stabilisation of the active conformation of the KD as well as regulation of nucleotide and ATP binding (Moosa Mohammadi et al., 1996). The activation loop is particularly important because it contains two tyrosine residues conserved across all studied FGFRs (the Y653 and Y654 in FGFR1, Y656 and Y657 in FGFR2 or Y649 and Y650 in FGFR3) that once phosphorylated induce a conformational change that activates the KD to an open configuration (Figure 1.7). The KD is then able to phosphorylate other tyrosine

residues outside the activation loop within both lobes of the KD, intracellular JM region and C-terminus, resulting in full activation of the receptor (M Mohammadi et al., 1996). The mechanism of activation seems to be conserved between FGFRs, but the number of phosphotyrosine residues on different receptors that can be phosphorylated upon receptor activation varies. For example, FGFR1 has 6 tyrosine sites (Y463, Y583, Y585, Y730, Y766, and Y776) that can be phosphorylated in a very precise and sequential way, whereas FGFR3 has 4 tyrosine sites (Y579, Y726, Y762 and Y772) (Furdui et al., 2006; Hart et al., 2001). In the inactive state, the αC helix on the N-lobe is known for anchoring the activation loop to a closed configuration that blocks protein substrate binding without impairing ATP binding (Moosa Mohammadi et al., 1996). Moreover, autoinhibition is regulated by a triad of residues in the kinase hinge loop that forms a network of hydrogen bonds mediating a “molecular brake” that keeps the KD in the inactive state (Chen et al., 2007). The activation and inactivation states of FGFR are a transient equilibrium regulated by structural features of the entire receptor, FGF ligand binding and intracellular regulatory mechanisms.

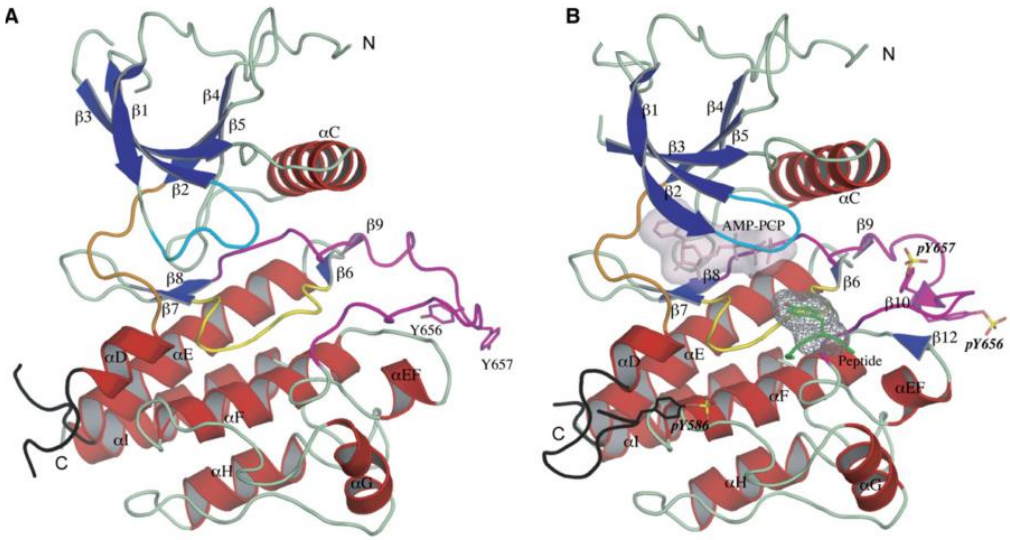

Figure 1.7 – Representation of the activation of FGFR2 KD. On the left is a representation of FGFR2 in the inactive state whereas on the right is the active state. The activation loop is shown in pink, the catalytic loop in yellow, the nucleotide binding loop in light blue and the kinase hinge region in orange. The ATP analog is shown by the pin surface and the tyrosine side chain of the substrate in green and grey mesh. The right image shows a conformational change of the activation loop upon phosphorylation of the tyrosine residue Y656 and Y657 that allows ATP to reach its binding site. Image adapted with permission from Molecular Cell, (Chen et al., 2007).

Upon phosphorylation in different tyrosine sites of the intracellular JM region, KD and C-terminus, these phosphorylated residues act as docking sites for adaptor proteins containing SH2 and PTB domains (Figure 1.8). One of these adaptor proteins is FRS2 that binds directly to the intracellular JM region of FGFR1 (Hart et al., 2001). FRS2 contains PTB domains in the N-terminus that binds to FGFR, myristyl anchors that facilitate localisation to the cell membrane and multiple tyrosine residues on the C-terminus region (Kouhara et al., 1997; Ong et al., 2000). Once docked to the active FGFR, FRS2 is phosphorylated at six different tyrosine sites, creating additional docking sites for other adaptor proteins, namely four binding sites (Y196, Y306, Y349 and Y392) for the growth factor receptor-bond 2 (GRB2) and two sites (Y436 and Y471) for the SH2-containing protein tyrosine phosphatase 2 (SHP2) (Hadari et al., 2001). The recruitment of docking molecules leads to the formation of specific complexes that result in the activation of different downstream signalling pathways. For example, the recruitment of GRB2 and son of sevenless (SOS) by FRS2, forms a complex that activates the proto-oncogene GTPase RAS and the MAPK pathway (Kouhara et al., 1997). The MAPK signalling cascade successively phosphorylates and activates MEK and Erk (Roskoski, 2012). MEK and Erk kinases can then translocate to the nucleus where they activate transcription factors that participate in immediate gene response (Andreadi et al., 2012). In the case of FGFR, the specific transcription factor that is activated by this pathway is the E26 transformation-specific (ETS) transcription factor which promotes cell survival, division, motility and differentiation (Ornitz and Itoh, 2015; Raible and Brand, 2001). FRS2 can also recruit GRB2 indirectly via SHP2 which regulates Src family kinase (SFK) activity and mediates RAS/Erk and PI3K/Akt pathway activation (Agazie et al., 2003; Zhang et al., 2004). Independently, another complex formed upon docking of FRS2 to FGFR is the GRB2 and GAB1 complex, which drives PI3K and Akt pathway activation (Hadari et al., 2001). In a study to understand the role of FRS2 in FGFR signalling, FRS2 -/- embryonic stem cells were generated, resulting in the impairment of MAPK and PI3K activity which caused a loss in cell proliferation and migration (Hadari et al., 2001). In the same study, the six tyrosine residues of FRS2 were also mutated to phenylalanine residues (four for GRB2 docking - Y196F, Y306F, Y349F, and Y392F; and two for SHP2 docking - Y436F and Y471F) in mouse embryonic fibroblasts (MEF) (Hadari et al., 2001).

Phenylalanine is identical to tyrosine but lacks the hydroxyl group in its side chain, impairing phosphorylation. The results showed that different tyrosine phosphorylation sites on FRS2 mediate different biological responses. Mutant forms of FRS2 in the GRB2 docking sites only partially reduced cell viability, whereas mutant forms of FRS2 in the SHP2 sites completely abolished the mitogenic response. A similar effect was seen in migration assays, although both mutations in SHP2 and GRB2 docking sites of FRS2 decrease chemotactic responses, the SHP2 docking sites were found to be more important than GRB2 sites for migration (Hadari et al., 2001).

In addition, C-terminus phosphorylated tyrosine residues act as docking sites for further adapter proteins. An example is the adaptor PLCγ, that upon phosphorylation by FGFR at Y762 in FGFR3, hydrolyses phosphatidylinositol 4,5-bisphosphate (PIP2) to produce diacylglycerol (DAG) and IP3 inositol 1,4,5-triphosphate (IP3) inducing the release of calcium and subsequent activation of protein kinase C (PKC) (Chen et al., 2005; Mohammadi et al., 1991). PKC in turn can also activate RAS (Huang et al., 1995). Furthermore, phosphotyrosine residues Y726 (on the KD) and Y762 (on the C-terminus) of FGFR3 are known to be required for optimal binding the SH2-Bβ adaptor protein which activates the STAT5 transcription factor (Kong et al., 2002). In particular, in constitutively active FGFR3 bearing the K652E mutation, the phosphorylation site Y726, was also found to be important for the phosphorylation of SHP2 and activation of PI3K, MAPK and STAT1 and STAT3 pathways, playing a crucial role in regulating cell proliferation (Hart et al., 2001).

Depending on the cellular context, other pathways have also been reported to be activated by FGFR such as p38 MAPK, Jun N-terminal kinase (JNK) and the p90 ribosomal protein S6 kinase 2 (RSK2) pathways (Hart et al., 2000; Kang et al., 2009; Klint and Claesson-welsh, 1999). Many of these activated pathways orchestrate key cellular processes including cell survival, proliferation, migration, differentiation and metabolism.

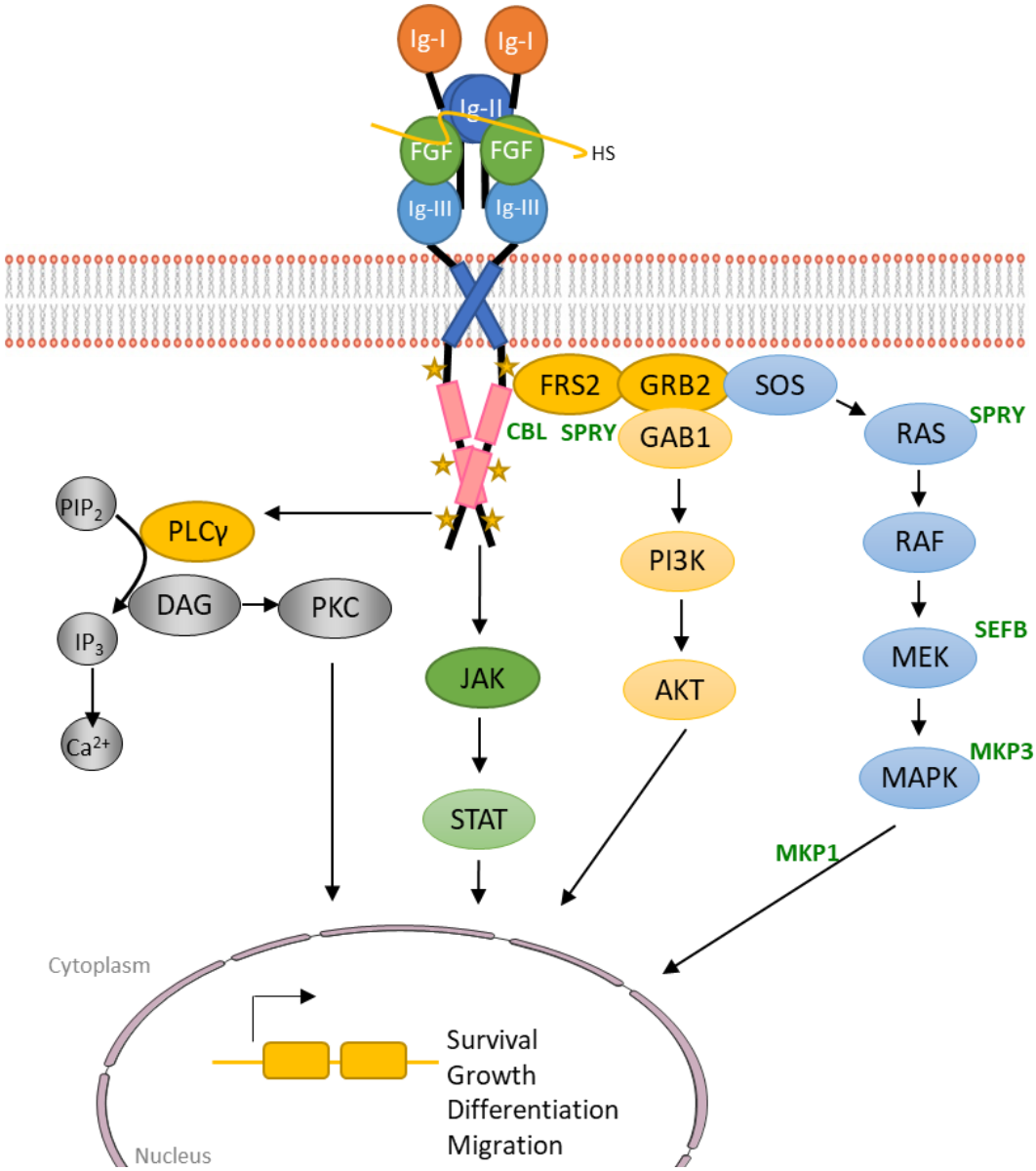

Figure 1.8 – Simplified overview of FGFR canonical signalling pathways. FGFs bind to FGFR in the presence of HS proteoglycan inducing receptor dimerisation which then allows the transphosphorylation of the tyrosine KD in the intracellular compartment of the cell inducing the recruitment of adaptor proteins responsible for the activation of several downstream signalling pathways. The intracellular compartment of active FGFR is phosphorylated in multiple tyrosine sites. In the C-terminus tyrosine phosphorylation works as a docking site for molecules containing SH2 domains such as PLCγ. Phosphorylation of PLCγ hydrolyses PIP2 to produce DAG and IP3 inducing the release of calcium cations and subsequent activation of PKC. In the intracellular JM region of FGFR, phosphorylation leads to the recruitment of FRS2 which then acts as a secondary docking protein to form two independent complexes. One complex is FRS2-GRB2-SOS that activates RAS which in turn activates the MAPK pathway. A second complex is FRS2-GRB2-GAB1 which drives the activation of PI3K/Akt pathway. Other pathways are also known to be activated by FGFR such as STAT, p38 MAPK, JNK, Src and RSK2 pathways. Collectively, these pathways play multiple roles in cell survival, growth, migration, differentiation and metabolism. FGFR signalling is regulated by receptor internalisation upon ubiquitination by CBL or by negative modulation by different proteins (shown in bold green) such as MKP, SEF and SPRY. *The yellow stars represent tyrosine phosphorylation sites; HS- heparin sulphate; FRS2- FGFR substrate 2; PLCγ- adaptor* (continuation of figure legend on following page)

(continuation of legend of Figure 1.8) *protein phospholipase Cγ; PIP2- phosphatidylinositol 4,5-bisphosphate; DAG- diacylglycerol; IP3- IP3 inositol 1,4,5-triphosphate; Ca2+- calcium; PKC- protein kinase C; GRB2- growth factor receptor-bond 2; SOS- son of sevenless; MAPK- mitogen-activated protein kinase; PI3K- phosphoinositide 3-kinase; MEK- intracellular mitogen-activated protein kinase/Erk kinase; RAF- Raf-1 proto-oncogene, serine/threonine kinase; RAS- proto-oncogene GTPase; GAB1- GRB2-associated binding protein 1; AKT- Akt serine/threonine kinase 1; JAK- janus kinase; STAT- signal transducer and activator of transcription; CBL- Cbl proto-oncogene E3 ubiquitin protein ligase; MKP- MAPK phosphatases; SEF- similar expression to fgf genes; SPRY- sprouty homolog.* Figure adapted with permission from Nature, (Turner and Grose, 2010).

1.2.4 - Regulation of FGFR signalling

FGFR signalling is regulated by different proteins, including SPRY, Cbl proto-oncogene E3 ubiquitin protein ligase (CBL), MAPK phosphatases (MKP) and SEF (Wesche et al., 2011) (Figure 1.8). SPRY are a ligand-inducible class of proteins antagonists of RTK signalling (Mason et al., 2006). This family is known to negatively regulate FGFR by different mechanisms that are not fully understood and there is conflicting information in the literature. SPRY is thought to either interact with the FRS2-GRB2-SOS complex, decoupling the cascade of downstream signalling, or directly inhibit RAS (Gross et al., 2001; Martínez et al., 2007). Studies show that SPRY1 and SPRY2 can translocate to the plasma membrane where they become phosphorylated on a conserved tyrosine and activated by FGFR (Hanafusa et al., 2002). While unphosphorylated SPRY constitutively binds to GRB2 at two proline-rich regions, only phosphorylated SPRY is able to inhibit the recruitment of GRB2-SOS to FRS2 or SHP2, impairing Erk pathway activation (Martínez et al., 2007). In addition, unphosphorylated SPRY results in prolonged Erk activation in response to FGF stimuli inducing outgrowth in PC-12 cell lines in monolayer cultures, in contrast to phosphorylated SPRY that significantly blocks PC-12 outgrowth (Hanafusa et al., 2002). Other studies refute the fact that SPRY can bind to GRB2, indicating that SPRY1 or SPRY2 do not prevent the formation of GRB2-SOS complex, but rather act downstream of this complex, directly blocking RAS or RAF activation, inhibiting cell growth and differentiation through MAPK pathway blockade (Gross et al., 2001; Yusoff et al., 2002). These results might indicate SPRY modes of action

that are not mutually exclusive, but rather reinforce the plasticity in SPRY activity in mediating negative regulation of FGFR.

CBL is a ubiquitin ligase that forms a ternary complex with GRB2 bound to FRS2 in response to FGF stimulation (Wong et al., 2002). In complex with FRS2 and GRB2, CBL conjugates ubiquitin to lysine residues of the active FGFR and FRS2 inducing clathrin-mediated endocytosis for subsequent degradation within the lysosome and signal termination (Lecker et al., 2006; Monsonego-ornan et al., 2002). However, in a later study aimed at understanding the role of ubiquitination in the internalisation and sorting of FGFR1, ubiquitination was found to be only important for internal cellular sorting of FGFR1 but not for its endocytosis (Haugsten et al., 2008). In this study, serial mutations of all the lysine residues (ubiquitination sites) of the intracellular domain of FGFR1 were generated in human cell lines. Results showed that for the mutations that did not impair kinase activity, ubiquitination levels were poor but the internalisation by endocytosis was not affected. In contrast, degradation of these mutants was hampered as mutants were inefficiently transported to the lysosomes. This indicates that internalisation of FGFR1 is not ubiquitin-dependent, but its degradation is.

Other modulators of FGFR such as SEF exert its regulatory effects upstream of RAS by directly preventing FGFR phosphorylation (Kovalenko et al., 2003). Cellular *in vitro* studies have demonstrated that in cells expressing constitutively active FGFR1, SEF can prevent MAPK pathway activation, but interestingly, the same if voided in cells with a constitutively active RAS, indicating the role of SEF directly through FGFR (Kovalenko et al., 2003). Dual phosphatases such as the MKP-1 and MKP-3 also play a role in FGFR signalling regulation. They are able to block the phosphorylation and enzymatic activity of Erk, negatively controlling FGFR (Sun et al., 1993). FGFR C-terminus tail was also found to be important in the regulation of receptor activation (Ahmed et al., 2010). FGFR2 was found to directly recruit GRB2 to a proline-rich region of FGFR2 SH3 C-terminus tail. But, GRB2 binding sterically impedes the phosphorylation of FGFR2 in other tyrosine residues resulting in an inhibition of the recruitment of other FGFR effectors such as SHP2 or PLCγ.

In parallel, MAPK has also been shown to play a role in the negative regulation of FGFR signalling through FRS2. MAPK can phosphorylate FRS2 on multiple threonine residues not only in response to FGFR stimulation by FGF but also in response to stimuli with EGF, insulin or platelet-derived growth factor (PDGF) (Lax et al., 2002). Increased threonine phosphorylation of FRS2 leads to a reduction in its levels of tyrosine phosphorylation, ultimately leading a reduction in GRB2 binding and attenuation of MAPK activation (Lax et al., 2002). FRS2 is therefore an important positive and negative regulator of FGFR signalling and is responsible for maintaining a precise control over its resultant biological activities.

Trafficking of FGFR within the cells is also a modulator of the spatial and temporal dynamics of its signalling (Miaczynska, 2013). The efficient internalisation and intracellular transport of RTKs through endocytic routes is a critical mean to attenuate or propagate extracellular ligand-induced signalling, via degradation or recycling respectively, ensuring a constant membrane flow maintaining the signalling balance (Miaczynska, 2013). However, signalling is not restricted to the plasma membrane, as evidence shows that activated receptors can associate with the membrane of internal organelles such as endosomes influencing the time, intensity and specificity of signalling (Disanza et al., 2009). Moreover, the signalling outcome within the cell has been shown to be dependent on the type of internalisation pathway used, either clathrin-mediated endocytosis or non-clathrin-mediated endocytosis (Roy and Wrana, 2005). One study on FGFR has shown that different FGFR family members display different endocytosis mechanisms (Haugsten et al., 2011). FGFR3 shows a much slower rate of endocytosis than FGFR1 and whereas FGFR1 internalisation, signalling termination and degradation is mediated by clathrin, FGFR3 is internalised by both clathrin and non-clathrin mechanisms. Clathrin depletion led to a prolonged and delayed signalling through FGFR1, suggesting that clathrin-mediated endocytosis of FGFR1 mediates the efficient activation of certain FGFR1 downstream pathways such as MAPK and it is important for signal termination. In contrast, clathrin depletion in FGFR3 only slightly delayed its degradation and signalling, showing that FGFR3 is dependent on alternative mechanisms to maintain signalling and receptor internalisation (Haugsten et al., 2011). This clathrin-dependent endocytosis for FGFR1 as well as for FGFR2 has been shown

to be regulated by Src and its phosphorylation target epidermal growth factor receptor kinase substrate 8 (Eps8) (Auciello et al., 2013). Src is recruited to active FGFR through FRS2 at the cell membrane and FGFR internalisation to the endosomes occurs after FGFR is released from complexes containing Src in an Eps8-dependent manner. Src and Eps8 have also been found to be key coordinators of immediate MAPK signalling for FGFR1 and FGFR2 and activation of PI3K for FGFR1 (Sandilands et al., 2007).

FGFR signalling is tightly regulated by a number of different modulators that control the spaciotemporal dynamics of FGFR network function and cell fate decisions.

1.3 - FGFR alterations in cancer

As described in earlier sections, FGFR activation and signalling is crucial for many physiological processes. Aberrations in FGFR or its downstream signalling components have been implicated in the initiation and progression of several cancer types (Ahmad et al., 2012). A recent study from 2015 has found through next-generation sequencing of almost 5000 tumours across all cancer types that FGFR aberrations are present in 7.1% of these tumours, the majority being activating mutations or gene amplifications (Helsten et al., 2015). Reported FGFR aberrations in cancer include receptor translocations, amplifications and point mutations. In addition to these mechanisms, a switch in FGFR splicing isoform, alterations in FGFR internalisation, impaired signalling termination and defective FGF ligand secretion have also been reported to affect FGFR canonical pathways leading to oncogenesis (Figure 1.9) (Babina and Turner, 2017; Tanner and Grose, 2015). A list of the FGFR alterations associated with cancer is summarised in Table 1.3.

FGFR amplification has been shown to occur as a result of gene duplication or aberrant gene transcriptional control (Dienstmann et al., 2014). Receptor overexpression can lead to accumulation at the cell surface and ligand-independent dimerisation arising from stochastic diffusion through the cell membrane. Of the four FGFR family members, cancer-associated amplification

is more common in FGFR1 and FGFR2 (Carter et al., 2015). For example, amplification of the *FGFR1* gene accounts for 10% of human breast cancers, being associated with poor prognosis (Reis-Filho et al., 2006). Whereas single nucleotide polymorphisms (SNPs) in *FGFR2* have been found to increase the risk of breast cancer by altering the binding affinity of transcription factors causing an increase in FGFR2 protein expression (Easton et al., 2007; Meyer et al., 2008). FGFR isoform switching is another mechanism that have been shown to drive tumourigenesis. With the affinity and specificity of FGF ligands being dependent on the isoform of FGFR expressed in cells, a switch in FGFR isoform could result in a change in ligand repertoire and as a consequence dysregulated signal transduction (Yan et al., 1993). For example, a spontaneous switch from FGFR2-IIIb isoform (enriched in epithelia) to FGFR2-IIIc isoform (enriched in mesenchyme) has been found in some subgroups of prostate cancer and in nearly 90% of clear cell renal cell carcinomas (ccRCC) (Kwabi-Addo et al., 2001; Zhao et al., 2013). Moreover, the mesenchymal-like bladder carcinoma cell line TSU-Pr1, that presents increasing metastatic ability in culture following systematic passaging and expresses FGFR1-3-IIIc, was found to spontaneously acquire epithelial characteristics (Chaffer et al., 2006).

In addition, amplification of FGF genes can alter the dimerisation rate of FGFR through increased paracrine or autocrine signalling, leading to a constitutive receptor activation which has been shown in breast and urothelial cancers (Reintjes et al., 2013; Rodriguez-vida et al., 2015). Chromosomal translocations of FGFR family members with other fusion protein partners have been identified in different cancers. The fusion of other genes to FGFR can increase the dimerisation of the receptors in a ligand-independent manner or increase its expression when the translocation event submits FGFR under the control of a different promoter (Kalff and Spencer, 2012; Yagasaki et al., 2001).

Point mutations are the most prevalent form of FGFR abnormalities accounting for one quarter of all FGFR aberrations found in cancer. Although more frequent in FGFR2 and FGFR3, mutations affect all four FGFR family members and happen across the entire length of the receptor (Patani, 2016). For instance, mutations in the Ig-III region can increase receptor's potential for dimerisation in a ligand-independent manner (Rousseau et al., 1996). Mutations on the KD are

known to induce constitutive receptor activation, whereas mutations of the C-terminus tail can impair the autoregulatory processes of ubiquitination and internalisation (Ahmad et al., 2012; Gallo et al., 2015). Examples of point mutations and fusions of FGFR3 will be discussed in detail in the next section.

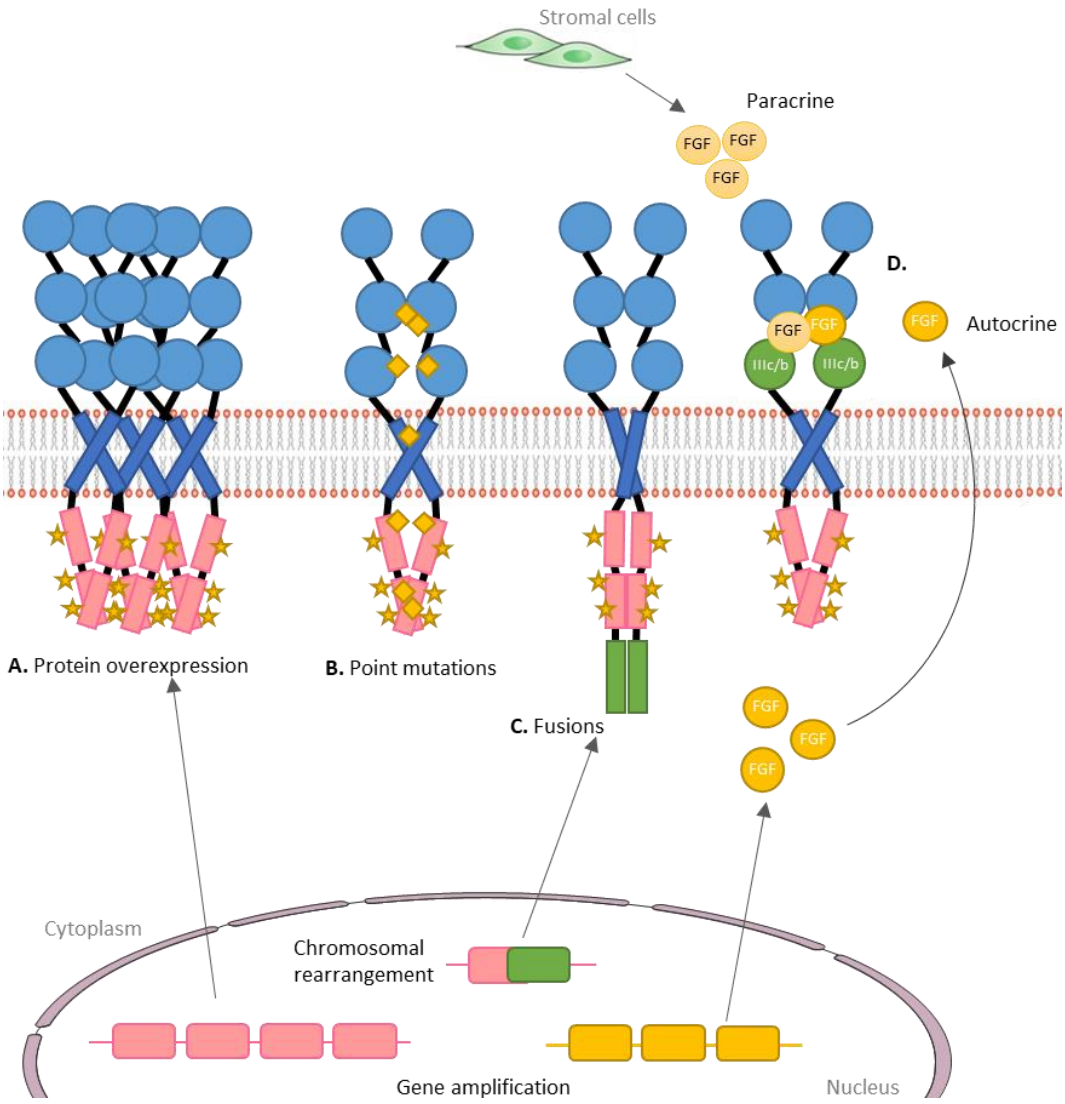

Figure 1.9 – Mechanisms of FGFR oncogenic activation. There are different mechanisms by which FGFR function and signalling can be altered in cancer. **A.** Amplification of FGFR gene can lead to receptor overexpression at the cell membrane which results in ligand-independent dimerisation by stochastic diffusion through the membrane. **B.** FGFR point mutations occur across the entire length of FGFR and have different outcomes. Mutations on the extracellular domain and TM domain can impair its autoinhibition or drive ligand-independent dimerisation and activation. Mutations on the KD are known to induce allosteric or direct constitutive activation of FGFR, whereas mutations on the C-terminus tail impair the autoregulatory mechanisms of ubiquitination and internalisation of FGFR. **C.** Chromosomal translocations result in fusions that can drive the constitutive ligand-independent dimerisation of the receptor. **D.** Gene amplification of FGF ligands can increase the secretion of FGFs and (continuation of figure legend on following page)

(continuation of legend of Figure 1.9) overstimulate FGFRs by autocrine or paracrine signalling. Alternative splicing of the Ig-III domain can also cause a switch on the FGFR isoform inducing FGFR response to a larger range of FGFs including those produced by neighbour cells such as stromal cells. *The yellow stars represent tyrosine phosphorylation sites. The yellow diamonds represent point mutations.* Image adapted with permission from Nature, (Babina and Turner, 2017).

Table 1.3 – Common FGFR genomic alterations found in cancer. Compiled from (Criscitiello et al., 2017; Dieci et al., 2013; Dienstmann et al., 2014; Pandith et al., 2010; Tiong et al., 2013; Touat et al., 2015; Wu et al., 2013; Xu et al., 2018)**.**

Gene	Alteration	Cancer type	Incidence %
FGFR1	Amplification	Lung cancer	6-20
		Head and Neck cancer	10-17
		Breast cancer	14
		Ovarian cancer	5
		Bladder cancer	3
	Mutation	Glioma (pilocytic astrocytoma)	5-8
		Melanoma	rare
	Translocation	Glioblastoma	na
		Breast cancer	na
		Lung cancer	na
		8p11 myeloproliferative syndrome	rare
		Chronic myeloid leukaemia	rare
FGFR2	Amplification	Gastric cancer	5-10
		Breast cancer	4
	Mutation	Endometrial cancer	12-14
		Squamous NSCLC	5
		Gastric cancer	rare
	Translocation	Cholangiosarcoma	14
		Prostate cancer	na
		Breast cancer	na
FGFR3	Amplification	Bladder cancer	na
		Salivary adenoid cystic cancer	na
	Mutation	Bladder cancer	40
		Spermatocytic seminoma	7
		Cervical cancer	5
		Myeloma	5
		Prostate cancer	3
		Colorectal cancer	na
		Oral squamous cancer	na
	Translocation	Myeoloma	15-20
		Glioblastoma	3-7
		Bladder cancer	3-6
		Lung cancer	3-5
		Head and Neck cancer	na
		Peripheral T-cell lymphoma	rare
FGFR4	Amplification	Colorectal cancer	5
		Gastric cancer	na
		Breast cancer	na
		Ovarian cancer	na
	Mutation	Rhabdomyosarcoma	6-8

1.3.1 - FGFR3 translocations and mutations

Genomic rearrangements or translocations involving FGFR3 are characterised by the fusion of FGFR3 with a partner gene on the N or C-terminus of the receptor. FGFR3 translocations have been identified in bladder cancers, MM and glioblastomas (Wu et al., 2013). A common example found in around 20% of MM is the t(4;14) translocation, that brings FGFR3 and MM SET domain (MMSET) genes under the control of IgH locus promoter, increasing their expression and aberrant signalling (Chesi et al., 1997). FGFR3 inhibition using the multi-targeting kinase SU5402 and the VEGFR and FGFR1/3 inhibitor PD173074 was shown to decrease the growth of two t(4;14) MM cell lines regardless MMSET activation, showing FGFR3 dependency in these cells and its potential as a target for MM therapy (Grand et al., 2004). Another cancer-driving translocation is the fusion of FGFR3 with TACC3, which is present in 3-6% of urothelial bladder carcinomas and 3-7% of glioblastomas (Dienstmann et al., 2014; Touat et al., 2015). TACC gene encodes for a motor spindle protein dimer known to stabilise the mitotic spindle during cell division (Schneider et al., 2007). FGFR3-TACC3 proteins are usually in-frame fusions of the FGFR3 N-terminus with TACC3 C-terminus. In bladder carcinomas, these fusions lack the last exon of FGFR3, resulting in the fusion of FGFR3 exon 1-18 with TACC3 exon 11 or exon 4, whereas in glioblastomas FGFR3 lacks the last three exons, and the fusion protein is formed by FGFR3 exon 1-16 coupled to TACC3 exon 8 (Singh et al., 2012; Williams et al., 2013). Due to the presence of a coiled-coil domain in TACC3 which enables TACC3 dimerisation, in FGFR3-TACC3 fusions the dimerisation and activation of cellular signalling in the absence of ligand is elevated (Sarkar et al., 2017; Singh et al., 2012). Because they are intracellular proteins and lack the C-terminus tail of FGFR3, these fusion proteins also often escape negative regulation mechanisms, impairing signal termination and protein degradation in the lysosomes (Lombardi et al., 2017; Wesche et al., 2011). Cells with this fusion protein are also particularly prone to aneuploidy, one of the hallmarks of cancer, due to the truncated form of TACC, essential to control mitotic spindle stability (Costa et al., 2016; Singh et al., 2012). Moreover, although studies have reported that this fusion protein localises to the mitotic spindle poles during mitosis

relocating to the midbody during late stage mitosis, it was also shown to display nuclear localisation in contrast to the WT-FGFR3 (Nelson et al., 2016; Singh et al., 2012). In addition, a recent study showed that the FGFR3-TACC3 fusion also exerts its oncogenic effects when it enters the secretory pathway or when it localises at the plasma membrane, leading to hyperactivation of MAPK pathway (Nelson et al., 2018).

Point mutations in FGFR3 are found in various cancers such as cancers of the bladder, head and neck, lung, prostate and colon, amongst others (Table 1.4) (Ahmad et al., 2012). Although FGFR3 mutations were first identified and studied in the context of germinal diseases, FGFR3 was the first receptor in the FGFR family to be reported as somatically mutated in cancer. Detected in around 40% of bladder cancers in all grades and stages, FGFR3 mutations are particularly frequent in non-muscle-invasive bladder cancer where they account for approximately 60 % to 70 % of the cases (Cappellen et al., 1999; Haugsten et al., 2010; Pandith et al., 2010). In addition, FGFR3 mutations are also found in 16 % to 20 % of the more aggressive muscle-invasive bladder cancers (Haugsten et al., 2010). Several missense mutations have been found in bladder cancers, including R248C, S249C, G372C and K652E, and are the same germinal activating mutations found in thanatophoric dysplasia, a lethal form of dwarfism (van Rhijn et al., 2002). Within the FGFR family, FGFR3 has one of the highest rates of point mutations found in cancer (Haugsten et al., 2010). The online database, cBioPortal, compiles sequencing data from just under 39,000 patients from 158 studies across all cancer types. Data indicates that FGFR3 is mutated in 261 unique different amino acid residues in 71 different cancer types and subtypes, with the most common mutation hotspot being S249C found primarily in urothelial carcinoma, the most common form of bladder cancer, with a smaller number of cases also found in lung, head and neck, cervical and oropharynx cancers.

The oncogenic potential of FGFR3 S249C mutation have been described in several studies. For example, in the MEF cell line NIH-3T3, the exogenous expression of FGFR3 S249C substitution has been shown to induce morphological transformation, cell proliferation, cell viability and anchorage-independent growth (Di Martino et al., 2009). Furthermore, FGFR3 S249C has

also been shown to enhance receptor phosphorylation and downstream signalling *in vitro,* through the activation of Erk and PLCγ1 in NIH-3T3 models and activation of Src, Akt and PLCγ1 in immortalized normal human urothelial cells TERT-NHUC (Bernard-Pierrot et al., 2006; Di Martino et al., 2009).

Table 1.4 – FGFR3 missense mutations associated with cancer. Amino acid numbers correspond to the FGFR3 isoform b. Compiled from (Cerami et al., 2012; Gallo et al., 2015; Gao et al., 2013; Haugsten et al., 2010; Tiong et al., 2013; Wesche et al., 2011)**.**

Disease	Mutation in FGFR3
Bladder cancer	E216K, D22N, G235D, R248C, S249C, P283S, V306I, G372C, S373C, Y375C, I378C, Y381C, G382R, F386L, A393E, N542S, K652E/M/N/Q/T, D648Y
Brain cancer	E468K
Cervical cancer	S249C
Colorectal cancer	C228R, R401C, V679I, E322K
Gallbladder cancer	R248C, S249C, G372C, Y375C, G382R, K652M, G699C
Head and neck cancer	Q209H, R248C, S249C, F388L, K415N, K652N, D619G, V632M, E688K, G699C
Lung cancer	T79S, R248C/H, S249C, S435C, K717M
Mesothelioma	D648Y
Multiple myeloma	G197S, Y241C, R248C, Y375C, G384D, S435C, K652E/M, L796R, P797A, F386L
Oral squamous cell carcinoma	G699C
Prostate cancer	S249C, F386L, A393E
Spermatocytic semioma	K652E/Q/M/N/T

Notably, cysteine mutations in the extracellular domain of FGFR3 are particularly prevalent in cancer (Visscher et al., 2017). Only in bladder cancer, S249C represent more than half of the mutations in FGFR3, comprising 61 % of all mutations, followed by Y375C, R248C and G372C accounting for 19, 8 and 6 % of all mutations, respectively (Di Martino et al., 2016). The introduction of a cysteine residue in the linker region between Ig-II and Ig-III of the extracellular domain (such as S249C and R248C) or in the JM region of the extracellular domain (such as G372C, S373C and Y375C) leads to ligand independent receptor dimerisation (Avis et al., 1998; Naski et al., 1996). The unpaired cysteine amino acid, in the reducing environment of the extracellular compartment, allows

the formation of a covalent intermolecular disulphide bond between parallel monomers, inducing receptor dimerisation, increased tyrosine phosphorylation and receptor activation (Gallo et al., 2015; Naski et al., 1996). However, receptor activation was found to be different between mutants, and despite R248C and S249C showing the highest dimerisation levels, G372C showed the highest kinase activity on *in vitro* assays, raising questions for a link between dimerisation and receptor activation (Avis et al., 1998).

Later studies for the analysis of R248C, S249C and Y375C extracellular mutations by Förster resonance energy transfer (FRET) indicate that these cysteine mutations only moderately stabilise FGFR3 dimerisation. Cysteine mutations are instead thought to structurally perturb FGFR3 dimers leading to the correct alignment of each monomer for full kinase activation (Del Piccolo et al., 2015). And although this effect occurs in the absence of ligand for R248C, S249C, G372C and S373C, ligand binding is required for correct juxtaposition and full activation of the extracellular JM mutant Y375C (Adar et al., 2002). The need for a correct dimer orientation was later confirmed with the non-cysteine mutation A391E in FGFR3 (Sarabipour and Hristova, 2016). In the absence of a disulphide bond, the glutamic acid (E) residue induces the receptor to be equally trapped in the active conformation in the absence of ligand, enforcing a tight closure of the TM domain of the dimer, inducing increased phosphorylation (Sarabipour and Hristova, 2016). In addition, mutations that affect the extracellular domain of FGFR3 such as R248C and Y375C, show reduced internalisation and degradation despite high ubiquitination levels leading to prolonged retention at the plasma membrane and sustained oncogenic signalling (Bonaventure et al., 2007).

Mutations in the TM domain of FGFR3 such as G382R/E found in bladder cancers result in the formation of hydrogen bonds between the two FGFR3 monomers, similarly leading to ligand-independent dimerisation and constitutive receptor activation (Bodoor et al., 2010; Webster et al., 1996).

Another class of mutations are found to occur in the intracellular domain of FGFR3. The most frequent KD hotspot mutation is located in the position K652 where variants such as K652E/Q/M/N/T have been identified in different cancers

including bladder cancer (Haugsten et al., 2010). K652 lies in the activation loop of the KD, which is essential for the kinase activity upon ligand binding. In contrast to mutations found in the ectodomain and TM of FGFR3 that induce ligand-independent receptor dimerisation, the K562 mutation induces a conformational change to the activation loop resulting in constitutive autophosphorylation of the receptor independent of its dimerisation status (Avis et al., 1998). Despite the absence of constitutive dimerisation, K652 mutations induce high levels of kinase activity, with K652E being reported as having 45-fold greater autophosphorylation than the WT FGFR3 (Patani, 2016). In fact, this effect is restricted to mutations in this particular residue, since a study where serial mutants were generated along the activation loop for positions Y649-L658 revealed that only mutations in K652 can activate the receptor (Webster et al., 1996). Moreover, it has been shown that K652E and K652M are more activating than the other variants (Bellus et al., 2000). Interestingly, despite the high kinase activity conferred by this mutation, expression of K652E in TERT-NHUC cells failed to activate PLCγ1 and led to a decrease in cell viability and proliferation rate when comparing to S249C and Y375C mutations (Di Martino et al., 2009). However, in the same study, the same effect was not seen in NIH-3T3 cell lines, where K652E shows the ability to transform cells in culture and activate Src, Akt and PLCγ1 pathways. The authors propose that in TERT-NHUC cells, receptor dimerisation is required for transphosphorylation of specific tyrosine residues on FGFR3 and consequent activation of some downstream signalling pathways (Di Martino et al., 2009). This observation indicates that the effects of mutant FGFR3, including K652E are likely to be cell line dependent, which might be due to tissue specificity and the expression of specific mediators for signalling (Sahni et al., 1999).

The crystallographic analysis of FGFR3-K652E clearly shows that the amino acid exchange from lysine to glutamic acid allows the KD to adopt a structure that mimics phosphorylation of the activation loop, by introducing a network of hydrogen bonds that stabilises the open conformation of the KD (Chen et al., 2013). This network is formed by the carboxylate group of the glutamic acid with R618 in the catalytic loop, plus the backbone amides of T653, T654 and R642 and with Y650 within the activation loop, which are reminiscent of the interactions on the active WT FGFR3. As with WT FGFR3, this conformational change is then

allosterically propagated to the kinase hinge region of the catalytic pocket (which has an autoinhibitory effect), causing a disengagement of the molecular brake resulting in kinase activation without dimerisation or ligand binding (Huang et al., 2013).

In addition, it has been shown in other RTK family members that distinct mutations result in alterations in the activation of downstream signalling pathways to the WT form of the receptor (Pines et al., 2010). Mutations in EGFR for example, can activate molecular pathways to different extents, showing differential MAPK and Akt activation levels for distinct mutants (Erdem-Eraslan et al., 2015). While this area of research is still in its infancy in the context of FGFR receptor signalling, the data presented above suggests that distinct FGFR3 mutations may affect the function and location of the receptor differently, leading to altered binding of signalling adaptors and activation of downstream signalling.

1.4 - Targeting FGFR3 in cancer

A subset of activating mutations in FGFR3 appear to be sensitive to targeted therapies. Studies have shown that the inhibition of FGFR3 is able to revert its oncogenic effects. For example, initial analysis of the 97.7 bladder cancer cell line bearing a FGFR3-S249C mutation, showed on knockdown with short-hairpin RNA (shRNA) a significant reduction in its ability to proliferate and survive in culture as well as to grow under anchorage-independent conditions, when compared to the WT control in telomerase immortalised normal human bladder cells (Tomlinson et al., 2007). This indicates that 97.7 tumour cells might be oncogene dependent on the mutation, and its inhibition is a useful therapeutic strategy.

There are several therapeutic approaches to target FGFR family members including FGFR3. Therapies include broad-spectrum multi-target tyrosine kinase inhibitors (TKIs), FGFR selective TKIs, monoclonal antibodies against FGFR and FGF traps (Touat et al., 2015). In general, TKIs are small molecule inhibitors that inhibit RTK activity by interfering with the binding pocket of ATP or substrates of the tyrosine KD, blocking their interaction and therefore inhibiting activation and

downstream signalling (Roskoski, 2015). Due to high homology between KDs of different RTKs, non-selective multi-target TKIs that inhibit FGFR often additionally exhibit inhibitory activity towards a varied range of other RTKs, including VEGFR, EGFR, PDGFR, Fms Related Tyrosine Kinase 3 (FLT3), KIT proto-oncogene (KIT) among others (Porta et al., 2017). As previously described, although this form of multi-target-based therapy has the potential to increase treatment efficacy by simultaneous blockade of redundant oncogenic pathways, it is associated with greater patient toxicity and lack of bioactivity against the main oncogenic target of interest, therefore limiting their efficacy in tumours driven by aberrant FGFR signalling (Giordano and Petrelli, 2008; Levitzki and Mishani, 2006). Moreover, as many of these multi-target RTKs also exert an inhibitory effect against angiogenic receptors such as VEGFR, it is difficult to associate the effect of these drugs to the inhibition of FGFR alone (Ferrara et al., 2003; Porta et al., 2017).

Selective FGFR inhibitors are a class of TKIs that have been specifically developed to exclusively target the FGFR family of receptors. Homology between the KDs of FGFR1/2/3 is higher compared to FGFR4 and, as a result, most of the TKIs in this class inhibit FGFR1-3 but not FGFR4 (Johnson and Williams, 1992). There are also some pan-FGFR inhibitors available that target all 4 isoforms of FGFR as well as some selective FGFR4 inhibitors (Katoh, 2016). On-target inhibitors are an attractive option in patients who harbour FGFR abnormalities.

PD173074 is an example of a small molecule selective FGFR1/3 inhibitor effective at suppressing cell proliferation in bladder cancer cell lines expressing mutant FGFR3 (S249C and Y375C) compared to cells expressing the WT receptor (Miyake et al., 2010). Further *in vitro* analysis linked this effect with a cell cycle arrest at G1-S transition, which was dose-dependent. The administration of PD173074 in mouse xenograft models of these mutant FGFR3 bladder cancer cell lines suppressed tumour growth and induced apoptosis in comparison to the untreated control (Miyake et al., 2010). Thus, this selective inhibitor shows a potential utility in tackling bladder cancers driven by FGFR3 mutations.

A similar effect is seen with the selective FGFR1-3 inhibitor BGJ398 (Infigratinib) in the treatment of cell line models harbouring extracellular mutations of FGFR3

including R248C and S249C. In cell line mouse models, this inhibitor was able to reduce the transformation effects of these cells in anchorage-independent conditions and reduce tumour volume in xenograft mouse models, proving once more that oncogenic effects driven by FGFR3 mutations can be reverted with the blockade of FGFR3 (Liao et al., 2013).

However, despite their success in preclinical *in vitro* and *in vivo* studies, selective inhibitors have faced many hurdles in clinical trials. Most have shown very poor efficacy in solid tumours, and there has been a substantial variation of clinical responses between different genetic aberrations and FGFR isoforms which will be discussed in greater detail in subsequent sections of this chapter (Babina and Turner, 2017).

Monoclonal antibodies (mAbs) are also being studied as an option to target FGFR or FGF ligands. Although more expensive than small-molecule inhibitors, these antibodies have a strong specificity for antigens of selected FGFR isoforms or FGF ligands, which is thought to limit the side effects and toxicities observed upon FGFR signalling blockade by TKIs (Tiseo et al., 2015; Touat et al., 2015). For example, antibody-based targeting of FGFR3 with R3Mab, an antagonistic anti-FGFR3 monoclonal antibody capable of blocking ligand binding and receptor dimerisation, was tested in mouse cells BaF3 transfected with the cancer-associated mutants S249C, Y375C, R248C, G372C, and K652E (Qing et al., 2009). R3Mab was able to inhibit the activation of FGFR3 and the immediate downstream signalling pathway MAPK. Constitutive proliferation was also suppressed on all cysteine mutants and ligand-induced proliferation was abolished for K652E (Qing et al., 2009).

Another alternative therapeutic approach is the use of FGF traps. An example is the compound FP-1039 (GSK3052230), which consists of the extracellular domain of FGFR1 fused to the fragment crystallizable (Fc) region of immunoglobulin G1 (IgG1) (Harding et al., 2013). FP-1039 selectively binds and neutralizes several FGFs that normally bind FGFR1, blocking the interaction between FGF-FGFR1 and therefore preventing receptor activation. But to date, this approach has not been applied to FGFR3 (Tolcher et al., 2016). A list of

FGFR agents both TKIs and mAbs that are currently undergoing clinical trials in solid tumours bearing FGFR3 alterations is summarised in Table 1.5.

Table 1.5 – Current ongoing clinical trials evaluating the effects of different FGFR targeted therapies in solid tumours bearing FGFR3 alterations. * *Docetaxel- microtubule associated inhibitor; Dexamethasone- corticosteroid that inhibits inflammation; JNJ-63723283- anti-PD-1 monoclonal antibody; AEs- adverse events; ORR- overall response rate.*

Inhibitor (manufacturer)	Target	Clinical trial identifier	Study purpose / Cancer type	Phase study	Remarks (reference)
Non-selective inhibitors					
Ponatinib (ARIAD Pharmaceuticals)	FGFR, PDGFR, VEGFR, EGFR, Abl, Src, RET, KIT, FLT1	NCT02272998	Advanced cancers with genomic alterations in FGFR1-4 and other genomic targets (KIT, PDGFRα, RET, FLT3, Abl1)	II	
Dovitinib (Novartis)	VEGFR1–3, PDGFRβ, FGFR1/3, FLT3, KIT, RET, TrkA, and CSF1	NCT01732107	BCG refractory urothelial carcinoma with FGFR3 mutations or over-expression	II	Discontinued due to high grade of AEs (Hahn et al., 2017)
Selective inhibitors					
AZD4547 (AstraZeneca)	FGFR1-3	NCT02965378	Second-line therapy for treating FGFR positive patients with recurrent stage IV squamous cell lung cancers	II/III	Phase II showed minimal activity on patients with FGFR1/3 amplification, FGFR3 (S249C) and FGFR3 fusion.
		NCT02824133	Recurrent malignant glioma expressing FGFR-TACC fusions	I/II	
NVP-BGJ398 (Novartis)	FGFR1-3	NCT01975701	Patients with recurrent glioblastoma with FGFR-TACC fusions and/or activating mutations in FGFR1, 2 or 3	II	
		NCT01004224	Advanced solid malignancies including bladder cancer with FGFR3 mutation or fusion	I	25.4% ORR in patients with metastatic bladder cancer (Pal et al., 2018)
		NCT02160041	Solid tumors and hematologic malignancies with FGFR genetic alterations	II	
		NCT01697605	Advanced solid tumor having alterations of the FGFR pathway in Asian patients	I	

Table 1.5 – Current ongoing clinical trials evaluating the effects of different FGFR targeted therapies in solid tumours bearing FGFR3 alterations. (Continuation)

Inhibitor (manufacturer)	Target	Clinical trial identifier	Study purpose / Cancer type	Phase study	Remarks (reference)
Selective inhibitors (Continuation)					
BAY1163877 (Bayer)	FGFR1-4	NCT01976741	Advanced solid tumours	I	
Erdafitinib (Astex Pharmaceuticals)	FGFR1-4	NCT01703481	Advanced or Refractory Solid Tumors or Lymphoma	I	Clinical activity and minimal toxicity in patients with advanced cholangiocarcinoma (CCA) and FGFR alterations
		NCT02699606	Advanced NSCLC, urothelial carcinoma, esophageal cancer or cholangiocarcinoma	II	
		NCT03210714	Pediatric advanced solid tumors, non-Hodgkin lymphoma, or histiocytic disorders with FGFR mutations	II	
		NCT02365597	Urothelial carcinoma with FGFR genomic alterations	II	
		NCT02952573	Relapsed MM in combination with dexamethasone* in patients with WT FGFR3 or mutated FGFR3	II	
		NCT03825484	Advanced cancers with FGFR genetic alterations		Approved for marketing
		NCT03390504	Urothelial carcinoma and selected FGFR gene aberrations in patients that exhausted all treatment options, including chemotherapy and immunotherapy	III	
		NCT03473743	Combination with JNJ-63723283* in patients with metastatic urothelial carcinoma with FGFR alterations	I	

Table 1.5 ─ Current ongoing clinical trials evaluating the effects of different FGFR targeted therapies in solid tumours bearing FGFR3 alterations. (Continuation)

Inhibitor (manufacturer)	Target	Clinical trial identifier	Study purpose / Cancer type	Phase study	Remarks (reference)
Selective inhibitors (Continuation)					
TAS-120 (Taiho Oncology)	FGFR1-4	NCT02052778	Advanced solid tumors with FGF or FGFR aberrations including urothelial carcinoma	I/II	
Debio-1347 (Debiopharm)	FGFR1-3	NCT03834220	Solid tumors harboring a fusion of FGFR1, FGFR2 or FGFR3	II	
		NCT01948297	Advanced solid tumours with FGFR alterations	I	
E7090 (Eisai)	FGFR1-3	NCT02275910	Solid tumours	I	
PRN1371 (Principia Biopharma)	FGFR1-4	NCT02608125	Solid tumors with metastatic urothelial carcinoma	I	
Monoclonal antibodies					
MFGR1877S (Genentech)	FGFR3	NCT02401542	Advanced or metastatic urothelial carcinoma with FGFR3 mutant/fusion. Dose escalation and efficacy alone or combination with Docetaxel*.	I	

1.5.1 - FGFR3 pre-clinical results and clinical trials

1.5.1.1 - Non-selective FGFR TKIs

Non-selective FGFR inhibitors have shown activity in the context of FGFR-dependent tumours. Several TKIs have been evaluated in clinical trials, or are still under investigation, and include ponatinib, dovitinib, lucitanib, cediranib, nintedanib and pazopanib (Liao et al., 2013; Wu et al., 2013). These are all multi-target TKIs that target several RTKs simultaneously including FGFR, PDGFR and VEGFR. Ponatinib and dovitinib are currently the only TKIs of this class that have been evaluated preclinically for treatment of cancers with FGFR3 genomic alterations including amplification and mutations. Ponatinib is an inhibitor of FGFR, PDGFR, VEGFR, EGFR, ABL proto-oncogene, non-RTK (Abl), Src, RET, KIT and FLT1. It is currently approved for the treatment of CML and acute lymphoblastic leukaemia (ALL) (Tan et al., 2019). In preclinical studies, it shows

growth inhibition and suppression of FGFR activation in cell line models harbouring FGFR2 or FGFR3 aberrations and is able to reduce tumour growth *in vivo* in xenograft mouse models (Gozgit et al., 2012). Dovitinib inhibits VEGFR1–3, PDGFRβ, FGFR1/3, FLT3, KIT, RET, TrkA, and colony stimulating factor 1 (CSF1) (Mazzola et al., 2014). In bladder cancer cell lines harbouring either the FGFR3-TACC3 fusion or FGFR3 point mutations, dovitinib was shown to reduce FGFR3 activation levels as well as phosphorylation of Erk, one of the downstream effectors of FGFR, which was correlated with increased levels of cellular apoptosis (Lamont et al., 2011). In the same study, the authors also established a relationship between high FGFR3 expression levels and higher drug sensitivity, suggesting that FGFR levels may act as a biomarker for therapeutic response. Interestingly, the sensitivity to dovitinib is also dependent on the inherent molecular characteristics of bladder cancer cells lines. In an *in vitro* study, dovitinib was tested in 10 different bladder cancer lines known to bear FGFR3 abnormalities such as mutations and fusions (Hänze et al., 2013). The study revealed that epithelial-like cells are more sensitive to dovitinib than mesenchymal-like cells, and that the measurement of epithelial and mesenchymal markers is a good indicative of anti-cancer response towards this inhibitor.

While both ponatinib and dovitinib show promising pre-clinical results supporting the rationale to investigate its potential as therapies for FGFR3-driven solid tumours such as bladder cancer, toxicities are a major concern for this class of non-selective FGFR inhibitors. Clinical trials are often withdrawn due to severe adverse events, which provides a strong argument towards the need for more selective and effective first-line therapies for cancers with FGFR3 aberrations.

1.5.1.2 - Selective FGFR TKIs

There is an array of different selective FGFR inhibitors that are currently being evaluated in the clinic (Table 1.5). This includes the FGFR1-3 inhibitors AZD4547, BGJ398, debio-1347, ARQ-087, E7090 and pan-FGFR inhibitors erdafitinib, TAS-120, PRN1371, BAY1163877. These are being tested in different

solid tumours harbouring FGFR alterations including FGFR3 mutations and/or fusions.

AZD4547 is a potent FGFR1-3 inhibitor that can block FGFR signalling and reduce cellular growth in cancer cells bearing FGFR alterations. In a preclinical study to test its efficacy, treatment with AZD4547 of KMS-11, a MM cell line that have a t(4;14) translocation and expresses a mutated form of FGFR3 (Y375C), led to the downregulation of the phosphorylation levels of FGFR, MAPK and FRS2 (Gavine et al., 2012). In addition, xenograft models of KMS-11 showed a 99% tumour growth inhibition upon treatment with this inhibitor, which is accompanied by a significant reduction in the proliferation marker Ki-67. These results support the use of AZD4547 as a treatment for cancers with FGFR3 alterations (Gavine et al., 2012). In a phase I clinical study (NCT00979134) for solid tumours, within a cohort of 21 patients with FGFR amplified tumours from different cancer types, AZD4547 showed a partial response for 1 patient with FGFR1-amplified NSCLC lasting for more than 12 weeks (Saka et al., 2017), and from the same cohort of patients, 2 of 3 bladder cancer patients showed disease stabilisation, with 1 of these patients also showing increased FGFR3 expression (Di Martino et al., 2016). However, there are no clinical trials assessing the response of this drug in bladder cancer patients with FGFR3 mutations. Current clinical trials for AZD4547 are being conducted for recurrent gliomas with FGFR1-TACC1 and FGFR3-TACC3 fusions (phase I/II) (NCT02824133), and for advanced recurrent squamous NSCLC (SqNSCLC) expressing FGFR gene mutations or amplifications that do not respond to first line therapies (phase II/III) (NCT02965378). Although the latter is still ongoing, early data has been published for the phase II study with a cohort of 27 patients with SqNSCLC (Aggarwal et al., 2019). Data showed minimal activity, where only 1 out of 23 patients with FGFR1 amplification achieved a partial response of less than 3 months, and where 1 out of 2 patients with FGFR3 mutation S249C had an unconfirmed partial response with a duration of response of 1.5 months (Aggarwal et al., 2019). However, the study has progressed into the phase III stage where additional FGFR alterations are being investigated in recurrent or advanced SqNSCLC.

BGJ398 (Infigratinib) is a selective ATP-competitive FGFR1-3 inhibitor discovered and optimised less than a decade ago. The first results with this compound in RT112 human bladder cancer rat xenograft model which harbours a FGFR3-TACC3 fusion, showed a significant tumour regression at low doses with minimal toxicity (Guagnano et al., 2011). Other studies describe its potential as a selective FGFR inhibitor in the context of FGFR2 and FGFR3 point mutations found in SqNSCLC. When treated with BGJ398, NIH-3T3 and Ba/F3 mouse model cell lines expressing FGFR2 W290C and S320C mutants or FGFR3 R248C and S249C mutants showed a significant reduction in cell survival, a reduction in cell transformation in anchorage-independent conditions and a reduction in tumour volume in xenograft mouse models (Liao et al., 2013). In a phase I clinical study (NCT01004224) for patients with solid tumours harbouring FGFR alterations, BGJ398 was well tolerated and there was a positive anti-tumour activity in 49 of 132 patients. Partial response was achieved in 4 out of 36 patients (11 %) with FGFR1-amplified sqNSCLC and in 3 out of 8 patients (38 %) with FGFR3-mutant bladder cancer. However, durable responses were limited and eventually most patients that initially displayed a partial response ended up with progressive disease and treatment failure (Nogova et al., 2017). In a recently completed phase I study for advanced or metastatic bladder cancer with FGFR3 alterations that do not respond to other therapies, there was a disease control rate (DCR) of 64.2 % from a cohort of 67 patients (expanded cohort from the initial open-label trial NCT01004224) (Pal et al., 2018). A reduction in tumour volume was observed in 25.4 % of patients and 38.8 % achieved disease stabilisation, however complete response was only observed in 1 patient out of the 67. The majority of responding patients harboured FGFR3 extracellular mutations (example: R248C, S249C, Y375C) and the FGFR3-TACC3 fusion. Patients with the intracellular FGFR3 mutation K652E showed a lower response towards BGJ398, which is thought to be caused by the destabilisation of the KD to which BGJ398 binds, reducing its activity by 5- to 10-fold when compared to the WT FGFR3 (Pal et al., 2018). Current studies are investigating the effect of BGJ398 in patients with solid tumours such as glioblastoma, haematologic malignancies and bladder cancer bearing FGFR alterations (Table 1.5).

Erdafitinib (JNJ-42756493), is an ATP-competitive pan-FGFR inhibitor and is a breakthrough in FGFR selective inhibitors, as it is the first and only pan-FGFR inhibitor approved earlier this year by the FDA, for the treatment of advanced or metastatic urothelial carcinomas with FGFR3 and FGFR2 alterations (Markham, 2019). Pre-clinical data showed that Erdafitinib has the potential to induce a prolonged inhibition of FGFR signalling which is accompanied by an antiproliferative effect in a range of human cancer cell lines with FGFR1-4 amplifications, FGFR3 translocations and FGFR4 mutations (Perera et al., 2017). Perera et al. also show that Erdafitinib administration results in a potent and dose-dependent antitumour activity in xenograft models of the same cell lines. A more recent phase II study (BLC2001) that led to the approval of Erdafitinib (NCT02365597) evaluated the drug in 99 patients with advanced and unresectable or metastatic urothelial carcinoma with FGFR3 mutations or FGFR2/3 fusions (Loriot et al., 2019). Data showed a response rate of 49 % among the 74 patients with FGFR3 mutations and an additional stable disease in 35 % of the patients with FGFR3 mutations. Moreover, responses were found across a range of FGFR3 mutations suggesting that the drug did not selectively inhibit some FGFR3 mutations over others. The response data with FGFR2/3 fusions were less promising. In the 25 patients with FGFR2/3 fusions, 11 had a FGFR3-TACC3 fusion, and of these patients a total of 4 (36 %) achieved a response to the treatment (Loriot et al., 2019). This trial is still active for metastatic or surgically unresectable urothelial carcinomas with FGFR genomic alterations. Erdafitinib is also currently being assessed for treatment of several other cancer types including cholangiocarcinoma, NSCLC, FGFR mutant or advanced urothelial carcinoma, lymphoma and oesophageal cancer (Table 1.5). For example, a phase I clinical study (NCT01703481) tested erdafitinib in 187 patients with various solid tumours with activating FGFR genomic alterations (Bahleda et al., 2019). Results identified that patients with urothelial carcinoma and cholangiocarcinoma were the most responsive across a range of cancer types, with an overall response rate (ORR) of 46.2 % and 27.3 %, respectively. Interestingly all of these patients carried FGFR mutations or fusions but not amplifications.

Although preclinical sensitivity to FGFR inhibitors is not readily translated into clinic, erdafitinib is an example where selective inhibitors have been shown to be efficacious in patients with bladder cancer. The collective experience gained from the development of FGFR inhibitors has shown that drug sensitivity varies according to the specific inhibitor under study and varies from one tumour type to another (Touat et al., 2015). Furthermore, there appears to be a selective response in patients bearing different FGFR alterations (Pal et al., 2018). In fact, previous preclinical studies show that distinct FGFR3 mutants present differential sensitivities to FGFR inhibitors *in vitro*. For instance, the FGFR3 N542K activating mutation is less sensitive to AZD4547 than K652E, whereas the TACC3-FGFR3 fusion displays the best response (Patani, 2016). The lack of response in some patients and the observation of disease progression on treatment, are indicators of intrinsic or acquired resistance respectively. Understanding FGFR inhibitor resistance is an area of active research and some of the mechanisms identified thus far will be discussed in the following section.

Several challenges remain which hinder the effective use of selective FGFR kinase inhibitors in the clinic. We do not fully understand why some mutations fare better than others when treated with these drugs which requires a deeper analysis of the biochemical and oncogenic properties of different FGFR3 mutations. There is also a need for the development of robust biomarkers for patient stratification to FGFR inhibitor therapy to enable better patient selection in order to improve the clinical effectiveness of these targeted therapies.

1.5.2 – Mechanisms of resistance to FGFR3 selective inhibitors

The two main types of resistance to FGFR kinase inhibitors such as AZD4547, BGJ398 and erdafitinib are intrinsic or primary resistance and acquired or secondary resistance. Intrinsic resistance is associated with the pre-existence of mutations or bypass mechanisms that allow cells to be unresponsive towards a selective inhibitor, whereas acquired resistance involves the assimilation of *de novo* mutations or mechanisms that evade the initial cell sensitivity to a selective inhibitor (Byron et al., 2013).

One of the common resistance mechanisms observed in clinic for other RTKs such as EGFR or ALK is mutations in the gatekeeper residue of the KD of the receptor (Chell et al., 2013). Gatekeeper mutations are usually amino acid substitutions involving larger hydrophobic residues in the ATP-binding pocket site, which sterically obstructs drug access to the ATP binding site or, stabilise the active conformation of the kinase (Byron et al., 2013). Although gatekeeper mutations in FGFR3 have not been identified in patients, *in vitro* assays have shown that the acquisition of a FGFR3 gatekeeper mutant V557M in the KMS-11 myeloma cell line (FGFR3-Y373C) is a mechanism of acquired resistance emerging from long-term exposure to the selective FGFR1-3 inhibitor AZ12908010, a closely related molecule to AZD4547, discovered during the development of AZD4547 that displays higher potency against FGFR1-3 and a more favourable selectivity profile (Chell et al., 2013). In this study, these resistant cells were also found to be cross-resistant to other FGFR inhibitors such as AZD4547 and PD173074, a FGFR1/3 and VEGFR2 kinase inhibitor.

Anticipating such resistant mechanisms to first generation FGFR inhibitors has led to the development of second generation covalent FGFR inhibitors. Covalent inhibitors such as the FGFR irreversible inhibitors 2 (FIIN-2) and 3 (FIIN-3) were designed to overcome clinical resistance by covalently binding to the ATP-binding pocket, potently inhibiting the proliferation of cells harbouring FGFR alterations including gatekeeper mutations (Tan et al., 2014). However, both of these covalent inhibitors proved to be unsuitable for *in vivo* treatment as they showed only moderate mouse liver microsomal stability, which is used as a readout for the metabolic stability of the compound *in vivo* (Brown et al., 2016). This issue required the development of an improved version FIIN-4 which showed improved mouse liver microsomal stability (Brown et al., 2016). FIIN-4 was shown to inhibit growth of metastatic breast cancer patient-derived xenografts models with FGFR1 amplification. Although there are no active clinical trials evaluating these covalent inhibitors at the moment, they are of great interest for future therapies, including their use in the context of resistance to first generation FGFR inhibitors.

Another known mechanism of resistance to selective kinase inhibitors is the activation of compensatory or bypass signalling pathways which compensate for the blockade of FGFR mediated survival signalling by activating similar or

alternative downstream effectors (Harbinski et al., 2012; Jänne et al., 2009). Due to the redundancy of intracellular signalling and the cross-talk that exists between different pathways, cells can trigger adaptive responses to counteract their dependency on a particular signalling pathway (in this case FGFR signalling) to enable cell survival and tumour growth in the presence of kinase inhibitors (Chandarlapaty, 2012). The acquisition of resistance by this mechanism has been reported in different cancer types driven by different oncogenes, including FGFR3 mutations in bladder cancer (Manstein et al., 2014). A number of different compensatory mechanisms to selective FGFR inhibitors in the preclinical setting have been described in the literature, such as the activation of the PI3K/Akt pathway upon FGFR inhibition with AZD4547 and BGJ398 and the activation of the RTKs ErbB2/3 and EGFR upon treatment with BGJ398 and PD173074 respectively.

The PI3K pathway has been shown in two studies to confer resistance to FGFR inhibitor treatment. In the first study aimed at identifying determinants of cell survival in the RT112 bladder cancer cell line (which harbours a FGFR3-TACC3 fusion) in the presence of the FGFR inhibitor AZD4547, a synthetic lethality screen was employed using a kinome-wide shRNA library, targeting all 518 human kinases (Wang et al., 2017). Multiple effectors in the PI3K pathway were identified as synergistically interacting with FGFR inhibitor treatment, suggesting that PI3K signalling is a compensatory mechanism that mediates FGFR inhibitor resistance. Consistent with this hypothesis, treatment with the PI3K inhibitor BKM12 in combination with AZD4547 resulted in a significant increase in RT112 apoptosis and a reduction in tumour size *in vitro* and *in vivo* compared to either drug as a single agent (Wang et al., 2017). A similar effect was observed in a different study for the same cell line RT112 but this time with the FGFR inhibitor BGJ398 (Datta et al., 2017). The authors generated an acquired resistant variant of this cell line by long-term exposure to the inhibitor. Analysis of this drug resistant cell line by a reverse-phase protein array (RPPA) led to the identification of upregulated phosphoproteins in the resistant cell line when compared to the parental cell line. The study showed that components of the PI3K pathway displayed increased phosphorylation, including Akt and its downstream target GSK3. Consistent with this observation, pharmacological inhibition of Akt activity

was able to restore sensitivity of the resistant cells to BGJ398, indicating the potential for combination therapy of FGFR and Akt inhibitors in bladder cancer with FGFR3 fusions (Datta et al., 2017).

Another mechanism of compensatory signalling in response to kinase inhibitor therapy is the activation of alternative RTKs. Pertinent to FGFR inhibitors, upregulation of components of the ErbB family of RTKs have been shown to confer resistance to this class of drugs. One study has shown that ErbB2 and ErbB3 can be activated as a compensatory mechanism upon FGFR inhibition with BGJ398 in multiple FGFR dependent cell lines, including NCI-H1581 and Kato-II which harbour amplified FGFR1 and FGFR2 respectively and the FGFR3-TACC3 fusion cell lines RT112 and RT4 (Wang et al., 2014). Additionally, an increased production of ErbB2/3 ligands was observed and this increase was found to be sufficient to drive BGJ398 resistance. Taken together, this data suggests that in a panel of cell lines, there is a switch in the dependency from FGFR to ErbB family members upon treatment with FGFR inhibitors suggesting a benefit in utilising ErbB inhibitors as a means to overcome resistance to FGFR inhibitor treatment (Wang et al., 2014).

The activation of ErbB1 or EGFR signalling pathway has also shown to influence resistance to FGFR inhibitors in cell lines expressing mutant and fusion forms of FGFR3 (Herrera-Abreu et al., 2013). An RNA interference (RNAi) genetic screen in cell lines harbouring FGFR1-4 aberrations in the presence of PD173074, showed that knockdown of EGFR sensitises cells to FGFR inhibitor treatment. The authors also showed that while MAPK signalling is downregulated by PD173074 treatment in mutant FGFR3 cell lines, this was rapidly rescued by EGFR activation, suggesting a role for EGFR as a compensatory RTK to overcome the loss of FGFR3 signalling. Consequently, the combination of FGFR and EGFR inhibition was effective in reducing cell viability in mutant FGFR3 expressing cells (Herrera-Abreu et al., 2013). Interestingly, it has been shown that the FGFR3-TACC3 fusion protein is similarly able to confer resistance to EGFR inhibition in cancers such as head and neck squamous cell carcinoma (HNSCC) (Daly et al., 2016), suggesting that there is a close interaction between the two RTK where either is able to compensate for the other when inhibited.

Despite some successes with FGFR inhibitors in the clinic, these therapies are not curative and do not achieve durable responses. Preclinical studies have shed light on some of the mechanisms of resistance to selective FGFR inhibitors (Guagnano et al., 2012). However, a better understanding of some of the signalling mechanisms that play a role in conferring resistance to this class of drugs is therefore important to unveil new ways of effectively targeting compensatory survival pathways to attain long-term responses in patients that harbour FGFR3 mutations.

1.6 - Conclusions and aims of the project

FGFR3 is one of the most commonly mutated isoforms of FGFR in cancer. With mutations being present in 40 % of bladder cancer cases, FGFR3 is a target of interest for therapy. Despite the promising results in a range of studies, the clinical data shows that there is a diverse range of responses to FGFR inhibitor therapy across patients harbouring mutant FGFR3. Resistance mechanisms to FGFR inhibition include gatekeeper mutations or the activation of compensatory mechanisms that evade oncogene dependency. Moreover, given the observation that response rates are variable between individual FGFR3 mutations, it is important to investigate the underlying biology of distinct FGFR3 mutants in order to discover new signalling dependencies that could be exploited for maximising the utility of selective FGFR inhibitors in the clinic.

While cancer genome sequencing data have provided detailed information about the distribution and frequencies of FGFR3 mutations in different cancer types and structural studies have elucidated the consequences of these mutations at the molecular level, the functional mechanisms by which these mutations promote cell survival has yet to be fully described. Similar to other RTKs like EGFR and ALK, distinct FGFR mutants might harbour different signalling dependencies, driving cancer progression by the activation of altered downstream pathways. These alterations are currently unknown and could be qualitative in nature, in that new signalling effectors are activated compared to WT FGFR3 or quantitative in

nature, wherein the same well-characterised FGFR3 signalling pathways are utilised but activated at different levels or in a distinct spatiotemporal fashion.

There is a gap in our knowledge of how FGFR3 mutations act on downstream oncogenic signalling pathways. Understanding the signalling alterations and transforming properties that accompany specific FGFR mutations will be key in establishing their mechanisms of action in driving oncogenesis. Furthermore, identifying these oncogenic properties of FGFR3 mutations will be necessary to anticipate resistance mechanisms to FGFR inhibitor therapy and identify new therapeutic strategies for drug discovery and repurposing to improve patient outcomes.

To achieve this objective, this thesis undertakes a systematic analysis of the functional effects in a panel of common and rare FGFR3 mutations across a range of cancer types, investigates the key signalling pathways activated by these mutants and characterises the role of FGFR inhibitor therapy in the treatment of cancers harbouring FGFR3 mutations.

Project aims:

1. Determine the oncogenic properties of common and rare FGFR3 mutants found in cancer;

2. Characterise mutant FGFR3 signalling dependencies in the presence and absence of selective FGFR inhibitors;

3. Assess the effects of identified targeted therapies in human cancer cell line models harbouring FGFR3 mutations.

Chapter 2

Materials and methods

2.1 - Molecular Biology

2.1.1 - Plasmids

The DNA constructs used on this project are listed in Table 2.1. pUMVC and pCMV-VSV-G, packaging and envelope plasmids, respectively, were used together to produce retroviral particles in most of the transductions generated for this project. pFB-Hyg-FGFR3b plasmid was used to build a library of FGFR3 mutants to be studied during this project. Src-Rescue has a wild-type (WT) c-Src insert and Src-Dasatinib-resistant (Src-T338I) has a dasatinib resistant gatekeeper mutation T338I insert.

Table 2.1 – List of plasmids and selectable markers

Plasmid	Bacterial Resistance	Selectable marker	Source	Reference
pFB-Hyg-FGFR3	Ampicillin	Hygromycin	Gift (M. Katan)	(Tomlinson et al., 2005)
pUMVC	Kanamycin	-	Addgene (8449)	(Stewart et al., 2003)
pCMV-VSV-G	Ampicillin	-	Addgene (8454)	(Stewart et al., 2003)
pBABE-Hygro	Ampicillin	Hygromycin	Addgene (1765)	(Morgenstern and Land, 1990)
pBABE-Src-Rescue	Ampicillin	Hygromycin	Addgene (26983)	(X. Zhang et al., 2009)
pBABE-Src-Dasatinib-resistant	Ampicillin	Hygromycin	Addgene (26980)	(X. Zhang et al., 2009)

2.1.2 - Bacterial transformation

XL10-Gold ultracompetent cells (Agilent Technologies) were thawed on ice and an aliquot of 45 µL was mixed with 2 µL of β-Mercaptoethanol for 2 minutes. 2 µL of DNA (1-10 ng) was then added and incubated a further 10 minutes on ice before heat shock in a water bath at 42 °C for 30 seconds, followed by 2 more minutes of incubation on ice. 500 µL of L-Broth medium at room temperature (RT) was then added to the mix and transformed cells were shaken at 220 rpm for 1 hour at 37 °C. Different volumes of the same cell suspensions (100 µL and 300 µL) were then spread on agar plates with selection antibiotic and incubated overnight at 37 °C (a maximum of 16 hours to avoid unspecific growth) until growth of individual colonies.

2.1.3 - Small- and large-scale plasmid preparation

Falcon tubes containing 6 mL of L-Broth medium and comprising selection antibiotic were inoculated with single bacterial colonies and incubated at 37 °C with shaking at 220 rpm for 8 hours. For small scale plasmid preparation, the 6 mL of bacterial suspensions were pelleted at 6,000 x g for 10 minutes followed by plasmid isolation with QIAprep Spin Miniprep Kit (Qiagen) using manufacturer's instructions. For larger amounts of plasmid preparation, 6 mL of the bacterial suspension was scaled up to 200 mL in L-Broth in an Erlenmeyer flask at 37 °C overnight, after which cells were pelleted at 6,000 x g for 10 minutes and plasmids isolated with the Hispeed Maxi kit (Qiagen) following manufacturer's protocol.

2.1.4 - Glycerol bacterial stocks preparation

Upon inoculation and growth of single bacterial colonies in L-Broth with selection antibiotic, cell suspensions were mixed with Glycerol 50 % in a 1:1 proportion, and frozen at -80 °C for long-term storage.

2.1.5 - Bacterial recovery from glycerol stocks

Bacterial stocks were retrieved from -80 °C and kept on dry-ice to prevent thawing. A small amount from the stock aliquot was scrapped frozen and plated in the appropriate agar plates with selection antibiotic following overnight incubation at 37 °C (up to a maximum of 16 hours). Single colonies were then inoculated on 6 mL of RT L-Broth with selection antibiotic and incubated for 8 hours at 37 °C, following small- or large-scale DNA plasmid preparation.

2.2 - Generation of FGFR3 variants

2.2.1 - FGFR3 construct

The human FGFR3-IIIb WT gene was expressed in the retroviral vector pFB (Stratagene) and modified by Prof. Matilda Katan laboratory (University College

of London (UCL)) from the original neomycin-resistant to contain a hygromycin resistance cassette (Tomlinson et al., 2005). The construct pFB-Hyg-FGFR3-IIIb was a gift from Prof. Matilda Katan laboratory. The different FGFR3 variants were generated in-house by site-directed mutagenesis.

2.2.2 - Site-directed mutagenesis (SDM)

Site-directed mutagenesis (SDM) was performed using two different commercialised kits as per the manufacturer's instructions: the QuikChange Lightning SDM Kit (Agilent) and the Q5® SDM kit (New England Biolabs).

For the first one, primers were designed using the QuikChange Primer Design online tool from Agilent [https://agilent.com/store/primerDesignProgram.jsp]. A list of primer sequences is shown in Table 2.2. Reactions were performed with 100 ng of template DNA on a thermocycler and when required, a gradient of annealing temperatures (Ta) 72-58 °C was applied to improve reaction efficiency. With the Q5® SDM kit (New England Biolabs), primers were designed with the online NEBaseChanger tool from New England Biolabs [https://nebasechanger.neb.com/]. Primer sequences are shown in Table 2.3. Reactions were carried out with 10 ng of template DNA on a thermocycler using the optimum Ta for each primer pair as per the manufacturer's instructions. Polymerase chain reactions (PCR) products were then digested for the parental DNA template with the enzyme DnpI (provided with each kit), followed by transformation in competent bacterial cells with 1-2 µL and 5 µL of the digested PCR product for QuikChange and Q5 reactions, respectively. After transformation and inoculation with overnight growth, up to 10 colonies were picked for scaling-up, followed by plasmid DNA isolation. DNA concentration was measured using a NanoDrop 2000 spectrophotometer (Thermo Fisher Scientific) to assess the quality of the samples. Samples were then screened by Sanger sequencing to select for clones with positive incorporation of the desired mutation. Positive plasmids were subsequently sequenced to discard false positives with potential extra mutations within the FGFR3 gene.

Table 2.2 – Primer sequences - QuikChange Lightning SDM Kit

FGFR3 mutation		Primers (5' → 3')		Template (pFB-Hyg-FGFR3)
S131L	TCG → TTG	Forward	GACAGACGCTCCATCCT**T**GGGAGATGACG	WT
		Reverse	CGTCATCTCCC**A**AGGATGGAGCGTCTGTC	
R248C	CGC → TGC	Forward	GACGTGCTGGAG**T**GCTCCCCGCACC	WT
		Reverse	GGTGCGGGGAGC**A**CTCCAGCACGTC	
S249C	TCC → TGC	Forward	ACGTGCTGGAGCGCT**G**CCCGCACC	WT
		Reverse	GGTGCGGG**C**AGCGCTCCAGCACGT	
S249T	TCC → ACC	Forward	TGCTGGAGCGC**A**CCCCGCACCGG	WT
		Reverse	CCGGTGCGGGG**T**GCGCTCCAGCA	
S373C	AGT → TGT	Forward	GACGAGGCGGGC**T**GTGTGTATGCAGG	WT
		Reverse	CCTGCATACACAC**A**GCCCGCCTCGTC	
Y375C	TAT → TGT	Forward	CGAGGCGGGCAGTGTGT**G**TGCAGGCAT	WT
		Reverse	ATGCCTGCA**C**ACACACTGCCCGCCTCG	
G382E	GGG → GAG	Forward	CATCCTCAGCTACG**A**GGTGGGCTTCTTCC	WT
		Reverse	GGAAGAAGCCCACC**T**CGTAGCTGAGGATG	
G382R	GGG → AGG	Forward	GCATCCTCAGCTAC**A**GGGTGGGCTTCTTC	WT
		Reverse	GAAGAAGCCCACCC**T**GTAGCTGAGGATGC	
R401C	CGC → TGC	Forward	TCTGCCGCCTG**T**GCAGCCCCCCC	WT
		Reverse	GGGGGGGCTGC**A**CAGGCGGCAGA	
N542K	AAC → AAG	Forward	GGAAACACAAAAACATCATCAA**G**CTGCTGGGCGCC	WT
		Reverse	GGCGCCCAGCAG**C**TTGATGATGTTTTTGTGTTTCC	
K652M	AAG → ATG	Forward	CTCGACTACTACAAGA**T**GACAACCAACGGCCGG	WT
		Reverse	CCGGCCGTTGGTTGTC**A**TCTTGTAGTAGTCGAG	
K652N	AAG → AAT	Forward	CAACCTCGACTACTACAAGAA**T**ACAACCAACGGC	WT
		Reverse	GCCGTTGGTTGT**A**TTCTTGTAGTAGTCGAGGTTG	
K652T	AAG → ACG	Forward	CTCGACTACTACAAGA**C**GACAACCAACGGCCGG	WT
		Reverse	CCGGCCGTTGGTTGTC**G**TCTTGTAGTAGTCGAG	
E629K	GAG → AAG	Forward	GCAATGTGCTGGTGACC**A**AGGACAACGTGATGAAG	WT
		Reverse	CTTCATCACGTTGTCCT**T**GGTCACCAGCACATTGC	
V679I	GTC → ATC	Forward	ACTCACCAGAGTGAC**A**TCTGGTCCTTTGGGG	WT
		Reverse	CCCCAAAGGACCAGA**T**GTCACTCTGGTGAGT	

Table 2.3 – Primer sequences – Q5 SDM kit

FGFR3 mutation		Primers (5' → 3')		Template (pFB-Hyg-FGFR3)
G372C	GGC → TGC	Forward	TGACGAGGCG**T**GCAGTGTGTATG	WT
		Reverse	GCCTCCACCAGCTCCTCC	
K652E	AAG → GAG	Forward	CTACTACAAG**G**AGACAACCAACGG	WT
		Reverse	TCGAGGTTGTGCACGTCC	
R248A*	CGC → GCC	Forward	CGTGCTGGAG**GC**CTCCCCGCAC	WT
		Reverse	TCCAGCGTGTACGTCTGC	
S249A	TCC → GCC	Forward	GCTGGAGCGC**G**CCCCGCACCGGC	WT
		Reverse	ACGTCCAGCGTGTACGTCTGCCGGATG	
G372A	GGC → GCC	Forward	GACGAGGCGG**C**CAGTGTGTATG	WT
		Reverse	AGCCTCCACCAGCTCCTC	
S373A	AGT → GCT	Forward	CGAGGCGGGCG**C**TGTGTATGCAGGC	WT
		Reverse	TCAGCCTCCACCAGCTCC	
Y375A	TAT → GCG	Forward	GGGCAGTGTG**GCG**GCAGGCATCCTCAG	WT
		Reverse	GCCTCGTCAGCCTCCACC	
R248C + S249C	CGC → TGC	Forward	CGTGCTGGAG**T**GCTGCCCGCA	S249C
		Reverse	TCCAGCGTGTACGTCTGCCG	
S373C + Y375C	TAT → TGT	Forward	GGCTGTGTGT**G**TGCAGGCATC	S373C
		Reverse	CGCCTCGTCAGCCTCCAC	
G372C + Y375C	TAT → TGT	Forward	GTGCAGTGTGT**G**TGCAGGCATCC	G372C
		Reverse	GCCTCGTCAGCCTCCACC	
G372C + S373C	AGT → TGT	Forward	CGAGGCGTGC**T**GTGTGTATGC	G372C
		Reverse	TCAGCCTCCACCAGCTCC	
G372C + S373C + Y375C	TAT → TGT	Forward	TGCTGTGTGT**G**TGCAGGCATC	G372C+ S373C
		Reverse	CGCCTCGTCAGCCTCCAC	

2.2.3 - Genomic DNA extraction

To extract genomic DNA from cell lines, cells were washed with phosphate buffered saline (PBS) and trypsinised for harvesting with growth medium. Cells were pelleted at 300 x g for 5 minutes and processed using a DNeasy Blood and Tissue Kit (QIAgen) following manufacturer's instructions.

2.2.4 - Polymerase chain reaction (PCR)

PCR were performed in a total volume of 50 µL, using the HotStarTaq DNA polymerase (QIAgen). Reaction mixtures contained 10 µL of extracted DNA, 20

pM – 200 nM of each forward and reverse primer, 2.5 U of HotStarTaq DNA polymerase, 1x reaction buffer, 200 µM of each dNTP, 1.5 mM of $MgCl_2$ and 0-3 % (v/v) of dimethyl sulphoxide (DMSO) and completed to the final volume with nuclease-free water (not DEPC-Treated) (Thermo Fisher Scientific). Reactions were performed on a thermocycler with an initial activation of the DNA polymerase at 95 ˚C for 15 minutes, followed by 40 cycles of 95 ˚C for 1 minute of denaturation, 67 ˚C for 1 minute of annealing and 72 ˚C for 1 minute of extension, with a final extension of 72 ˚C for 10 minutes. For optimisation, primers concentration and DMSO percentage were changed. PCR products were then subjected to electrophoresis on a 2 % agarose gel. The products were visualised under UV and specific band-size cut and extracted with QIAquick Gel Extraction Kit (QIAgen) following manufacturer's instructions to clean-up the samples before Sanger sequencing using Eurofins Genomics.

2.2.5 - Agarose gel electrophoresis

Samples were diluted in nuclease-free water (not DEPC-Treated) (Thermo Fisher Scientific) to a minimum of 300 ng of DNA and prepared with a 6x gel loading dye buffer (R0611 - Thermo Fisher Scientific). Samples were loaded onto a 1-2 % (w/v) agarose gel dissolved in 1x TAE (Tris-acetate-EDTA) buffer with 0.5 µg/mL of ethidium bromide. Electrophoresis was conducted in 1x TAE running buffer at 150 V for 30 minutes to 1 hour. Gels were visualised with a UV transilluminator (UVP, LLC).

2.2.6 - Sanger sequencing

All samples were sequenced through Eurofins Genomic tube sequencing service. Chromatograms were aligned to the original nucleotides sequence using the CLC Sequence Viewer software tool from Qiagen and using the online tool Benchling [https://benchling.com/]. A list of the sequencing primers used on this project is shown on Table 2.4.

Table 2.4 – Sequencing primers

Gene	Primers (5' → 3')		Reference
PCR and genomic sequencing of FGFR3:			
FGFR3_249-249C	Forward	CGGCAGTGGCGGTGGTGGTG	Y. Dodurga, 2011
	Reverse	AGCACCGCCGTCTGGTTG	
FGFR3_372-375C	Forward	CAGGCCAGGCCTCAACGCCC	
	Reverse	AGGCCTGGCGGGCAGGCAGC	
FGFR3_Ex18	Forward	AGAGGCCCACCTTCAAGC	Sarah V. Williams, 2012
TACC3_Ex11	Reverse	CTCACACCTGCTCCTCAGC	
pFB-FGFR3 sequencing:			
pFB-Hyg	Forward	CCTTACACAGTCCTGCTGACC	
	Reverse	AACAGACCTTGCATTCCTTTG	
FGFR3_1	Forward	GAGCGTGTCCTGGTGGGG	
FGFR3_2	Forward	CATCCTGCAGGCGGGGCT	
FGFR3_3	Forward	CCTGTTCATCCTGGTGGTGG	
FGFR3_4	Forward	GACAAGGACCTGTCGGACC	
FGFR3_5	Forward	CAAGAAGACAACCAACGGC	
pBABE-Src sequencing:			
p-BABE5'	Forward	CTTTATCCAGCCCTCAC	Weinberg Lab
Src-1	Forward	ATGGGGAGCAGCAAGAG	
Src-2	Forward	GGGAACCTTCTTGGTCC	
Src-3	Forward	AGGGCTGCTTTGGAGAG	
Src-4	Forward	GGACAACGAGTACACAG	
Src-5	Forward	CTGGAGGACTACTTCACC	
Src-R	Reverse	AAGAGCTTGGGCTCGGT	

2.3 - Mammalian cell culture

2.3.1 - Maintenance of cell lines

All cell lines were kept in a humidified incubator on an atmosphere of 37 °C at 5 % CO_2. The origin and growth medium conditions used to grow the cell lines used in this project are described in Table 2.5. All cell lines were also supplemented with 10 % (v/v) of Fetal Bovine Serum (FBS) (Life Technologies), 100 IU/ml penicillin and 100 µg/ml streptomycin. The selection antibiotic used to grow retroviral transduced cell lines was kept throughout their passaging but removed during the course of an experiment.

Cells were passaged when they reached 80-90 % confluence and split 1:5–1:20 depending on the cell line. Adherent cells were washed once with Dulbecco's PBS and detached with Trypsin 0.05 % in Versene 0.02 % at 37 °C for up to 5 minutes. Trypsin was then neutralised with growth medium and the suspension of cells split into a new flask with fresh growth medium. Cells were discarded after a maximum of 10 passages.

Table 2.5 – Cell lines and growth conditions. Non-essential amino acids (NEAA) (Thermo Fisher Scientific 11140035); FGFR3 constructs include: pFB-Hyg, pFB-Hyg-FGFR3b-WT and all other pFB-Hyg-FGFR3b-mutants. Src constructs include: pBABE-Hyg, pBABE-Src rescue and pBABE-Src-Dasatinib-resistant plasmids.

Cell line	Retroviral transduction	Growth medium; L-Glutamin; NEAA 100x	Selection antibiotic (µg/mL)	Source
NIH-3T3	-	DMEM	-	Gift (M.Katan)
NIH-3T3	pFB-Hyg-FGFR3b-(WT, S249C, N542K, V557M, K652E)	DMEM	Hygromycin (100)	Gift (M.Katan)
NIH-3T3	FGFR3 constructs	DMEM	Hygromycin (100)	
NIH-3T3	RT112Fus	DMEM	Geneticin (800)	Gift (M.Katan)
PC9	-	RPMI 1640	-	ECCAC (90071810)
PC9	FGFR3 constructs	RPMI 1640	Hygromycin (100)	
BFTC905	-	DMEM; 2 mM	-	Gift (M.Katan)
BFTC905	Src constructs	DMEM; 2 mM	Hygromycin (100)	
RT112M	-	RPMI 1640; 2 mM; 1x	-	Gift (N. Turner)
RT112M	Src constructs	RPMI 1640; 2 mM; 1x	Hygromycin (12.5)	
MGHU3	-	MEM with Earle's salts; 2 mM; 1x	-	Gift (N. Turner)
MGHU3	Src constructs	MEM with Earle's salts; 2 mM; 1x	Hygromycin (50)	
639V	-	DMEM; 2 mM	-	Gift (M.Katan)
639V	Src constructs	DMEM; 2mM	Hygromycin (100)	
HEK293T	-	DMEM	-	ATCC (CRL-3216)
Phoenix-Eco™	-	DMEM	Hygromycin (300)	Gift (M.Katan)

2.3.2 - Freezing and thawing of cell lines

After being detached from a flask, cells suspension was transferred into a falcon tube and cell number counted. The cells were then centrifuged at 300 x g for 5 minutes at RT. Upon removal of the supernatant, the pellet was resuspended in freezing medium, comprised of FBS with 10 % (v/v) of DMSO (Sigma-Aldrich) in a concentration of 1 x 10^6 cells per mL. Cells were transferred to cryovials (Thermo Fisher Scientific) and stored overnight at -80 °C, after which they were moved to liquid nitrogen for long-term storage.

For the thawing, the cryovial was immerged in a 37 °C water bath for approximately 1 minute. The content of the cryovials was then transferred to flasks with pre-warmed medium and left in the incubator overnight. On the following day cell medium was changed.

2.3.3 - Cell counting

To count cells, 10 µL of cell suspension was mixed with 10 µL of Trypan blue solution 0.4 % (w/v). 10 µL of this mix was then pipetted into a countess slide and the number of viable cells was read on a Countess™ II Automated Cell Counter (Thermo Fisher Scientific).

2.4 - Generation of stable cells lines

2.4.1 - Production of sable cell lines by retroviral transduction for expression of plasmid constructs

To achieve equal expression levels of FGFR3b and its variants in NIH-3T3 cell lines, retroviruses were produced using two different packaging cell lines. HEK293T cell line was used in alternative to the standard retrovirus competent Phoenix-Eco cell line to overcome the reduced efficiency of the later to produce retroviral particles after long passaging and high confluency (Yang and Allen, 2018). The generation of all the remaining stable cell lines used in this project was conducted using HEK293T cells, including the expression of pFB-Hyg

constructs in PC9 cells, as well as pBABE-Src constructs in the RT112M, MGHU3, 639V and BFTC905 cell lines.

2.4.1.1 - Production of retroviral particles with Phoenix-Eco cells

On day 1 Phoenix-Eco cells were seeded in 25 cm^2 flasks at low density to give cells a confluence of 50–70 % on the following day. On day 2 cells were transfected with the plasmid of interest (1.25-5 µg of DNA) using the transfection reagent Polyethylenimine (PEI) (1 mg/mL, Sigma-Aldrich). For each plasmid, a falcon tube was set with 11 µL of PEI plus 520 µL of serum-free medium and incubated at RT for 20 minutes. Then DNA was added, and samples were incubated a further 20 minutes at RT to allow the formation of PEI-plasmid complexes, after which 5mL of DMEM medium was added to the mixture. This solution was used to change medium to Phoenix-Eco cells to start viral production. Medium was changed at 24 hours and then again at 48 hours but with a smaller volume of medium (4 mL) to concentrate the shedding virus. On day 4, the target NIH-3T3 cells were seeded in 25 cm^2 flasks at low density to give 50-60 % confluent cells on the following day. On day 5 virus supernatant was harvested and filtered through 0.45 µm sterile syringe filters units (Merck Millipore) to remove cell debris. Target cells were infected with two different virus titrations (1:2 and 1:4) in an attempt to improve plasmid transduction. In this way, 2 mL or 4 mL of the filtered retrovirus suspension was added to 6 mL or 4 mL of DMEM respectively with 8 µL of 8 mg/mL polybrene (Sigma-Aldrich), a cationic polymer used to increase transduction efficiency. Then 4 mL of this solution was used to change medium to the target NIH-3T3 cells. Infection was carried out for 4 hours in the incubator. Viral supernatant was exchanged with fresh media and cells maintained in culture for 3 days before passaging and antibiotic selection initiation. Successfully transduced cells were propagated in selection antibiotic for 2 more weeks upon which cells with the constructs were considered fully selected and stable.

2.4.1.2 - Production of retroviral particles with HEK293T cells

HEK293T cells were seeded on day 1 at approximately 4.6 x 10^4 cells per cm^2 of culture flasks. For most of the retrovirus production, 75 cm^2 flasks were used. On day 2, cells at 50–70 % confluency were transiently transfected with three

different plasmids: the envelope plasmid pCMV-VSV-G, the packaging construct pUMVC and the insert plasmid. For each 75 cm^2 flask, an eppendorf was set with 15 µg of the insert plasmid and pUMVC and 1.88 µg of pCMV-VSV-G in a volume made up to 500 µL with 0.9 % (w/v) sterile NaCl solution. PEI was used as transfection reagent at a ratio of 4:1 to the total amount of DNA used and was diluted in 0.9 % (w/v) sterile NaCl solution to make up 500 µL. Both tubes were incubated for 10 minutes at RT. After this step, the PEI solution was added to the plasmids tube and incubated for a further 10 minutes at RT. During incubation, fresh media was added to the HEK293T cells and finally the mixture PEI-plasmids was added to the flask. On the following day, flasks were replenished with fresh media. On day 4, 75,000-150,000 target cells were seeded in 6 well plates to be infected with retrovirus. On day 5, the retrovirus suspension was harvested and filtered through 0.45 µm sterile syringe filters units. The retrovirus was used to change media to the target cells at a neat, half dilution and one quarter dilution with a final concentration of 8 µg/mL of polybrene. Cells were placed in the incubator for 4 hours before changing media, followed by a further 72 hours in the incubator. At this point, when necessary, cells were used for a second round of transfection following the same previous steps. Otherwise, cells were split and antibiotic selection initiated. Upon 2 weeks cells were stably expressing the constructs of interest.

2.4.2 - Determination of selection antibiotic concentration

To find out the ideal antibiotic concentration to select transduced cells, a pre-assay was performed on uninfected cells, where escalating doses of antibiotic were used to evaluate cell response as a colony formation assay, described on section 2.6.2. The minimum antibiotic dose able to kill 100 % of the cells after 7 days was used for selection after transduction. Cells were then maintained on half dose of the determined selection antibiotic.

2.5 - Protein analysis procedures

2.5.1 - Protein extraction

For protein extraction from cell cultures, cell lines were generally seeded on day 1 with 4 x 10^5 cells per 25 cm^2 flask, or when higher amount of protein was required 1 x 10^6 cells per 25 cm^2 flask, and 2 x 10^6 cells and 4 x 10^6 cells per 75 and 175 cm^2 flask, respectively. Cells were kept in culture for 48 hours before any treatment or assay took place. For cell lysis, cells were placed on ice and washed once with ice-cold PBS before adding RIPA lysis buffer (50 mM Tris-HCl, pH 7.6, 150 mM NaCl, 1 % (v/v) NP40, 0.5 % (w/v) sodium deoxycholate, 0.1 % (w/v) sodium dodecyl sulphate (SDS)) with 1x Halt™ Protease and Phosphatase Inhibitor Cocktail with EDTA (Pierce, Thermo Fisher Scientific). Depending on the cell number, 150-300 µL of RIPA was added to 25 cm^2 flasks, 1mL and 3 mL added to 75 and 175 cm^2 flasks, respectively. RIPA buffer was spread evenly through the flask and cells were kept on ice for 5 minutes before being scrapped and collected into an Eppendorf tube. Lysis was processed for a further 10 minutes on ice with regular vortexing. Tubes were stored at -80 °C overnight before sample preparation.

2.5.2 - Protein quantification

The day after protein extraction, lysates were thawed on ice and carefully sonicated with 2 pulses of 5 seconds with 5 seconds interval on ice. Lysates were cleared out by centrifugation at 15,000 x g for 10 minutes and the supernatant transferred to a clean tube.

At this point, the amount of protein was quantified with bicinchoninic acid (BCA) Protein Assay Kit (Pierce, Thermo Fisher Scientific), using 10 µL of each sample including the standard Albumin according to manufacturer's instructions. The wavelength of 562 nm was used on a Spectramax M5 plate reader (Molecular Devices) to measure the absorbance for calculation of protein concentration.

2.5.3 - Sodium dodecyl sulphate-polyacrylamide gel electrophoresis (SDS-PAGE)

Samples were prepared immediately after protein quantification. Between 15-70 µg of protein was diluted in 4x NuPAGE LDS Sample Buffer and 10x NuPAGE Sample Reducing Agent (Thermo Fisher Scientific) up to a volume of 20 µL with water. Samples were boiled at 95 °C for 5 minutes. When analysing non-reducing samples, the sample reducing agent was not added to the preparation and the samples were not boiled, but the subsequent steps of the protocol remained the same. Samples were loaded into a 4-12 % gradient gel (Novex, Thermo Fisher Scientific) and immerged on 1x NuPAGE™ MOPS SDS Running Buffer (Invitrogen™ Novex™, Thermo Fisher Scientific). Proteins were separated by electrophoresis at 150 V for 90 minutes.

2.5.4 - Western blotting

Separated proteins were transferred from the SDS gel into polyvinylidene fluoride (PVDF) membranes either by wet or dry transfer. Wet transfer was performed for 3 hours at 30 V in transfer buffer (Tris 25 mM, glycine 192 mM, pH 8.3) with 20 % (v/v) methanol. Dry transfer was carried out on an iBlot™ 2 dry blotting machine (Thermo Fisher Scientific), within iBlot™ Transfer Stacks with increased voltage for 7 minutes (20 V for 1 minute, 23 V for 4 minutes and 25 V for 2 minutes). Protein transfer was visualised with Ponceau stain (0.1 % (w/v) Ponceau S dye, 1 % (v/v) acetic acid in water) to facilitate molecular weight (MW) sorting and consequent immunoblotting.

To avoid non-specific antibody binding, membranes were incubated in blocking buffer with 5 % (w/v) bovine serum albumin (BSA) (Sigma-Aldrich) in Tris-buffered saline solution with 0.01 % (v/v) Tween (TBS-T) for 30 minutes at RT with shaking at 60 rpm. Membranes were then incubated overnight at 4 °C on a shaker (60 rpm) with a solution of the primary antibody in blocking buffer. Three washes of 10 minutes each in TBS-T at RT on a shaker, were used to remove unbound antibody before incubation for another hour at RT at 60 rpm with the secondary antibody in blocking buffer. Antibody details and used concentrations

are listed in Table 2.6. Three more washes were carried out after secondary antibody incubation, and membranes were developed with Supersignal™ West Pico PLUS Chemiluminescent Substrate (Pierce, Thermo Fisher Scientific) for 1-5 minutes. Signal was visualised by x-ray film or on the ChemiDoc system (Bio-Rad).

When blotting for proteins with equal MW, different gels were run, and membranes blot separately. Otherwise, membranes were strip from the antibody no more than once, using Restore Plus Western Blot Stripping Buffer (Thermo Fisher Scientific) for 10 min and washed once with TBS-T for 5 minutes, both at RT on a shaker at 60 rmp, before blocking and reprobing with the antibodies of interest.

Table 2.6 – Primary and secondary antibodies

Protein	Source (species, clonality)	Vendor	Dilution in blocking buffer	MW (kDa)
FGFR3	Mouse monoclonal	Santa Cruz Biotecnology #sc-13121	1:500	105, 115 and 130
pY1000	Rabbit polyclonal	Cell Signaling #8954	1:2000	N/A
EGFR	Rabbit polyclonal	Cell Signaling #2232	1:1000	175
pSTAT3 Y705	Rabbit polyclonal	Cell Signaling #9145	1:500-1:1000	79, 86
STAT3	Rabbit monoclonal	Cell Signaling #8768	1:1000-1:5000	86
pSrc Y416	Rabbit polyclonal	Cell Signaling #2101	1:500	60
Src	Rabbit polyclonal	Cell Signaling #2108	1:1000	60
pAkt S473	Rabbit monoclonal	Cell Signaling #4058	1:250-1:500	60
Akt	Rabbit monoclonal	Cell Signaling #4691	1:1000-1:2000	60
pErk T202/Y404	Rabbit monoclonal	Cell Signaling #4370	1:2000	42, 44
Erk	Rabbit monoclonal	Cell Signaling #4695	1:2000-1:5000	42, 44
a-Tubulin	Mouse monoclonal	Sigma-Aldrich #T5168	1:10,000	50
Anti-rabbit HRP	Goat monoclonal	Cell Signaling #7074	1:2000-1:10,000	N/A
Anti-mouse HRP	Goat polyclonal	SignalChem #G32-62G-1000	1:10,000	N/A

2.5.5- Luminex assay

Cell lysates were prepared as previously described in RIPA buffer with protease and phosphatase inhibitors, followed by protein quantification with BCA assay. For multiplex assay, 10 µg of lysate was used as analyte per well on a 96-well plate format. A list of the successful proteins used for this assay is presented in Table 2.7. The protocol followed the manufacturer's instructions and prepared

samples were run on the dual-laser flow-based detection instrument Luminex® 200™ by Adam Stewart from Prof. Udai Banerji laboratory.

Table 2.7 – Luminex proteins

Protein (phosphorylation site)	Source
CHK1 (S345)	Homegrown
CHK2 (T68)	Homegrown
ßCATENIN (S33/37)	Homegrown
GSK3ß (S9)	Millipore - #48-611MAG
FAK (Y397)	Homegrown
JAK1 (Y1022/1023)	Homegrown
PRAS40 (T246)	Homegrown
RAF1 (S259)	Homegrown
LCK (Y394)	Homegrown
Src (Y419)	Millipore - #46-710MAG
NFkB (S536)	Millipore - #46-702MAG
FGFR1 (Y653/654)	Homegrown
Rb (S760)	Homegrown
PTEN (S380)	Millipore - #48-611MAG

2.6 - Phenotypic assays

2.6.1 - Anchorage independent assay – soft agar

Colony formation assays in soft agar were performed with NIH-3T3 cells in 6 well plates with 20,000 cells per well seeded in triplicate. Due to the temperature sensitivity of the assay, because agar solutions solidify bellow 40 °C, and the physiologic temperature of cells is 37 °C, a water bath was pre-set at 42 °C along with a water filled beaker. Two stock solutions of 1.2 % and 1.4 % (w/v) of Noble Agar (Sigma-Aldrich) in water were melted for 2 minutes in the microwave and then stabilised at 42 °C for at least 1h. Two-times concentrated (2x) DMEM with 20 % FBS was also prepared and incubated at 37 °C. Once temperature was equilibrated, the plates were coated with a layer of 1.5 mL of 1.2 % agar and 2x DMEM (1:1) to give a final concentration of 0.6 % agar in 1x DMEM plus 10 % FBS. Plates were set aside until agar solidification, for a minimum of 15 minutes at RT. In the meanwhile, cells were trypsinised, counted and twice the number of cells to be seeded (i.e. 40,000 cells) were transferred to a tube and mixed with

2x DMEM and 1.4 % agar in a volume proportion of 2:1:1, respectively. Then, 1.5 mL of this solution of cells was used to cover the base layer of the pre-coated plates. Plates were placed in the incubator at 37 °C for 30 minutes. Then 1mL of full medium was added to the plates. To avoid premature agar solidification, solutions were mixed with tubes placed inside the prewarmed water filled beaker, and all the solutions were kept in the water bath when not in use.

Media was changed every 3 days. After 3 weeks medium was removed and colonies were stained with Giemsa Stain Modified Solution (48900, Sigma-Aldrich) with 1 part Giemsa to 5 parts glycerol:methanol (5:24 parts) for 20 minutes with gentle shaking. Plates were washed several times in water, including overnight de-staining. The plates were then scanned and the number of colonies with a diameter greater than 10 pixels was analysed on ImageJ software.

2.6.2 - Colony formation assay

Cells were trypsinised, counted and seeded in 6 well plates at low density. Therefore, 1000 cells per well were used for all assays with NIH-3T3 cells and 15,000 cells were used for all other cell lines. On the following day, drug was added to the plates and replaced with fresh medium and drug. Media and drug replacement were performed twice a week. Plates were kept in culture for 13 or 14 days before staining. After medium removal, cells were fixed to the plate with Carnoy's solution (1 acetic acid: 3 methanol) and incubated for a minimum of 5 minutes at RT. Fixative was removed and plates were air-dried and then stained with 1 % (w/v) crystal violet (Sigma-Aldrich) for 5 minutes at RT. Plates were washed throughout with tap water and scanned with ChemiDoc. The percentage of colonies covering the plates were calculated with ImageJ tool.

2.6.3 - Small molecule inhibitors preparation

The lyophilised chemical inhibitors were resuspended in DMSO to a concentration of 1-10mM depending on their solubility factor. Aliquots were

prepared and stored for long-term at -20 °C. The entire list of small molecule inhibitors used in this project is shown in Table 2.8.

Table 2.8 – Small molecule chemical compounds

Compound	Source	Compound (continuation)	Source (continuation)
AZD4547	LC Labs #A-1088	MK-8776	Selleckchem #S2735
AZD5363	Selleckchem #S8019	Momelotinib	Selleckchem #S2219
BEZ235	LC Labs #N-4288	MRT67307	Sigma-Aldrich #SML0702
BGJ398	Selleckchem #S2183	NVP-AUY922	LC Labs #N-5300
Binimetinib	LC Labs #B-2332	NVP-TAE684	Selleckchem #S1108
Bosutinib	LC Labs #B-1788	Palbociclib	Selleckchem #S1116
BX-795	Sigma-Aldrich #SML0694	Pazopanib	LC Labs #P-6706
Cediranib	LC Labs #C-4300	PD173074	Selleckchem #S1264
Ceritinib	Selleckchem #S7083	PF562271	Selleckchem #S2890
Crizotinib	LC Labs #C-7900	Ponatinib	LC Labs #P-7022
Dabrafenib	Selleckchem #S2807	GSK126	Selleckchem #S7061
Dasatinib	LC Labs #D-3307	Saracatinib	Selleckchem #S1006
Foretinib	LC Labs #F-4185	Silmitasertib	Selleckchem #S2248
Gefitinib	LC Labs #G-4408	Sorafenib	LC Labs #S-8599
Imatinib	LC Labs #I-5577	Sunitinib	LC Labs #S-8877
JQ1	Selleckchem #S7110	Trametinib	LC Labs #T-8123
Lenvatinib	LC Labs #L-5400	Vandetanib	LC Labs #V-9402
MK2206	Selleckchem #S1078		

2.6.4 - Inhibitor dose response viability assay

Dose response assays were done in a 96 well format. Plate edges and space in between wells were carefully filled with PBS to avoid medium evaporation and thus improve reproducibility across biological replicates. Cells were trypsinised, counted and 1000-3000 cells were seeded per well in triplicate. The number of cells used was calculated to reach 80-90% confluence at the end-point assay. Thus, 1000 cells were used for NIH-3T3 cells, 2000 cells for PC9 cells and 3000 cells for the other cell lines. After 24 hours, serial dilutions of the inhibitor of interest were prepared in 12-well reservoirs (9 dilutions ranging from 5nM to 50μM). Medium was replaced from the plates with the appropriate drug dosage and vehicle control. After 72 hours, cell viability was calculated using a measure of the ATP concentration with CellTitre-Glo (CTG) (Promega) reagent, as per the manufacturer's guidelines. Luminescence was read using a Victor plate reader (PerkinElmer). Values were normalised against the DMSO vehicle control and

viability percentages were plotted on GraphPad Prism 7 which were then analysed with a four-parameter non-linear regression curve-fitting with 5000 points. The points of the curve allowed the half maximal inhibitory concentration (IC_{50}) calculation by taking the closest inhibitor concentration correspondent to 50 % cell viability. A minimum of three biological replicates were obtained to calculate the average IC_{50} value.

2.6.5 - Anchorage independent assay – spheroids

Cells were seeded on Corning® Costar® Ultra-Low Attachment 96 well round bottom plates (Sigma-Aldrich) on a density of 1000 cells per well per 100 µL. Plates were spun down at 300 x g for 1 minute before incubation at 37°C.

2.6.6 - Inhibitor response – Spheroid size

After 24 hours in round bottom plates, spheroids were formed and 100 µL of a 2x concentrated inhibitor solution was added to each well. Spheroids were kept in culture for up to 10 days and image acquisition data using the CeligoS Imaging Cytometer (Nexcelom Bioscience) were acquired on days 4, 7 and 10. The area of the spheroids was calculated using ImageJ software with a modified automated macro processing (Ivanov et al., 2014). Well media was replenished on day 4 and 7 with careful removal of 100 µL of medium from each well prior to the addition of 100 µL of 2x inhibitor or DMSO control.

2.6.8 - Targeted small molecule inhibitor screen

A set of 32 small molecule inhibitors were selected to build a library to target a broad range of signalling pathways. A template was pre-made in 96 well plates with the different drugs including the vehicle DMSO control at the concentration of 1 µM which was then stored at -80 °C. Cells were seeded at 1000 cells / well in 96 well plates in duplicate. After 24 hours, inhibitor library plates were thawed at RT and cells were treated with the inhibitors up to a volume of 100 µL per well and to a final concentration of 500 nM. After 72 hours cell viability was measured

by CTG assay. Raw data was normalised against the DMSO control and the average of three biological replicates was plotted on a heat map.

Chapter 3

Assessment of FGFR3 cancer-associated mutations

3.1 - Introduction

Although FGFR3 mutations have long been associated with skeletal syndromes, it was only later that FGFR3 alterations were found in cancer (Richelda et al., 1997). The FGFR3 chromosomal translocation t(4;14) (p16.3;q32) was first identified in MM and associated with the occurrence of FGFR3 mutations such as Y375C and K652E/M in different myeloma cell lines. (Chesi et al., 1997; Fracchiolla et al., 1998; Ronchetti et al., 2001). This finding prompted further investigations and many other FGFR3 gene mutations associated with human skeletal disorders were subsequently linked to cancer development, such as R248C, S249C or G372C (Cappellen et al., 1999). Later, with the arrival of large-scale cancer genome sequencing projects, hundreds of other FGFR3 somatic mutations were identified in diverse human cancers (Helsten et al., 2015), and are now catalogued in different online databases.

FGFR3 somatic missense mutations account for the development and progression of different human cancer types, in particular bladder cancer (van Rhijn et al., 2002). Most common FGFR3 mutations have been studied for their functional consequences at the receptor level. For instance, kinase hyperactivation and ligand-independent receptor activation are known to result in downstream signalling exacerbation leading to uncontrolled cell proliferation, growth and survival in diverse types of cancers (Naski et al., 1996; Ornitz and Itoh, 2015). However, the way distinct FGFR3 mutations modulate downstream signalling pathways to drive oncogenesis is poorly understood. Therefore, this thesis seeks to study the signalling mechanisms involved in the development of FGFR3 mutation-dependent cancers in order to improve patient outcomes.

This first chapter of results aims to identify and select the most common FGFR3 somatic point mutations found in cancer, through the analysis of curated public online databases in order to develop relevant models for its study. The generation of cellular models bearing relevant FGFR3 mutations and the optimisation of mutant FGFR3 expression levels will be presented along with model validation by analysis of transforming phenotype and response to FGFR3 inhibitors. Moreover, FGFR3 mutants will be analysed for their downstream signalling activity in the presence and absence of ligand stimulation.

3.2 - Selection of relevant missense somatic FGFR3 point mutations in cancer

There are several online databases that compile somatic FGFR3 mutations on an ongoing basis, including cBioportal for cancer genomics [https://www.cbioportal.org/] and the Catalogue of Somatic Mutations in Cancer (COSMIC) [cancer.sanger.ac.uk], which curate data from diverse worldwide studies including The Cancer Genome Atlas (TCGA) [cancergenome.nih.gov] and the International Cancer Genome Consortium (ICGC) [icgc.org]. At the beginning of this project, FGFR3 cancer-associated missense mutations were gathered from cBioportal, which at the time (October 2015) comprised data from just under 200 samples, but now includes more than 42,000 samples from 159 studies. For this project, relevant FGFR3 mutants were selected based on a threshold of 3 or more cases per mutation. With the number of samples being deposited in the database rapidly increasing, additional mutations were included to accommodate other high frequency mutations according to the set threshold. In some cases, residues that are frequently mutated but associated with lower frequency mutant variants were also included in the panel in order to explore if different mutations in the same amino acid residue had functional and biological consequences. One case is for the residue S249 that is frequently mutated to a cysteine (179 samples out of 659, according to cBioportal) but is also found to be mutated to a lower frequency to a threonine (1 sample out of 659, according to cBioportal) (Figure 3.1) (Cerami et al., 2012; Gao et al., 2013). In order to further increase the number of samples from which mutations were selected, FGFR3 mutations identified in an individual study by Helsten and colleagues, which analysed nearly 5000 tumour samples specifically to assess the mutation status of FGFRs, were also included for this study (Helsten et al., 2015).

The panel of FGFR3 mutations included in this study was finalised at the end of 2017, making a total of 16 FGFR3 point mutations across the entire length of the receptor (Figure 3.1). Mutations include S131L that occurs in the acidic box region within the linker Ig-I-Ig-II, known to play a role in the receptor autoinhibition (Kalinina et al., 2012). The panel also includes mutations in the linker region between Ig-II-Ig-III, namely the most common FGFR3 mutation S249C along with

a lower frequency mutation S249T and the third most common FGFR3 mutation R248C. Both residues R248 and S249 are known to form disulphide bonds between homodimers in a ligand-independent manner, driving the constitutive activation of the receptor (Bernard-Pierrot et al., 2006). Three other selected mutations localise at the JM region of the extracellular domain. These are all cysteine variants and include residues G372, S373 and Y375. The unpaired cysteine on these residues is also thought to drive constitutive dimerisation of the TM domain in the absence of ligand, resulting in a conformational change of the TM domain that is propagated to the KD which becomes active (Bodoor et al., 2010). Interestingly, cysteine variants are the most common type of mutation in FGFR3 making up around 95% of all cancer-associated mutations found in FGFR3, most of which can be found in bladder cancers (Di Martino et al., 2016). A mutation on the TM domain was also selected on residue G382, where the mutation arginine (R) is more commonly found in cancer than the glutamic acid (E) (Bodoor et al., 2010). And on the JM region of the intracellular compartment of FGFR3 a cysteine mutation on residue R401 was also included. Further along the receptor, cancer-associated mutations include residues on the KD, such as E629, K652 and V679. Residue K652 is most frequently mutated to glutamic acid (E) but lower frequency mutations such as methionine (M), threonine (T) and asparagine (N) are also found in cancer (van Rhijn et al., 2002). K652 is found within the activation loop of the KD, known to play a role in the activation of the receptor (Webster et al., 1996).

Along with the selected 16 FGFR3 cancer-associated mutations, positive and negative controls were also included in the panel. The gatekeeper mutation control V557M, that is known to hinder inhibitor binding and confer resistance to FGFR inhibitors, was selected as a negative control for the response to FGFR inhibitors (Chell et al., 2013). In parallel, the translocation RT112Fus that harbours the fusion of WT FGFR3 with TACC3 was used as positive control due to its high transformation potential *in vitro* and in xenograft models as described in chapter 1 (Patani, 2016; Williams et al., 2013). A final variant N542K, only described in germline diseases, was also included in the panel as a positive control due to its reported high kinase activity when compared to other FGFR3 mutants (Greulich and Pollock, 2011; Patani, 2016).

Upon mutant selection, information about the nucleotide exchange for each mutant was identified in COSMIC, where there is a detailed description of each mutation. It is important to note that some mutations are found in both FGFR3 isoforms III-c and III-b, depending on their tissue of origin, however in this work mutations are referred to using the residue numbering of the FGFR3-b isoform, in contrast to the canonical isoform c commonly used in publications.

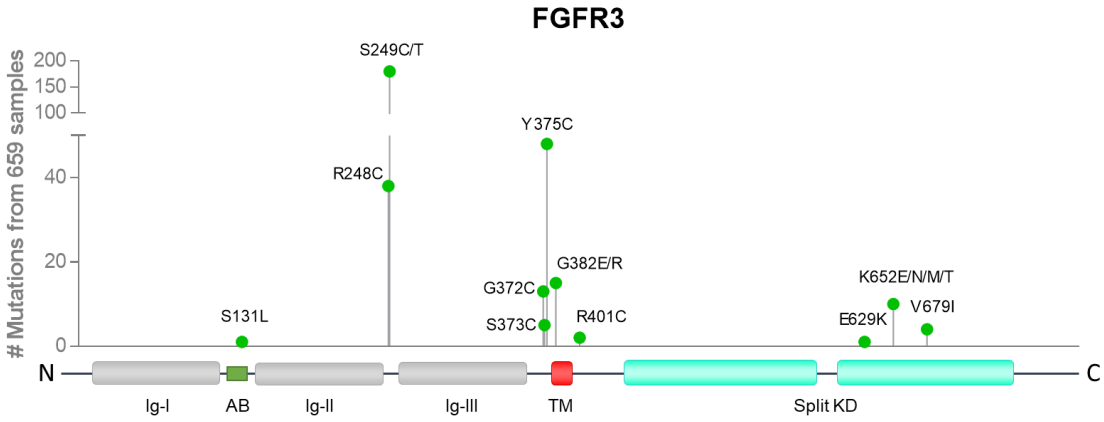

Figure 3.1 – Distribution of all FGFR3 cancer-associated mutations selected for this project. FGFR3 mutations represented here were selected from cBioportal curated database (Cerami et al., 2012; Gao et al., 2013) and from an article where around 5000 tumours were screened for FGFR alterations (Helsten et al., 2015). The lollipop plot shows on the y-axis the number of samples from different patients presenting the correspondent FGFR3 mutation. At the end of 2017 when the panel was complete, all mutations for each residue were found in more than three patients except E629K which was only identified in 1 patient from the screen by Helsten et al. (Helsten et al., 2015). Their distribution across the different domains of FGFR3 is indicated by the coloured bar at the bottom of the lollipop plot. From left to right is FGFR3 from (N)-terminus to (C)-terminus, where the grey bars represent each Ig domain of the extracellular region with Ig-I being followed by the acidic box (AB), which is therefore followed by Ig-II and Ig-III. The red box represents the TM domain whereas the blue boxes represent the split KD.

3.3 - Generation of FGFR3 mutant NIH-3T3 cell line models

3.3.1 - Construction of FGFR3 mutant plasmids and cell line transduction

The aim of this project is to characterise individual FGFR3 mutations to improve targeted therapies and to define the resistance mechanisms of FGFR3 mutations towards selective inhibitors. Hence, it was important to utilise the same cell line

model which allowed the execution of diverse experimental assays, from phenotypic assessment to the determination of molecular signalling effectors that play a role in cancer development as well as enable evaluation of the efficacy of inhibitors. The use of the same model cell line for the expression of FGFR3 mutants facilitated the assessment of mutant specific characteristics in the same genomic background to minimise confounding genetic and epigenetic factors that may arise when using a panel of cell lines from a number of different cancer types. Therefore, the NIH-3T3 mouse fibroblast cell line was used to generate FGFR3 mutant models. This cell line is a workhorse for evaluating oncogenic effects and has been widely used in diverse cancer studies. It is a valuable tool for screening the oncogenic effects of transduced genes as the cells have a high degree of contact-inhibition in culture (which is lost in cancer cells) (Alvarez et al., 2014; Williams et al., 2013), and are amenable for signalling pathway analysis and drug assays (Chang et al., 2015; Yeh et al., 2008).

In order to express FGFR3 mutants in NIH-3T3 cells, a retroviral vector pFB (Stratagene) containing full length FGFR3-WT modified to have a hygromycin resistant cassette was obtained from Prof. Matilda Katan (UCL). The plasmid contained the FGFR3b spliced isoform, selected due to the frequency of FGFR3 mutations in bladder cancer and epithelial tissues, where this isoform b is most commonly expressed (Tomlinson et al., 2005). Point mutations were introduced in this pFB-FGFR3-Hyg backbone using SDM followed by full Sanger sequencing of FGFR3b gene in order to confirm the successful introduction of the single mutation of interest (method details are described in section 2.2.2) (Appendix Figure 8.1). The generated plasmid library of FGFR3 mutants, along with the WT FGFR3 control were then used to engineer stable cell lines in mouse fibroblast NIH-3T3 background. Moreover, a pFB-Hyg construct lacking the FGFR3 gene was also transduced into NIH-3T3 cells and used as an empty vector (EV) control. Plasmids were used to produce retroviral particles in packaging cells lines (Phoenix-eco or HEK293 cells) that were then able to infect the host NIH-3T3 cells. Hygromycin antibiotic was used for the selection of positively infected cells, and after a further 2 weeks in culture, populations of cells stably expressing mutant FGFR3 were generated (refer to section 2.4.1 to see full method details).

3.3.2 - Optimisation of FGFR3 expression levels

In order to attain comparable data between mutant cell line models, I set out to establish if the engineered cells express similar levels of mutant FGFR3 by western blotting analysis. The theoretical MW of FGFR3 is 88 KDa, however as a result of post-translational modifications, immunoblots often display additional bands due to the presence of different glycoforms that confer different mobilities in SDS-PAGE gels (Gibbs and Legeai-Mallet, 2007). Therefore, the unglycosylated form of FGFR3 exists at 105 KDa and the low and high glycosylation levels appear at 115 KDa and 130 KDa, respectively (Gibbs and Legeai-Mallet, 2007). RT112Fus (FGFR3-TACC3 fusion protein) has a distinct MW due to the presence of the fusion protein TACC3 coupled to FGFR3. Some of the FGFR3 mutant cell lines were originally a gift from Prof. Matilda Katan, including FGFR3-WT, RT112Fus, S249C, N542K, V557M and K652E (Figure 3.2A). However, the expression levels of these cell lines were confirmed to be considerably higher than the mutants generated in-house (denoted with the suffix "L") as part of this project (Figure 3.2B). Moreover, in-house generated cell lines also shown to express distinct FGFR3 levels.

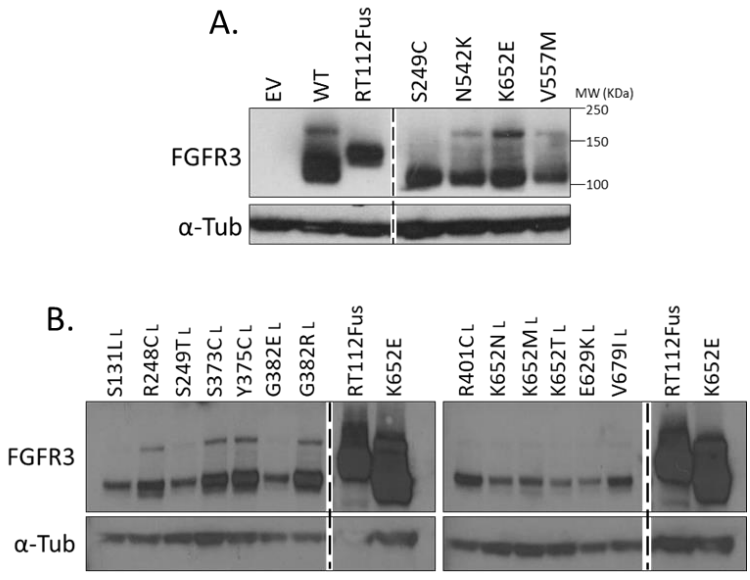

Figure 3.2 – FGFR3 expression levels in NIH-3T3 cell lines. A. FGFR3 expression of cell lines obtained from Prof. Matilda Katan's laboratory in UCL in comparison to the EV control generated in-house. The MW of FGFR3 protein is indicated in KDa. **B.** Part of the panel of FGFR3 cell lines transduced in-house (L) shows reduced and uneven levels of expression when compared to the cell lines RT112Fus and K652E from panel A.

In order to obtain cells with similar higher mutant FGFR3 expression levels as those obtained from UCL, different approaches were taken. These included utilising an alternative retroviral production technique, using different virus titrations and generating clones from parental mutant cell lines. In the first round of viral particle production, Phoenix-Eco packaging cells were used. However, despite further attempts at cell line generation using 1.25-5 µg of plasmid template and ½ (v/v) of virus for infection of NIH-3T3 cells, the resultant receptor expression levels were still reduced compared to the cell lines from UCL. To address this issue, an alternative viral production method was utilised. HEK293 cells were infected with 15 µg of the FGFR3 vector of interest along with two other plasmids encoding viral packaging components. NIH-3T3 cells were then transduced with ½ or ¼ (v/v) of virus with either one or two consecutive rounds of infection in an attempt to increase transduction levels (see full details in section 2.4.1.2). The results were more promising, and the FGFR3 expression levels of the generated stable cell lines were very similar across the panel and similar to the S249C cells obtained from UCL (Figure 3.3A and Appendix Figure 8.2). Moreover, I found that the concentration of virus used for transduction and the number of repeated infections did not have an impact on the receptor expression levels of these cells. Therefore, I proceeded with the generation of the remaining mutants (including G372C, R401C, E629K and V679I) with the same protocol, using ½ (v/v) of virus and one round of infection. Moreover, at this point, due to the previously unsuccessful generation of high expressing mutant cell lines, I decided to re-generate in-house the cell lines from UCL (including WT, RT112Fus, S249C, N542K and V557M) through the same method, in an attempt to obtain similar expression levels across all mutant cells, in case the remaining mutants fail to express high levels of FGFR3. K652E cell lines were not re-generated as cells did not survive upon antibiotic selection. However, finally when the expression of FGFR3 levels was compared across all generated cell lines, there were still discrepancies, and the FGFR3 expression levels were still very low for the in-house generated mutants compared to those acquired from UCL (Figure 3.3B). Moreover, across the in-house generated mutant cell lines, FGFR3 expression levels were uneven, with cell lines such as $G382R_L$ expressing higher levels than $K652M_L$ for example.

To further attempt to generate similar high-expressing cell lines, single-cell clones were generated from the engineered cells. The rationale for this assumes that within the population of engineered cells, the expression levels for FGFR3 in individual clones vary, following a normal distribution. Hence, isolating and growing up individual clones from the original population would permit the generation of cell lines with different expression levels. Therefore, the previously generated in-house and UCL cell lines were used to generate single-cell clones, in an attempt to achieve equally high FGFR3 expression levels. The UCL cell lines were used to generate lower expression clones, whereas the in-house cell lines were used to generate higher expressing clones. The process consisted of consecutive serial cell dilutions in full growth media and seeding in 96-well plate format on day 1. On day 2, wells containing only one cell (in up to 10 wells) were selected for follow up and monitored through time for cell multiplication until full well confluency, allowing the expansion of these clones to generate cell lines. However, the generation of cell lines with high FGFR3 expression again proved to be challenging using this method (Figure 3.3C and Appendix 8.3).

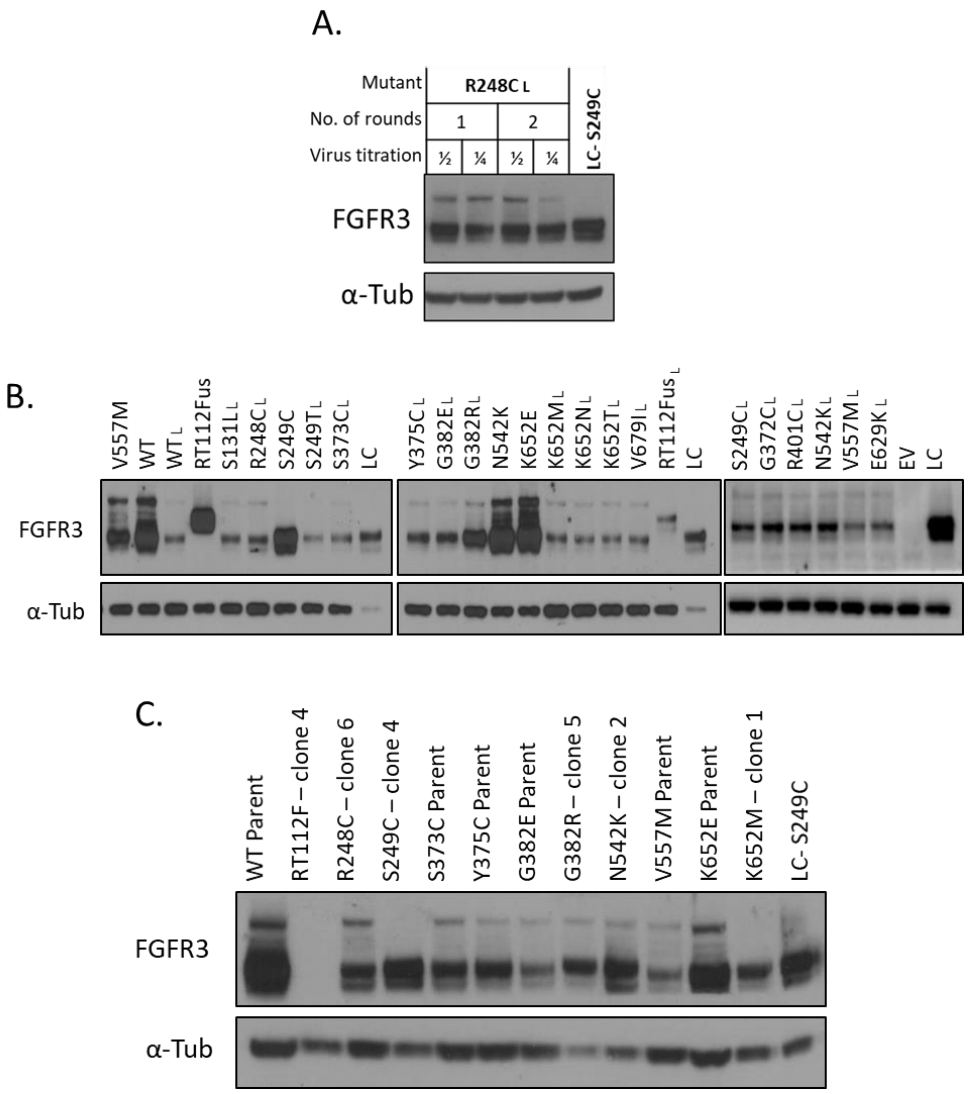

Figure 3.3 – Optimisation of FGFR3 expression levels in NIH-3T3 cell lines. A. Representative example of the resulting transduction of FGFR3 mutants after virus production with HEK293 cells, one and two rounds of infection and different virus titrations. The full panel of generated cell lines can be seen on Appendix Figure 8.2. **B.** Cell lines transduced in A by virus production with HEK293 cells using one round of transfection and ½ virus titration, were run together with the panel of cell lines acquired from UCL shown in Figure 2A, and the remaining generated FGFR3 mutant cells. Differences in FGFR3 expression levels are still clear. **C.** Collection of FGFR3 mutants and parental cell lines generated after single cell clones sorting and growth. Selected clones derived from parental cells are numbered according to the originated clone number. WT, RT112Fus, S249C, N542K, V557M and K652E from UCL were used as parental cell lines to obtain lower levels of FGFR3 expression. The remaining cell lines used the in-house generated cell lines to obtain higher FGFR3 expression levels. The represented cell lines were picked out of all generated clones according to their similar expression levels. The full panel of generated cell lines can be seen on Appendix Figure 8.3. However, results still show an uneven and low expression of FGFR3 for some mutant cells when comparing to the loading control (LC) for high expression S249C from UCL.

Despite several attempts, the generation of FGFR3 mutant cell lines with equal FGFR3 expression levels as the UCL cell lines proved to be challenging. Therefore, the entire panel of generated FGFR3 mutants were divided into two classes: the high expressing mutants, and the low expressing mutants (Figure 3.4). To distinguish these two groups of cell lines, all low expression mutant cells generated in-house are denoted with the suffix “L” throughout this entire work.

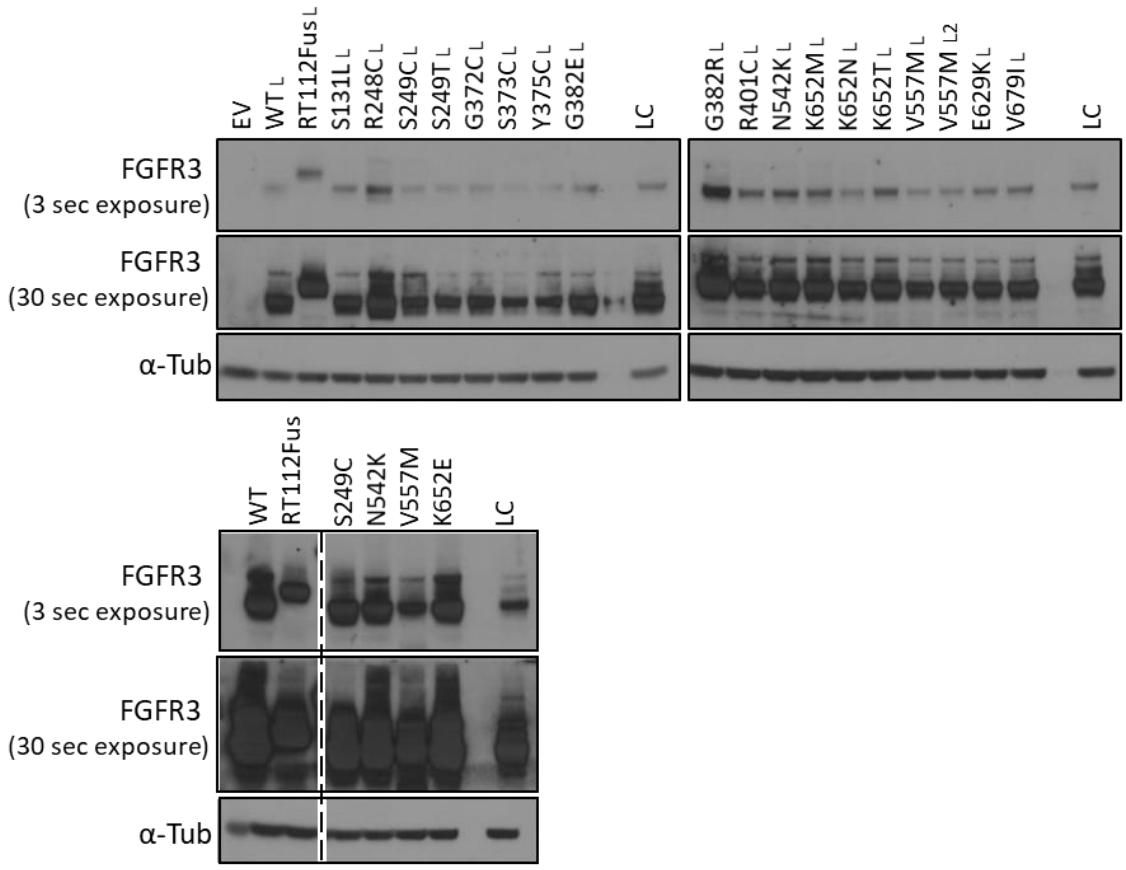

Figure 3.4 – FGFR3 expression of the final panel of FGFR3 cell lines. The entire panel of FGFR3 mutants employed in this thesis is shown and divided in low expressing mutants (L) generated in-house on the top panel, and high expressing mutants on the bottom panel acquired from UCL. On the top panel L2 represents a second generated mutant cell line. Two different FGFR3 film exposures are shown in order to facilitate the visualisation of the different expression levels between panels. The loading control (LC) is here a mere reference to compare FGFR3 expression between blots run at the same time but on different gels.

3.4 - Effects of FGFR3 mutations on cellular morphology

It has previously been shown that expressing oncogenes in NIH-3T3 cells results in loss of contact inhibition leading to a dramatic change in cellular morphology (Bernard-Pierrot et al., 2006; Di Martino et al., 2009). Morphologic assessment thus allows for the selection of the most transforming mutations which are often associated with their potential to grow tumours *in vivo* (Bernard-Pierrot et al., 2006). Along these lines, I evaluate the effects of FGFR3 mutant expression on the morphology of NIH-3T3 cells using EV and WT FGFR3 expressing cells as negative controls and the RT112Fus expressing cells as a positive control. Cells expressing RT112Fus have a high transformation potential in culture due to its loss of contact-inhibition, resulting in the ability to form clusters of cells with a distinct morphology from WT FGFR3 expressing cells (Williams et al., 2013).

Each cell line was seeded and observed under the microscope after 3 days in culture (Figure 3.5 and 3.6). Presented images represent the morphology of engineered cell lines at high and/or low confluency at an early passage number (≤ 3). On day 3, confluency of cells varies between 60 % - 95 % across cell lines, which might indicate different growth rates between mutants. Morphological effects were clearly visible upon expression of particular mutants. Across the high expressing mutants obtained from UCL, RT112Fus had the most markedly pronounced change in cellular morphology (Figure 3.5). These cells formed clear elongated protrusions with compact cells. Unlike the flattened morphology of the EV and WT FGFR3 cells, all the mutants in the high expression panel of cells from UCL showed a round spindle-like morphology at low and high confluency. Moreover, RT112Fus cells grew as dense aggregates at high density that were visible to the naked eye. Cells expressing the high kinase activity mutants N542K and K652E, also formed aggregates similar to RT112Fus expressing cells when grown at high confluency, suggesting that these mutants may have similar transformation ability as RT112Fus.

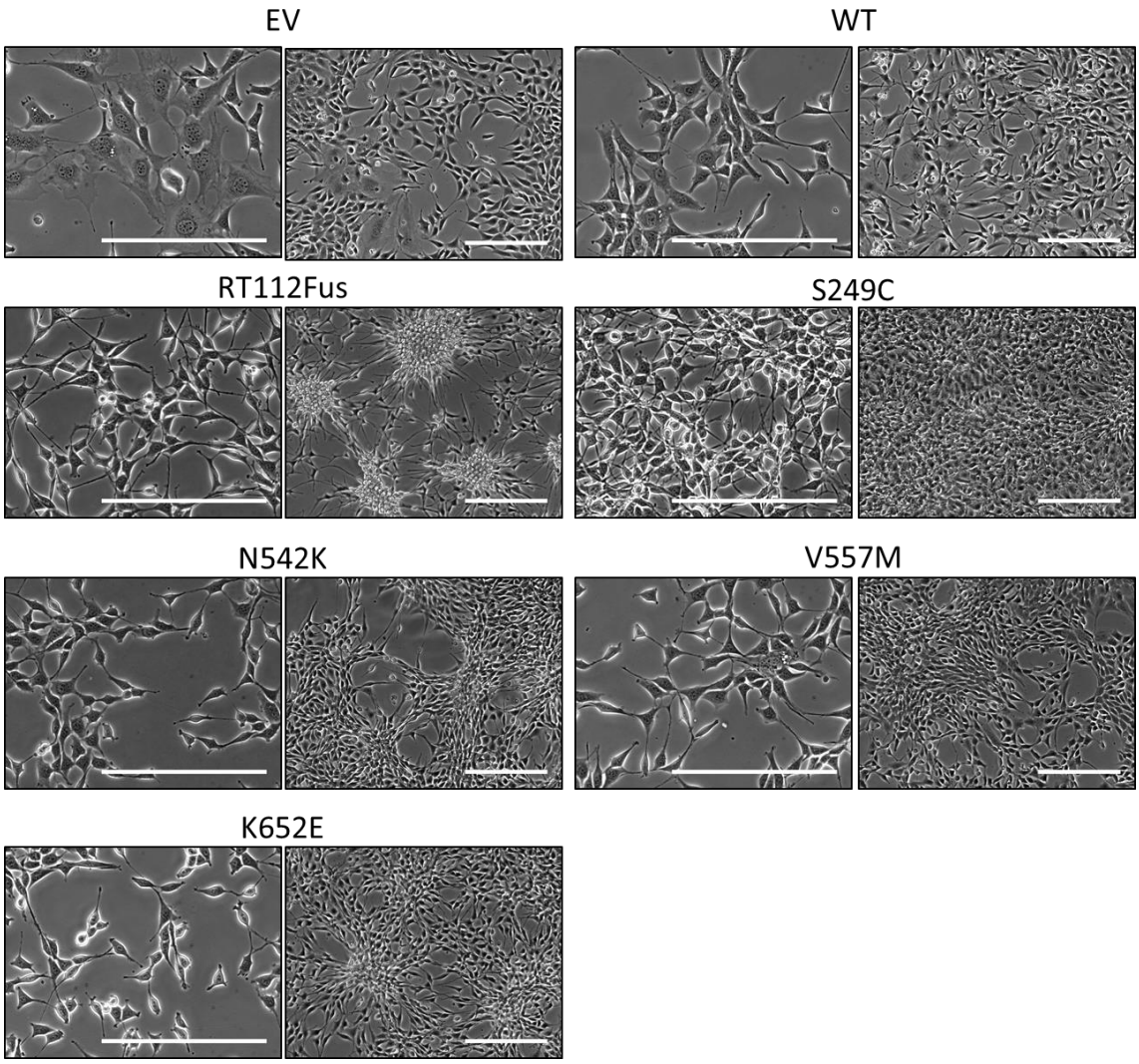

Figure 3.5 – Morphology of stably transduced FGFR3 cell lines obtained from UCL. Evaluation of the morphology of FGFR mutant cell lines highlight that a subset of cells has spindle-like morphology with extended protrusions. Cells with strong transforming potential grew as dense aggregates at high confluency that were visible to the naked eye. Cell lines expressing high levels of mutant FGFR3 (obtained from UCL) are represented here with either low confluency (left image) and high confluency (right image). The scale bar represents 200 μm.

Evaluation of the in-house low expressing mutant cells finds a wide range of different cellular morphologies across the range of distinct FGFR3 mutants (Figure 3.6). For instance, whereas the WT_L cells displayed a flattened morphology, cells expressing the cysteine mutants and $RT112Fus_L$ were characterised by spindle-like cells with long extended filaments, along with the ability to form aggregates that were visible to the naked eye. Interestingly, $S249T_L$ has a distinct morphology from $S249C_L$ despite there being a difference in just

one single amino acid substitution suggesting that the signalling pathways activated by these two mutants were distinct. Similarly, there are morphological differences in K652M$_L$ versus K652N$_L$ and K652T$_L$ although the effects are less apparent compared to S249C$_L$ and S249T$_L$. Moreover, whereas some mutants displayed a similar morphology to the WT$_L$ cells composing a very flat monolayer of cells, without apparent transformation potential such as V557M$_L$ cells, others also displayed different morphologies from the WT$_L$, as well as RT112Fus$_L$. Collectively the similarity in morphology between the RT112Fus cells and the cysteine mutants in the in-house panel of cells showed that these cells are likely to have the highest transformation potential amongst all mutants being studied in this panel.

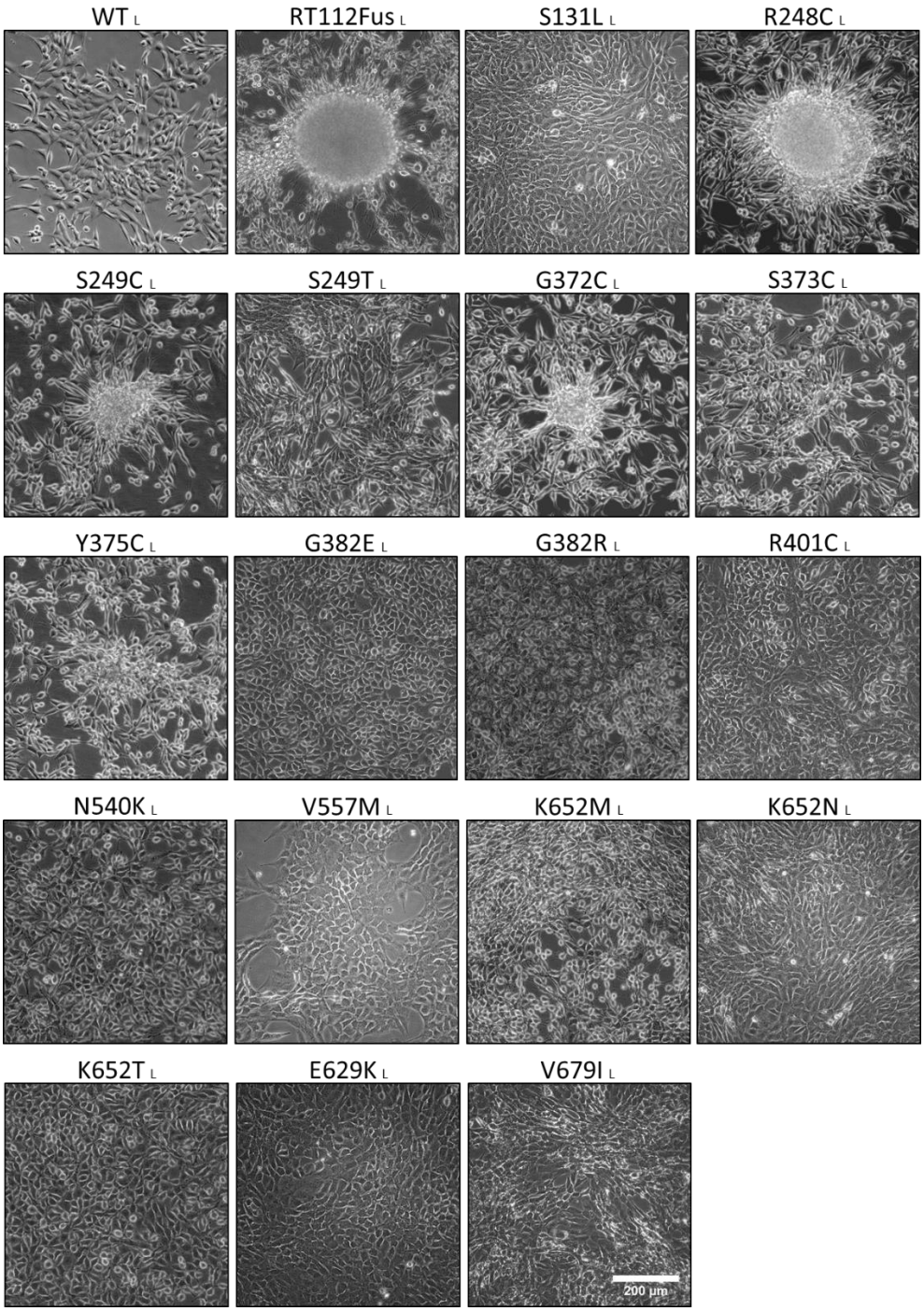

Figure 3.6 – Morphology of stably transduced FGFR3 cell lines generated in-house. Evaluation of the morphology of FGFR mutant cell lines highlight that a subset of cells has spindle-like morphology with extended protrusions. Cells with strong transforming potential grew as dense aggregates at high confluency that were visible to the naked eye. Representative pictures are shown for high confluency cell lines expressing low levels of FGFR3 mutants generated in-house. The scale bar is equal for all pictures and represents 200 µm.

3.5 - Anchorage independent growth of FGFR3 mutants

A subset of FGFR3 mutant cell lines were tested for their ability to grow under anchorage-independent conditions in soft agar, a widely used assay to assess the transformation potential of cell lines *in vitro*, a hallmark of carcinogenesis. This assay tests the ability of cells to grow from single cells into colonies, without a physical support like the walls of a tissue culture plate. The soft agar assay is considered a rigorous test for malignant transformation, where cells that do grow are associated with a more oncogenic phenotype (Borowicz et al., 2014). Rat1A cell lines expressing the FGFR3-TACC3 gene have previously been shown to be able to grow under such conditions, confirming their oncogenic potential (Singh et al., 2012) and thus RT112Fus NIH-3T3 cells were used in my experiments as a positive control.

For this assay, I first assessed the cells expressing high levels of mutant FGFR3 and compared them with the negative control EV and WT FGFR3 expressing cells that are known for not growing colonies in soft agar, and the positive control RT112Fus cell line that was shown before to form colonies in soft agar (Williams et al., 2013). Each cell line was seeded in triplicate in freshly prepared agar and after four weeks, colonies were imaged and quantified for the percentage of surface covered with colonies (Figure 3.7A). All tested mutant cell lines formed numerous colonies in soft agar, which was significantly higher than the EV or WT cells, with RT112Fus, S249C and N542K mutants displaying an average well coverage between 16.5 - 21.3%, and K652E and average of 9.3% well coverage (Figure 3.7B). As expected, there were no colonies visible in the EV control and a very low number of colonies in the WT FGFR3 expressing cells (1.5% well coverage). In order to confirm that the effect seen is due to the presence of the mutant FGFR3, the same assay was done in parallel with the addition of the pan-FGFR inhibitor BGJ398. Treatment with this inhibitor completely abolished the formation of colonies in soft agar for all tested cells confirming that the observed anchorage independence is driven by mutant FGFR3 signalling.

I then evaluated a subset of the low expression mutant FGFR3 expression models that were generated in-house (Figure 3.7C). The extracellular mutations $R248C_L$ and $S249C_L$ were selected due to their transforming morphology (Figure

3.6) and ability to grow as aggregates in monolayers. As a comparator, the $S249T_L$ cell line which displayed a distinct morphology to $S249C_L$ despite being mutated at the same amino acid was also selected for evaluation. Alongside, the WT_L cell line was used as a negative control. The assay was performed only with two biological replicates and so it was not quantified. However, results showed that the two cysteine mutants $R248C_L$ and $S249C_L$ were able to form colonies in soft agar, despite their low expression levels of FGFR3. In contrast, the control mutant cells $S249T_L$ were not able to form colonies in soft agar, suggesting that that the two distinct mutations on the same amino acid S249 showed very different phenotypes, where the cysteine substitution was more transforming than the threonine mutation.

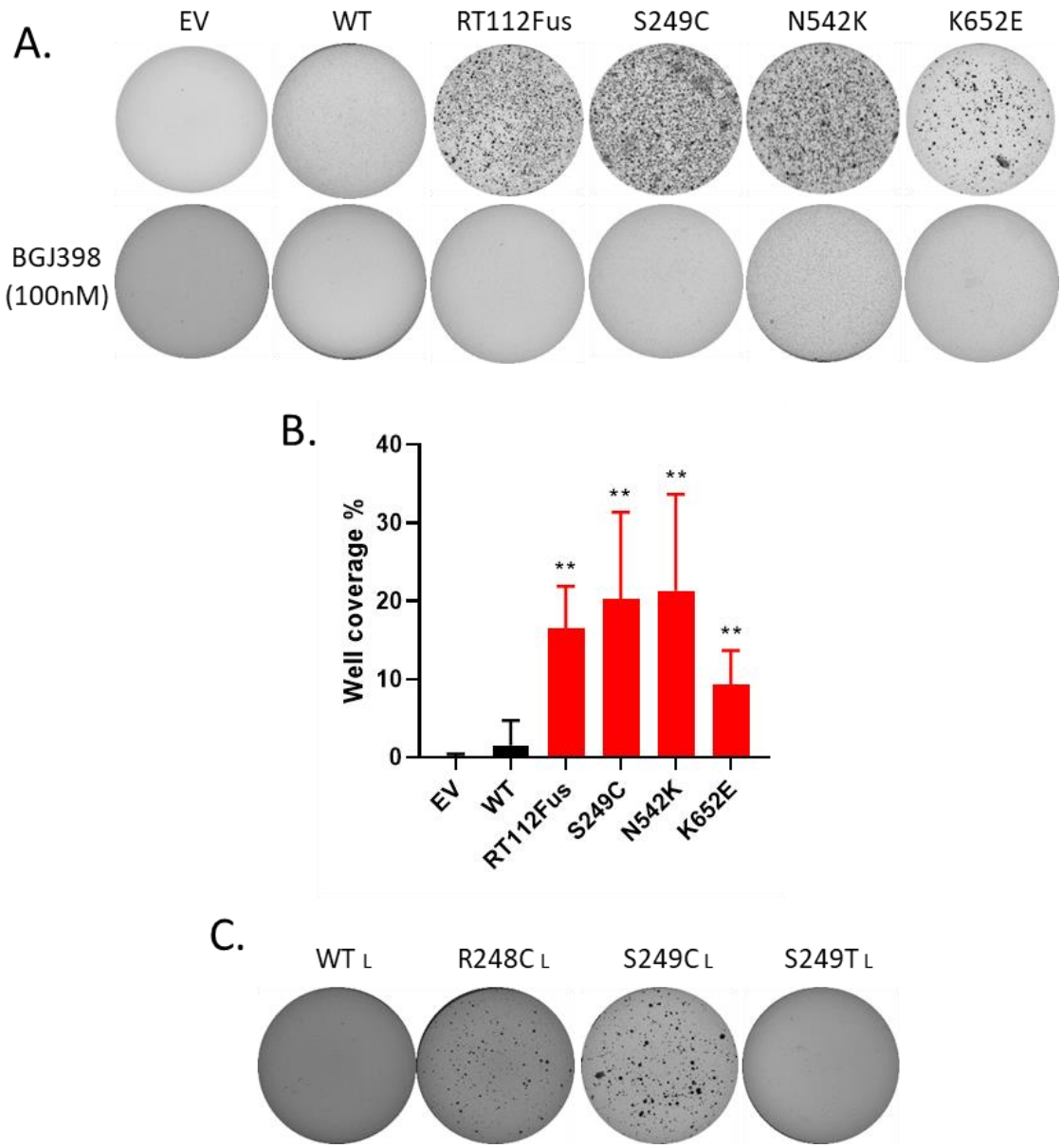

Figure 3.7 – Colony formation of FGFR3 mutant cell lines under anchorage-independent conditions. Cell lines were seeded in soft agar and kept in culture for 4 weeks before staining and quantification. **A.** Representative images of one biological replicate for the high expressing FGFR3 mutants and its negative controls EV and WT cell lines and positive control RT112Fus cell line. The top row represents cells growing in normal media, whereas on the bottom row cells were treated with 100nM of BGJ398. **B.** Quantification of 6 biological replicates of well coverage from the soft agar assay is represented by the bar chart, ** p-value< 0.01. **C.** Representative images of the soft agar assay for a selected subset of low expressing FGFR3 mutants and control WT_L generated in-house.

3.6 - Sensitivity to the pan FGFR inhibitor, BGJ398

It has previously been demonstrated that the total expression levels of mutant FGFR is important in its ability to drive oncogenesis. Notably, sensitivity to FGFR inhibitors has been shown to be confined to bladder cancer cell lines expressing high levels of either FGFR3-S249C or FGFR3-TACC3 (Chell et al., 2013). In this study, Chell et al. evaluated the sensitivity of the FGFR inhibitors AZD4547 and PD173074 in two bladder cancer cell lines 97-7 and 97-29, which express high and low mRNA levels of FGFR3-S249C, respectively. The results indicated that only 97-7, with high levels of mutant FGFR3, showed strong dependency on FGFR3, showing to be sensitive to the FGFR inhibitors in contrast to the 97-29 cell line (Chell et al., 2013).

To assess if the NIH-3T3 models obtained from UCL and generated in-house were dependent on FGFR3 signalling, I undertook a systematic investigation of the sensitivity of the FGFR3 mutant cell line models towards the FGFR inhibitor BGJ398. Each cell line in the panel was subjected to drug treatment to evaluate the dose dependent effects of BGJ398 on cell viability. Each cell line was seeded in 96-well format plates on day 1, following inhibitor treatment after 24 hours with serial dilutions of BGJ398. After a further 72 hours in culture cell viability was measured using the luminescence CTG assay. The resulting data was normalised against the vehicle DMSO control to plot the dose response curves (Figure 3.8). The data was also used to calculate the half maximal inhibitory concentration (IC_{50}) value, which corresponds to the dose of inhibitor required to inhibit cell viability by 50% when compared to the vehicle-treated counterpart.

Treatment of the high expressing mutant cells resulted in a distinct separation in the dose response curves between the mutants and the controls, EV, WT and gatekeeper mutant V557M (Figure 3.8A). The dose response curves showed a shift towards the left for all three mutants S249C, N542K and K652E and fusion RT112Fus, indicating a higher sensitivity of these cells towards BGJ398 than the controls. The IC_{50} have mean values ranging from 0.2 µM to 0.4 µM for the mutants and fusion, and an average of 1.7 µM for the control WT and EV, showing a significant difference of around 5-fold between controls and mutants. As

anticipated, the gatekeeper mutant V557M which is unable to bind to the drug had an average IC_{50} of 1.3 µM which is similar to the controls.

In contrast, when the same drug treatments were administered to the low mutant FGFR3 expressing cell lines that were generated in-house, this therapeutic window between the WT and mutant receptors was lost (Figure 3.8B). Here, the dose response curves were very similar across the panel, without significant differences observed between mutants and controls. The mean IC_{50} values range from between 1.5 µM and 3.1 µM. This data is consistent with the previous study by Chell et al., and demonstrates that only cells which express high levels of mutant FGFR3 harbour a strong dependency on FGFR signalling (Chell et al., 2013).

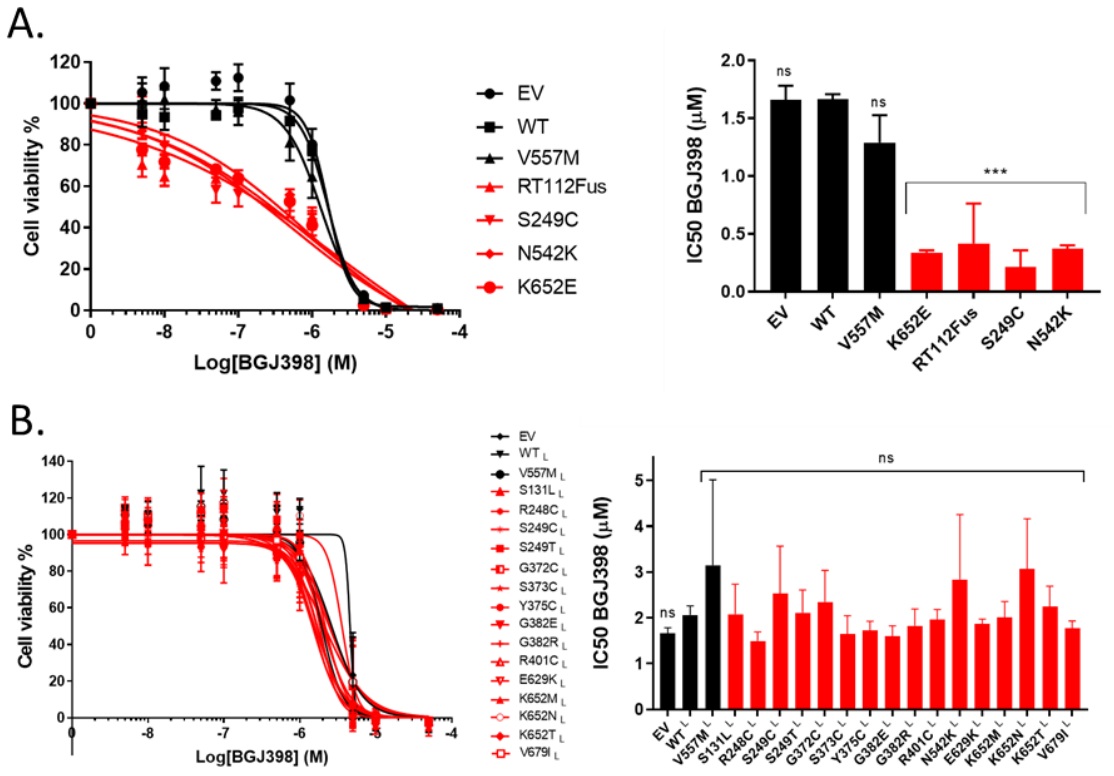

Figure 3.8 – Sensitivity of FGFR3 cell lines towards BGJ398. Cells were seeded in 96 well plates and treated with nine serial dilutions of BGJ398 across a broad range of drug doses as stated, for 72h. Viability was measured with CTG assay and normalised to the vehicle-treated DMSO control. IC_{50} values were calculated using four-parameter non-linear regression analysis and statistical analysis was performed with one-way ANOVA multiple comparisons against the WT of each panel with GraphPad Prism software. Curves represent the mean of three biological replicates and the bar charts are the mean IC_{50} calculated from those replicates. **A. B.** Drug dose curve (left) and IC_{50} values (right) for the high (A) and low (B) expressing FGFR3 mutant cells and controls. *** p-value< 0.0001; ns- not significant.

3.7 - Effect of FGFR3 mutations on the cell signalling

The impact of FGFR3 mutations on downstream cellular signalling was also investigated by western blotting. As distinct mutations in different regions of the receptor may have unique consequences on the constitutive activity of FGFR3, the basal levels of the main downstream signalling effectors of FGFR3 in the absence of ligand were investigated and compared against the controls EV and WT. Given that the BGJ398 drug response data previously described in Figure 3.8A showed that only the high expressing FGFR3 panel of cell lines harboured a dependence on FGFR signalling, I focussed on these cell lines for these signalling experiments. Cells were seeded in media with 10% FBS and harvested 48 hours later. Lysates were run on a gradient gel where proteins were separated prior to immunoblotting for total (t) and phospho (p) proteins with antibodies recognising components of the MAPK pathway (tErk/ pT202/Y204 Erk), PI3K/Akt pathway (tAkt/ pS473 Akt), Src pathway (tSrc/ pY416 Src) and STAT3 pathway (tSTAT3/ pY705 STAT3) (Figure 3.9). Despite multiple attempts at optimising phospho-specific FGFR3 antibodies as well as immunoprecipitation experiments to evaluate the phosphorylation levels of FGFR3, I was unable to successfully measure the phosphotyrosine status of FGFR3. As an alternative, I have used the pY1000 antibody, which generally recognises phosphorylated tyrosine residues in cell lysates as a readout of the levels of the tyrosine residues phosphorylated in the same mass range as FGFR3.

All mutant cells showed stronger tyrosine phosphorylation (pY1000 antibody) at the same MW as FGFR3 (~130 KDa) compared to the EV cells, indicating that the bands shown by pY1000 is likely to be due to FGFR3 phosphorylation. STAT3 phosphorylation was reduced in the FGFR3 mutants and RT112Fus expressing cells when comparing to the EV and WT FGFR3 controls, however this decrease was also accompanied by a decrease in the total levels of STAT3, suggesting that expression of FGFR3 mutations leads to the suppression of the STAT3 pathway via the downregulation of the total STAT3 protein levels. Src tyrosine phosphorylation was upregulated in all FGFR3 mutants and the fusion RT112, comparing to the controls EV and WT indicating that constitutive activation of FGFR3 mutations leads to increased activation of the Src pathway. In contrast,

there were no apparent differences in Akt and Erk activation across the panel of different cell lines. Overall, these comparisons suggested that mutations in FGFR3 as well as translocations of FGFR3 with TACC3 gene results in constitutive activation of the receptor and have an impact in the main downstream signalling effectors, namely an increase in Src pathway activity and a downregulation of total STAT3 levels.

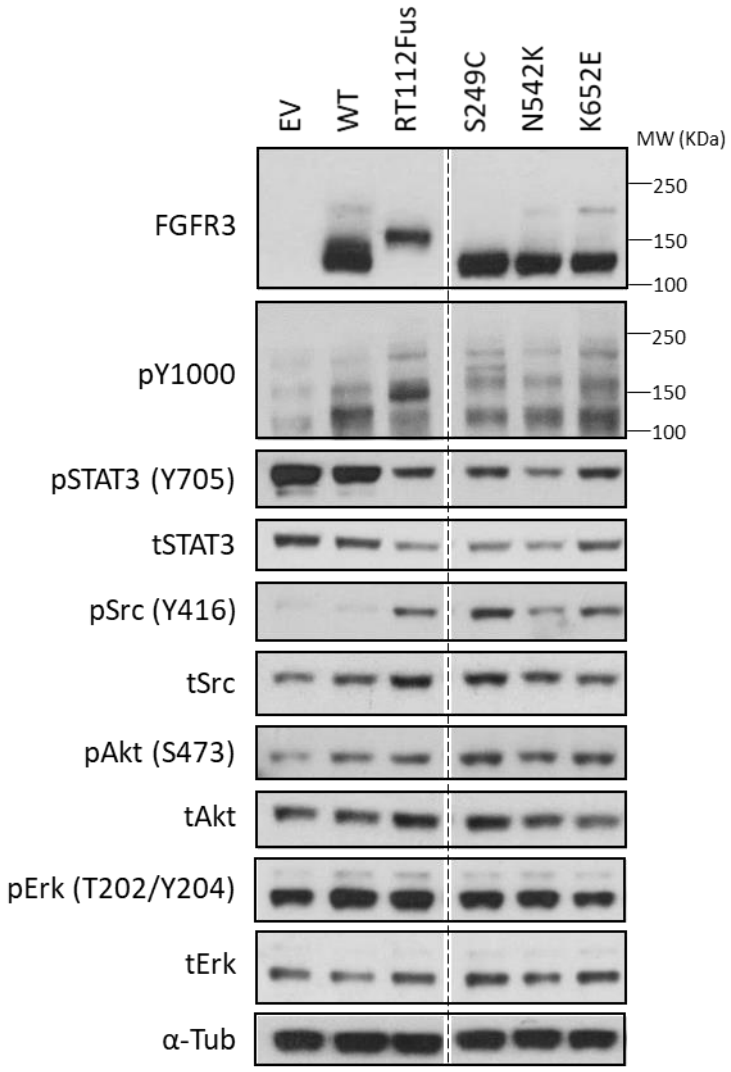

Figure 3.9 – Comparison of basal levels of expression of the major FGFR3 downstream signalling components in the high expressing FGFR3 mutant cell line panel. Cell lines were seeded in full growth medium and cells lysed after 48h in culture, when cells were approximately 80% confluent. Proteins were analysed by western blotting with antibodies against total proteins or phosphosite-specific proteins as indicated. Tubulin was used as a loading control.

3.8 - Effect of ligand stimulation on the downstream signalling of FGFR3 mutants

To gain further insights about the signalling pathways activated by FGFR3 mutants, I assessed the phosphorylation of the key downstream pathways (MAPK, PI3K/Akt, Src and STAT3) upon receptor activation by the addition of the FGF1 ligand. Confluent cells were starved for at least 16h under serum starvation conditions to avoid any confounding signalling arise from the addition of FBS and, subsequently treated with 25 ng/mL of FGF1 in fresh serum free media prior to lysis at 5, 10 and 30 minutes. For each cell line, lysates were also prepared at the 0 minute (no ligand time point). Lysates were resolved and analysed by western blotting (Figure 3.10).

The data showed that FGF1 stimulation did not have an impact on the total levels of FGFR3 at the time points analysed, but it did increase the levels of tyrosine phosphorylation (pY1000) in the same mass range as FGFR3 for the EV and WT cells but not the FGFR3 mutants and fusion expressing cells. The mutants S249C, N542K and K652E and fusion presented the same tyrosine phosphorylation levels across all time points despite ligand stimulation, and these were higher than the non-stimulated EV and WT cells. There was also a marked decrease in STAT3 tyrosine phosphorylation activity after 30 minutes of stimulation in all cell lines. A similar outcome was observed for Akt phosphorylation for RT112Fus, K652E and to a less extent S249C, where FGF1 stimulation resulted in reduction of Akt phosphorylation after 5 minutes. An opposite effect was however seen for the EV cells, where pAkt increased after 5 minutes and was maintained up to 30 minutes. In turn, Src tyrosine phosphorylation activity was not affected in any of the cell lines. Interestingly, phosphorylation of Erk activity was significantly increased for all cell lines except the fusion which remained invariant to ligand stimulation with FGF1. Although S249C also showed pErk increase at 5 minutes, this effect is attenuated to almost basal levels upon 30 minutes of stimulation.

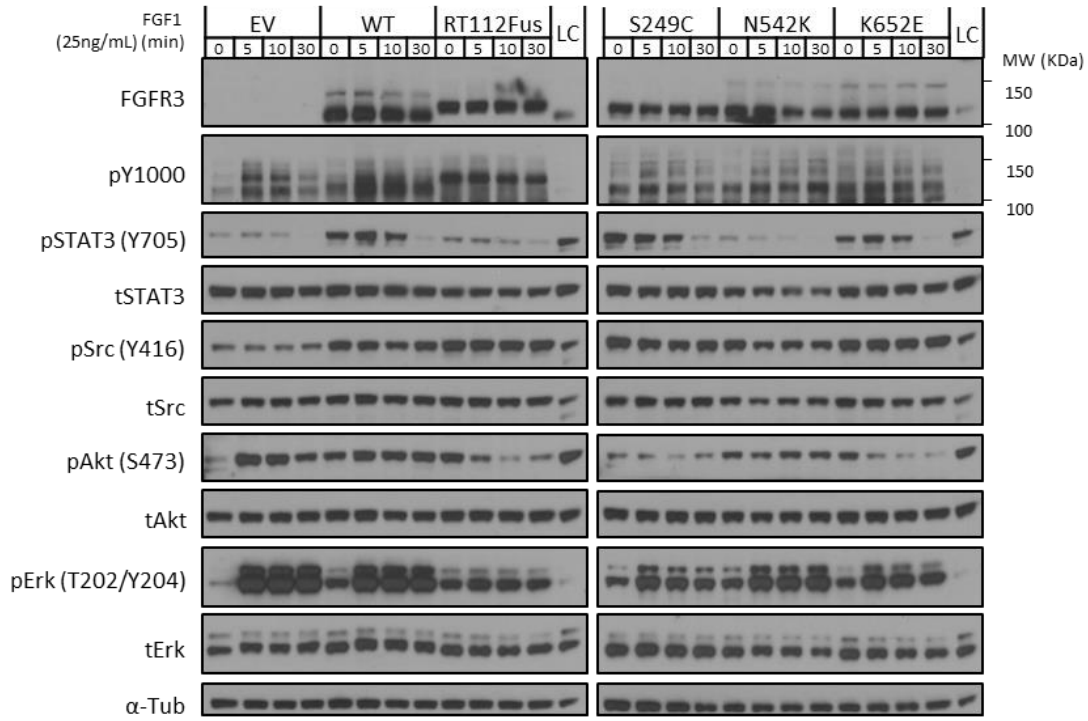

Figure 3.10 – FGFR3 downstream signalling after ligand stimulation with FGF1 in the high expressing FGFR3 mutant cell line panel. Cell lines were seeded in full growth medium and starved after 24h for at least 16h with medium without FBS. Cells where then stimulated with 25ng/mL of FGF1 for 5, 10 and 30 minutes. As a comparator, the same panel of cells were serum starved but not subjected to ligand stimulation and are here represented by the 0 min time point. Cells were lysed and proteins were analysed by western blotting with antibodies against total proteins or phosphosite-specific proteins as indicated. Tubulin was used as a loading control. The loading control (LC) is here used to compare blots run at the same time but in separate gels.

3.9 - Discussion

In this chapter, a panel of cancer-associated FGFR3 mutants was generated and stably transduced into NIH-3T3 cells, along with the respective controls. Engineered cell lines were subdivided into a group of cells expressing high levels of FGFR3 mutants (obtained from UCL) and a group of cell lines expressing low levels of FGFR3 mutant ($_L$). Cancer-associated mutations were then characterised for their transformation and oncogenic potential in culture and the downstream pathways were investigated under basal and ligand stimulated conditions in the subset of high expressing FGFR3 mutant cells.

In the extracellular region of FGFR3, the hotspot S249C is the most frequent mutation in FGFR3-driven cancers and is a well validated oncogenic driver as previously described (Di Martino et al., 2009). Consistent with these reports, I have confirmed its oncogenic activity by demonstrating that NIH-3T3 cells that express this S249C mutant are able to form colonies under anchorage-independent conditions in both the high and low expressing mutant. Interestingly, all the cysteine mutants ($R248C_L$, $S249C_L$, $G372C_L$, $S373C_L$ and $Y375C_L$) showed a morphology that was more similar to known transforming mutants (e.g. $RT112Fus_L$) such as a spindle cell morphology and the ability to form aggregates at high confluence. This was similarly observed in the soft agar functional assay, where cysteine variants $R248C_L$ and $S249C_L$ showed a strong ability to confer anchorage independent growth while $S249T_L$ mutant did not. This demonstrates that there is a variant specific effect where substitution of a cysteine selected amino acid within the extracellular domain of FGFR3 is a strong driver of oncogenicity. This observation is in line with the idea that the cysteine variants promote the formation of covalent disulphide bonds between monomers, leading to the constitutive dimerisation of the receptor in a ligand-independent manner and consequently increased and uncontrolled activation of FGFR3 (Avis et al., 1998).

Mutations in the TM domain ($G382E/R_L$) or JM intracellular region ($R401C_L$) of FGFR3 as well as mutations $E629K_L$ and $V679I_L$ on the KD did not seem to exert a particular transforming phenotype in this model, indicating that they might not be as oncogenic as some of the other mutants. In contrast, the KD mutants K652E and N542K were shown to be capable of forming colonies in the soft agar assays with a similar capacity as the positive control RT112Fus. K652 is the most frequently mutated residue in the FGFR3 KD in cancer and is known for its ability to transform cells in culture and grow in soft agar (Di Martino et al., 2009). N542K has also been described in the literature to induce a transforming morphology and grow in soft agar (Patani, 2016). This effect seen for N542K and K652E can be associated with their high baseline kinase activity. In *in vitro* kinase purified assays, it has been shown that these two mutants harbour a 45-fold increase in baseline kinase activity when compared to WT FGFR3 (Patani, 2016). This is in line with historical data that demonstrates that the kinase activity of K652E is a

100-fold above that of WT FGFR3 (Webster et al., 1996). I further showed that the anchorage independent growth was driven by mutant FGFR3 signalling given that the addition of the pan-FGFR inhibitor BGJ398 completely abolished the capacity of the FGFR3 mutant cell lines to grow in soft agar. Taken together, these results indicate that different mutants display distinct levels of transformation. This is likely to be the result of the specific structural effects that each mutant confers on the receptor, with some mutations driving constitutive dimerisation of the receptor and other mutations harbouring high basal constitutive receptor activation.

In the FGFR3 inhibitor BGJ398 dose response experiments, I showed that there is a correlation between high FGFR3 mutant expression and sensitivity to BGJ398. My results demonstrate that the high expressing mutant cell lines were more dependent on FGFR3 signalling as illustrated by their higher sensitivity towards BGJ398. In contrast, the low expressing mutants generated in-house showed similar levels of sensitivity to the WT FGFR3 and EV cells. These results were consistent with previously published data, where low expression of FGFR3-S249C in the human bladder cancer cell line 97-29, did not confer a strong FGFR3 dependency, whereas the same mutation expressed at higher levels in the human bladder cancer cell line 97.7 was associated with a strong dependency on FGFR3 signalling (Chell et al., 2013). In general, the high expressing mutants displayed a response that better mimics the results reported in the literature, with a significant increased sensitivity to FGFR inhibitors observed for all the cancer-associated mutants and fusion when comparing to the WT FGFR3 (Guagnano et al., 2011; Lamont et al., 2011). Moreover, the V557M gatekeeper mutant response was consistent with the expected results (Chell et al., 2013), where its inability to bind to kinase inhibitors resulted in a low sensitivity towards the ATP-competitor BGJ398, with an IC_{50} similar to the WT control. Despite different levels of FGFR3 expression having a clear impact on the sensitivity towards FGFR inhibitors, the transforming profile of some strong oncogenes such as S249C was not affected by its expression levels in the soft agar assay where both the low and high expressing cell lines formed colonies in an anchorage independent manner. Therefore, the panel of low expressing mutants may be suitable for studying the functional and molecular effects of

strongly oncogenic mutants, whereas high expressing mutants may be used to explore the downstream dependencies of distinct mutant variants including dependencies to FGFR3 inhibitors.

Western blot analysis of the basal signalling in the high expressing mutant FGFR3 cell lines showed that FGFR3 mutants had distinct signalling profiles compared to WT FGFR3. For instance, there was a marked increase in Src tyrosine phosphorylation in all the mutants and fusion receptors when comparing to the WT FGFR3. This finding suggests that the FGFR3 mutants activate a different signalling network to the canonical WT receptor which may have implications on an altered dependency on the Src pathways which will be explored in more detail in subsequent chapters. This data highlights the need to further examine the role of each mutation in influencing downstream signalling networks in order to drive oncogenesis, which may create new pathway dependencies that can be targeted by therapeutics. Src activation had been seen before in the context of FGFR3 mutants in NIH-3T3 cells (Di Martino et al., 2009). This event was investigated in bladder cancer cell lines expressing the fusion FGFR3-TACC3 in the presence of the Src inhibitors such as dasatinib, where dasatinib was shown to have anti-cancer effects in these cells and in mouse model xenografts of the same cell lines (Levitt et al., 2010). However, other studies have shown that Src inhibition promote the ability for bladder cancer cells to migrate and metastasise (Thomas et al., 2011). Moreover, a phase II clinical study (NCT00706641) have not found any benefit for the use of dasatinib alone as a therapy for muscle-invasive urothelial carcinomas (Hahn et al., 2016). Src had also been associated with the activation and signalling modulation of FGFR1 (Sandilands et al., 2007), and for that reason might also play an important role in the regulation of FGFR3 mutants which will be the subject of experiments described in subsequent chapters.

Upon evaluation of the signalling profiles of the panel of cell lines stimulated with the FGF1 ligand, my data highlighted two interesting aspects. The first is that the majority of FGFR3 mutants did not respond to the addition of FGF1 with an increase in pY1000 signal, suggesting the constitutive activation of these mutant receptors is not impacted by the addition of ligand at least at the level of receptor tyrosine phosphorylation. The second observation is that FGF1 ligand stimulation

induced an increase in pY1000 signal in the ~130kDa mass range of FGFR3 in the EV cells, indicating that there are cellular proteins that are tyrosine phosphorylated at the same MW as FGFR3 on the EV control cells. As the NIH-3T3 cells do not express endogenous FGFR3, these results may indicate that there are other FGFR family members that are activated by FGF1. NIH-3T3 cells have previously been shown to express the FGFR1 receptor which also binds to FGF1 which may account for the increase in receptor phosphorylation levels observed in the EV cells (Citores et al., 1999). The activation of FGFR1 may therefore mask the effects of FGFR3 WT and mutant signalling readouts in these ligand stimulation experiments. For instance, the upregulation of pErk across the cell line panel including the EV cells may be indicative of an FGFR1 rather than a FGFR3 effect.

Collectively, my experiments demonstrate that a subset of FGFR3 mutants are oncogenic and harbour constitutive activity that is not responsive to the addition of FGF1. It also suggests that the Src pathway may be an important signalling node that drives the oncogenic signalling downstream of mutant FGFR3. These models will be used to investigate the signalling pathway dependencies activated by mutant FGFR3 in subsequent chapters.

Chapter 4

Functional mechanisms and dependencies of FGFR3 mutants

4.1 - Introduction

Activating cancer-associated FGFR3 mutants have been described as good candidate targets for therapy, with *in vitro* and *in vivo* preclinical studies showing a good response towards a number of different FGFR3 inhibitors (Tomlinson et al., 2007; Touat et al., 2015). However, to date only one selective FGFR inhibitor has been licensed by the FDA (Tony et al., 2019). Clinical trials that evaluate FGFR inhibitor efficacy often do so in a range of different cancer types that encompass a large number of different FGFR family members and genetic alterations. Collectively, there is clinical evidence that patients with the best clinical responses are those with FGFR1 amplifications, FGFR2 fusions or FGFR3 mutations (Dienstmann et al., 2014; Javle et al., 2018). However, it should be noted that although patients with FGFR3 mutations display partial responses to FGFR inhibitors, tumours often relapse due to drug resistance (Nogova et al., 2017). Moreover, clinical trial data indicate that FGFR inhibitor response rate is linked to the specific types of FGFR3 alterations, with patients harbouring extracellular mutations responding better than KD mutations (Pal et al., 2018).

Therefore, there is a need to find new ways to better target FGFR3 cancer associated mutations to overcome acquired resistance to selective FGFR inhibitors and achieve durable responses or improve the efficacy of these inhibitors in mutants that are intrinsically resistant. In this chapter, the high expressing FGFR3 mutant models were subjected to further characterisation to investigate mutant-specific sensitivity to the FGFR inhibitor BGJ398 and other inhibitors of interest, utilising cell viability assays, colony formation assays and spheroid formation assays (Figure 4.1). In parallel, cell line models were assessed for their downstream signalling profiles to better characterise the temporal cellular signalling responses to FGFR inhibitor treatment (Figure 4.1).

There is currently a gap in our knowledge of the signalling pathway dependencies associated with FGFR3 mutations in cancer. A better understanding of the oncogene addiction pathways attributed to different FGFR3 mutations may reveal new candidate targeted therapies which can delay the acquisition of FGFR inhibitor resistance and achieve long-term durable drug responses.

To identify these vulnerabilities and key signalling pathways responsible for conferring oncogene addiction in distinct FGFR3 mutants, a targeted small molecule inhibitor screen and a Luminex assay were used to characterise the FGFR mutant cell line panel. For the targeted small molecule inhibitor screen, a library of pharmacological compounds designed to disrupt a broad range of different signalling pathways was employed to probe the major pathway dependencies in different FGFR3 mutant expressing cells. This analysis was aimed at identifying mutation-specific signalling effectors that are necessary for survival in the context of FGFR mutants but not in WT FGFR3 control cells. The Luminex assay is an orthogonal approach employed to determine the levels of basal activity of major downstream signalling effectors driven by mutant FGFR3. It is a technique where colour-coded beads are coated with analyte-specific capture antibodies to provide a readout of the analyte levels in cell lysates. This technique has the potential to assay a larger number of downstream effectors than the conventional western blotting and was employed in my studies as a tool aimed at detecting key differences on the activated signalling pathways in FGFR3 mutants.

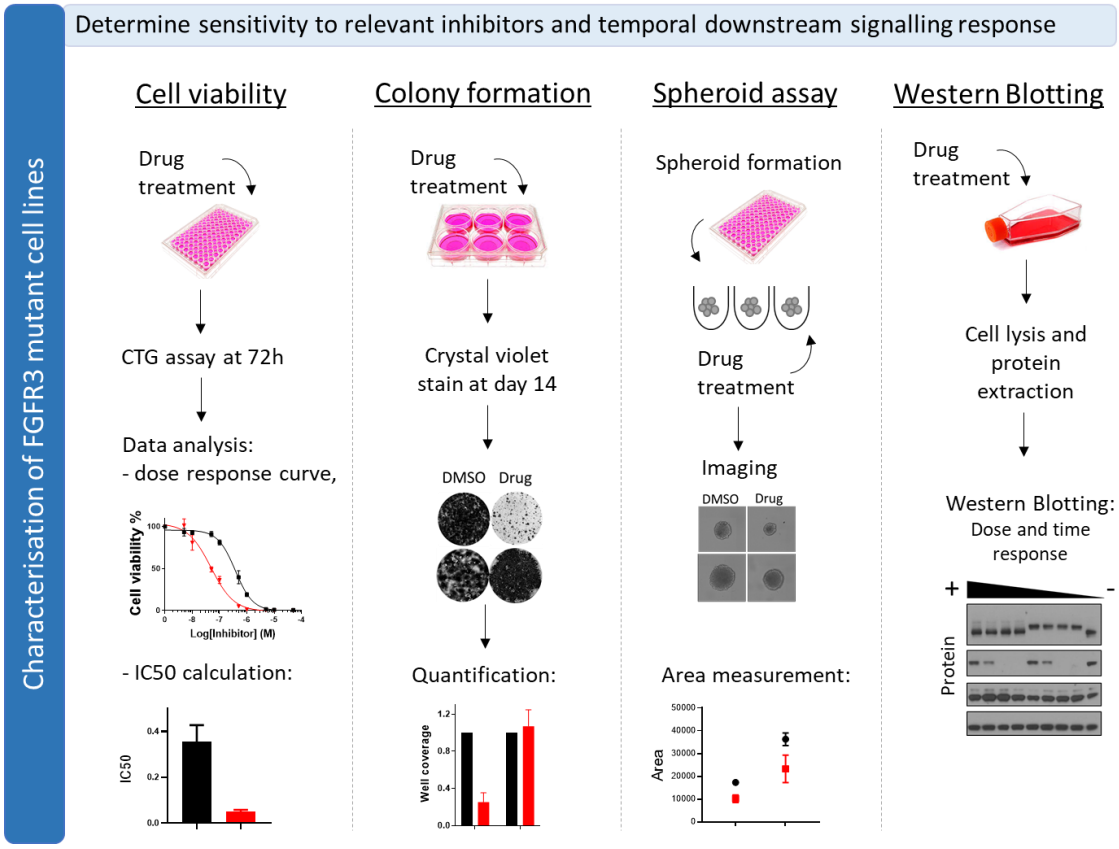

Figure 4.1 – Diagram of the proposed experiments for the characterisation of FGFR3 mutant cell lines. Different techniques were utilised to characterise mutant FGFR3 cell lines sensitivity and dependencies.

4.2 - BGJ398 is ineffective in a subset of FGFR3 mutations in long-term survival assays

The FGFR3 mutant cell models were further characterised for their survival and growth properties in the presence of BGJ398. While 72 hours cell viability assays described in chapter 3 (Figure 3.8A) showed that BGJ398 had a clear therapeutic window between the FGFR3 mutants and controls, it is unknown if such FGFR inhibitors achieve durable effects upon long-term drug exposure. To investigate this further, colony formation assays were performed to evaluate the efficacy of the FGFR inhibitor in long-term culture over the course of 2 weeks. For this assay, FGFR3 mutant cells, RT112Fus expressing cells and three controls EV, WT and gatekeeper V557M cell lines were seeded in 6-well plates and treated with 1 µM and 2 µM of BGJ398 after 24 hours. Media was replenished with fresh drug every

3 days. Cells that are sensitive to BGJ398, die over time and are washed out upon media change. The survival fraction of cells after 2 weeks was stained with crystal violet for quantification (Figure 4.2A, C). After 14 days in culture the number of colonies for 1 μM of BGJ398 was high for all cell lines, with no significant difference when comparing to the vehicle-treated DMSO control. There was no statistical difference between the mutants, fusion and WT FGFR3 cells at this dose, with a mean well coverage between 76-93 % for the mutants and fusion and a mean of 94-99 % for the three controls. Despite similarly high well coverage across all the cell lines in the panel, BGJ398 had an impact on the morphology of all mutants compared to the WT FGFR3 (Figure 4.2B). In particular, RT112Fus and S249C cell lines were found to be flatter and with an enlarged cytoplasm when compared to the DMSO control or the WT FGFR3 (Figure 4.2B). With an increased dose of drug (2 μM), there was a significant reduction in colony formation for all cell lines apart from the WT, when compared to the DMSO counterpart, with well coverage dropping to a mean of ~20 % (Figure 4.2C). It should be noted that this reduction in colonies was also observed in the negative control gatekeeper V557M, suggesting that the reduction in colony formation observed in the panel of cell lines is likely due to the non-specific toxic effects of the inhibitor at this higher dose (Figure 4.2C).

Spheroid-based assays were used as a measure for the ability of cells to grow under anchorage-independent conditions, a hallmark of cancer. In contrast to soft agar assays where single cells are seeded in an agarose matrix, in spheroid-based assays, a large number of cells are seeded into wells with a low-adherent surface to form spheroids. Such spheroid cell cultures are thought to better recapitulate the three-dimensional properties of tumours including maintaining a gradient of hypoxia, nutrients, metabolism and proliferation between its core and surface (Hirschhaeuser et al., 2010). It has previously been shown from gene expression studies that spheroids can more accurately mimic clinical expression profiles than those observed in monolayer cultures (Schmidt et al., 2016). To evaluate the effects of BGJ398 in spheroid cultures, cells were seeded into 96-well low-adherent plates and grown in culture for 24 hours to allow for spheroid formation prior to treatment with BGJ398. After 72 hours of treatment, brightfield images of the spheroids were captured using the Celigo high content microscope,

and the largest cross-section area of the spheroid was measured as a readout for their growth (Figure 4.3A). Cells in the vehicle DMSO control were found to display different propensities to growth in the spheroid assays. Spheroids for RT112Fus and K652E formed significantly larger spheres than the WT FGFR3 control, with a 2-fold and 1.6-fold increase in cross-sectional area respectively (Figure 4.3B). The EV cells formed the smallest spheroids followed by the V557M and WT. When treated with BGJ398, the FGFR mutant and fusion spheroids failed to grow resulting in the same baseline cross-sectional area as the EV cells. This data demonstrates that the growth effect observed under DMSO conditions is driven by FGFR3 signalling. As expected, the reduction in spheroid cross-sectional area is observed across the cell line panel except for the EV and V557M gatekeeper mutation (Figure 4.3C).

Overall, these experiments have shown that while BGJ398 was effective at reducing spheroid growth in the FGFR3 mutant expressing cells under low attachment conditions in short-term 72 hours assays, similar to the monoculture experiments described in chapter 3, this effect is lost when undertaking longer-term colony formation assays. These data indicate that consistent to the lack of durable responses observed in patients that have been treated with FGFR inhibitors, BGJ398 is ineffective in long-term cellular assays highlighting the need for better strategies to overcome resistance to this class of drugs.

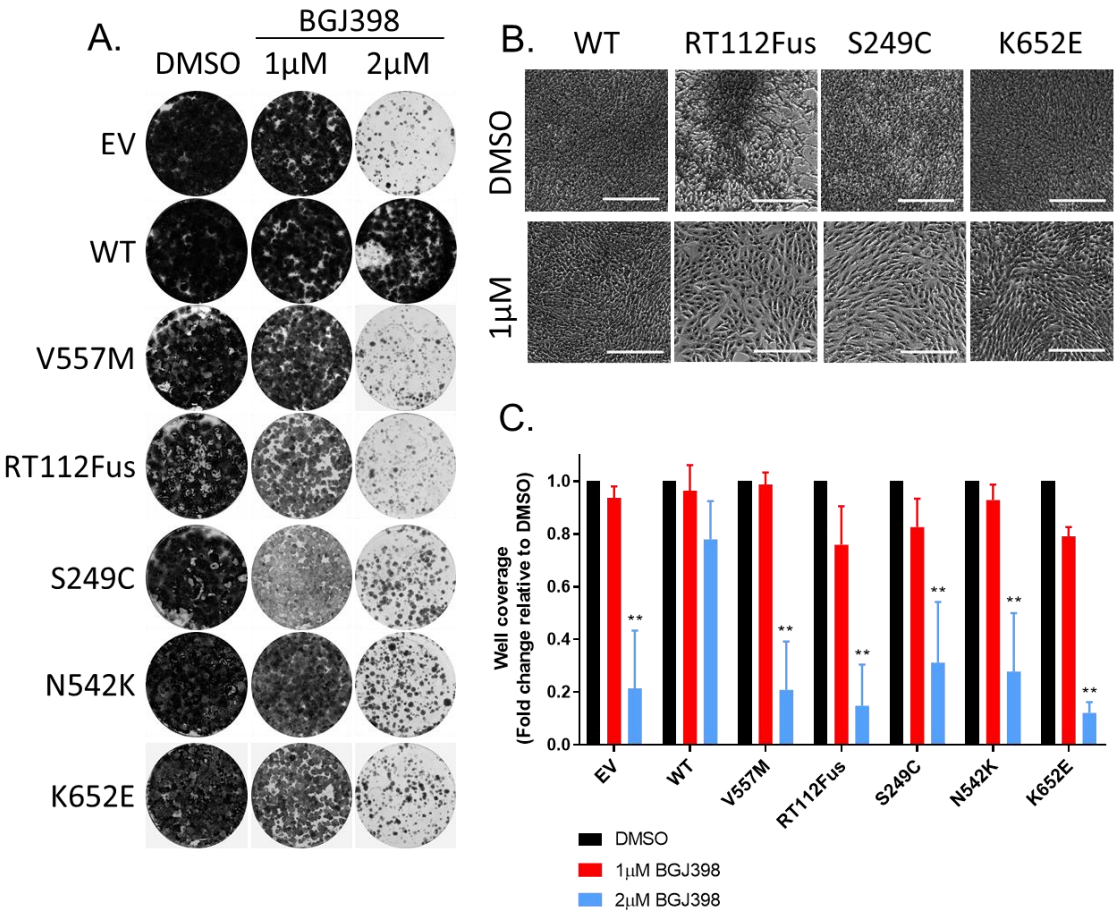

Figure 4.2 – Effect of BGJ398 in long-term colony formation assays. FGFR3 expressing cells and controls were seeded in 6-well plates at low density (1000 cells/well) and treated with 1µM and 2µM of BGJ398 for 14 days. **A.** Representative images of colony formation staining with crystal violet. **B.** Microscopic images showing the morphologic changes associated with BGJ398 treatment. Images were acquired from the colony formation plates on day 14 before staining **C.** Colony formation quantification. The percentage of the wells being covered by cells was calculated using imageJ software. Results are normalised for each cell line relative to its vehicle-control DMSO. Statistical analysis was performed with two-way ANOVA compared to the WT. ** p-value< 0.01. (n=3 biological replicates).

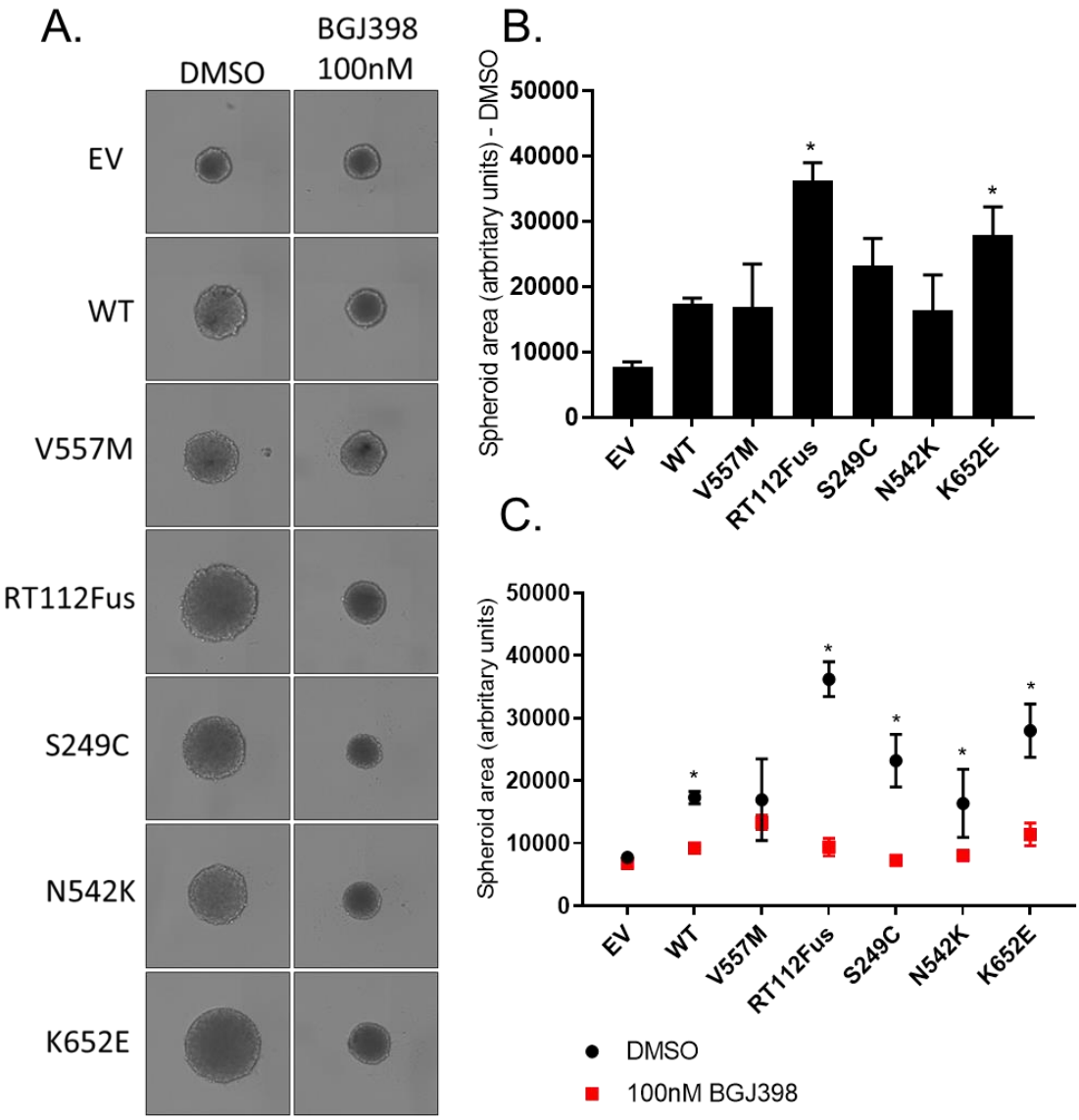

Figure 4.3 – Growth potential of FGFR3 expressing cell lines under anchorage-independent conditions in spheroid assays. 1000 cells were seeded on low-adherent 96-well plates and treated with DMSO vehicle or BGJ398 for 72 hours before scanning for cross-sectional area quantification. **A.** Representative images of spheroids after 72 hours of treatment with 100 nM of BGJ398 and DMSO control. **B.** Spheroid area for cell lines treated with DMSO vehicle control was calculated using imageJ and plotted for comparison. **C.** Spheroid area is here shown when comparing to spheres treated with 100nM of BGJ398 or DMSO. Statistical analysis was performed on GraphPad Prism with one-way ANOVA for B relative to the WT and two-way ANOVA for C between BGJ398 and DMSO control treatments for each cell line. * p-value< 0.05. (n=3 biological replicates).

4.3 - FGFR3 mutants mediate their signalling and functional effects through the MAPK pathway

To understand the signalling pathway alterations that are modulated as a result of FGFR3 blockade by BGJ398, western blotting analysis was performed in the cell line panel upon being subjected to different drug doses and time points. Four major signalling nodes (Src, STAT3, Akt and Erk) were investigated along with total levels of FGFR3 and phosphotyrosine using the pY1000 antibody. To test the effect of different doses of BGJ398, FGFR3 mutant cells and the relevant controls were seeded on day 1 and treated on day 3 when confluency was ~80 %. Cells were treated for 6 hours with DMSO vehicle and 10 nM, 100nM and 1 μM of BGJ398. Cells were harvested for protein extraction, resolved and subjected to immunoblotting. Treatment with BGJ398 led to a decrease in the phosphotyrosine levels in the WT FGFR3 and FGFR3 mutant cell lines but not the EV and V557M gatekeeper cells (Figure 4.4A). This result is consistent with the view that the phosphorylation signals being detected by pY1000 in this mass range is likely to be representative of FGFR3 tyrosine phosphorylation. Moreover, it was noted that at the highest doses of BGJ398, there was a reduction in the total levels of FGFR3 in all cell lines including the V557M and WT cells. Interestingly, the only downstream signalling node that consistently showed a dose dependent response upon drug treatment is pErk. Phosphorylation of Erk was decreased when the mutant FGFR3 cells were treated with BGJ398 compared to the DMSO vehicle but not in the three EV, WT FGFR3 and V557M controls (Figure 4.4A). In contrast, pSrc levels remained invariant to the treatment with BGJ398, although the phosphorylation levels of this signalling node were much higher in the FGFR3 fusion and mutants compared to the EV and WT FGFR3 cells.

To examine the temporal effects of BGJ398 treatment on cell signalling, cell lysates were collected at 1 and 6 hours after treatment with 100 nM BGJ398 and subjected to western blot analysis (Figure 4.4B). The data shows rapid inhibition on pErk levels at 1 hour which is partially restored at 6 hours in the RT112Fus, S249C and K652E mutant cell lines. The same effect was also visible but to a lesser extent in the N542K cells. BGJ398 had no effects on pErk phosphorylation

in the control cell lines, confirming that mutant FGFR3 signalling is primarily mediated by the MAPK pathway. The RT112Fus cell line also showed a decrease for both total FGFR3 levels and a decrease in pY1000 signals after 1 and 6 hours of treatment with BGJ398. In addition, there was a slight increase in pSTAT3 levels at 6 hours for the EV, WT, S249C and V557M cell lines, for both the DMSO control and BGJ398, and a slight decrease in pAkt levels at 1 hour for WT, N540K, K652E and V557M cell lines upon BGJ398 treatment.

This analysis demonstrates that of the measured proteins, pErk signalling is selectively inhibited by BGJ398 in the FGFR3 mutants examined as well as the RT112Fus expressing cells, indicating that this is a major signalling node downstream of altered FGFR3 signalling.

A.

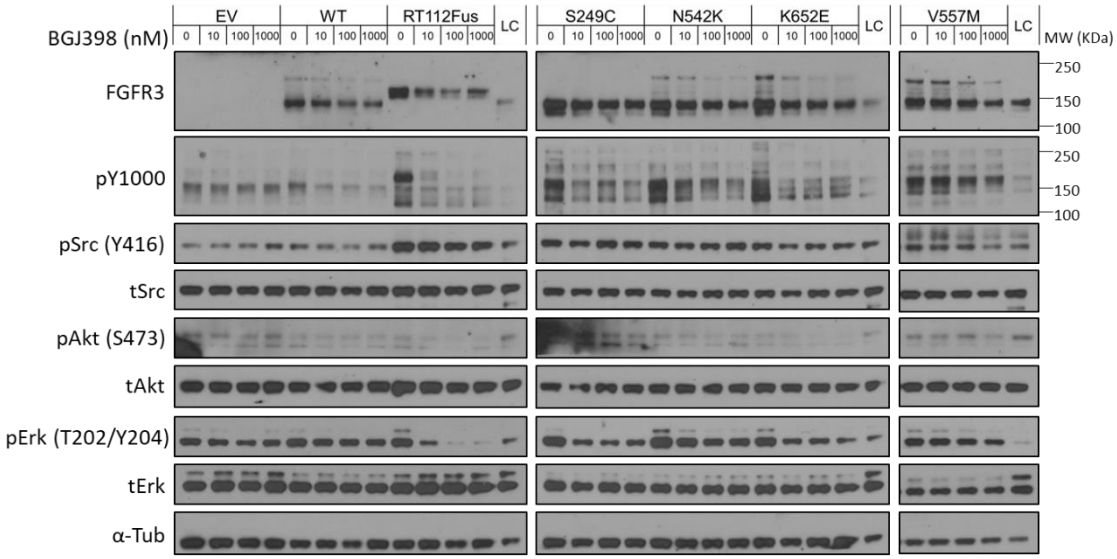

B.

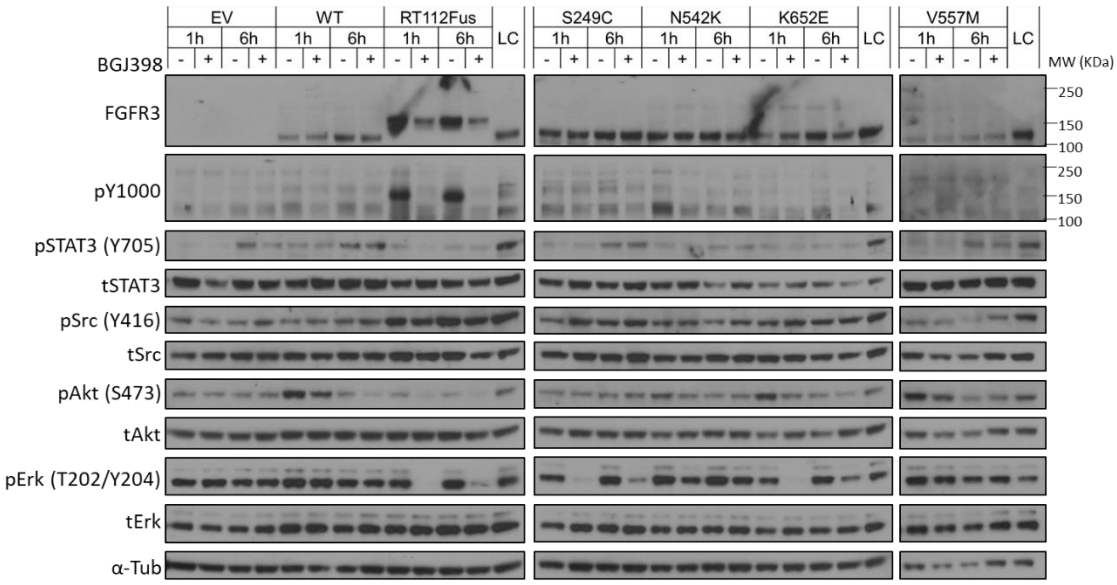

Figure 4.4 – The effect of BGJ398 in mutant FGFR3 expressing cells signalling pathways. A, B. Cells were seeded in full growth media and after 48 hours were treated with BGJ398. Cells were lysed, and protein extracts resolved by SDS-PAGE for immunoblotting with antibodies for the indicated proteins. **A.** Increasing concentrations of BGJ398 was added to cells for 6 hours to evaluate signalling alterations associated with drug treatment. The DMSO vehicle control is represented here as 0 nM and uses the same DMSO volume used to treat cells at 1000 nM. **B.** 100 nM of BGJ398 was added to the cell line panel for 1 and 6 hours. The DMSO vehicle control is represented here as (-) and uses the same DMSO volume used to treat cells at 100 nM. The loading control (LC) was used to compare protein levels between different gels and tubulin was used as a housekeeping protein. Representative images are shown from 3 biological replicates.

4.4 - MAPK signalling is important in driving the functional effects of FGFR3 activating mutants

Given that the MAPK pathway was found to be a key downstream component of mutant FGFR3 signalling, I hypothesised that the functional effects of BGJ398 on mutant FGFR3 cells in the phenotypic assays (cell viability, colony formation and spheroid assays) described in Figure 3.8A and section 4.2 may be the result of suppression of the MAPK pathway. To test this hypothesis, the small molecule kinase inhibitor trametinib that selectively blocks MEK, the upstream kinase of Erk, was used to establish if downregulation of the MAPK pathway will phenocopy the effects of BGJ398. Colony formation assays showed that in contrast to treatment with BGJ398, the ability for cells to form colonies was completely abolished under long-term treatment with 100 nM of trametinib for all cell lines including the controls (Figure 4.5A). I then undertook a cell viability assay using CTG assay to evaluate the dose dependent effects of trametinib in the cell line panel. This assay showed that at 72 hours treatment, there was a statistically significant decrease in IC_{50} values for all the FGFR3 mutant and RT112Fus cells when compared to the EV and WT FGFR3 control cells (Figure 4.5B). Whereas the FGFR3 mutants and fusion cells had an average IC_{50} value of between 15-45 nM, the WT FGFR3 cells had an average IC_{50} of 123 nM, 3-fold higher compared to RT112Fus and 8-fold higher compared to the K652E mutant (Figure 4.5B). It should be noted that comparing the IC_{50} values for BGJ398 (calculated from Figure 3.8A), the IC_{50} for trametinib treatment was significantly lower than that of BGJ398 treatment in all cell lines investigated (Figure 4.5C). In spheroid-based assays where cells were subjected to 72 hours trametinib treatment, I observed a reduction in spheroid size in all mutant and WT FGFR3 expressing cells to a baseline cross sectional area equivalent to the EV control (Figure 4.5D). In this assay, the effect between BGJ398 (previously calculated in Figure 4.3C) and trametinib treatment was very similar, with a Pearson r^2 correlation of 0.86 (Figure 4.5E).

Western blotting experiments confirm that trametinib treatment led to a reduction in the phosphorylation of Erk (Figure 4.6). Interestingly, there appears to be a reciprocal increase in Akt phosphorylation levels upon trametinib treatment which

was not seen with BGJ398 treatment (Figure 4.4B). Moreover, there was an increase of pSTAT3 levels at 6 hours for the EV, WT and V557M control cell lines, under both the DMSO and trametinib treatment conditions. pSTAT3 was also increased with trametinib at 6 hours for RT112Fus, S249C, N542K and the K652E expressing cells.

This analysis shows that the inhibition of MEK by trametinib leads to a reduction in cell survival of FGFR3 mutant and fusion cell lines, indicating that MAPK pathway is a major signalling node downstream of mutant FGFR3 signalling. These results indicate that the effects seen with BGJ398 in the phenotypic assays in Figure 3.8A and section 4.2, where a reduction in cell viability was observed along with a reduction in spheroid growth for all FGFR3 alterations are a result of MAPK pathway suppression.

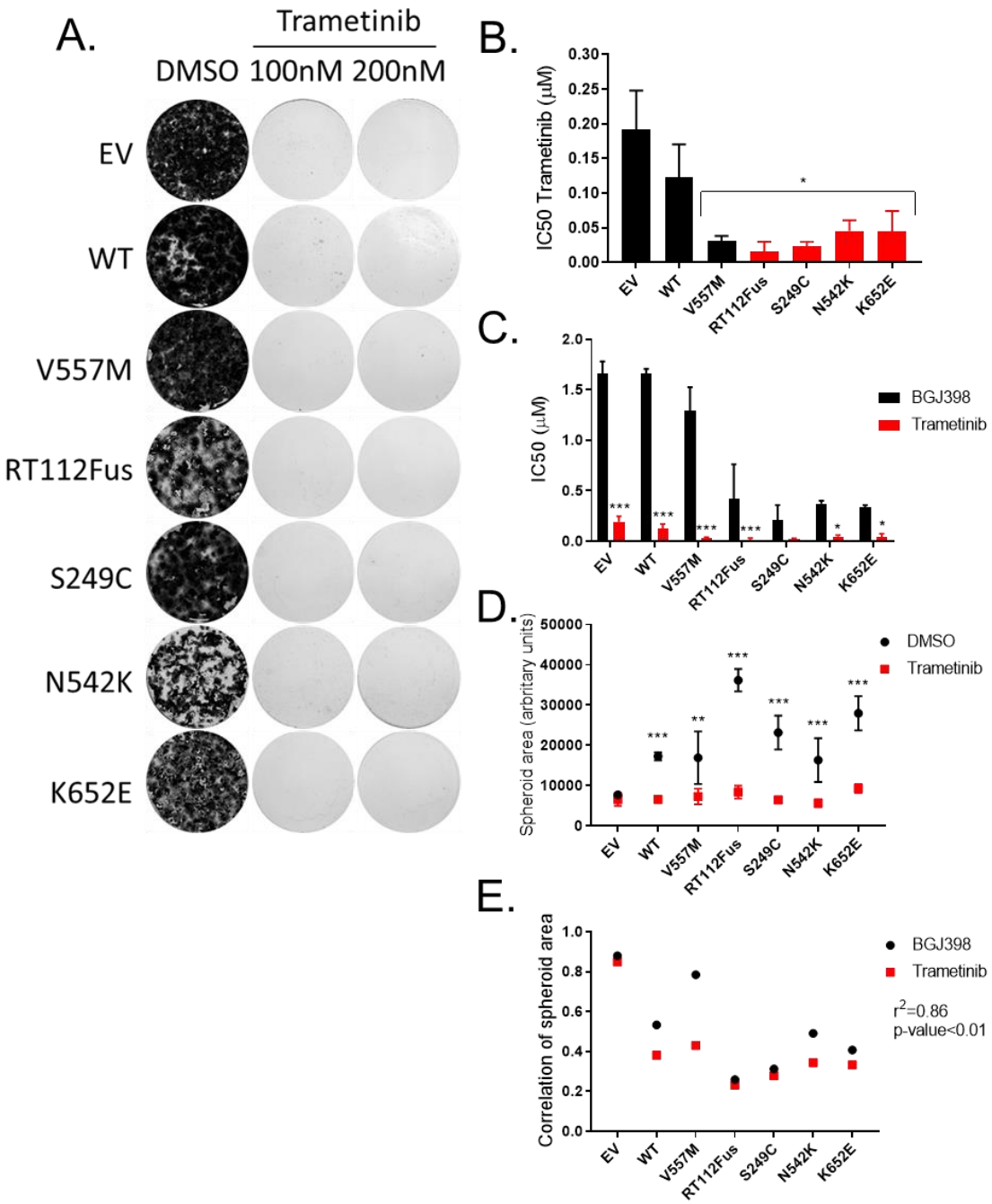

Figure 4.5 – Functional effects of Trametinib on mutant FGFR3 cell line panel across a range of phenotypic assays. The MEK inhibitor trametinib was used to investigate the sensitivity of each cell line to the suppression of MAPK pathway. **A.** Colony formation assays: representative example of colony formation in the presence of 100 nM and 200 nM of trametinib. Cells were seeded at low density (1000 cells/well) and treated after 24 hours in culture. Media was replenished every 3 days and cells were fixed and stained with crystal violet at day 14. **B.** IC_{50} values of trametinib treatment across the cell line panel in cell viability assays. Cells were seeded in 96-well plates and treated with 9 increasing doses of trametinib (5 nM – 50 μM). After 72 hours the viability of the cells was measured with CTG assay and results normalised against the DMSO vehicle control. Data was plotted and fitted to a curve with four-parameters on GraphPad Prism to calculate the IC_{50} values. Statistical analysis was performed with one-way ANOVA compared to the WT. * p-value< 0.05. (n=3 biological replicates). **C.** Comparison of the (continuation of figure legend on following page)

(continuation of legend of Figure 4.5) IC_{50} values of B with the IC_{50} values previously shown for BGJ398 treatment in Figure 3.8A. Two-way ANOVA statistics was employed to compare between trametinib and BGJ398 treatment for each cell line. *** p-value< 0.001, * p-value< 0.05. (n=3 biological replicates). **D.** Cross sectional area data generated from trametinib treatment in the panel of cell lines in the spheroid growth assay. 1000 cells from each cell line were seeded on a round-well low adherent plate for 24 hours before treatment with 100 nM of trametinib and a further 72 hours in culture. Spheroids were screened and the area of the largest cross-section calculated using imageJ. Results were plotted along with the DMSO control for comparison. Statistical analysis to compare the data between trametinib and vehicle control were performed for each cell line with two-way ANOVA. *** p-value< 0.001, ** p-value< 0.01. (n=3 biological replicates). **E.** Comparison of spheroid assay data between trametinib treatment from D and BGJ398 treatment from Figure 4.3C. The fold change between the relevant inhibitor and its DMSO vehicle control are here plotted to establish the correlation coefficient factor between the trametinib and BGJ398 treatments. Pearson correlation coefficient r^2 was calculated. (n=3 biological replicates). All statistical analysis was performed on GraphPad Prism.

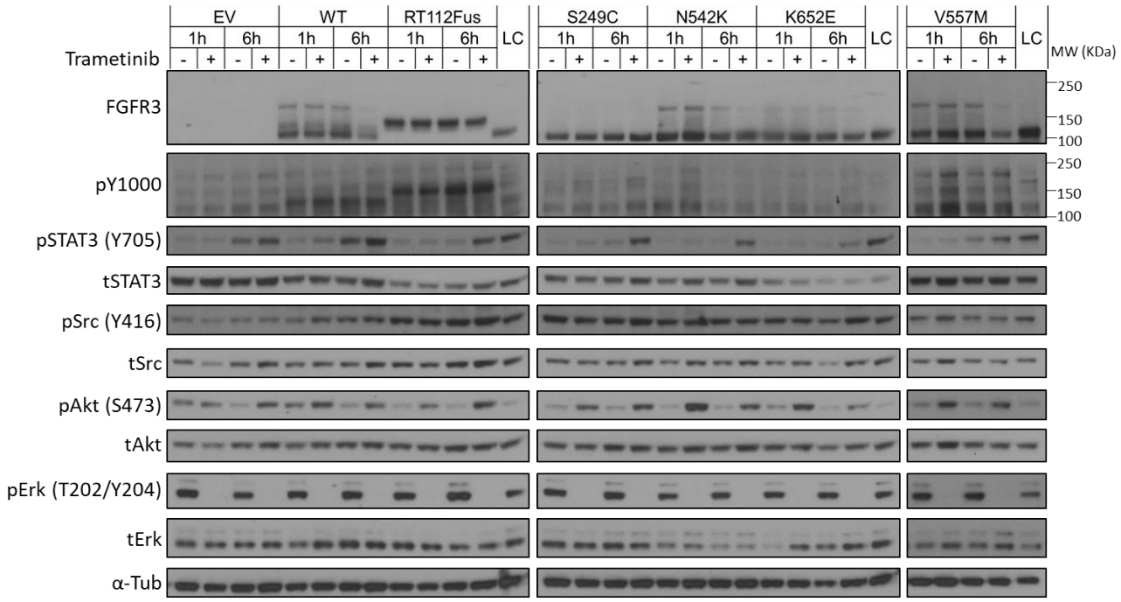

Figure 4.6 – The effect of trametinib on the downstream signalling pathways in the panel of NIH-3T3 cell lines. Cells were seeded in full growth media and treated after 48 hours with 100 nM of trametinib for 1 hour and 6 hours, along with the DMSO vehicle control (-) for each condition, which uses the same DMSO volume used to treat cells at 100 nM. Cells were lysed and proteins extracted prior to SDS-PAGE for immunoblotting with antibodies for the indicated proteins. The loading control (LC) was used to compare protein levels between different gels and tubulin was used as a loading control between samples of the same gel. Representative images are shown from 2 biological replicates.

4.5 - Multiplex assay reveals that Src phosphorylation is increased in the context of FGFR3 alterations

Functional characterisation of FGFR3 cancer-associated mutant cell lines indicated that high expressing FGFR3 mutants and the fusion RT112Fus were oncogenic and transforming in culture. Moreover, cells were sensitive to the pan-FGFR inhibitor BGJ398 either on monolayer or spheroid cultures and this was accompanied by a mutant- and fusion-specific downregulation of the MAPK pathway. However, the mutant FGFR3 expressing cells lacked sensitivity to BGJ398 in long-term colony formation assays and this phenotype was accompanied by a restoration of Erk phosphorylation levels at 6 hours.

In order to identify the downstream signalling pathways activated by individual FGFR3 mutants across a broad-spectrum of signalling effectors, a Luminex multiplex experiment was performed in the RT112Fus, S249C and K652E FGFR3 mutant expressing cells and compared to the WT FGFR3 control. RT112Fus was selected due to its high transformation potential and the S249C and K652E were selected because they are the most frequent mutations on the extracellular domain and KD of FGFR3, respectively.

Cells were harvested after 48 hours in culture and lysates were processed for coupling with antibody coated beads. Luminex integrates coloured labelled microbeads coated with analyte-specific capture antibodies. Each bead colour is associated with a specific phospho-specific antibody that could be recognised by the dual-laser flow-based detection multiplex instrument. The cell lysates were then mixed with the beads prior to biotinylation for detection in the Luminex 200^{TM} instrument. The output for this data is the number of detected beads for each analyte with the associated fluorescence intensity. Analysis excluded all proteins for which the number of counts was inferior to 20 beads to avoid background interferences. A panel of proteins was quantified across the FGFR3 mutants investigated and the data was normalised against the WT FGFR3 cell line control which is depicted as a heatmap in Figure 4.7. Table 4.1 shows the list of the phosphorylated proteins used, which includes amongst others, effectors of the major downstream signalling pathways of FGFR3, providing a basal readout for the signalling activity of cellular networks. This analysis finds that basal

phosphorylation levels of Src was increased 3.5-fold, 2.3-fold and 3.7-fold for the fusion, S249C and K652E, respectively, compared to the WT FGFR3. This result is consistent with the previous baseline analysis of major signalling pathways performed by western blotting in section 3.7, demonstrating that the Luminex methodology can effectively measure phosphorylated proteins in the NIH-3T3 cells. This analysis further shows that the phosphorylation of the pro-inflammatory signalling protein nuclear factor kappa B (NFkB) was decreased in the fusion FGFR3 expressing cell but, increased 2.6-fold in S249C cells when compared to the WT FGFR3. It is interesting to note that the majority of proteins measured such as GSK3β (WNT signalling), retinoblastoma-associated protein (Rb) and phosphatase and tensin homolog (PTEN) (tumour suppressor genes), along with proteins RAF1 and janus kinase (JAK1) (growth signalling), generally showed a slight reduction in protein phosphorylation in the FGFR3 mutants and fusion cells compared to the WT FGFR3 control. This analysis demonstrates that across all the proteins examined, only phosphoSrc levels were consistently increased in all the FGFR3 mutants and may serve as a key functional candidate signalling pathway by which these mutations mediate their oncogenic effects.

Table 4.1 – Overview of the proteins measured in the Luminex assay and the major pathways they are involved in. All proteins and respective phosphorylation sites are described with their associated biology function and involvement in major pathways.

Protein (phosphorylation site)	Function and major pathway
CHK1 (S345)	DNA damage response and cell cycle checkpoint response.
CHK2 (T68)	DNA damage response.
ßCATENIN (S33/37)	Regulation of cell–cell adhesion and gene transcription. WNT signalling pathway.
GSK3ß (S9)	Regulator in the glucose homeostasis, transcription factors and microtubules. WNT signalling.
FAK (Y397)	TK plays critical roles in integrin-mediated signal transductions.
JAK1 (Y1022/1023)	TK membrane adaptor, phosphorylates STAT proteins. JAK/STAT signalling pathway.
PRAS40 (T246)	Substrate of Akt and a component of mTORC1.
RAF1 (S259)	Upstream of MEK. MAPK signalling pathway.
LCK (Y394)	Developing of T-cells. Is a member of the Src family of protein tyrosine kinases.
Src (Y419)	Non-receptor TK proto-oncogene, is involved in cell adhesion, growth, movement and differentiation.
NFkB (S536)	Pro-inflammatory signalling pathway. Transcription of DNA, cytokine production and cell survival.
FGFR1 (Y653/654)	RTK
FGFR3 (Y649/650)	RTK
Rb (S760)	Tumour suppressor.
PTEN (S380)	Tumour suppressor.

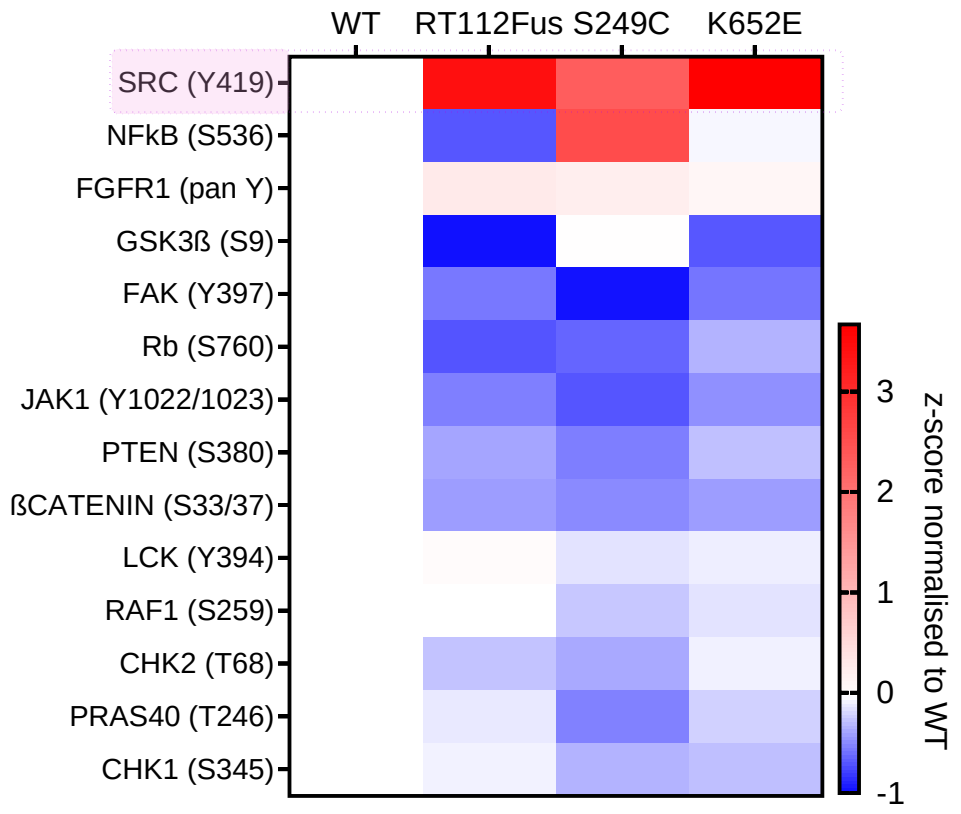

Figure 4.7 – Luminex assay to identify the levels of phosphorylation of 14 different proteins in the context of FGFR3 mutant and fusion cell lines. Cells were seeded in full growth media and lysed after 48 hours. Proteins were extracted and processed for antibody coupling with capture colour-coded beads. Samples were then run on a Multiplexing processor for analyte detection and quantification. Results were analysed and filtered to avoid background and data was normalised across cell lines by z-score. Results were plotted on a heat map for each cell line according to the levels of phosphorylation of each protein in comparison to the WT control.

4.5 - Targeted small molecule inhibitor screen reveals that specific FGFR3 alterations confer a protective effect to dasatinib

To interrogate the key signalling dependencies in the FGFR3-mutant cell models, I undertook a small molecule inhibitor screen in the WT FGFR3 control and S249C, N542K, K652E and RT112Fus mutant FGFR3 cells. This screen was designed to identify signalling dependencies by utilising small molecule inhibitors that target major downstream signalling pathways and RTKs. The screen is composed by 32 small molecule inhibitors which is administered at 500 nM. A list of all compounds used in the screen and their key targets is shown in Table 4.2.

The inhibitors include broad-spectrum kinase inhibitors, which are able to target multiple kinases such as imatinib (targets Abl, KIT and PDGFR) and foretinib (targets VEGFR and MET). It also has selective kinase inhibitors such as BGJ398 (FGFR), Binimetinib (MEK) or AZD5363 (Akt). And it also comprises a small number of inhibitors for non-kinase proteins such as NVP-AUY922 (Hsp90), GSK126 (enhancer of zeste homolog 2 (EZH2) methyltransferase) and JQ1 (bromodomain and extra-terminal (BET) family members). This assay was used to identify small molecule inhibitors that selectively reduced cell viability in mutant FGFR3 expressing cell but not in the WT FGFR3 cells. This strategy would identify unique mutant-specific dependencies with a suitable therapeutic window and also provide information on the signalling effectors that drive cell survival in the FGFR3 mutants but not the WT FGFR3.

Cells were seeded in 96-well plates and 24 hours later, cells were treated with the panel of inhibitors in fresh media. After 72 hours, cell viability was measured using CTG. Results from three biological replicates and two technical replicates each, were normalised to WT FGFR3 expressing cells and represented as a heatmap in Figure 4.8. To assess reproducibility of the assay, Pearson correlation was calculated, with a strong correlation of $r^2 > 0.7$ shown for all replicates in each cell line (Figure 4.9). The screen demonstrated that the distinct FGFR3 mutants and fusion expressing cells displayed differential sensitivity to individual inhibitors in the panel. Moreover, the analysis revealed that some mutants conferred a survival advantage to selected inhibitors when compared to the WT FGFR3 control cells. For example, JQ1 that is a selective inhibitor of bromodomain containing (BRD)1-4, is more potent in WT FGFR3 cells compared to the mutants. A similar effect was seen with BEZ235, an inhibitor of PI3K and mammalian target of rapamycin (mTOR) pathways, where only N542K and K652E expressing cells conferred survival to this drug when compared to the WT FGFR3 expressing cells.

In contrast, there was a subset of inhibitors that were selective for FGFR3 mutants compared to WT FGFR3. These group of inhibitors included selective FGFR inhibitors such as BGJ398 and AZD4547, and broad-spectrum kinase inhibitors such as ponatinib or cediranib and foretinib which also target all FGFR family members. Dasatinib, a broad-spectrum kinase inhibitor that potently

targets Src and Abl (Kwarcinski et al., 2016), was also found to decrease the cell viability in the N542K and K652E mutant expressing cells. Interestingly the RT112Fus and S249C mutants conferred a survival advantage to this drug compared to the WT control. Interestingly, bosutinib, a more selective Src inhibitor, also showed the same effect, although to a lesser extent. Taken together, these data suggest that the Src protein may be an important mediator for mutant FGFR3 signalling and should be further investigated.

Table 4.2 – List of inhibitors in small molecule inhibitor screen. The major cellular targets of inhibitors included in the screen are indicated.

Compound	Target	Major pathway
AZD4547	FGFR1-3	FGFR
AZD5363	Akt	PI3K/Akt/mTOR
BEZ235	PI3K, mTOR	PI3K/Akt/mTOR
BGJ398	FGFR1-3	FGFR
Binimetinib	MEK1/2	MAPK
Bosutinib	Src	Src
BX-795	PDK1, TBK1, IKKϵ	NFkB and TBK1
Cediranib	Broad-spectrum: VEGFR, Flt1/4, KIT	Broad-spectrum TKi
Ceritinib	ALK	ALK
Crizotinib	Met, ALK	ALK
Dabrafenib	BRAF V600E	MAPK
Dasatinib	Broad-spectrum: SFK, Abl, KIT	Src
Foretinib	Broad-spectrum: VEGFR, MET	Broad-spectrum TKi
Imatinib	Broad-spectrum: Abl, KIT, PDGFR	Broad-spectrum TKi
JQ1	BRD1-4	BET bromodomain family
Lenvatinib	Broad-spectrum: VEGFR2/3	Broad-spectrum TKi
MK2206	Akt	PI3K/Akt/mTOR
MK-8776	CHK1	ATR-CHK1
Momelotinib	JAK1/2	JAK/STAT
MRT67307	IKKϵ, TBK1	NFkB and TBK1
NVP-AUY922	Hsp90	Hsp90
NVP-TAE684	ALK	ALK
Palbociclib	CDK4, CDK6	Cell cycle regulator
Pazopanib	Broad-spectrum: VEGFR1-3, PDGFR	Broad-spectrum TKi
PF562271	FAK, Pyk2	FAK
Ponatinib	Abl, PDGFRα, VEGFR2, FGFR1, Src	Broad-spectrum TKi
GSK126	EZH2	EZH2 methyltransferase
Silmitasertib	CK2	CK2
Sorafenib	Broad-spectrum: VEGFR2, BRAF, RAF	Broad-spectrum TKi
Sunitinib	Broad-spectrum: VEGFR2, PDGFRß	Broad-spectrum TKi
Trametinib	MEK1/2	MAPK
Vandetanib	Broad-spectrum: VEGFR2/3, EGFR	VEGFR

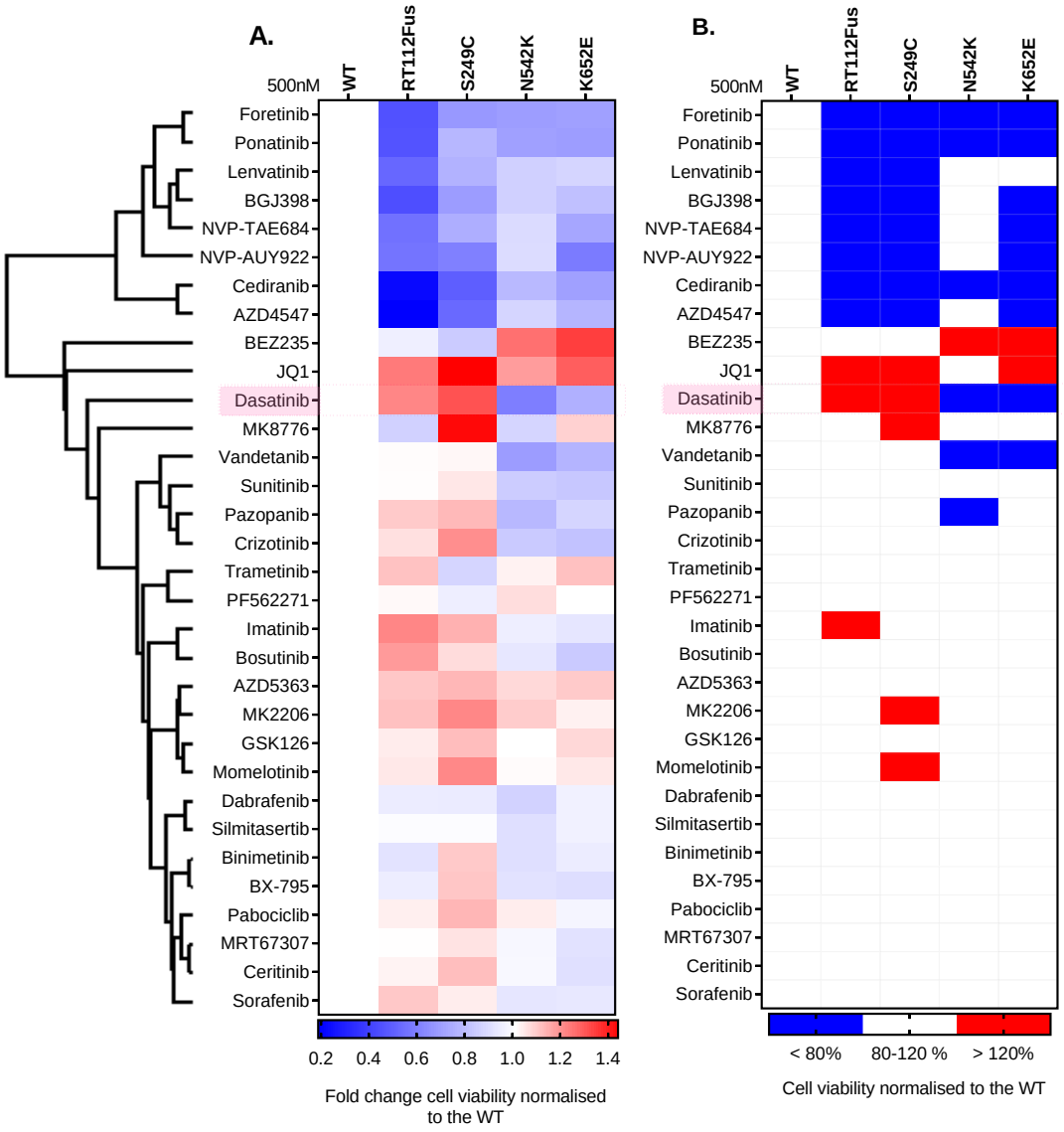

Figure 4.8 – A targeted small molecule inhibitor screen of the panel of FGFR3 mutant expressing cells. Cells were plated in 96-well plates and treated after 24 hours with the panel of inhibitors at a final concentration of 500 nM. Data is represented as heat map relative to the WT FGFR3 control cells. The dendrogram represents a hierarchical clustering of all drugs calculated with Perseus software. **A.** Cell viability for each inhibitor and each cell line was normalised to the viability of the FGFR3 WT cell line, and fold changes are represented as a heat map. **B.** Results are plotted as a categorical map where for each drug a 20 % threshold was applied between each FGFR3 altered cell line and the WT FGFR3. Therefore, blue represents the conditions for which the cell viability was 20 % lower than the WT FGFR3 control, and red represents those conditions where cell line viability was 20 % higher compared to the WT FGFR3 for the same inhibitor. (n=3 biological replicates, 2 technical replicates each).

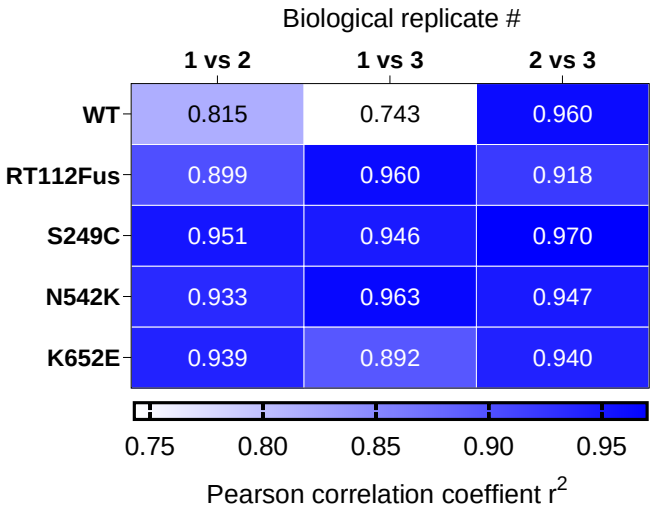

Figure 4.9 – Pearson correlation coefficient between biological replicates from the targeted small molecule inhibitor screen. Pearson correlation coefficient r^2 was calculated on GraphPad Prism for each cell line across three biological replicates. Each column represents the r^2 between the indicated pair of biological replicates.

4.6 - RT112Fus and S249C are resistant to Src inhibitors, dasatinib and saracatinib

Given that the western blotting and Luminex assay data showed an increased Src phosphorylation in the context of FGFR3 alterations; and that dasatinib (a multi-target kinase inhibitor that blocks Src activity) had a unique sensitivity profile across the FGFR3 mutants examined, I sought to further investigate the effects of dasatinib in the NIH-3T3 cell line panel across a range of phenotypic assays. These assays include cell viability in short-term CTG assays, cell survival in long-term colony formation assays and cell growth and survival under non-adherent conditions in spheroid-based assays. Evaluation of the key downstream signalling alterations upon treatment with dasatinib was also evaluated to assess the signalling effects of this drug.

Dose response measurements by the CTG assay showed that consistent with the kinase inhibitor screen data, the RT112Fus and S249C FGFR3 mutant cell lines were more resistant compared to the WT FGFR3 control cells after 72 hours treatment with dasatinib (Figure 4.10A). This was reflected in the IC_{50} values with

the RT112Fus and S249C cells having an average IC_{50} value of 3 µM and 4.4 µM respectively, compared to the WT FGFR3 cells with a mean of 0.6 µM (Figure 4.10B). This analysis was extended to another more selective but less potent Src inhibitor Saracatinib (Green et al., 2009). Results obtained with this drug were comparable to dasatinib with mean IC_{50} values of 4 µM and 6 µM for RT112Fus and S249C expressing mutant cells respectively compared to the WT FGFR3 expressing cells (1.6 µM) (Figure 4.10C, D). Together, the cell viability data suggests that the translocation RT112Fus and the cysteine mutation S249C confer a significant protective effect against Src inhibitors that is not observed with the other FGFR3 mutants.

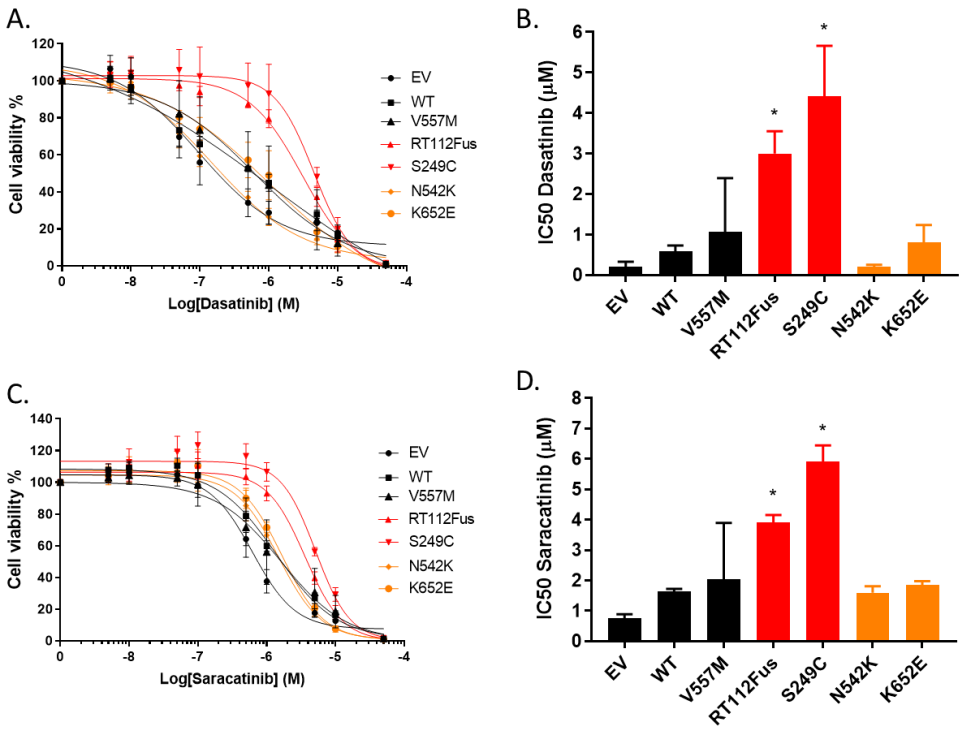

Figure 4.10 – Evaluation of dasatinib and saracatinib dose response effects on cell viability in the panel of mutant FGFR3 expressing cells. Cells were seeded and treated over a range of concentrations with the indicated inhibitors for 72 hours. Viability was measured by CTG assay and normalised against the DMSO vehicle control. **A, C.** Viability data was plotted against inhibitor concentration and a four-parameter non-linear regression was fitted with GraphPad Prism. **B, D.** IC_{50} values were extrapolated from the fitted dose response curves and plotted. One-way ANOVA was used for statistical analysis compared to the WT control. * p-value< 0.05. (n=3 biological replicates).

In long-term colony formation assays performed at 3 different doses of dasatinib (100nM, 1uM and 2uM), the RT112Fus and S249C FGFR3 mutant expressing

cells had more colonies across all drug doses after 14 days of treatment compared to the EV, WT FGFR3 and V555M gatekeeper controls as well as the other FGFR3 mutants N542K and K652E (Figure 4.11A, B). In contrast, spheroid-based assays did no fully recapitulate the effects seen in the CTG viability and colony formation assays. Here, data showed that only the RT112Fus mutant conferred a survival advantage to dasatinib in the cell line panel (Figure 4.11C, D). This discrepancy is likely to be due to the limitations of this assay where the small spheroids formed by the control cell lines (EV and WT FGFR3) limits the sensitivity of the assay in detecting small changes in spheroid cross-sectional area upon dasatinib treatment in these cells.

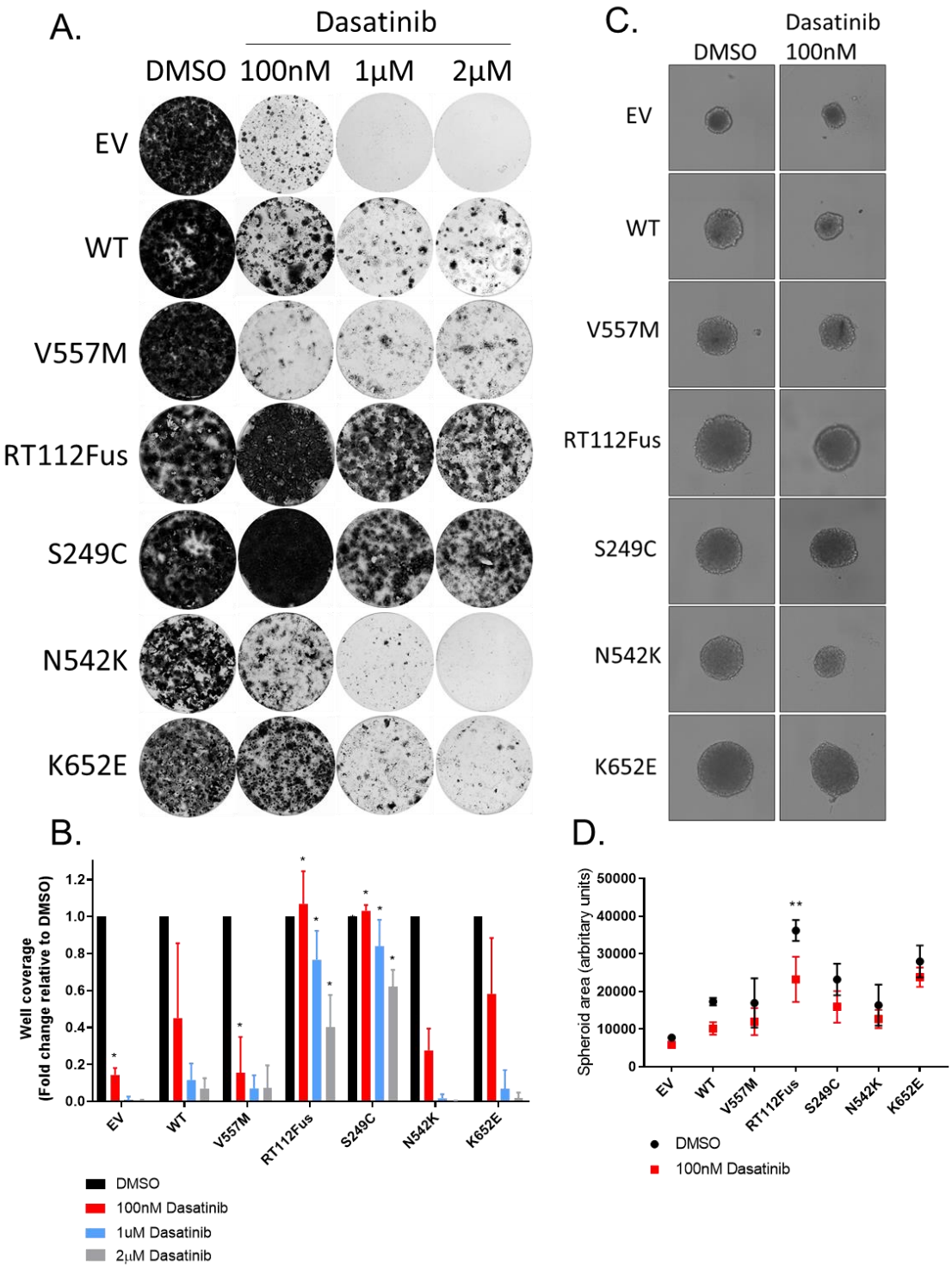

Figure 4.11 – Evaluation of dasatinib effects in colony formation and spheroid assays in the panel of mutant FGFR3 expressing cells. A. Representative images of crystal violet staining of colony formation assays. Cells were seeded in 6-well plates for 24 hours and treated with the indicated concentration of dasatinib for 14 days. **B.** Quantification of colony formation from A. Colonies were first measured as a percentage of well coverage for each condition with imageJ. Data was normalised against the DMSO control of each cell line. Statistics were performed with two-way ANOVA. * p-value< 0.05. **C.** Representative images from spheroid assay. Cells were seeded on a round-well low adherent plate for 24 hours and treated with 100 nM of dasatinib along with the vehicle control (continuation of figure legend on following page)

(continuation of legend of Figure 4.11) DMSO for 72 hours before imaging. **D.** The area of the largest cross-section of the spheroids from C was calculated using imageJ. Results were plotted along with the DMSO control for comparison. Statistics comparing between dasatinib and vehicle control were performed for each cell line with two-way ANOVA. ** p-value< 0.01. (n= 3 biological replicates).

To better understand the signalling mechanisms that may be driving the differential survival effects observed in the RT112Fus and S249C FGFR3 mutants, I assessed the dose response effects of dasatinib on a small number of key FGFR3 downstream signalling nodes (MAPK, Akt and Src) by western blotting. Cells were lysed after 6 hours of treatment with increasing doses of dasatinib (10 nM, 100 nM and 1000 nM) (Figure 4.12). As expected, dasatinib potently supressed phosphorylation levels of Src in all cell lines at the intermediate dose of 100 nM. Dasatinib did not alter the total levels of FGFR3 for any of the cell lines, however there was a dose dependent decrease in the pY1000 signal in all cell lines except RT112Fus. This mutant only showed a slight reduction of pY1000 at 1 µM of dasatinib. The pY1000 signal for WT FGFR3 cells for the DMSO vehicle control was here similar to RT112Fus cell line, which is not consistent with previous blots (e.g. Figure 4.4A) where in contrast to WT FGFR3 cells only the fusion cell line and the FGFR3 mutant cells display and increased phosphorylation at the same MW as FGFR3. This effect denotes activation of WT FGFR3 or phosphorylation of FGFR1 (that is known to be expressed by NIH-3T3 cells) that could be a sporadic result of media change upon DMSO treatment. Media contains FBS that has growth factors that can transiently activate FGFR in the WT setting. In contrast, Akt phosphorylation levels appeared to be reduced for all cell lines only at the highest dasatinib doses of 100 nM and 1 µM but not in the WT FGFR3 expressing cells. The phosphorylation levels of Erk varied across cell lines. For instance, pErk was markedly suppressed at the intermediate dose of 100 nM for the EV control cells, whereas in the WT FGFR3 and V557M gatekeeper cell, the phosphorylation levels of this protein remained constant. For the non-responsive cell lines RT112Fus and S249C, pErk levels appear to increase upon drug treatment. Collectively, I have shown that dasatinib consistently reduces Src phosphorylation levels in a dose dependent fashion in all the cell lines examined. However, there is variation in the response of the other

signalling nodes to dasatinib across the distinct FGFR3 mutants, suggesting that each mutant responds differently to treatment with this inhibitor.

The effects of saracatinib were also analysed by western blotting. Consistent with the more selective but less potent nature of this compound, the data showed that phosphorylation levels of Src was only inhibited at the highest drug concentrations of 1uM (Figure 4.13). There were no other alterations in any of the other proteins examined.

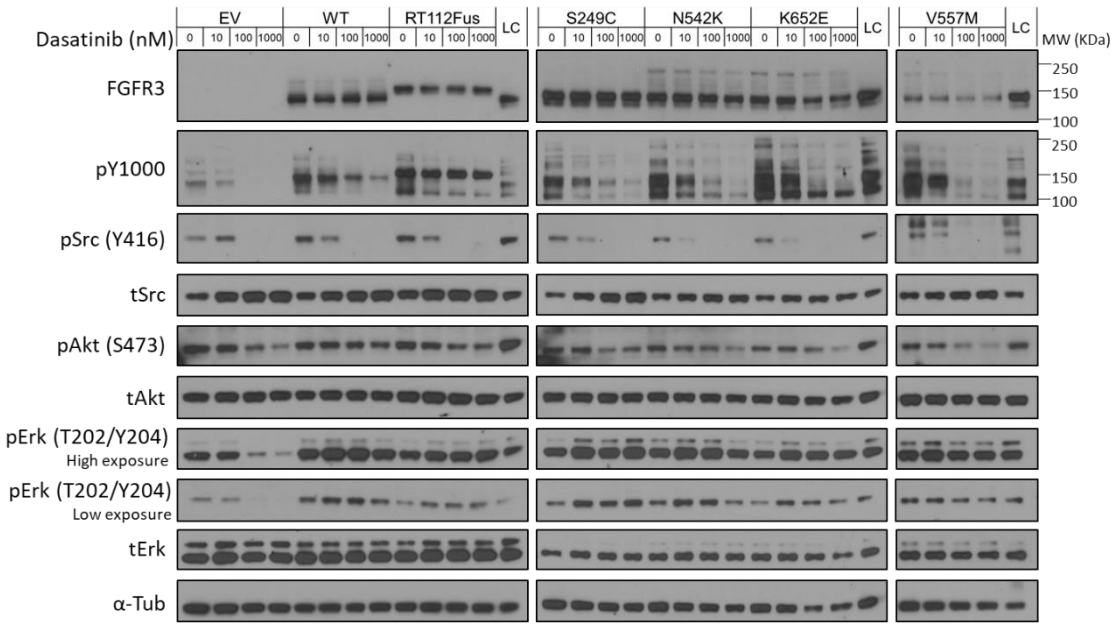

Figure 4.12 – Investigation of the signalling effects of dasatinib treatment in the panel of mutant FGFR3 cells. Cells were seeded for 48 hours and treated with the indicated doses of dasatinib for 6 hours. The DMSO vehicle control is represented here as 0 nM and uses the same DMSO volume used to treat cells at 1000 nM. Extracted proteins from lysates were run on an SDS-PAGE for immunoblotting with the indicated proteins. The MW of the correspondent blotted protein is indicated in KDa. The loading control (LC) was used to compare protein levels between different gels and tubulin was used as a loading control between samples of the same gel. This blot is a representative image from 2 biological replicates.

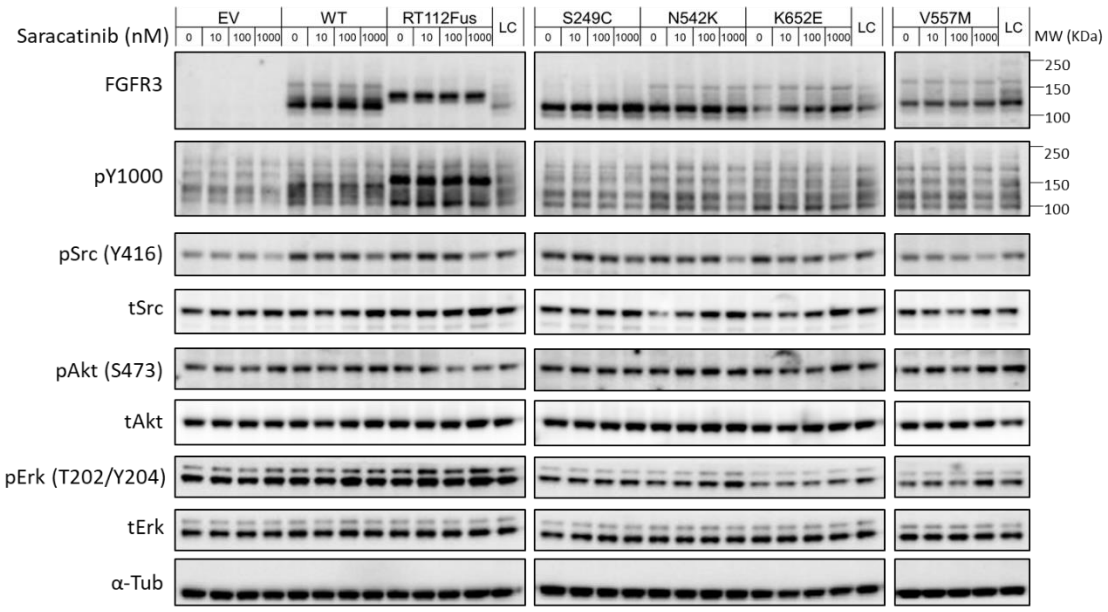

Figure 4.13 – Assessment of the signalling effects of dasatinib treatment in the panel of mutant FGFR3 cells. Cells were seeded for 48 hours and treated with the indicated doses of saracatinib for 6 hours. The DMSO vehicle control is represented here as 0 nM and uses the same DMSO volume used to treat cells at 1000 nM. Lysates were processed for protein extraction and samples were resolved by SDS-PAGE for immunoblotting with the indicated proteins. The MW of the correspondent blotted protein is indicated in KDa. The loading control (LC) was used to compare protein levels between different gels and tubulin was used as a loading control between samples of the same gel.

4.7 - Dasatinib in combination with BGJ398 synergises to reduce cell survival in RT112Fus and S249C FGFR3 expressing cells

The use of combination therapy as a means to suppress multiple signalling pathways to overcome drug resistance is a well-established concept in cancer biology (Faivre et al., 2006). It has been extensively shown that many cancer cells are resistant to single agent targeted therapies as a result of the activation of compensatory signalling mechanisms, which can be overcome by the addition of a second agent that inhibits said compensatory signalling. To investigate whether the addition of dasatinib could modulate the sensitivity of mutant FGFR3 expressing cells to BGJ398, the panel of cell lines was subjected to combination treatment with both inhibitors (Figure 4.14). Cell viability assays after 72 hours of treatment with both inhibitors showed that while all cells were sensitive to the

combination, the FGFR3 mutants were significantly more sensitive than the control cell lines with a mean IC_{50} value of 10-18 nM for the mutants versus the WT FGFR3 control cells which had a mean IC_{50} value of 69 nM (Figure 4.14A, B). When comparing the inhibitor dose response curves of single agents dasatinib and BGJ398 versus the combination in the WT FGFR3, RT112Fus and S249C cells, there was a clear demonstration that the effect of the combination was more potent than each inhibitor as a single agent (Figure 4.14C). Statistical analysis showed that the difference between both inhibitors as single agents versus the combination was significant for drug doses between 50 nM and 1 µM in the WT FGFR3 expressing cell, and between 10 nM and 1 µM in the RT112Fus and S249C mutant cells. To establish if the combination therapy was synergistic, the combination index (CI) was calculated according to the Chou-Talalay method, in which CI values < 1 indicate drug synergism (Figure 4.14D) (Chou, 2010). This analysis revealed that synergy was observed for the dasatinib and BGJ398 combination at all assayed doses for all three cell lines, RT112Fus, S249C and WT FGFR3. Extending this analysis to saracatinib and BGJ398 led to very similar findings, indicating that a structurally distinct inhibitor of Src could recapitulate the phenotypic effects observed with dasatinib (Figure 4.15).

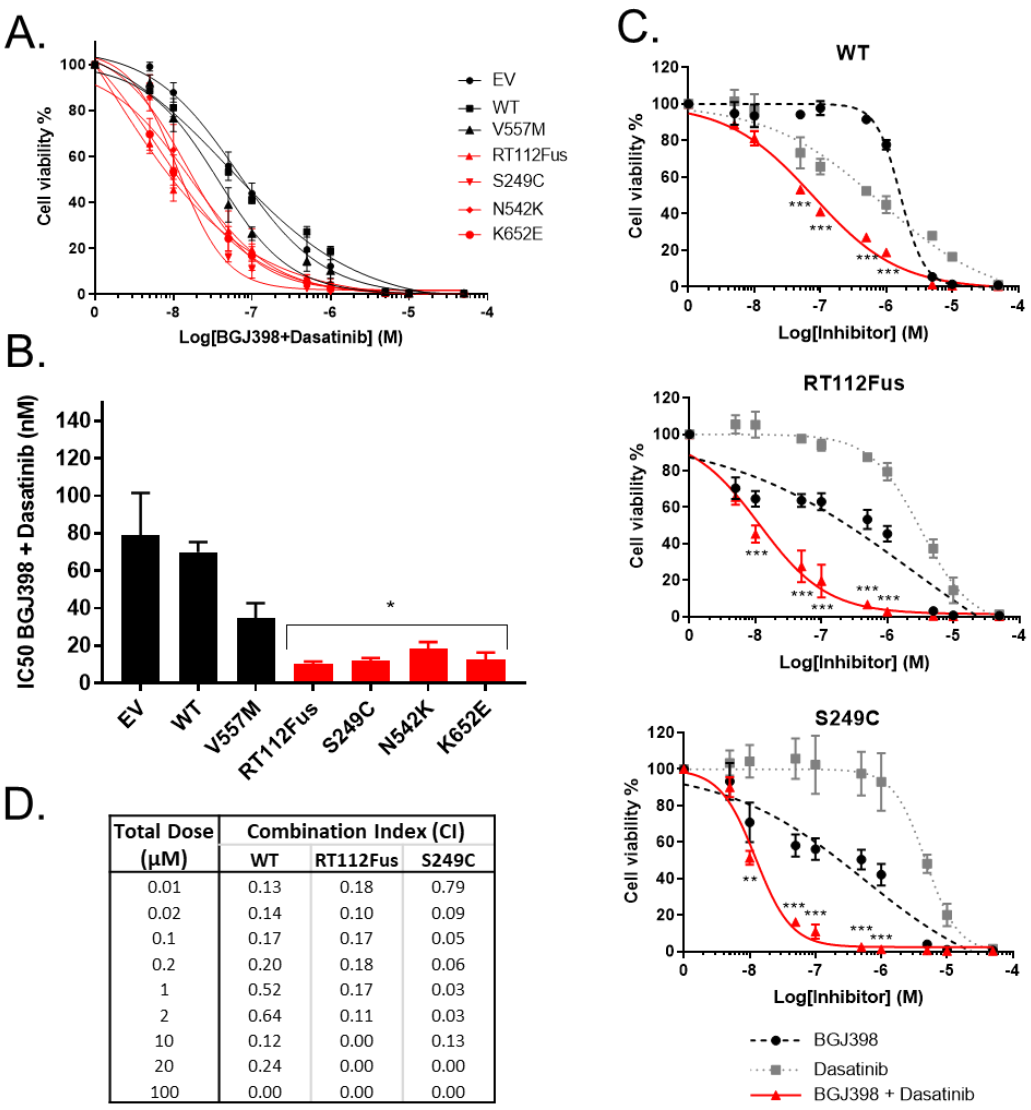

D.

Total Dose (μM)	Combination Index (CI)		
	WT	RT112Fus	S249C
0.01	0.13	0.18	0.79
0.02	0.14	0.10	0.09
0.1	0.17	0.17	0.05
0.2	0.20	0.18	0.06
1	0.52	0.17	0.03
2	0.64	0.11	0.03
10	0.12	0.00	0.13
20	0.24	0.00	0.00
100	0.00	0.00	0.00

Figure 4.14 – Valuation of dasatinib and BGJ398 combination effects on cell viability in the panel of mutant FGFR3 expressing cells. A-C. Cells were seeded in 96-well plates for 24 hours and treated with a range of doses of the combination of BGJ398 plus dasatinib in a 1:1 ratio. Cell viability was measured after 72 hours of treatment utilising the CTG assay. **A.** Cell viability data from the CTG assay was normalised against the DMSO vehicle control and plotted to fit a four-parameter non-linear regression on GraphPad Prism. **B.** IC_{50} was extrapolated from the curves from A. Statistical analysis was performed with a one-way ANOVA against the WT control. * p-value< 0.05. **C.** Dose response curves for BGJ398 and dasatinib as single agents and their combination were plotted together for comparison for the WT, RT112Fus and S249C. BGJ398 and dasatinib single agent data was previously shown in Figures 3.8A and 4.10A. Statistical analysis was performed with two-way ANOVA for each individual dose across the three treatments. ** p-value< 0.01, *** p-value< 0.001 and it is indicated only when statistical significance was found between the combination of BGJ398 plus dasatinib versus both inhibitors alone. **D.** The combination index (CI) was calculated using the dose response data employing the Chou-Talalay method (Chou, 2010). Values < 1 indicate drug synergy.

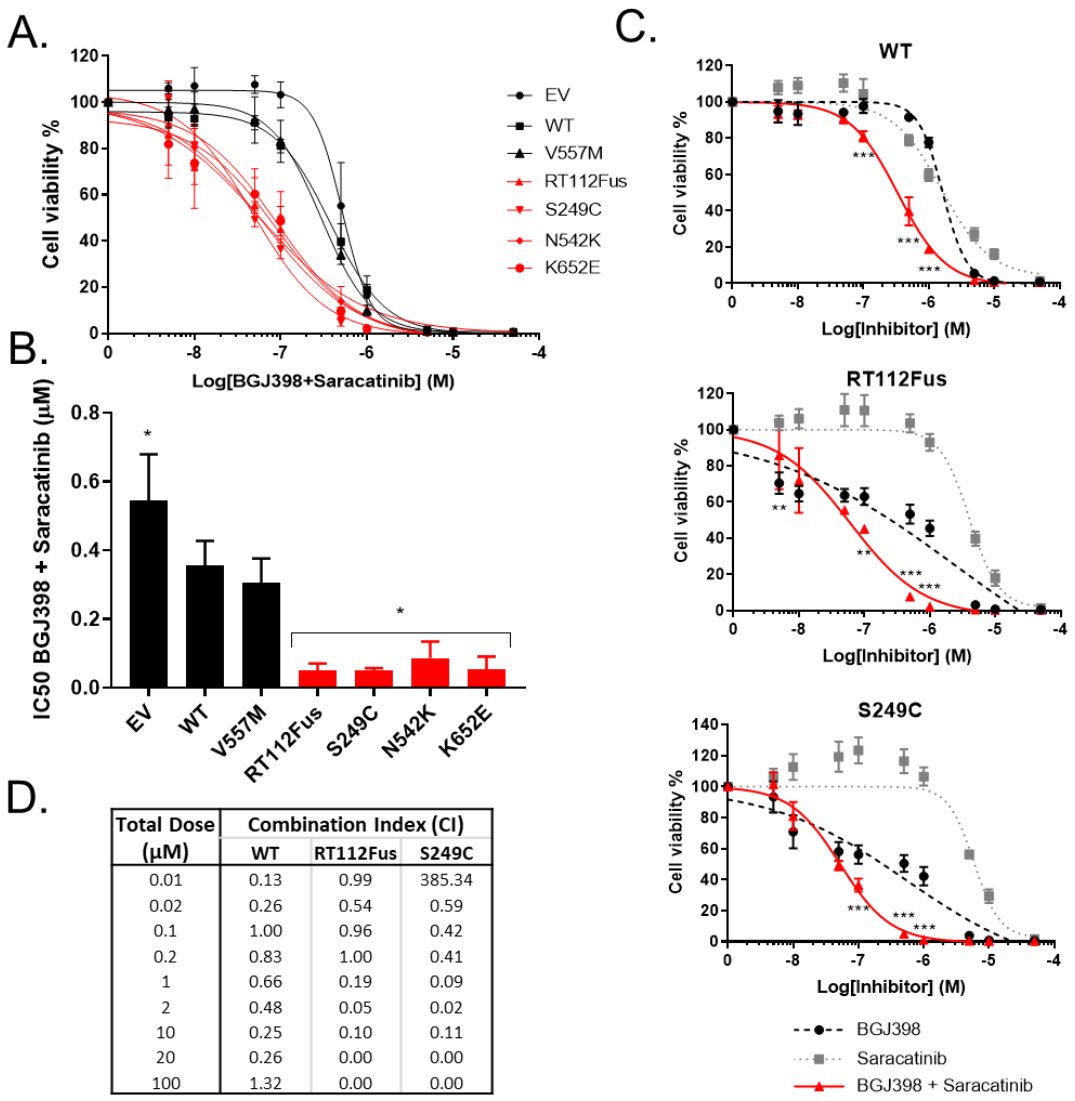

D.

Total Dose (µM)	Combination Index (CI)		
	WT	RT112Fus	S249C
0.01	0.13	0.99	385.34
0.02	0.26	0.54	0.59
0.1	1.00	0.96	0.42
0.2	0.83	1.00	0.41
1	0.66	0.19	0.09
2	0.48	0.05	0.02
10	0.25	0.10	0.11
20	0.26	0.00	0.00
100	1.32	0.00	0.00

Figure 4.15 – Evaluation of saracatinib and BGJ398 combination effects on cell viability in the panel of mutant FGFR3 expressing cells. A-C. Cells were seeded in 96-well plates for 24 hours and treated with a range of doses of the combination of BGJ398 plus saracatinib in a 1:1 ratio. Cell viability was measured after 72 hours of treatment utilising the CTG assay. **A.** Cell viability data from the CTG assay was normalised against the DMSO vehicle control and plotted to fit a four-parameter non-linear regression on GraphPad Prism. **B.** IC_{50} was extrapolated from the curves from A. Statistical analysis was performed with a one-way ANOVA against the WT control. * p-value< 0.05. **C.** Dose response curves for BGJ398 and saracatinib as single agents and their combination were plotted together for comparison for the WT, RT112Fus and S249C. BGJ398 and saracatinib single agent data was previously shown in Figures 3.8A and 4.10C. Statistical analysis was performed with two-way ANOVA for each individual dose across the three treatments. ** p-value< 0.01, *** p-value< 0.001 and it is indicated only when statistical significance was found between the combination of BGJ398 plus saracatinib versus both inhibitors alone. **D.** The combination index (CI) was calculated using the dose response data employing the Chou-Talalay method (Chou, 2010). Values < 1 indicate drug synergy.

Further assessment of the combinatory effects of BGJ398 and dasatinib in long-term colony formation assays showed a complete abrogation of colony formation in all mutant FGFR3 expressing cell lines (Figure 4.16). Notably, all the three controls used, EV, WT FGFR3 and the gatekeeper mutant V555M had residual colonies in the low dose combination (1 μM BGJ398 and 100 nM dasatinib), suggesting that the effects of the combination were selective for the FGFR3 mutants.

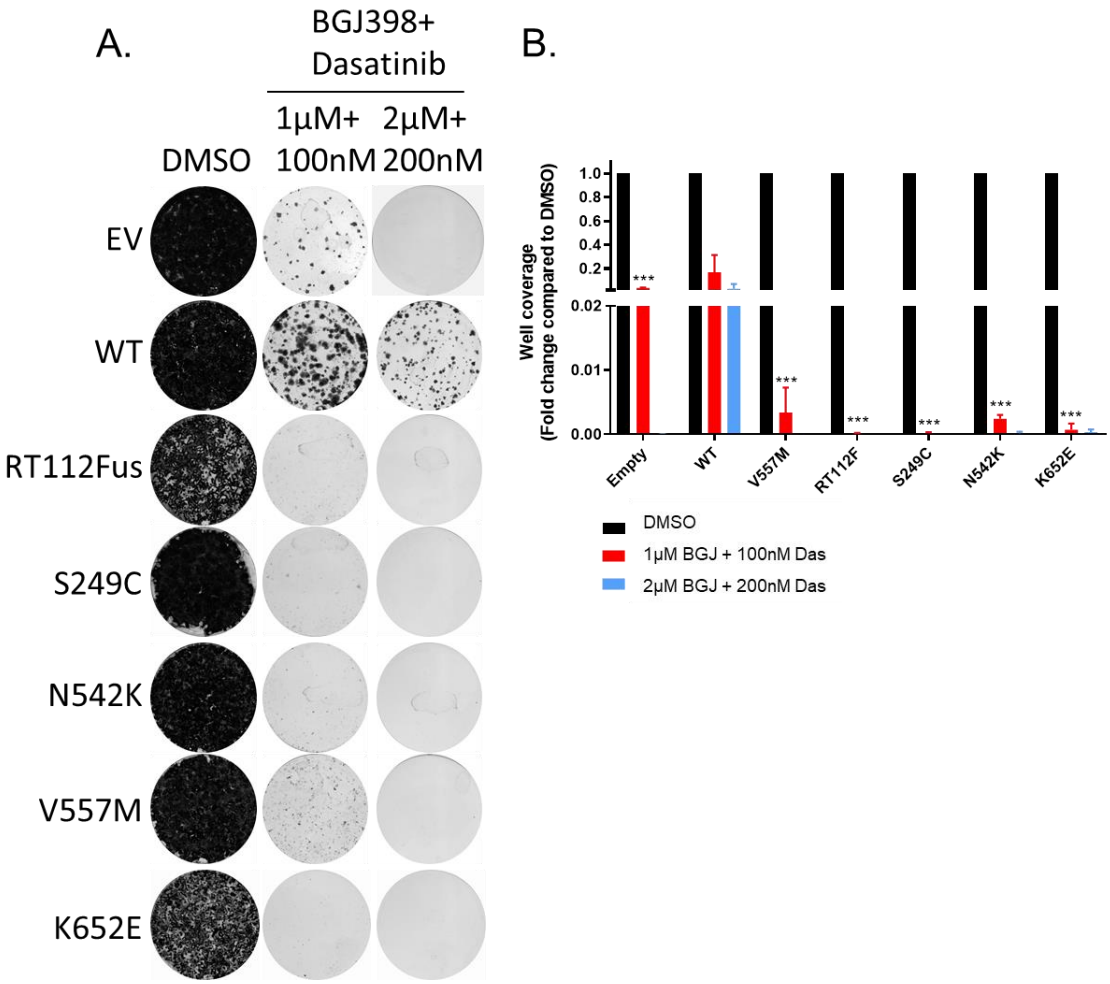

Figure 4.16 – BGJ398 in combination with dasatinib treatment in long-term colony formation assays. **A.** Representative images of colony formation in the presence of BGJ398 plus dasatinib combination. Cells were seeded at low density (1000 cells/well) for 24 hours and treated with the indicated doses. Cells were stained with crystal violet after 14 days. **B.** Quantification of well coverage normalised to the DMSO control. Statistical analysis was performed on GraphPad Prism with two-way ANOVA compared to the WT control for each drug concentration. *** p-value< 0.001. (n=3 biological replicates). *BGJ- BGJ398, Das- dasatinib*

To identify candidate signalling mechanisms that may explain the synergistic effect of these two drugs, I evaluated the signalling alterations in the panel of cells after treatment for 6 hours with increasing doses of a combination of both BGJ398 and dasatinib (in a 1:1 ratio) (Figure 4.17). As expected, for the EV, RT112Fus, S294C, N542K and K652E cells the data showed that the phosphorylation levels of Src, Akt and Erk were downregulated upon treatment with the combination, which is the result of the independent effects of dasatinib and BGJ398 as single agents (see Figures 4.4 and 4.12). Notably, in some mutants (S249C and K652E) there was a more potent inhibition of pErk in the combination compared to single agent treatment with BGJ398 alone (Figure 4.4A). Interestingly, the combination also had the added effect of suppressing the phosphorylation levels of Erk in the WT FGFR3 and V557M cell lines at 1 μM, that was not previously observed in the single agent treatment of either inhibitor alone (Figures 4.4 and 4.12).

Overall, this section demonstrates that BGJ398 in combination with dasatinib induces a greater reduction in cell survival for all FGFR3 mutant cell lines and RT112Fus cell line, than each of the inhibitors alone. Moreover, the growth advantage observed for the RT112Fus and S249C FGFR3 cell lines with dasatinib (Figure 4.11A) and the resistance observed in the presence of BGJ398 in long-term colony formation assays for all FGFR3 altered cell lines (Figure 4.2) was abrogated by the combination of both BGJ398 and dasatinib. The synergy between both inhibitors was linked to the more potent inhibition of pErk signalling and added inhibition of pAkt signalling.

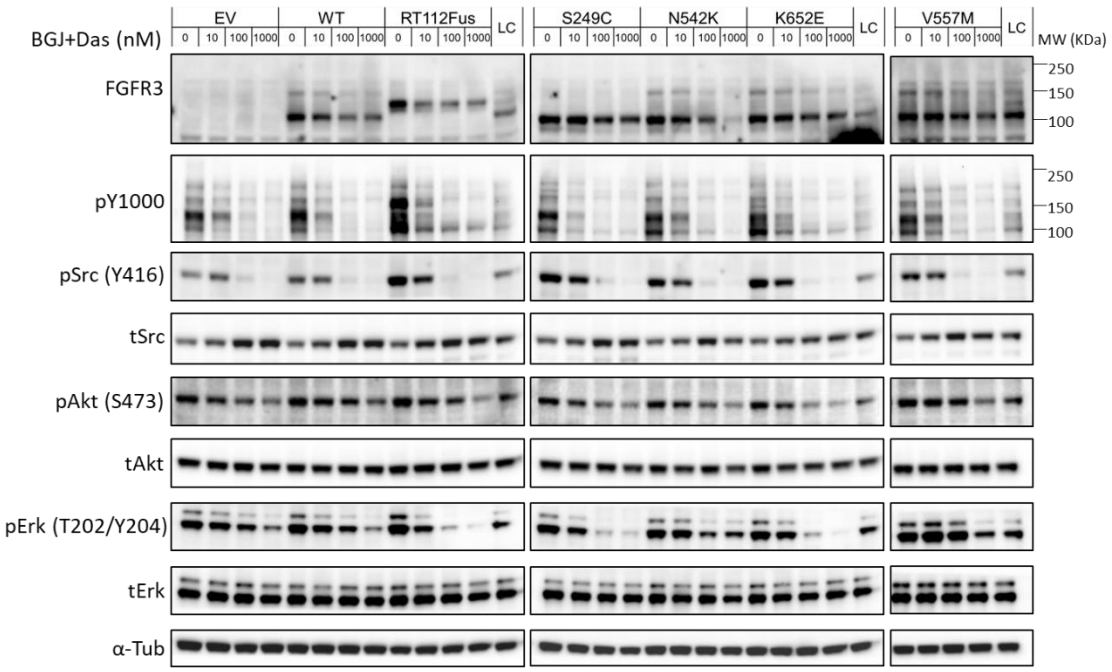

Figure 4.17 – Assessment of key FGFR3 downstream signalling alterations upon combined treatment of FGFR3 mutant cells with BGJ398 and dasatinib. Cells were seeded for 48 hours and treated with dasatinib plus BGJ398 for 6 hours at the indicated doses. The DMSO vehicle control is represented here as 0 nM and uses the same DMSO volume used to treat cells at 1000 nM. Inhibitors were administered in a 1:1 ratio, and the indicated concentration represents the total concentration used. Cells were lysed for protein extraction and resolve by SDS-PAGE prior to immunoblotting with antibodies against the indicated proteins. The MW is indicated in KDa. The loading control (LC) was used to compare protein levels between different gels and tubulin was used as a loading control between samples of the same gel. This blot is a representative image from 2 biological replicates. *BGJ- BGJ398, Das- dasatinib.*

4.8 - Discussion

In this chapter, an analysis of the phenotypic profile and signalling response of FGFR3 mutant expressing cells in the presence of BGJ398 was performed along with the investigation of the signalling pathway dependencies of FGFR3 mutants. This analysis led to the identification the Src pathway as a candidate signalling protein which may be important for regulating FGFR3 mutant biology. Importantly, I show that the multi-target kinase inhibitor dasatinib was able to sensitise mutant FGFR3 expressing cells to BGJ398 in long-term colony formation assays.

Although BGJ398 was capable of decreasing the cell viability of FGFR3 mutant expressing cells as shown in Figure 3.8A in chapter 3, these cells were ultimately resistant to BGJ398 treatment in the long-term colony formation assays (Figure 4.2). In fact, there was no significant reduction on cell survival and growth of cancer-associated FGFR3 mutants expressing cells at a high dose of 1 µM of drug. This data is consistent with the clinical observation that many patients that harbour FGFR3 mutations ultimately become resistant to selective FGFR inhibitors with tumour relapse (Katoh, 2019; Nogova et al., 2017).

To better understand the molecular mechanisms associated with the lack of response to BGJ398, I investigated the dose-dependent and temporal effects of the drug on the MAPK, Akt and Src pathways in the panel of mutant FGFR3 cells. My studies show that 1 hour treatment of BGJ398 was accompanied by a reduction of phosphorylation levels of Erk in all mutant cell lines compared to the controls, suggesting that one of the key signalling pathways directly regulated by FGFR3 is the MAPK pathway. It also suggests that this pathway may be a key driver of the oncogenic properties of mutant FGFR3 receptors. My findings are consistent with previously published studies, where pErk levels have been found to be reduced with BGJ398 treatment in bladder cancer cell lines expressing FGFR3 fusions and mutations. This includes the RT112 and RT4 (FGFR3-TACC3 fusions), KMS-11 (FGFR3-Y375C) and OPM2 (K652E) cell lines (Guagnano et al., 2012, 2011). Notably, pErk levels start to reappear after 6 hour treatment with BGJ398 which may be a potential reason why this drug is ineffective in long-term assays. This data is consistent with a published study data showing complete suppression of pErk levels in the human bladder cancer cell line RT112M (FGFR3-TACC3 fusion) after 1 hour treatment with the selective FGFR3 inhibitor PD173074, which was similarly partially restored after 6 hours treatment (Herrera-Abreu et al., 2013). There were also some changes observed in the phosphorylation levels of Akt and STAT3 that were independent of BGJ398 treatment, such as pAkt activation for the DMSO control condition at 1 hour and pSTAT3 activation at 6 hours. Such observations are likely to be an artefact of the fresh media change upon drug addition, as full serum media contains growth factors and cytokines responsible for inducing pathways of cell survival.

Given that the MAPK pathway was downregulated by BGJ398 treatment in the mutant FGFR3 cell lines, I sought to test the hypothesis that this pathway may be implicated in mediating the oncogenic properties of cancer-associated mutations of FGFR3. Treatment of cells with trametinib (MEK inhibitor), showed a reduction in pErk levels that was accompanied by a decrease in cell survival in colony formation, cell viability and spheroid-based assays. A similar effect has recently been reported in NIH-3T3 cells expressing the RT112Fus and K652E FGFR3 mutants (Nelson et al., 2018). I further showed that trametinib was more potent in reducing the viability in all cell lines examined compared to BGJ398. Trametinib completely suppressed pErk levels in all cell lines at both 1 and 6 hours. This is in contrast to BGJ398 treatment where the suppression of pErk levels was transient. Taken together, this data demonstrates that the MAPK pathway is a critical pathway essential for the survival of all cell lines examined, including the controls. It also provides additional evidence that the reduction in pErk levels observed downstream of mutant FGFR3 upon treatment with BGJ398 is a key signalling driver for their oncogenic properties.

Since BGJ398 treatment is ineffective in long-term colony formation assays, identifying additional signalling dependencies may shed light on therapeutics that could serve as salvage therapies in the context of FGFR inhibitor resistance. I undertook a multipronged approach to address this including the Luminex bead-based assay as well as a targeted small molecule inhibitor screen. The Luminex assay was very informative, highlighting not only the proteins that were differentially phosphorylated between the WT and FGFR3 mutants, but was also helpful in identifying differences in signalling between the three FGFR3 mutants. This analysis confirmed that distinct mutations activate different signalling pathways, raising the possibility that each mutation may have a unique set of pathway dependencies. One observed difference is in the phosphorylation levels of NFkB, that increased in the S249C expressing cells but was decreased in the RT112Fus cells compared to WT FGFR3. NFkB plays a crucial role during the inflammatory response in cancer development and is being exploited as a target for anti-cancer and anti-inflammatory drugs (Perkins, 2012). NFkB has previously been shown to be activated by mutant FGFR3 via TGFβ-activated kinase 1 (TAK1) in the bladder cancer cell line MGHU3 which harbours the Y375C

mutation and in HEK293 cells expressing the K652E FGFR3 mutation (Salazar et al., 2014). The Luminex data also showed an increased Src phosphorylation levels in the S249C, K652E and RT112Fus mutants compared to the WT FGFR3 expressing cells. Src is a non-receptor tyrosine kinase that is involved in many different cellular processes including cell adhesion, motility and survival (Paul A Bromann, 2004), and its deregulation is known to contribute to oncogenesis in a range of cancer types (Zhang and Yu, 2012). Src has been explored as a target for cancer therapy and has particularly been studied for its role as a key signalling node driving acquired and intrinsic resistance to tyrosine kinase inhibitors (Rexer et al., 2011). For instance, in HER2-overexpressing human breast cancer cell lines, the Src inhibitor AZD0530 was found to overcome resistance to lapatinib, a dual HER2 and EGFR inhibitor (Rexer et al., 2011). In this study, combined inhibition with AZD0530 and lapatinib was effective in preventing acquisition of lapatinib resistance (Rexer et al., 2011). However, studies exploring the potential of Src as a target for therapy in the context of FGFR3 mutant-driven cancers such as bladder cancer has been very limited.

In parallel, I conducted a targeted small-molecule inhibitor screen to perturb major signalling pathways and kinases implicated in cancer, facilitating the identification of signalling nodes that have a functional role in driving mutant FGFR3-mediated oncogenesis. Interestingly, my data demonstrates that distinct FGFR3 mutants harbour unique dependencies compared to the WT FGFR3 expressing cells. As expected, FGFR inhibitors and some broad-spectrum inhibitors that target the FGFRs such as ponatinib, cediranib and foretinib were found to sensitise all mutant FGFR3 expressing cell lines when comparing WT FGFR3. This is consistent with previously published studies in cancer cell lines that harbour FGFR3 mutation and validates the targeted small molecule inhibitor screen as a valid strategy to identify mutant-specific dependencies (Gozgit et al., 2012; Kataoka et al., 2012). The PI3K/mTOR inhibitor BEZ235 had selectivity for the S249C and RT112Fus mutants, suggesting that these mutants may preferentially utilise the PI3K-Akt-mTOR pathway to mediate their oncogenic effects. However, since there have been previous studies reporting the use of Akt pathway inhibitors to overcome resistance to FGFR3 inhibitors, this strategy was not pursued further (Datta et al., 2017).

Dasatinib, a broad-spectrum tyrosine kinase inhibitor whose targets include Src, also showed a distinct sensitivity profile across the mutants. Specifically, the RT112Fus and S249C mutants were found to confer a protective effect against dasatinib compared to the other mutants and WT FGFR3. Collectively my experiments show that despite the phosphorylation levels of Src being elevated across all the FGFR3 mutants profiled, there was contrasting functional effect when a Src inhibitor was investigated. These findings demonstrate that measuring protein phosphorylation levels alone is insufficient in predicting pathway dependencies and phenotypic assays remain the gold standard for evaluating functional effects. Although the number of studies reporting the role of Src in FGFR3 cancer-associated cell lines have been very limited, Vallo et al. found that Src suppression by dasatinib treatment can inhibit tumour growth and invasion in RT112 xenograft mouse models that are not resistant to the therapy regimen with gemcitabine (Vallo et al., 2016). In addition, studies in FGFR1 have shown that Src is able to modulate the activation, localisation and signalling dynamics of this receptor (Sandilands et al., 2007). This study showed that Src activity can regulate FGFR1 activation and transport to the plasma membrane through a RhoB in an actin-dependent mechanism. Moreover, in the same study, Src was found to function as a positive and negative regulator of FGFR1 signalling. Treatment of FGF2-stimulated MEFs with dasatinib failed to activate Akt, delayed Erk activation and failed to attenuate MAPK signalling. These results showed that activation of the Akt pathway through FGFR1 is dependent on Src and that Src is essential to activate Erk and regulate its signalling through FGFR1 (Sandilands et al., 2007). In the same study, the authors also suggested that Src inhibitors might be useful in the treatment of cancers which harbour FGFR1 mutations.

Based on my findings and evidence for the role of Src in modulating other FGFR family members, the next step of my studies sought to validate and further explore the differential sensitivities of distinct FGFR3 mutants to Src inhibitors. A full dose response cell viability assay as well as long-term colony formation assay confirmed the effects observed by the small molecule inhibitor screen, with the RT112Fus and S249C FGFR3 mutant expressing cells displaying resistance to dasatinib compared to the other mutations and controls. A similar phenotype was

also observed with the more selective but less potent Src inhibitor saracatinib, which provides additional evidence that this observed phenotype is a Src-mediated effect. Downstream signalling pathway analysis by immunoblotting confirmed that the phosphorylation levels of Src was equally suppressed across all cell lines upon treatment with dasatinib. Interestingly, in the N542K and K652E FGFR3 mutant expressing cells, this reduction in Src phosphorylation was accompanied by concomitant decrease in the phosphorylation of Erk at 1 µM. This data suggests that in these mutants dasatinib interferes with MAPK pathway and that this may be the reason why these cells are sensitive to treatment with this inhibitor. Supporting this idea, no reduction in the phosphorylation levels of Erk was observed in the for RT112Fus and S249C FGFR3 expressing cells. In fact, pErk levels were shown to increase at 1 µM of dasatinib. It is therefore possible that the inability of dasatinib to suppress pErk levels is the reason why these cells were not sensitive to treatment with this inhibitor.

The potential for Src inhibitors to sensitise cells to inhibitors of other RTKs such as EGFR have been previously reported (Rexer et al., 2011). To determine if a similar effect is observed in the context of FGFR inhibitors, I undertook inhibitor combination experiments of BGJ398 and dasatinib and showed that both drugs have synergistic effects when used together in mutant FGFR3 expressing cells. In particular, I show that low dose dasatinib was able to overcome resistance to BGJ398 in long-term colony formation assays. Analysis of downstream signalling showed that the combination led to a significant suppression of both the pErk and pSrc levels and a slight decrease in pAkt in the FGFR3 mutant expressing cells. This data demonstrates that combining low doses of dasatinib together with BGJ398 is an effective strategy to overcome resistance of mutant FGFR3 expressing cells to selective FGFR inhibitors.

In conclusion, I show that Src phosphorylation levels were elevated in the cancer-associated FGFR3 mutations investigated in this study. However, a subset of mutants (RT112Fus and S249C) harboured resistance to the broad-spectrum inhibitor dasatinib which was shown to downregulate the Src pathway. I further demonstrate that dasatinib was able to sensitise all FGFR3 mutant expressing cells to BGJ398 in long-term assays, highlighting the utility of this strategy as a

means of overcoming FGFR inhibitor resistance and potentially achieving more durable responses in mutant FGFR3 driven cancers.

Chapter 5

Investigation of the role of Src in a panel of FGFR3 altered human bladder cancer cell lines

5.1 - Introduction

In chapter 4, I have shown that Src phosphorylation increases upon expression of activating FGFR3 alterations in NIH-3T3 cells. However, the RT112Fus and S249C mutants were found to confer a survival and growth advantage to broad-spectrum Src inhibitors such as dasatinib and saracatinib, showing a differential dependency towards the Src pathway when compared to the other FGFR3 mutants and controls. Moreover, treatment of RT112Fus and S249C expressing cells with both dasatinib and the FGFR inhibitor BGJ398 led to a synergistic reduction in cell viability in long-term colony formation assay. To establish if the observations made in the NIH-3T3 model are also present in human cancer cell lines harbouring endogenous FGFR3 mutants, in this chapter, I evaluated the effects of dasatinib and BGJ398 in a panel of human bladder cancer cell lines (Table 5.1). The RT112M cell line was directly used to compare the effects observed with RT112Fus NIH-3T3 model while the 639V and MGHU3 cells which harbour extracellular cysteine mutations, were used to compare the phenotypic effects seen with the FGFR3 S249C NIH-3T3 expressing cells.

Table 5.1 – Panel of human bladder cancer cell lines with FGFR3 alterations.

Cell line	FGFR3 status	Reference
BFTC905	WT	(Nakanishi et al., 2015)
RT112M	FGFR3-TACC3	(Acquaviva et al., 2014)
639V	R248C	(Elliott et al., 1977)
MGHU3	Y375C	(Lin et al., 1985)

Previous studies have shown that other RTKs and alternative compensatory signalling pathways can bypass mutant FGFR3 dependency in cancer cells. For example, in the RT112 bladder cancer cell line, HGF ligand-mediated activation of MET was found to compensate for the loss of FGFR3 signalling induced by BGJ398 treatment (Harbinski et al., 2012). In a subsequent study, the activation of PI3K/Akt pathway was also found to induce resistance to the FGFR inhibitor AZD4547 in RT112M cells, and PI3K inhibitors were found to act in synergy with FGFR inhibitors in this cell line (Wang et al., 2017). However, targeting these compensatory pathways into effective clinical strategies has been a challenge. A

phase I clinical trial has shown that the combination of BGJ398 with the PI3K inhibitor BYL719 lead to a partial response in 8 patients over 24, one of which with bladder carcinoma bearing the FGFR3-TACC3 fusion achieved a complete response (NCT01928459). Although there is one ongoing clinical trial to explore the effect of BGJ398 together with the MEK inhibitor (MEK162) plus the RAF inhibitor (LGX818) in advanced BRAF mutant melanoma (NCT02159066), there are currently no clinical trials exploiting the combination of FGFR3 inhibitors with other signalling effectors in mutant FGFR3-driven bladder cancers.

Although Src has been found to be overexpressed and highly activated in a variety of cancers such as breast and liver cancers (Irby and Yeatman, 2000), the combination of Src inhibition with FGFR3 blockade has never been tested. This chapter investigates the potential of inhibiting Src signalling as a means of achieving durable drug responses in bladder cancer

5.2 - Bladder cancer cell lines respond differently towards FGFR3 inhibitors, and are resistant to Src inhibitors

Based on the observation that the combination of BGJ398 and dasatinib have a more potent effect in reducing long-term cell survival in RT112Fus and S249C expressing NIH-3T3 cells, four human bladder cancer cell lines were evaluated for their response to FGFR3 and Src inhibitors. Initially, to confirm the presence of R248C and Y375C FGFR3 mutations in 639V and MGHU3 bladder cancer cell lines, respectively, genomic DNA was isolated from each cell line and sequenced using Sanger sequencing, which confirmed the mutational status of these cell lines (Figure 5.1A). The FGFR3 expression levels of each cell line were also assessed by western blotting analysis (Figure 5.1B). 639V was found to express lower levels of FGFR3 when compared to the other cell lines. As expected, the FGFR3 protein from the RT112M cell line displayed a higher MW band which is consistent with the expression of the FGFR3-TACC3 fusion protein.

To investigate the phenotypic effects of FGFR inhibitors (BGJ398 and PD173074) and Src inhibitors (dasatinib and saracatinib) in the panel of bladder cancer cell lines, dose response assessment utilising the CTG assay was

performed. Consistent with data in the FGFR3 altered NIH-3T3 cell line models, all the bladder cancer cell lines were more sensitive to BGJ398 treatment comparing to the WT FGFR3 cell line BFTC905 (Figure 5.2A, E). Moreover, this sensitivity was more pronounced in the RT112M and MGHU3 cell lines which expressed higher levels of FGFR3 mutant receptor and correspondingly had lower IC_{50} values than BFTC905 and 639V (Figure 5.2E). In order to establish if the observed phenotype was specific to BGJ398, another FGFR inhibitor with a different molecular structure (PD173074) was also tested. PD173074 showed similar effects to treatment with BGJ398 with similar sensitising effects on the RT112M and MGHU3 cell lines comparing to BFTC905 (Figure 5.2B, E). Interestingly, the IC_{50} values for 639V and BFTC905 with PD173074 was considerably higher than with BGJ398. This suggests that different FGFR inhibitors might result in the downregulation of distinct pathways and/or have different potencies. For 639V and BFTC905 cell lines, it can be that the downstream pathways affected by PD173074 are not detrimental for cell survival, or in contrast to BGJ398, it results in a weaker downregulation of essential pathways for these cells.

When the panel of cell lines were subjected to dasatinib treatment, there was no significant difference in drug sensitivity across the panel of bladder cancer cell lines (Figure 5.2C, E). This observation is in contrast to the NIH-3T3 model where the expression of the RT112 fusion induced a protective effect towards dasatinib in the NIH-3T3 cells (Figure 4.10). Assessment of a second Src inhibitor saracatinib showed that this drug was ineffective in the bladder cancer cell lines with IC_{50} values >14 µM across all cell lines (Figure 5.2D, E).

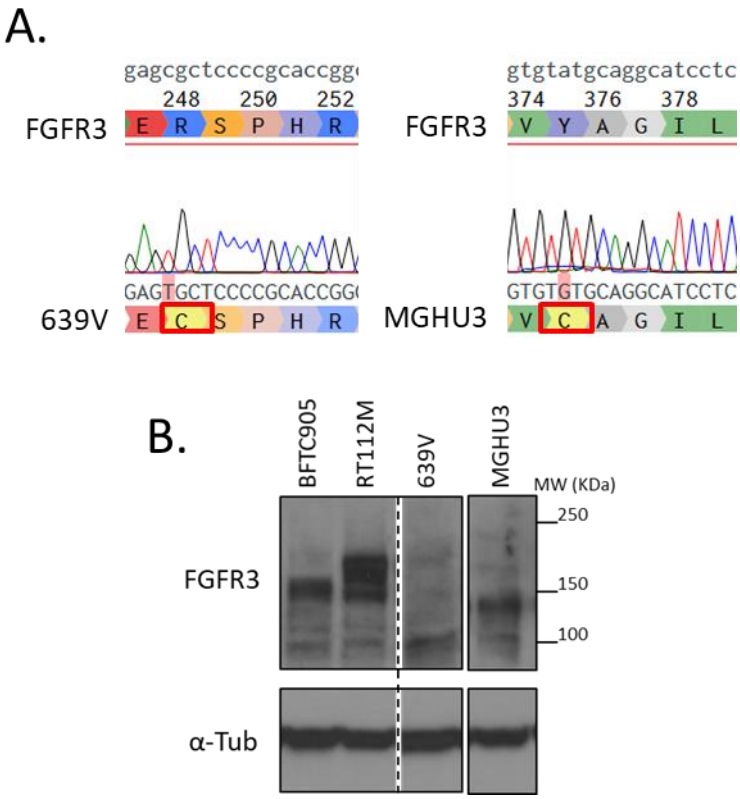

Figure 5.1 – Confirmation of FGFR3 mutation status in bladder cancer cell lines. A. Sanger sequencing was performed on the two FGFR3 mutant cell lines 639V and MGHU3 and results were aligned to the WT-FGFR3 sequence for comparison. Altered nucleotides are highlighted in red and mutated amino acid residue shown in the red square. **B.** Cells were lysed and extracted protein was subjected to a western blotting for verification of the expression levels of FGFR3.

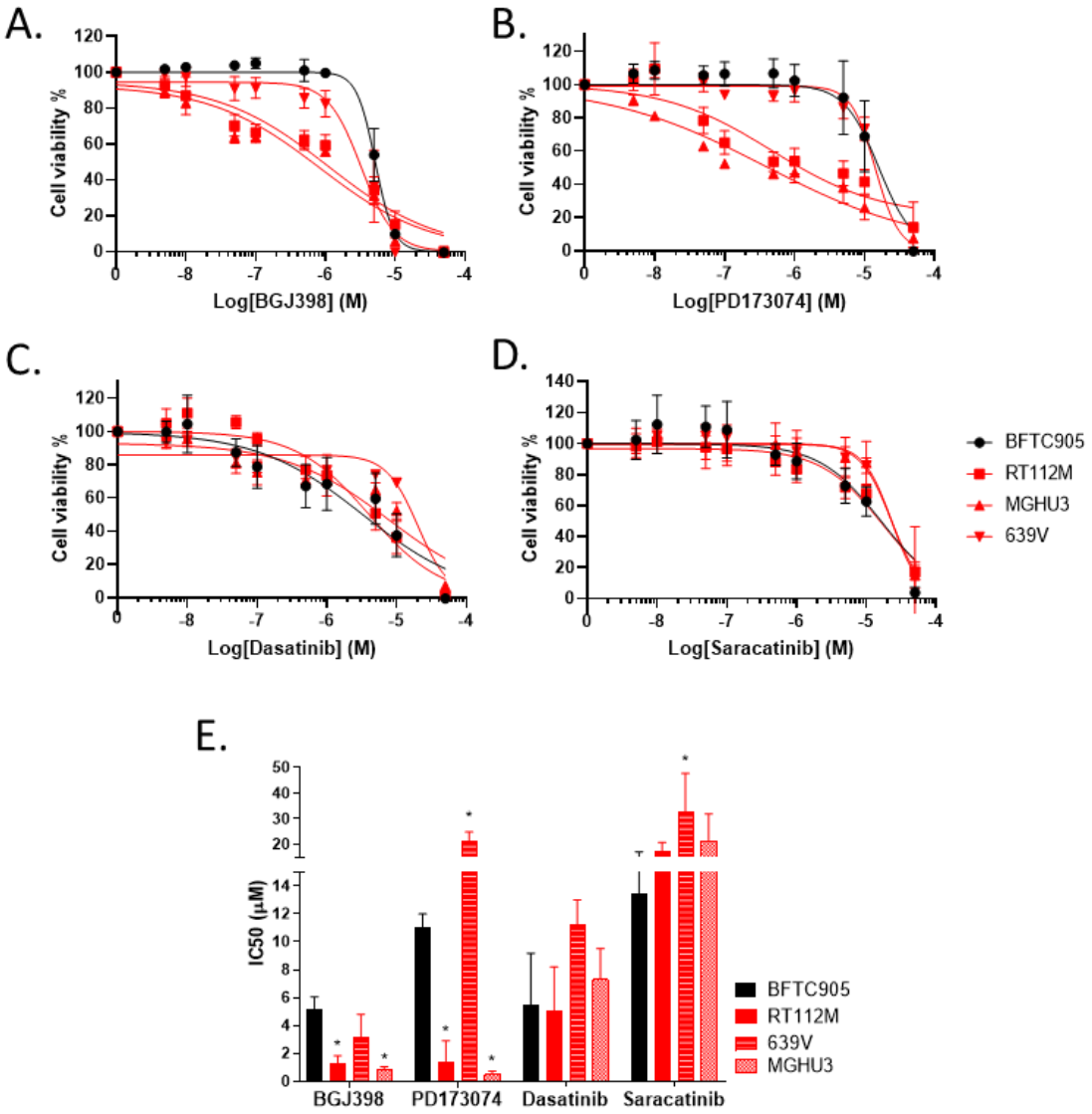

Figure 5.2 – Dose response curves of bladder cancer cell lines to FGFR3 and Src inhibitors. A-D. Cells were seeded in full media and treated with a range of 9 concentrations with the indicated inhibitors for 72 hours. Viability was measured by CTG assay and normalised against the DMSO vehicle control. Viability data was plotted and fitted with four-parameter non-linear regression with GraphPad Prism. **E.** IC_{50} values were extrapolated from the fitted dose response curves. Two-way ANOVA was used for statistical analysis against the WT BFTC905 control for each inhibitor. * p-value< 0.05. (n=3 biological replicates).

5.3 - The combination of FGFR inhibitors and dasatinib has synergistic effects in bladder cancer cell lines

Given the limited effects of single agent dasatinib treatment in the bladder cancer cell lines, I sought to investigate the cell line panel to the combination of FGFR

inhibitors with dasatinib (Figure 5.3A, B). The dose response curves showed that while the cell lines harbouring the fusion and FGFR3 mutants were insensitive to dasatinib alone, the combination of BGJ398+dasatinib was more effective than BGJ398 alone. Notably, the combination was also more effective at reducing cell viability in the control BFTC905 cell line when compared to the single agent BGJ398 but, required higher doses (above 1μM) than the cell lines harbouring FGFR3 alterations (below 0.5 μM). However, statistical significance was not achieved between single and combination treatment in the RT112M and MGHU3 cell lines (Figure 5.3B).

To assess if there is synergy between both inhibitors, the CI was calculated (Figure 5.3C). Synergy (CI<1) was observed in the 10 nM to 200 nM combined drug dose in RT112M, 639V and MGHU3 cell lines but only for 100 nM and 200 nM combined drug dose for BFTC905. Taken together, the results showed that the combined effect of BGJ398+dasatinib was more effective in all cell lines investigated and although the overall IC_{50} value of the combination was not statistically significant compared to BGJ398 treatment alone in the RT112M and MGHU3 cell lines, this combination showed a synergistic effect at lower combined drug doses compared to BFTC905.

A.

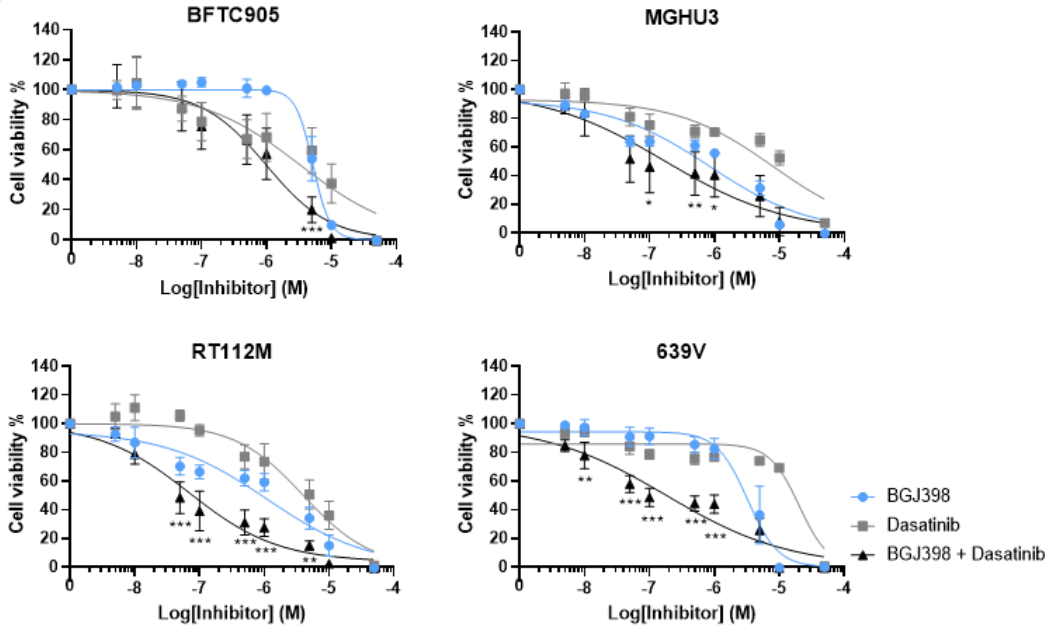

B.

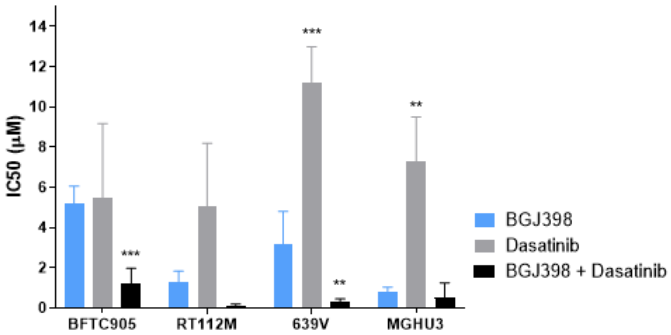

C.

Total Dose (µM)	Combination Index (CI)			
	BFTC905	RT112M	639V	MGHU3
0.01	1.55	0.41	0.11	0.40
0.02	3.10	0.20	0.13	0.47
0.1	0.38	0.22	0.24	0.34
0.2	0.36	0.30	0.35	0.53
1	1.30	1.01	1.52	2.14
2	1.91	1.68	2.98	4.08
10	2.67	3.66	7.86	9.55
20	0.53	0.88	0.05	4.03
100	0.09	0.02	0.25	0.01

Figure 5.3 – Dose response assessment of BGJ398 and dasatinib treatment as single agent or in combination in a panel of bladder cancer cell lines. A. Cell viability was measured with CTG assay after 72 hours treatment with serial dilutions of BGJ398 and dasatinib as single agent or in combination. In the combination arm, an escalating dose in 1:1 ratio was maintained. Data was fitted with a four-parameter non-linear regression on GraphPad Prism. Data for BGJ398 and dasatinib are the results from the previous Figure 5.2 and is displayed here for comparison (continuation of figure legend on following page)

(continuation of legend of Figure 5.3) purposes and visualisation of the effects exerted in the combination arm. Statistical analysis was performed with two-way ANOVA for each individual dose across the three treatments. * p-value< 0.05, ** p-value< 0.01, *** p-value< 0.001 and it is indicated only when statistical significance was found between the combination of BGJ398 plus dasatinib versus each inhibitor alone. **B.** IC_{50} values were calculated for independent replicates from dose response curves shown in A. Two-way ANOVA was applied to calculate the significance between dasatinib and BGJ398+dasatinib in comparison to BGJ398 alone for each cell line. ** p-value< 0.01, *** p-value< 0.001. **C.** The combinations index (CI) of BGJ398 plus dasatinib was calculated using the drug dose response data employing the Chou-Talalay method (Chou, 2010). Values <1 indicate a synergistic interaction between the two inhibitors. (n= 3 biological replicates).

Treatment of PD173074 with dasatinib, showed an analogous response in some of the cell lines. All cell lines investigated apart from MGHU3 showed a reduction in cell viability with the combination treatment compared to the FGFR3 inhibitor as single agent (Figure 5.4A). The IC_{50} value of the PD173074+dasatinib combination also did not show a significant cell survival decrease for RT112M when comparing to PD173074 alone (Figure 5.4B). CI calculation showed that there was no synergy observed across the majority of combined drug doses in the 639V cells (Figure 5.4C). As with BGJ398 treatment, synergy was shown in the RT112M cell line at multiple low drug doses. MGHU3 displayed synergy only in a subset of doses examined. The fact that PD173074 and BGJ398 display different synergy profiles in combination with dasatinib for different cell lines, in particular for 639V cells (Figure 5.3 C and 5.4C), suggests that these selective FGFR inhibitors interact with dasatinib in distinct ways affecting cell viability differently.

Overall, the data suggests that while dasatinib as a single agent has minimal effects on the viability of bladder cancer cells harbouring FGFR3 alterations, the combination of FGFR inhibitors and dasatinib is effective in reducing cell viability in a synergistic manner across a number of different drug concentrations.

A.

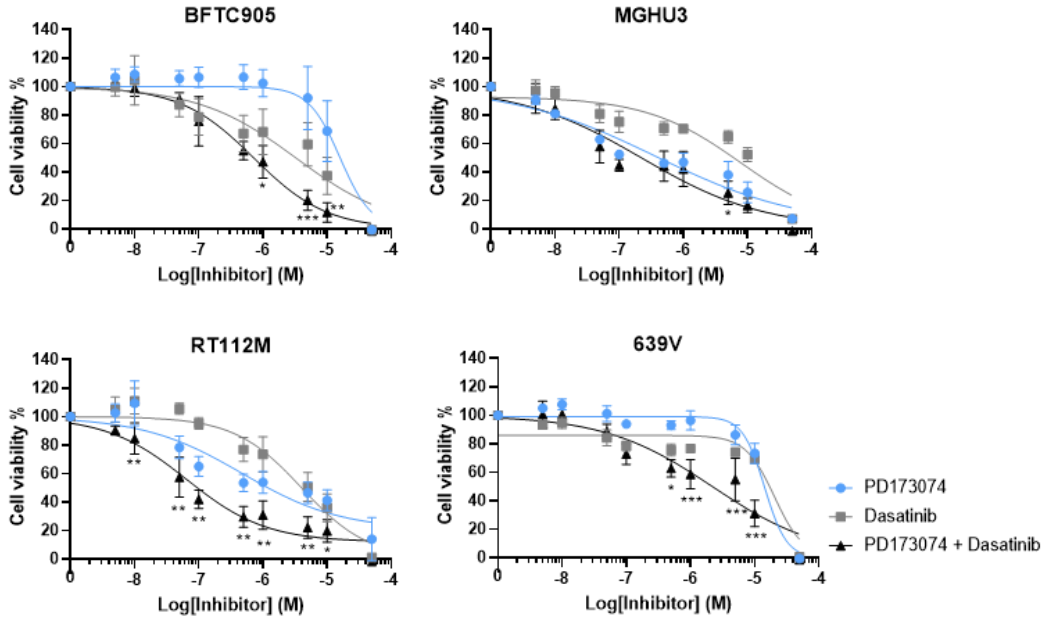

B.

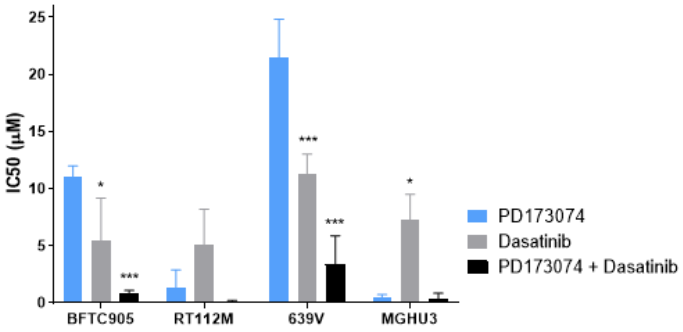

C.

Total Dose (µM)	Combination Index (CI)			
	BFTC905	RT112M	639V	MGHU3
0.01	1.53	0.04	422.33	4.08
0.02	0.43	0.05	844.66	1.44
0.1	0.42	0.05	1.08	0.30
0.2	0.33	0.06	0.40	0.17
1	0.78	0.17	1.01	0.81
2	1.23	0.35	1.56	1.34
10	2.28	1.13	6.31	1.16
20	2.74	1.97	3.54	0.68
100	0.05	0.00	0.02	0.00

Figure 5.4 – Dose response assessment of PD173074 and dasatinib treatment as single agent or in combination in a panel of bladder cancer cell lines. A. Cell viability was measured with CTG assay after 72 hours treatment with serial dilutions of PD173074 and dasatinib as single agent or in combination. In the combination arm, an escalating dose in 1:1 ratio was maintained. Data was fitted with a four-parameter non-linear regression on GraphPad Prism. Data for PD173074 and dasatinib are the results from the previous Figure 5.2 and is displayed here for comparison purposes and visualisation of the effects exerted in the combination arm. Statistical analysis was performed (continuation of figure legend on following page)

(continuation of legend of Figure 5.4) with two-way ANOVA for each individual dose across the three treatments. * p-value< 0.05, ** p-value< 0.01, *** p-value< 0.001 and it is indicated only when statistical significance was found between the combination of PD173074 plus dasatinib versus each inhibitor alone. **B.** IC_{50} values were calculated for independent replicates from dose response curves shown in A. Two-way ANOVA was applied to calculate the significance between dasatinib and PD173074+dasatinib in comparison to PD173074 alone for each cell line. * p-value< 0.05, *** p-value< 0.001. **C.** The combinations index (CI) was calculated using the drug dose response data employing the Chou-Talalay method (Chou, 2010). Values <1 indicate a synergistic interaction between the two inhibitors. (n= 3 biological replicates).

5.4- Dasatinib sensitises bladder cancer cell lines to FGFR inhibitor treatment in long-term colony formation assays.

To assess the effects of the single agent FGFR inhibitors in the human bladder cancer cell lines in longer-term colony formation assays, the panel of cells were seeded at low density and treated with the FGFR inhibitors BGJ398 and PD173074. After 14 days in culture, the surviving population was fixed and stained for imaging and quantification (Figure 5.5A, B). The data shows that, consistent with the short-term viability assays, the RT112M and MGHU3 cell lines were more sensitive to both inhibitors compared to BFTC905 and 639V. It should be noted that despite the increased sensitivity of these two cell lines, there were still a large proportion of residual colonies, suggesting that a significant proportion of cells were resistant to single agent FGFR inhibitor treatment. In contrast to FGFR inhibitors, dasatinib was effective across all four cell lines with dramatic reduction in colony formation in the BFTC905 and MGHU3 cells and to a lesser extent the RT112M and 639V lines. The combination of either of the two FGFR3 inhibitors with dasatinib showed a significant reduction in colony formation compared to the DMSO control for all cell lines, with colonies covering less than 20% of the well (Figure 5.5B, C). However, no significant statistical differences in well coverage area were seen between any of the cells harbouring FGFR3 alterations and the BFTC905 WT FGFR3 expressing cell line. Moreover, when comparing the enhanced effects of the combination treatment with single agent FGFR3 inhibitor alone, there was only statistical significance for the BFTC905 and 639V cell lines (Figure 5.5B), which is consistent with the results obtained in short-term viability assays (Figures 5.3B and 5.4B). Overall, long-term cell survival was reduced with the combination of BGJ398 or PD173074 with

dasatinib for all tested cell lines, prompting further analysis on the mechanistic processes involved in cell survival reduction with the combinations.

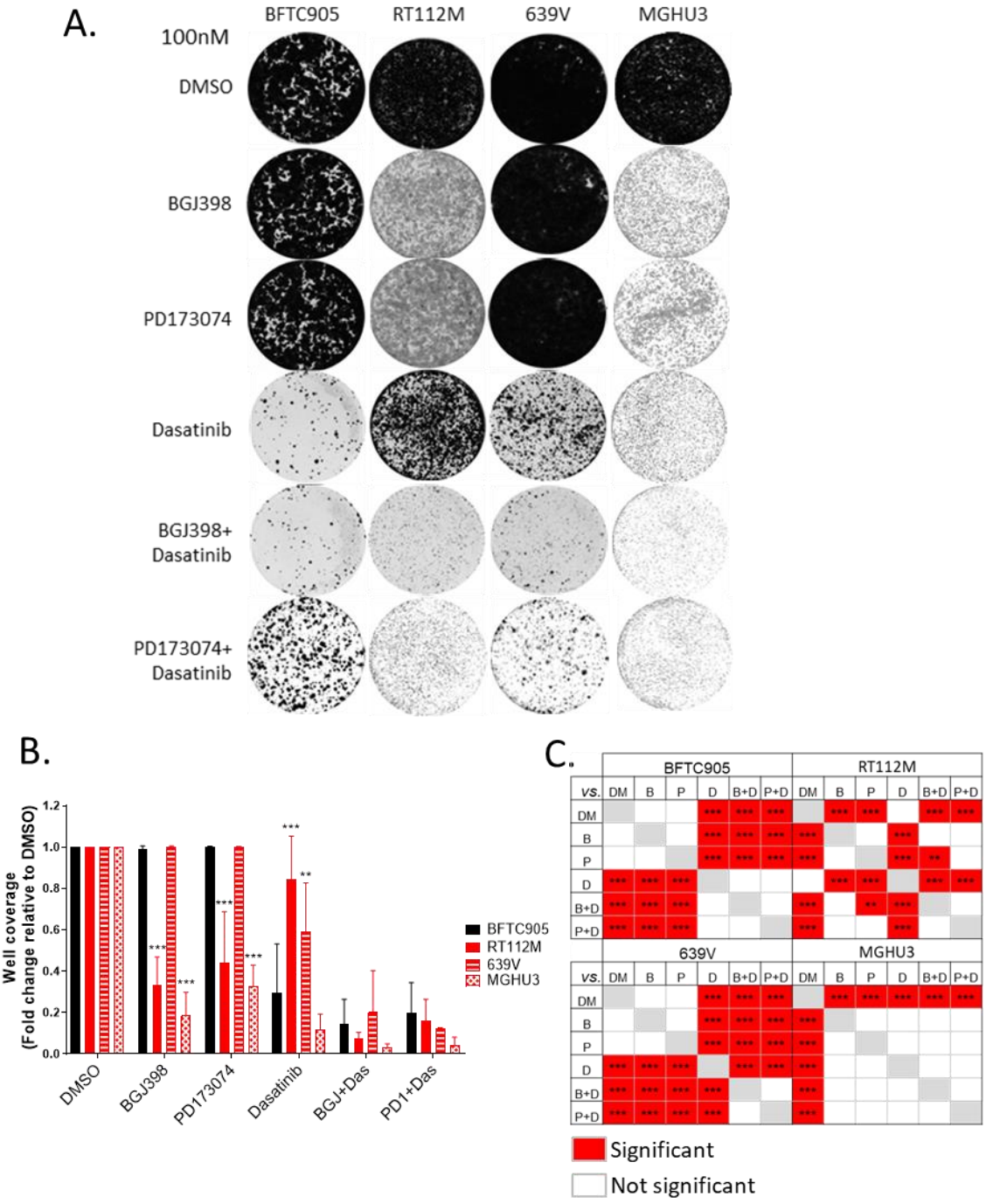

Figure 5.5 – Effects of FGFR inhibitors and dasatinib as single agents and in combination in colony formation assays. Colony formation assay was assessed by seeding cells at low density (15,000 cells/well) in 6 well plates and after 24 hours 100 nM of the corresponding inhibitors was added. The total dosage of inhibitor combination was 100 nM in a 1:1 ratio. (continuation of figure legend on following page)

(continuation of legend of Figure 5.5) Inhibitors were replenished every 3 days with fresh media for 14 days. **A.** Representative crystal violet staining of colony formation at day 14. **B.** The percentage of cells covering each well on the colony formation plates was calculated with imageJ and then normalised to the DMSO vehicle control. Two-way ANOVA statistical analysis was performed across cell lines for the same inhibitor when comparing to BFTC905. **C.** Two-way ANOVA statistical analysis was performed for each cell line across different drugs for pairwise combinations of the values displayed in B. ** p-value< 0.01, *** p-value< 0.001. (n=3 biological replicates). *DM- DMSO, B- BGJ398; P- PD173074; D- dasatinib.*

To characterise the temporal signalling changes associated with the addition of BGJ398 or dasatinib as single agents or in combination, I performed a western blot analysis in the RT112M cell line. Cells were lysed after 2, 4, 6 and 24 hours of treatment with the stated inhibitor to investigate the signalling dynamics in response to these inhibitors of interest (Figure 5.6). In the presence of BGJ398, pErk levels decreased at 2 hours but started to reappear at 4 and 6 hours post-treatment. This result is consistent with the signalling dynamics observed in the NIH-3T3 cell line model expressing the fusion protein (Figure 4.4). However, at 24 hours Erk phosphorylation was completely abolished by the addition of BGJ398 and this was accompanied by the suppression of pAkt. As expected, the addition of dasatinib treatment showed a complete suppression of pSrc for all time points up to 24 hours, accompanied by a small decrease in pAkt at 2 hours. The combination of both inhibitors displayed an additive effect of the individual inhibitors with concomitant decrease in the activation of both the Erk and Src signalling pathways. However, there was a lower decrease of pAkt at 24 hours compared to BGJ398 treatment alone.

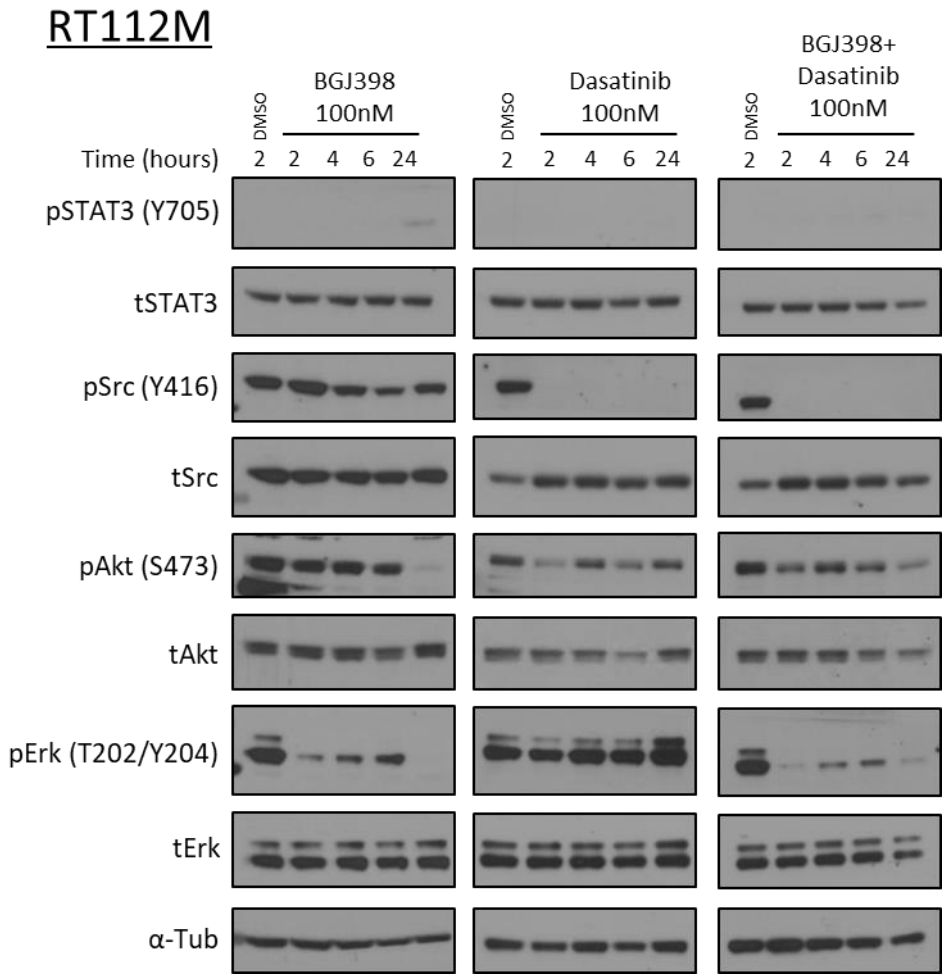

Figure 5.6 – Immunoblot of temporal signalling response of inhibitor treatment in RT112M cells. Cells were seeded in full media for 48 hours and treated with the indicated inhibitors at 100 nM. The combination arm consists of a total drug concentration of 100 nM in a 1:1 ratio for each inhibitor. Cells were lysed after 2, 4, 6 and 24 hours post-treatment. DMSO vehicle control cells were also collected at 2 hours. Protein extracts were resolved by SDS-PAGE for immunoblotting with the indicated proteins. Western blot is a representative image from 2 biological replicates.

5.5 - Investigating if the link between mutant FGFR3 and EGFR signalling is mediated through the Src pathway

Several molecular mechanisms have been shown to drive resistance to selective FGFR inhibitors in bladder cancer (see section 1.5.2). One of these mechanisms is the upregulation of EGFR signalling to compensate for the loss of mutant FGFR3 activity in the presence of the FGFR inhibitor PD173074 (Herrera-Abreu et al., 2013). The study by Herera-Abreu et al. further showed that the RT112M,

639V and MGHU3 cell lines were only partially dependent on FGFR3 signalling and inhibition by PD173074 induced EGFR phosphorylation leading to pErk reactivation after 6 hours of drug treatment. Consistent with this mechanism, dual blockade of FGFR3 and EGFR with a combination of PD173074 and gefitinib (an EGFR inhibitor) led to sustained downregulation of pErk signalling for up to 48 hours and a durable drug response (Herrera-Abreu et al., 2013). Given that Src is a major downstream signalling node of both FGFR3 and EGFR (Paul A Bromann, 2004), and that the combination of dasatinib and FGFR inhibitors was synergistic, I sought to investigate if the drug resistance induced by EGFR in the presence of FGFR inhibitors was due to the activation of the Src tyrosine kinase by this receptor.

Viability assays were therefore conducted to assess the dose response effect of gefitinib alone or in combination with either FGFR inhibitors or dasatinib in the panel of bladder cancer cell lines (Figure 5.7). Gefitinib as a single agent was ineffective in all four cell lines investigated (Figure 5.7A). To test if EGFR blockade exerts the same effect as Src blockade when used in combination with BGJ398, the combination of gefitinib plus BGJ398 was assess, however I found that this combination had no added benefit compared to single agent BGJ398 (Figure 5.7A-C). In addition, dual inhibition of the EGFR and Src with the combination of gefitinib and dasatinib was no more effective than dasatinib treatment alone (Figure 5.7A-C). To validate the observations made by Herrera-Abreu et al., I also assessed the response of PD173074 in combination with gefitinib in the panel of bladder cancer cell lines. The data showed that unlike BGJ398, combined treatment of gefitinib plus PD173074 shows a significant reduction in cell viability in the BFTC905 and 639V cell lines compared to PD173074 alone.

I further sought to establish the effects of gefitinib as a single agent or in combination in long-term colony formation assays (Figure 5.8). Consistent with the short-term cell viability assays, there is no additional benefit of adding gefitinib to BGJ398 or dasatinib in combination compared to single agent treatment alone.

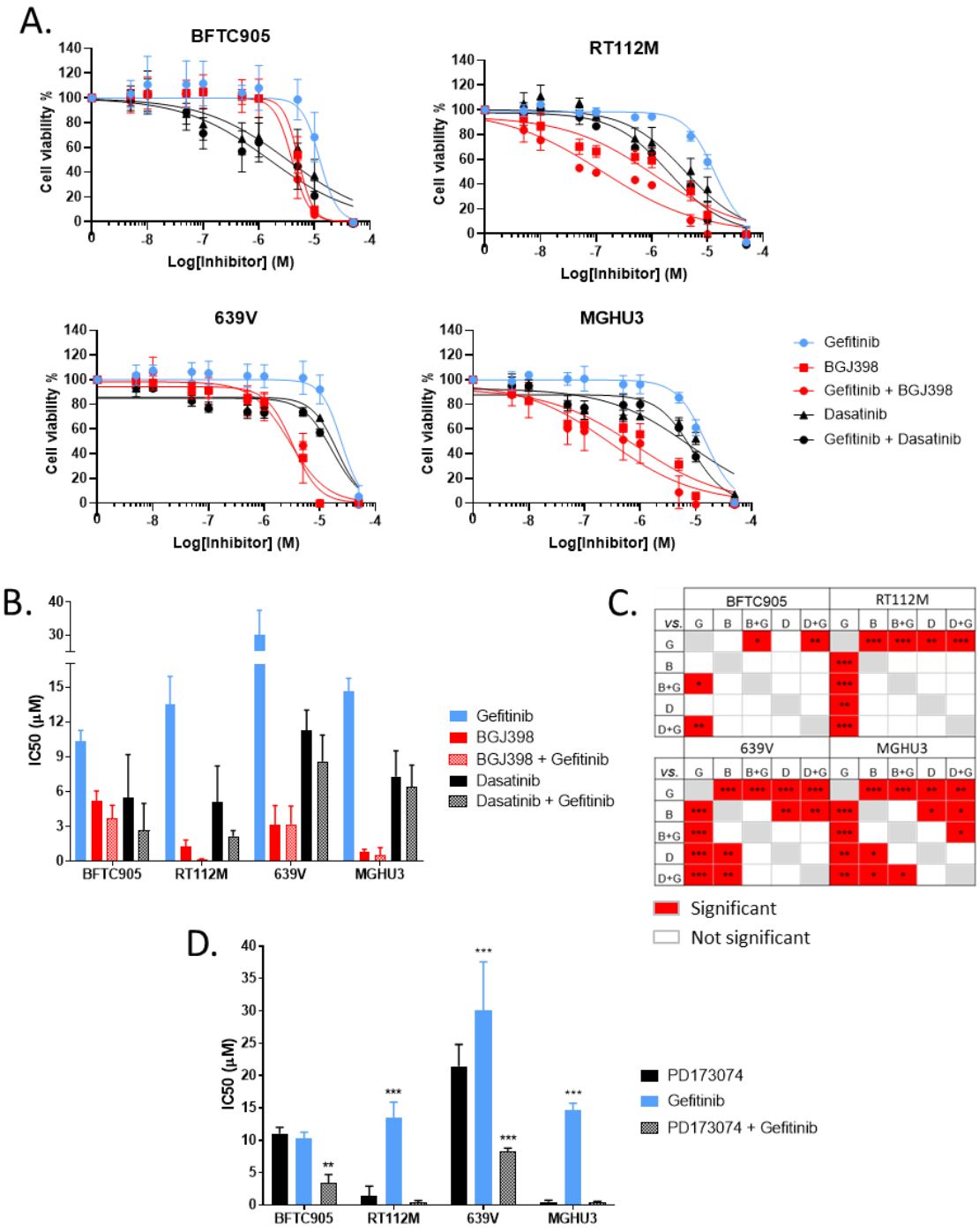

Figure 5.7 – Dose response profiles of a panel of bladder cancer cell lines upon treatment with FGFR, EGFR and Src inhibitors as single agents or in combination. A. Cell viability was measured with CTG after 72 hours treatment with serial dilutions of the indicated inhibitors. The combination arm used a 1:1 ratio for each drug with simultaneous escalating concentrations as indicated. Data was fitted with a four-parameter non-linear regression on GraphPad Prism. **B.** IC_{50} values were calculated from the data points of each individual regression in A for independent replicates. **A, B.** Data for BGJ398 and dasatinib are the results from the previous Figures 5.2A, 5.2C and 5.2E and is used here for comparison purposes and visualisation of the effects exerted with the combined agent. **C.** Two-way ANOVA statistical analysis was performed for each cell line across different drugs (continuation of figure legend on following page)

(continuation of legend of Figure 5.7) for pairwise combinations of IC_{50} values displayed in B. **D.** The dose response profiles were also evaluated for the combination of gefitinib and PD173074. The extrapolation of the correspondent IC_{50} values are here represented for the indicated inhibitors. PD173074 data was shown before in Figure 5.2E and is represented for comparison purposes. Statistical analysis used two-way ANOVA test to compare the effect of the combined agent and gefitinib to PD173074 alone. * p-value< 0.05, ** p-value< 0.01, *** p-value< 0.001. (n= 3 biological replicates). *G- gefitinib, B- BGJ398, D- dasatinib.*

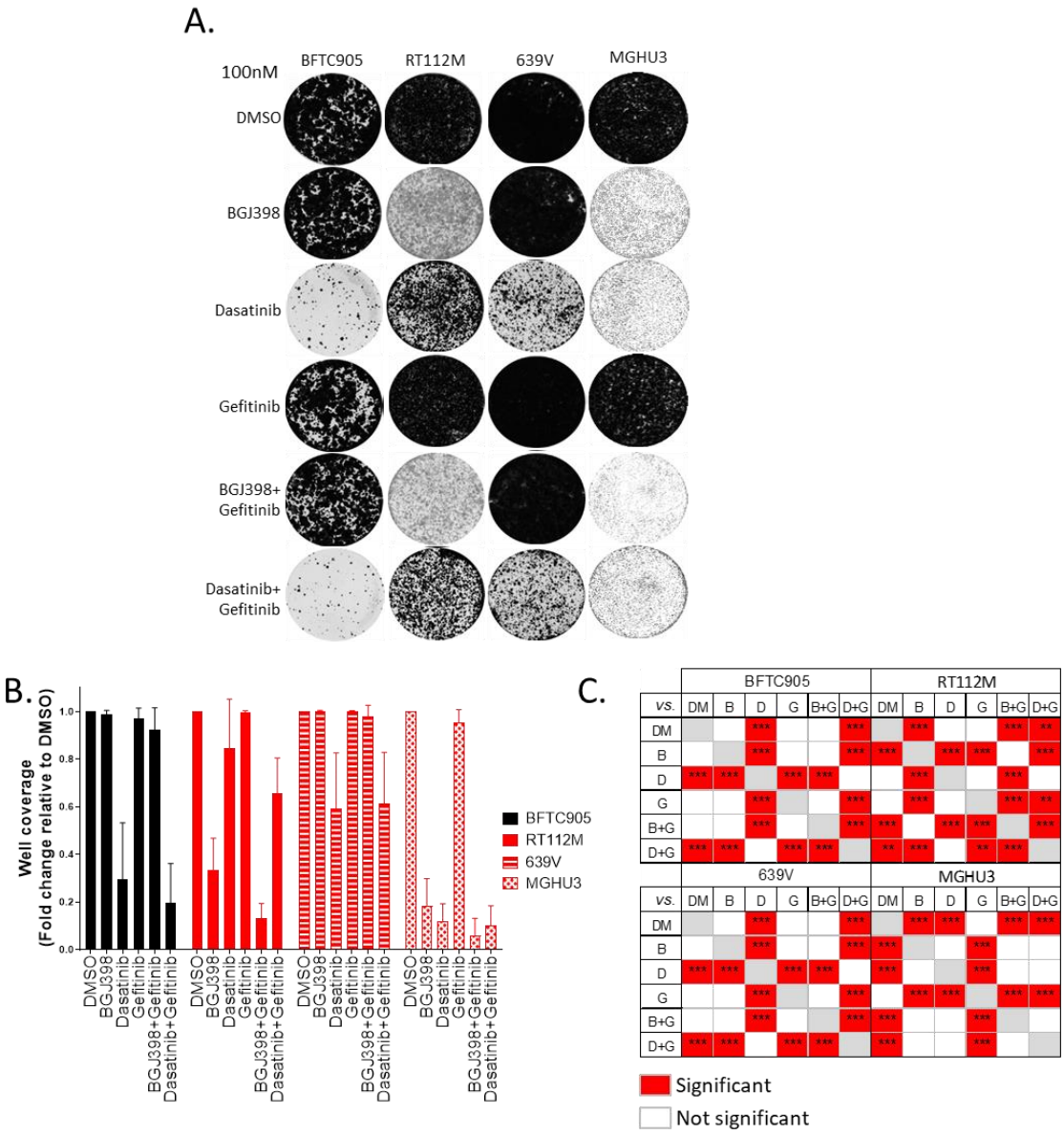

Figure 5.8 – Colony formation assay assessing the long-term effects of FGFR, EGFR and Src inhibitors as single agents or in combination. Colony formation assay was assessed by seeding cells at low density (15,000 cells/well). Cells were treated with 100 nM of the corresponding inhibitors after 24 hours in culture. The total dosage of combined inhibitors was 100 nM in a 1:1 ratio. Fresh inhibitor was replenished every 3 days for 14 days. **A.** Representative crystal violet staining of colony formation at day 14. Images for BGJ398 and dasatinib were previously represented in Figure 5.5A and here represented for comparison. **B.** The percentage of colonies covering each well was (continuation of figure legend on following page)

(continuation of legend of Figure 5.8) calculated with imageJ and then normalised to the DMSO control. DMSO, BGJ398 and dasatinib data was presented previously and is plotted for comparison. **C.** Statistical analysis was performed with two-way ANOVA for each cell line across different drugs for pairwise combinations the values displayed in B. (n=3 biological replicates). *DM- DMSO, G- gefitinib, B- BGJ398, D- dasatinib.*

To study the signalling mechanisms driving the observed phenotypes in the bladder cancer cell lines upon treatment with BGJ398, dasatinib and gefitinib as single agents or in combination, western blot analysis of the key signalling nodes was performed. Cancer cell lines were treated with the indicated drugs for 1 hour prior to cell lysis and immunoblotting (Figure 5.9).

Similarly to what was observed in the NIH-3T3 cell line models, BGJ398 and PD173074 treatment did not affect pErk levels for BFTC905 (WT FGFR) but it completely abolished pErk levels for the RT112M (FGFR3-TACC3 fusion) and MGHU3 (Y375C mutant) cell lines. Notably, these latter two cell lines were found to be the most sensitive to FGFR inhibitor treatment within the cell line panel (Figure 5.2A, E). Interestingly, both FGFR inhibitors did not reduce pErk levels in the 639V cells, which was shown to be non-responsive to both BGJ398 or PD173074 in cell viability assays (Figure 5.2A, E). For all four cell lines, dasatinib treatment suppressed Src phosphorylation and this was accompanied by an increase of total Src. The combination of inhibitors showed an additive effect of each inhibitor as single agents in the BFTC905, RT112M and MGHU3 cell lines. Therefore, for RT112M and MGHU3 cell lines, there was a decrease in pErk and pSrc as it was seen with FGFR3 inhibitors and dasatinib alone, respectively, and for BFTC905 cell line, there was a decrease in pSrc as seen with dasatinib alone. Notably, in the 639V cell line, the combination of either BGJ398 or PD173074 and dasatinib was now able to reduce pErk levels compared to treatment with any of the FGFR inhibitors or dasatinib alone.

Gefitinib as a single agent also induced an increase of pSrc for MGHU3 and had no effect on any of the remaining cell lines. Importantly, given that Src has previously been shown to be a downstream mediator of EGFR signalling (Paul A Bromann, 2004), treatment of all the cell lines with gefitinib did not lead to a reduction of the phosphorylation levels of Src, indicating that for these cell lines Src signalling is not dependent on upstream EGFR activity. On the other hand,

the combination of either FGFR inhibitor with gefitinib reduced the phosphorylation levels of Erk for RT112M and MGHU3 cell lines, as seen with BGJ398 and PD173074 alone, and partially reduced pErk levels for 639V cell line, which was not seen with either drug alone.

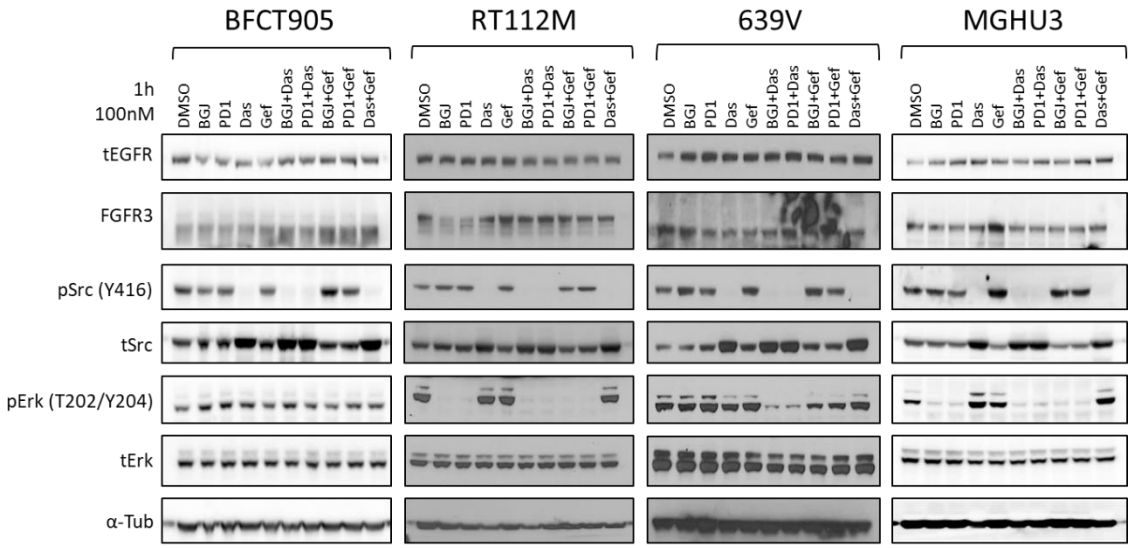

Figure 5.9 – Assessment of key signalling proteins in bladder cancer cell lines upon treatment with FGFR, EGFR and Src inhibitors as single agents or in combination. Cells were seeded for 48 hours and treated with the indicated inhibitors at 100 nM or vehicle control DMSO for 1 hour. The combination arm consists of a total concentration of 100 nM in a 1:1 ratio for each drug. Protein extracts were resolved by SDS-PAGE for immunoblotting with the indicated proteins. Representative images are shown from 2 biological replicates. *BGJ- BGJ398; Das- dasatinib; PD1- PD173074; Gef- gefitinib.*

Based on the data that pErk was reduced upon BGJ398 and PD173074 treatment in the RT112M and MGHU3 cell lines (Figure 5.9) and that this treatment was sufficient to reduce cell viability as a single agent (Figure 5.2A, B, E), I sought to investigate if the pErk pathway is a driver for cell survival in the panel of bladder cancer cell lines. Dose response assessment of trametinib, a MEK inhibitor, was performed in the panel of four bladder cancer cell lines (Figure 5.10). Consistent with the treatment with BGJ398 or PD173074 (Figure 5.2A, B, E), trametinib caused a dose dependent reduction in cell viability in the RT112M and MGHU3 cell lines (Figure 5.10). Interestingly this inhibitor had a more potent effect on the BFTC905 cells and showed no response in the 639V line, suggesting that the 639V cell line was not dependent on the MAPK pathway for survival.

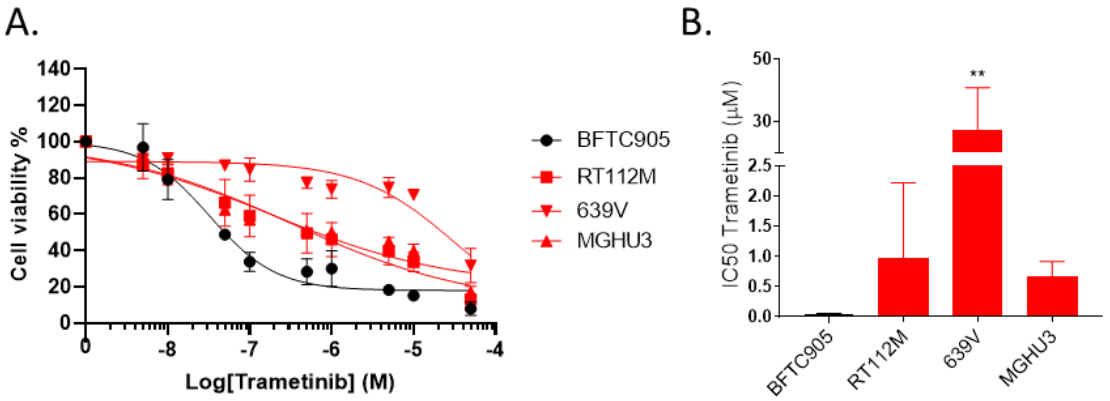

Figure 5.10 – Dose response assessment of trametinib treatment in the panel of bladder cancer cell lines. A. Cells were seeded for 24 hours and treated with the indicated range of concentrations of trametinib. Viability was measured with CTG assay after 72 hours and data fitted with a four-parameter non-linear regression on GraphPad Prism. **B.** IC_{50} values were calculated from the data points of each individual regression in A for independent replicates. Statistical analysis used one-way ANOVA test to compare IC_{50} between RT112M, MGHU3 and 639V cell lines compared to BFTC905. ** p-value< 0.01. (n= 3 biological replicates).

5.6 - Src gatekeeper mutation rescues phenotypes associated with dasatinib treatment

To determine if the action of dasatinib in the panel of bladder cancer cell lines was due specifically to the inhibition of Src activity, we utilised a gatekeeper mutant of Src. A point mutation of T338I in the avian *Src* gene has previously been shown to selectively block the binding of dasatinib (X. H. F. Zhang et al., 2009). By expressing this dasatinib-resistant gatekeeper mutant in the panel of bladder cancer cell lines, one can establish if Src is the target of this multi-target kinase inhibitor should the mutant rescue the phenotype induced by the treatment of dasatinib. As comparator, the WT *Src* gene and an EV control plasmid were used. Plasmids were transduced into the four bladder cancer cell lines, BFTC905, RT112M, 639V and MGHU3 by retroviral transfection and expression of gene maintained by selection with hygromycin. Stable expression was confirmed by western blotting and compared to the untransduced parental cell lines and EV controls (Figure 5.11). When comparing to the parental cells and the EV control, an increase in Src was only obtained for 639V cell line. Notably, there is an

increase in the levels of Src expression upon transduction of the EV plasmids in the BFTC905, RT112M and 639V cell lines for reasons that are unclear. An increase Src expression was obtained in the MGHU3 cell line when compared to the EV control, but expression was still lower than the parental cell line. Overall, high ectopic expression of Src was not achieved in any of the cell lines, which might be explained by the ability for cells to adapt and change their gene expression to accommodate and limit expression of the exogenous gene (Eguchi et al., 2018; Grubera et al., 2008).

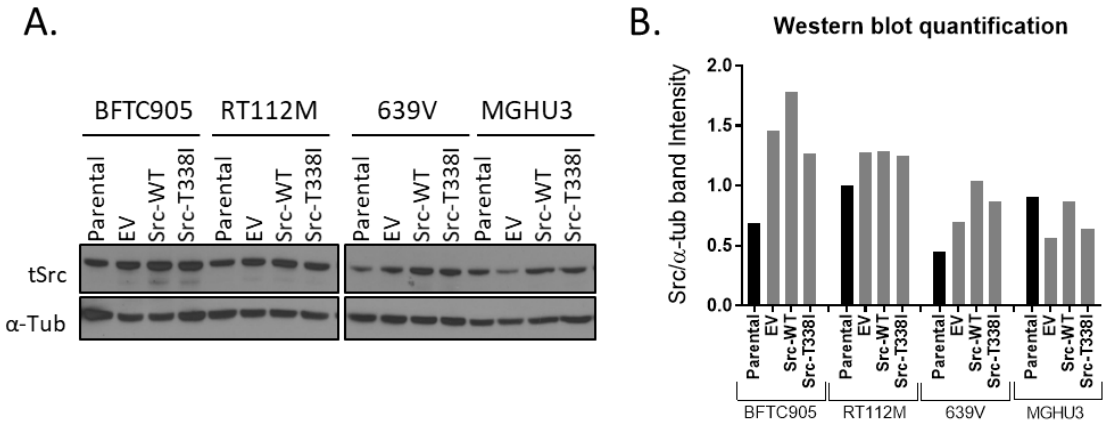

Figure 5.11 – Evaluation of ectopic Src expression in the panel of bladder cancer cell lines. Retroviral transduced cells were lysed and protein extracts separated on an SDS-PAGE for immunoblotting with tSrc. **A.** Levels were run along with the parental non-transduced cell line and the EV control. Tubulin was used as a loading control. **B.** Levels of tSrc were quantified with imageJ and normalised to the tubulin loading control.

Despite lack of an observable increase in Src expression levels in the gatekeeper mutant expression cells, the transduced cell line panel was subjected to long-term colony formation assays in the presence of 100 nM and 500nM of BGJ398 and dasatinib as single agents or in combination (Figure 5.12). After 14 days in culture, there was a clear rescue effect in the cells expressing the Src-T338I gatekeeper mutant in the presence of dasatinib, indicating that low ectopic protein expression levels were still capable of inducing a phenotype on these cells. Compared to the EV and Src-WT controls, cells displayed a lack of sensitivity towards dasatinib and the combination of dasatinib plus BGJ398 for all four cell lines. These data provide evidence that the phenotypic effects observed with dasatinib treatment or the combination of dasatinib with FGFR inhibitors is due to

the selective targeting of Src by the drug. When short-term cell viability assays were performed, a similar trend of a rescue effect was observed in the presence of dasatinib, with all cells except 639V presenting a higher IC_{50} when expressing the Src gatekeeper mutant compared to the EV control, although statistical significance was not reached (Figure 5.13). The exception for the 639V cells where the rescue effect was not pronounced is due to the parental cell line being already resistant to dasatinib (Figure 5.2E). In the presence of BGJ398 plus dasatinib, Src-T338I expressing cells were able to revert the phenotype to BGJ398 alone for all cell lines, and a significant increase the cell viability was observed for all cell lines compared to the EV control cells, except in MGHU3 cells (Figure 5.13B).

Taken together, these experiments demonstrate that the observed sensitisation effect of dasatinib on BGJ398 treatment in the panel of FGFR3 dependent bladder cancer cell lines is due to the selective inhibition of the Src protein.

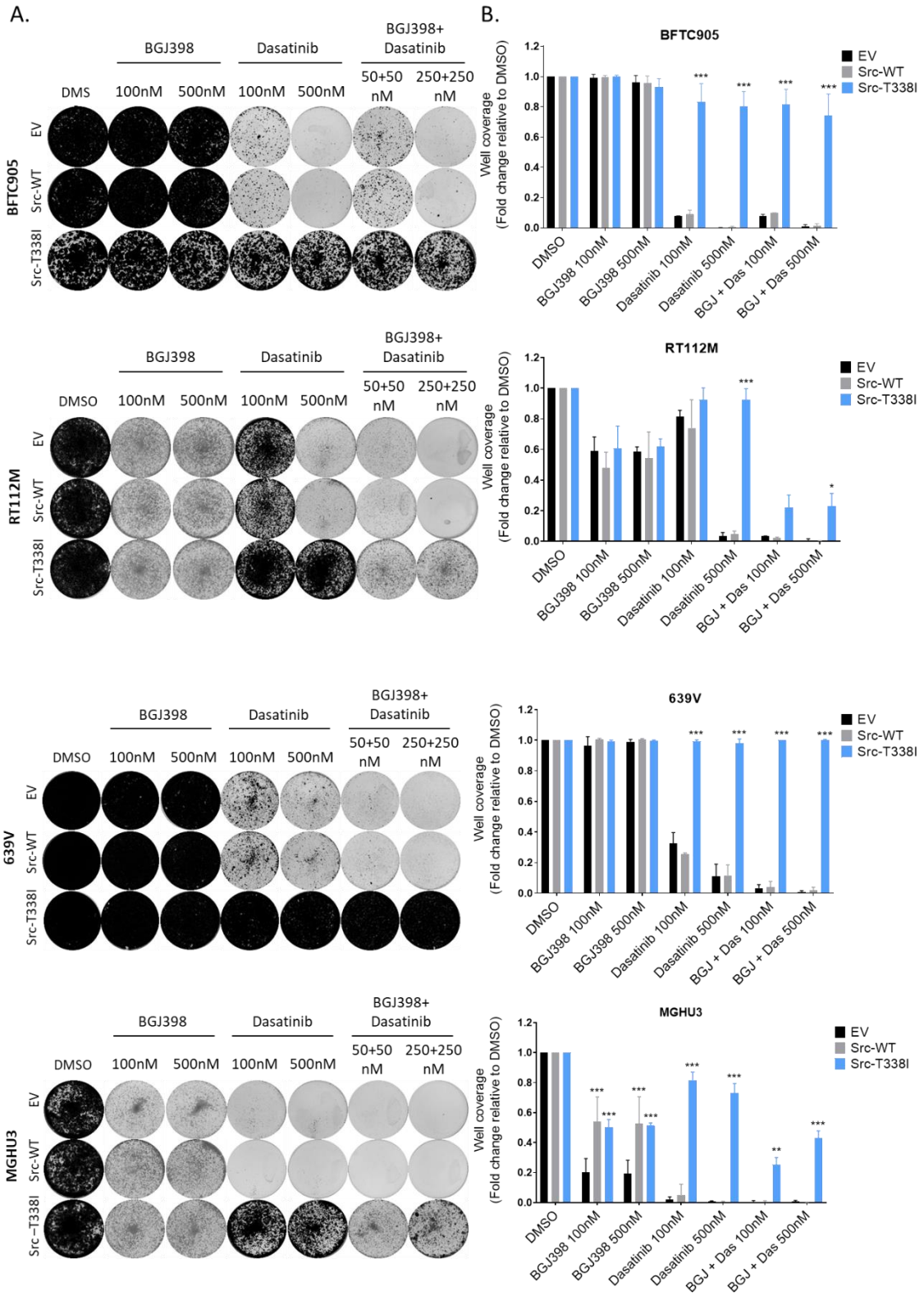

Figure 5.12 – Colony formation assays of Src transduced bladder cancer cell lines upon treatment with BGJ398 and dasatinib. A. Cells were seeded at low density (15,000 cell/well) on 6-well plates. After 24 hours, cells were treated with the indicated dose of the corresponding inhibitors along with the vehicle control DMSO. Fresh inhibitor was replenished every 3 days for 14 days. On day 14 cells were fixed and stained for visualisation with crystal violet. **B.** Quantification of the colony formation assay. The percentage of colonies covering each well was calculated with (continuation of figure legend on following page)

(continuation of legend of Figure 5.12) imageJ and then normalised to the DMSO control. Statistical analysis was performed with two-way ANOVA for each inhibitor of each cell line against the EV control. * p-value< 0.05, ** p-value< 0.01, *** p-value< 0.001. (n=2 biological replicates). *BGJ- BGJ398; Das- dasatinib.*

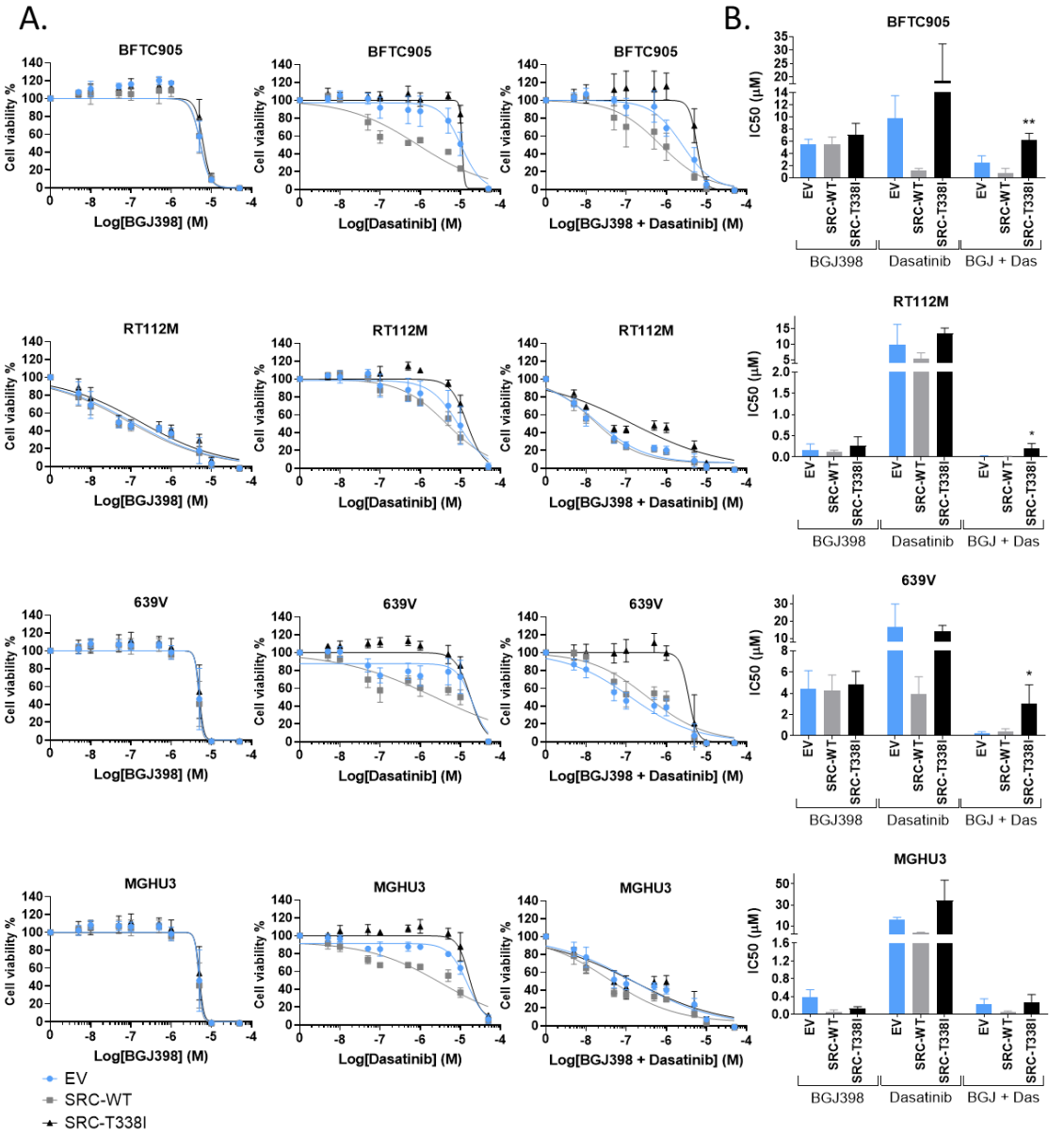

Figure 5.13 – Dose response assessment of Src transduced bladder cancer cell lines upon treatment with BGJ398 and dasatinib. A. Cells were treated with a dose range of the indicated inhibitors after seeding for 24 hours in culture and viability was measured after 72 hours of treatment using the CTG assay. The combination arm was performed using a 1:1 ratio with escalating drug concentrations as indicated. Data was normalised against the DMSO control and data fitted with a four-parameter non-linear regression on GraphPad Prism. **B.** IC_{50} values were calculated from the data points of each individual regression in A for independent replicates. Statistical analysis used one-way ANOVA test to compare IC_{50} compared to the EV control for each inhibitor in each cell line. * p-value< 0.05, ** p-value< 0.01. (n= 3 biological replicates). *BGJ- BGJ398; Das- dasatinib.*

5.7 - Dissecting the pathway dependencies in the FGFR3 mutant bladder cancer cell lines

In section 5.5, I showed that treatment with BGJ398 in combination with dasatinib led to pSrc suppression in the BFTC905 cell line, and dual pSrc and pErk suppression in MGHU3, RT112M and 639V cell lines. To establish which signalling pathways are critical for maintaining cell survival in each of the FGFR3 bladder cancer cell lines, small molecular inhibitors for key signalling pathways were used. Specifically, the MEK inhibitor trametinib was used to inhibit the Erk pathway, the PI3K/mTOR inhibitor BEZ235 was employed to suppress the Akt pathway and dasatinib the Src pathway. These inhibitors were added to the panel of bladder cancer cell lines either as single agents or in combination and evaluated in short-term (72 hour) cell viability assays (Figure 5.14). Western blotting was also undertaken to evaluate pathway suppression in the cell lines upon drug treatment (Figure 5.15).

This analysis found that of all the single agent inhibitor treatments in the BFTC905 cell line, only trametinib was able to reduce cell viability, while BEZ235 and dasatinib had no activity as single agents, although no statistical significance was found (Figure 5.14A). Interestingly, the combination of dasatinib plus BEZ235 was able to reduce BFTC905 cell viability to a similar degree as trametinib alone. This data indicates that in addition to the Erk pathway, this cell line was dependent on the simultaneous activation of both the Src and Akt pathways (Figure 5.15). In the case of the RT112M FGFR3 fusion cell line, blockade with any of the three inhibitors as single agents did not have an effect on cell viability (Figure 5.14B). However, targeting any combination of the three inhibitors or the addition of all three inhibitors simultaneously, although not significant, led to a reduction in cell viability which demonstrates that the suppression of at least two of the three pathways under investigation (MAPK, Akt and Src) is required to reduce survival in this cell line (Figure 5.15). In contrast, the 639V cell line which harbours the R248C FGFR3 mutation, was only sensitive to trametinib plus BEZ235 and dasatinib plus BEZ235 combination but not the trametinib plus dasatinib combination (Figure 5.14C). This finding shows that in this cell line, cell survival requires the activation of the Akt pathway and either the Erk or Src

pathways (Figure 5.15). Notably, given that dual blockade of Src and Erk (with trametinib plus dasatinib) was insufficient to cause a reduction in cell viability, one can conclude that the presence of the Akt pathway alone is able to maintain survival in the 639V cell line (Figure 5.15). In the case of the MGHU3 cell line, a strong dependency on the Akt pathway was observed, as BEZ235 treatment led to a reduction in cell viability, which was not observed for dasatinib and to a lesser extent trametinib (Figure 5.14D). A dependency on the Akt pathway for MGHU3 cells was previously described with BKM120 (PI3K inhibitor) and AZD5363 (Akt inhibitor) (Davies et al., 2015; Wang et al., 2017). In these studies, tumour growth of MGHU3 xenograft models was reduced by BKM120 or AZD5363 treatment, and both inhibitors were found to act synergistically with FGFR3 inhibition by AZD4547. This effect was demonstrated to be caused by an activating mutation on *AKT1* (E17K) gene on MGHU3 cell line, which drives PI3K/Akt pathway activation and dependency (Davies et al., 2015).

Taken together, this data demonstrates that the bladder cancer cell lines bearing distinct FGFR3 mutants are dependent on different downstream signalling pathways. Whereas different combinations of inhibitors targeting the main downstream signalling pathways could lead to cell sensitivity in the different cell line models, only the BGJ398 plus dasatinib combination was able to selectively reduce cell viability in the panel of FGFR3 altered bladder cancer cell lines examined, in comparison to the BFTC905 cell line (Figure 5.3B).

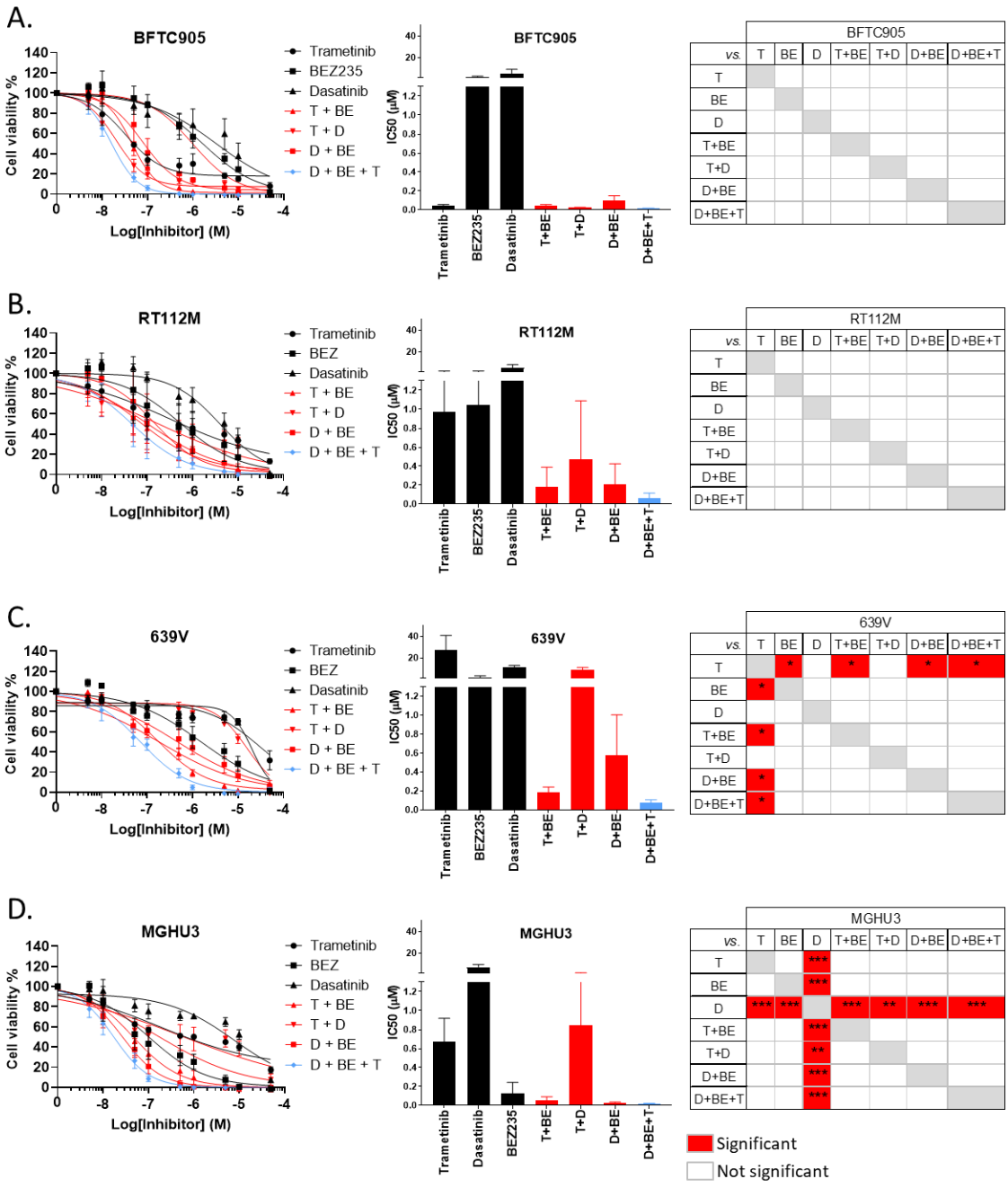

Figure 5.14 – Dose response assessment in bladder cancer cell lines upon treatment with trametinib, BEZ235 and dasatinib. A-D. FGFR3 bladder cancer cell lines. The dose response curves (on the left) represent cell viability that was measured with CTG assay upon 72 hours treatment with a range of concentrations of the indicated inhibitors. The double and triple combination arms used a 1:1 and a 1:1:1 ratio respectively, with escalating drug concentrations as indicated. Data was fitted with a four-parameter non-linear regression on GraphPad Prism. Data for dasatinib and trametinib are the results collected previously (Figures 5.2 and 5.10) and are used here for comparison. The bar charts (in the middle) represent the IC_{50} values calculated from the data points of each individual regression for independent replicates. Two-way ANOVA statistical analysis (on the right) was performed for each cell line across different drugs for pairwise combinations of each IC_{50} value. ** p-value< 0.01, *** p-value< 0.001. (n=2 or 3 biological replicates). *BE- BEZ235; T- trametinib; D- dasatinib.*

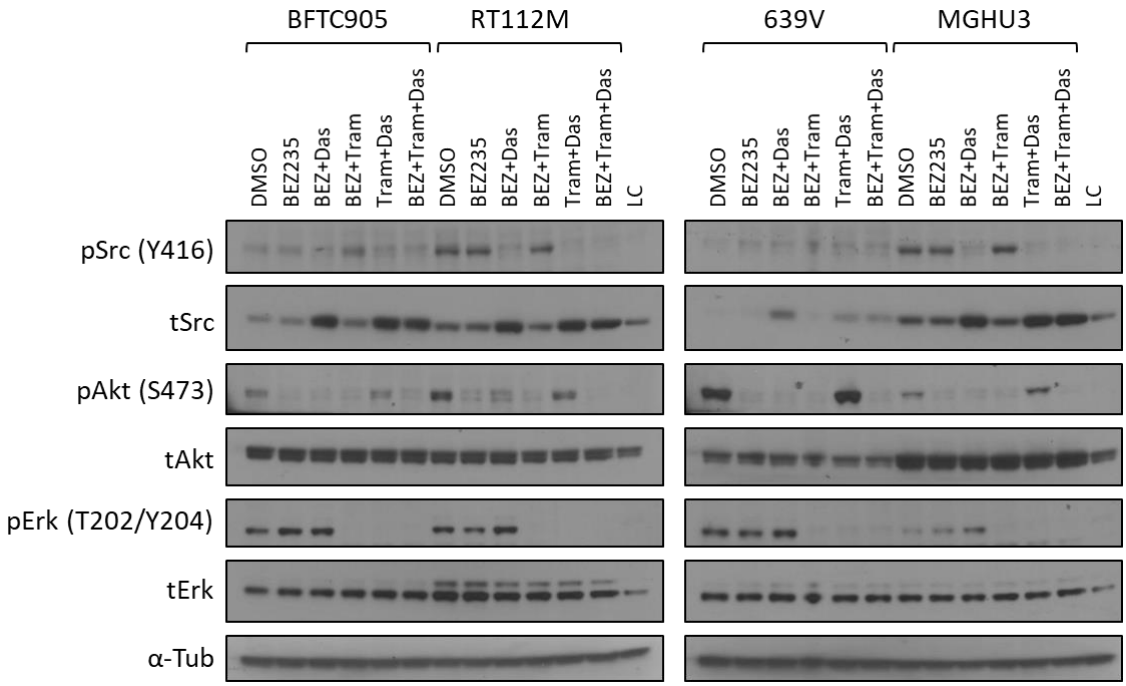

Figure 5.15 – Assessment of key signalling proteins in bladder cancer cell lines upon treatment with trametinib, BEZ235 and dasatinib as single agents or in combination. Cells were seeded for 48 hours in culture and treated with the indicated inhibitors at 100 nM or vehicle control DMSO for 1 hour. The combination arm utilised drug doses at 100 nM each. Protein extracts were resolved by SDS-PAGE for immunoblotting with the indicated proteins. The loading control (LC) was used to compare samples between different blots. *BEZ- BEZ235; Tram- trametinib; Das- dasatinib.*

5.8 - Discussion

In this chapter, I undertook a characterisation of the phenotypic and signalling effects of a number of inhibitors for key signalling pathways in a panel of bladder cancer cell lines that harbour endogenous FGFR3 mutations (Table 5.2). This analysis included the FGFR inhibitors BGJ398 and PD173074 and the Src inhibitor dasatinib which were previously shown to be effective as a combination strategy for some FGFR3 mutants in the NIH-3T3 models in chapter 4. As single agents, the FGFR inhibitors BGJ398 and PD173074 had variable effects in the bladder cancer cell lines investigated. In both the short-term cell viability assay and colony formation assay, the 639V (R248C) cell line was found to lack sensitivity to both inhibitors when compared to the MGHU3 (Y375C) and RT112M (TACC3-FGFR3 fusion) cell lines. In our experiments, both MGHU3 and RT112M

displayed comparable sensitivity to these drugs which is inconsistent with the previous study by Acquaviva et al, which demonstrated that RT112M was significantly more sensitive to BGJ398 than MGHU3 (Acquaviva et al., 2014). Notably, the 639V cells were considerably more sensitive to BGJ398 than to PD173074 in cell viability assays, which demonstrates that distinct selective FGFR inhibitors induce different responses in the same cell line and may allude to FGFR3 mutant specific selectivity to structurally distinct FGFR inhibitors.

Table 5.2 – Summary of the results from the phenotypic assays and signalling effects executed for the panel of bladder cancer cell lines. For the cell viability and colony formation assays the comparison evaluated is indicated on the 'vs' column. Cell viability summary is based on Figures 5.2-5.4, 5.7 and 5.10. Colony formation summary is based on Figures 5.5 and 5.8. Western blot summary is derived from Figures 5.6 and 5.9. *S↓- significantly inferior; S↑- significantly superior; NS- not sensitive; ↑- increased levels of phosphorylation; ↓- decreased levels of phosphorylation (small arrow represents small decrease); (=)- phosphorylation levels remain the same; (—)- not evaluated; na- not applicable; BGJ- BGJ398; Das- dasatinib; PD1- PD173074; Gef- gefitinib; BFTC- BFTC905.*

	Inhibitor	*vs (Cell viability | Colony formation)*	Cell viability	Colony formation	Western blotting (1h)	
					pSrc	pErk
BFTC905	BGJ398	BFTC | DMSO	na	NS	=	=
	PD173074	BFTC | DMSO	na	NS	=	=
	Dasatinib	BFTC | DMSO	na	S ↓	↓	=
	Trametinib	BFTC | DMSO	na	—	—	—
	Gefitinib	BFTC | DMSO	na	NS	=	=
	BGJ+Das	BGJ | BGJ	S ↓	S ↓	↓	=
	PD1+Das	PD1 | PD1	S ↓	S ↓	↓	=
	BGJ+Gef	BGJ | BGJ	NS	NS	=	=
	PD1+Gef	PD1 | PD1	S ↓	—	=	=
	Das+Gef	Das | Das	NS	NS	↓	=
639V	BGJ398	BFTC | DMSO	NS	NS	=	=
	PD173074	BFTC | DMSO	NS	NS	=	=
	Dasatinib	BFTC | DMSO	NS	NS	↓	=
	Trametinib	BFTC | DMSO	S ↑	—	—	—
	Gefitinib	BFTC | DMSO	NS	NS	=	=
	BGJ+Das	BGJ | BGJ	S ↓	S ↓	↓	↓
	PD1+Das	PD1 | PD1	S ↓	S ↓	↓	↓
	BGJ+Gef	BGJ | BGJ	NS	NS	=	↓
	PD1+Gef	PD1 | PD1	S ↓	—	=	↓
	Das+Gef	Das | Das	NS	NS	↓	=

	Inhibitor	*vs (Cell viability | Colony formation)*	Cell viability	Colony formation	Western blotting (1h)	
					pSrc	pErk
RT112M	BGJ398	BFTC | DMSO	S ↓	S ↓	=	↓
	PD173074	BFTC | DMSO	S ↓	S ↓	=	↓
	Dasatinib	BFTC | DMSO	NS	NS	↓	=
	Trametinib	BFTC | DMSO	NS	—	—	—
	Gefitinib	BFTC | DMSO	NS	NS	=	=
	BGJ+Das	BGJ | BGJ	NS	NS	↓	↓
	PD1+Das	PD1 | PD1	NS	S ↓	↓	↓
	BGJ+Gef	BGJ | BGJ	NS	NS	=	↓
	PD1+Gef	PD1 | PD1	NS	—	=	↓
	Das+Gef	Das | Das	NS	NS	↓	=
MGHU3	BGJ398	BFTC | DMSO	S ↓	S ↓	=	↓
	PD173074	BFTC | DMSO	S ↓	S ↓	=	↓
	Dasatinib	BFTC | DMSO	NS	S ↓	↓	=
	Trametinib	BFTC | DMSO	NS	—	—	—
	Gefitinib	BFTC | DMSO	NS	NS	↑	=
	BGJ+Das	BGJ | BGJ	NS	NS	↓	↓
	PD1+Das	PD1 | PD1	NS	S ↓	↓	↓
	BGJ+Gef	BGJ | BGJ	NS	NS	=	↓
	PD1+Gef	PD1 | PD1	NS	—	=	↓
	Das+Gef	Das | Das	NS	NS	↓	=

In the short-term cell viability assays, all four bladder cancer cell lines were insensitive to single agent treatment with the Src inhibitors dasatinib and saracatinib. However, in the colony formation assays, three of the four cell lines (BFTC905, MGHU3 and 639V) displayed a significant reduction in colony

formation upon treatment with dasatinib when compared to the DMSO control as a single agent, with the BFTC905 and MGHU3 cell lines harbouring the greatest sensitivity to this drug. This data is consistent with that observed in the NIH-3T3 models which show that ectopic expression of the RT112Fus (TACC3-FGFR3 fusion) and the S249C mutant (adjacent to the R248C mutant in 639V cells) are resistant to dasatinib treatment. Given that the WT FGFR3 expressing cell line is also sensitive to Src inhibition, it is difficult to establish if the observed phenotypic effects are intrinsic dependencies associated with specific FGFR3 mutations. This is one of the limitations of utilising cancer cell lines with endogenous FGFR3 mutations as they do not share an isogenic background and may harbour other heterogeneous genomic and epigenetic aberrations that impact drug sensitivity.

Despite the efficacy of single agent BGJ398 in some of the cell lines e.g. MGHU3 and RT112M, combination treatment with dasatinib and BGJ398 shows synergy at low drug dose (<200nM) in all three FGFR3 mutant cell lines. This effect was replicated in the colony formation assay where the combination was particularly effective in reducing the number of colonies across all four bladder cancer cell lines. Consistent with the effect seen in the NIH-3T3 cells, my data demonstrates that the combination of these two agents is likely to be an effective strategy for targeting FGFR3 mutant-driven bladder cancers, in particular for patients who display intrinsic resistance to single agent FGFR inhibitors (e.g. 639V cells).

When the signalling alterations associated with drug treatment were examined by immunoblotting, my data shows that BGJ398 and PD173074 treatment led to a downregulation of Erk phosphorylation levels in the cell lines which were sensitive to FGFR inhibitors (RT112M and MGHU3) but not the cells which are resistant (BFTC905 and 639V). This data is consistent with the NIH-3T3 data and suggests that the MAPK pathway is key cell survival node in some of the mutant FGFR3 bladder cancer cell lines. I confirmed this hypothesis by showing that the RT112M and MGHU3 cells but not the 639V cell line were sensitive to treatment with the MEK inhibitor trametinib. This analysis further confirms that the 639V cell line is not dependent on the MAPK pathway for survival. Treatment of the bladder cancer cell line panel with dasatinib led to a reduction in the phosphorylation of Src in all four cell lines which was accompanied by an increase in the total levels

of Src. The upregulation of total Src levels upon dasatinib treatment has previously been reported in CML cells (Konig et al., 2008) and also been observed in other cell lines used in our laboratory. Combined treatment of both FGFR inhibitors and dasatinib led to a decrease in both pErk and pSrc levels for RT112M and MGHU3 cells as expected, and also for the 639V cell line that didn't show pErk reduction with either inhibitor alone. Since low nanomolar concentration of this combination was able significantly reduce cell viability in the FGFR3 mutant cell lines in a synergistic manner, the data suggests that simultaneous blockade of both parallel pathways is necessary to overcome survival in these cells.

Herrera-Abreu et al., previously demonstrated that in a subset of FGFR3 mutant bladder cancer cell lines, EGFR activation is a compensatory mechanism by which cells achieve intrinsic resistance to FGFR inhibitors (Herrera-Abreu et al., 2013). Specifically, the authors showed that in the RT112M cells, combination treatment of PD173074 and gefitinib led to a durable and complete suppression of the pErk pathway. Given that dasatinib was similarly able to sensitise cells to FGFR inhibitor therapy, I sought to determine if the Src pathway was the key pathway downstream of EGFR activation responsible for conferring drug resistance in the bladder cancer cell line panel. In contrast to the data presented by Herrera-Abreu, my experiments show that there was no additive effect of adding gefitinib to BGJ398 or PD173074 in the RT112M cells. There was however a statistically significant difference in the combination of PD173074 with gefitinib compared to PD173074 alone for the BTFC905 and 639V cell lines. Furthermore, the combination of gefitinib to dasatinib did not have an additive effect in the phenotypic assays compared to dasatinib as a single agent in all cell lines tested. Notably, dasatinib was more effective than gefitinib at reducing cell survival in all cell lines when combined with BGJ398. Immunoblotting analysis finds that phosphorylation of Src does not decrease with the addition of the EGFR inhibitor indicating that Src is not downstream of EGFR activation but rather a parallel resistance signalling pathway in the bladder cancer cell lines.

While there is a consistent correlation between the decrease in phosphorylation levels of Src and dasatinib treatment in the bladder cancer cell lines, given that this drug is a broad-spectrum multi-target TKI, it was necessary to show that Src

was the causative driver of cell survival and resistance to FGFR inhibitors. I used a gatekeeper mutant of Src (Src-T338I) which is unable to bind to TKIs such as dasatinib as a means to demonstrate that Src was the primary target of dasatinib in these cells. Ectopic expression of this mutant conferred a robust resistance to dasatinib in all cell lines and rescued the survival phenotype in the colony formation assays compared to the expression of the WT Src control. This effect was less evident in the short-term cell viability assays, but nevertheless there was a significant phenotype rescue in the presence of both BGJ398 and dasatinib in all cell lines except MGHU3 due its high sensitivity towards BGJ398 as a single agent in these assays. Taken together, this data demonstrates that dasatinib mediates its effect on cell viability (as a single agent and in combination with FGFR inhibitor) in the bladder cancer cell lines through the suppression of Src signalling.

There is limited knowledge regarding the role of Src in FGFR3-driven cancers. In bladder cancer cell lines expressing the RT112 fusion (TACC3-FGFR3), studies have shown that the Src inhibitor dasatinib is able to inhibit tumour growth and muscle invasion in xenograft mouse models (Vallo et al., 2016). Nevertheless, this effect was shown to be compromised in cell lines expressing the same RT112 fusion from patients resistant to first-line conventional therapy regimen with gemcitabine. In RT112 gemcitabine resistant mouse xenografts, dasatinib showed to induce an increase in tumour size and growth (Vallo et al., 2016). Moreover, a phase-II clinical study have not shown benefit for the use of dasatinib as a single agent in invasive bladder cancer patients (NCT00706641), where out of 25 patients treated with dasatinib only 4 showed a non-significant decrease in the proliferation marker Ki-67 (Hahn et al., 2016). To date, the use of Src inhibitors alone as a therapy for bladder cancer remains controversial.

Finally, to further assess the involvement of the MAPK, PI3K/Akt and Src pathways on maintaining cell survival in each of the bladder cancer cell lines within the panel, I conducted cell viability assays to determine the dose dependent effects of selective inhibitors of these pathways either as single agents or in combination. The data demonstrates that cell lines bearing different FGFR3 alterations harboured distinct signalling dependencies. For BFTC905 cells, MAPK suppression by trametinib or the combined suppression of Src and Akt by

dasatinib and BEZ235 induce a reduction in cell viability. Regarding the RT112M fusion cell line, the inhibition of any two pathways (from MAPK, Akt and Src) is enough to reduce cell viability. For 639V, Akt plays a fundamental role only when combined with the suppression of either Src or MAPK pathway. And finally, MGHU3 showed to be the most dependent on the Akt pathway. This analysis provided insights of the major dependencies of different cell lines and reinforces the need for personalised therapies for bladder cancer and FGFR3 mutations. One limitation of the data outlined in this chapter is that only a small number of bladder cancer cell lines with a limited number of FGFR3 mutations was assessed. As such it is not possible to attribute the phenotypes observed in these cancer cell lines entirely to the specific FGFR3 mutation under study. To address this limitation, future work could include CRISPR engineering of specific FGFR3 mutations into the same cancer cell line to generate isogenic lines for the validation of the pathway dependencies identified in this chapter.

Despite these limitations, some of results were consistently observed in both the NIH-3T3 models in chapter 4 as well as the cancer cell line panel employed in this chapter. This gives one, additional confidence that these observations are specific to the selected FGFR3 mutations under study. For instance, pErk was consistently suppressed across all FGFR3 mutants by the addition of the FGFR inhibitors which is associated with sensitivity to this class of drugs. Furthermore, the fusion protein and to a lesser extent the R248C and S249C mutations were resistant to dasatinib as a single agent in both NIH-3T3 models and cancer cell lines. Finally, the addition of dasatinib is able to sensitise both NIH-3T3 and cancer cell line models that harbour FGFR3 mutations to FGFR inhibitors. Collectively, this data demonstrates that this combination is a promising therapy to either overcome drug resistance to FGFR inhibitors in the salvage therapy setting or be used as upfront strategy to achieve durable drug responses in bladder cancer patients.

Chapter 6

Evaluation the phenotypic properties and sensitivity of FGFR3 cysteine mutations to therapy with BGJ398 and dasatinib

6.1 - Introduction

The most common FGFR3 mutations found in cancer involve cysteine substitutions on the extracellular domain of the receptor. These include mutations R248C, S249C and Y375C which constitute more than 85 % of the mutations found in bladder cancer (Di Martino et al., 2016). Early studies demonstrate that the introduction of a cysteine residue leads to ligand-independent receptor dimerisation by the formation of a disulphide bond, promoting constitutive activation of FGFR3 (Cappellen et al., 1999). However, later studies suggest that this dimerisation of FGFR3 may be a transient effect (Del Piccolo et al., 2015). Cysteine mutations are now known to perturb the structure of FGFR3 dimers leading to the correct alignment of each monomer inducing full kinase activation (Del Piccolo et al., 2015). Moreover, studies have shown that the position of the cysteine mutations in the receptor can affect its activation levels (Adar et al., 2002), and that some less activating mutations such as Y375C only become fully activated in the presence of FGF ligand (Adar et al., 2002). These studies suggest that cysteine mutations might lead to the differential activation of FGFR3 that could modulate downstream signalling in distinctive ways to drive oncogenesis.

Several studies have revealed the importance of FGFR3 cysteine mutations as cancer drivers (Bernard-Pierrot et al., 2006; Di Martino et al., 2009; Miyake et al., 2010). For instance, mutations such as S249C are able to induce morphological transformation, cell proliferation, cell viability and anchorage-independent cell growth in NIH-3T3 cell models (Di Martino et al., 2009). In addition, cells expressing FGFR3 S249C were shown to hyperactivate several downstream signalling pathways including Erk and PLCγ1 in NIH-3T3 models and Src, Akt and PLCγ1 in TERT-NHUC cells (Bernard-Pierrot et al., 2006; Di Martino et al., 2009). Furthermore, bladder cancer cell lines expressing S249C and Y375C cysteine mutations were found to induce tumour growth in xenograft mouse models, and this effect could be inhibited by FGFR3 inhibitors such as PD173074 (Miyake et al., 2010a).

The enrichment of cysteine mutations found in FGFR3-driven cancers, highlights its importance for cancer development and progression, as well as the need to

study these mutations in greater detail to find new effective treatment options. The results presented in the chapters 4 and 5 show that cell lines bearing FGFR3 mutations, such as S249C in NIH-3T3 cell models as well as R248C (MGHU3) in the bladder cancer cell lines, are resistant to dasatinib but sensitive to the combination of BGJ398 plus dasatinib in long-term colony formation assays. It remains unclear if this sensitivity is caused by the acquisition of the cysteine mutation and if this combination has utility across other FGFR3 cysteine mutations. To address these outstanding questions, in this chapter I engineered a series of matched FGFR3 cysteine and alanine/glycine mutant expressing cell lines to investigate if the potent effects of the BGJ398 and dasatinib combination was specific to the cysteine mutants and if the combination could be expanded to a broader range of FGFR3 cysteine mutations found in cancer patients.

6.2 - FGFR3 cysteine mutants display a growth advantage in anchorage-independent conditions

My hypothesis is that due to the high frequency of FGFR3 cysteine mutations found in cancer, these mutations possess a higher ability to activate FGFR3 and therefore form tumours. Correspondingly, it is likely that these mutations are more susceptible to the combination of FGFR inhibitors and dasatinib. To test this hypothesis, I first undertook an anchorage independent spheroid assay to compare the cysteine mutants (R248C, S249C, G372C, S373C, Y375C and R401C) versus the remaining low expressing FGFR3 mutant NIH-3T3 cell lines generated in chapter 3. As controls, I utilised the EV and WT FGFR3 cell lines, along with the gatekeeper mutant cells V557M and the non-cysteine negative control S249T mutant cells, which is used to compare the specificity of the cysteine mutation in the same residue as S249C. Cells were seeded in low-attachment 96-well plates to generate spheroids and treated after 24 hours with BGJ398 or DMSO as a vehicle control. After 72 hours in culture, cells were screened and spheroid cross-sectional area was measured (Figure 6.1A). Under baseline DMSO conditions, a subset of mutants was found to have markedly higher spheroid area compared to WT_L FGFR3 expressing cells (Figure 6.1B). These mutants are $R248C_L$, $S249C_L$, $S373C_L$, $Y375C_L$, $G382R_L$ and $K652M_L$.

Notably, all the cysteine mutations in the extracellular domain of FGFR3 ($R248C_L$, $S249C_L$, $S373C_L$ and $Y375C_L$), with the exception of $G372C_L$ displayed increase spheroid area compared to WT_L FGFR3 expressing cells. Moreover, this growth effect was driven by FGFR3 signalling as BGJ398 treatment completely abolish spheroid growth (Figure 6.1C).

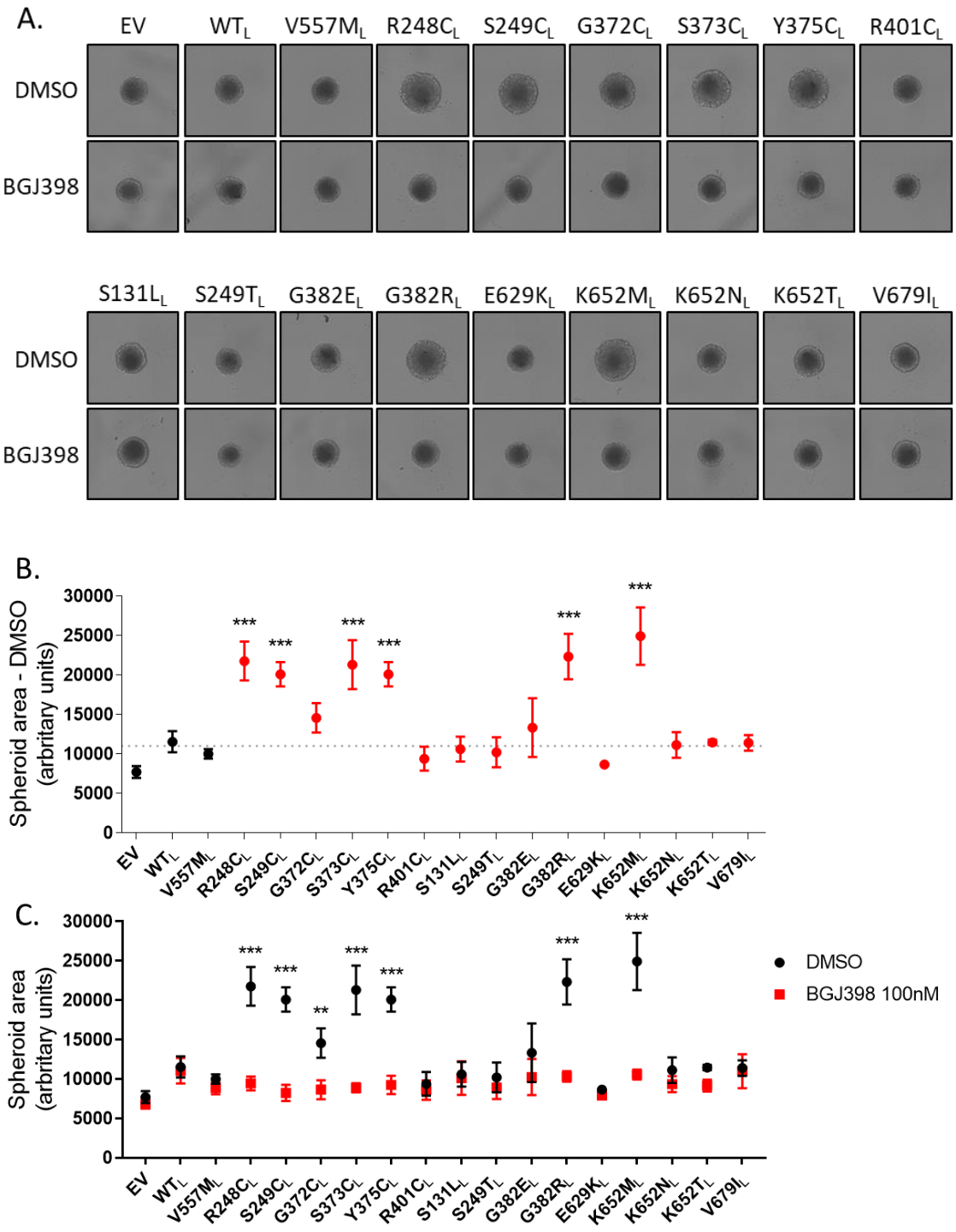

Figure 6.1 – Evaluation of spheroid formation and growth of cancer-associated FGFR3 mutations. FGFR3 mutant expressing NIH-3T3 cells were seeded on round-bottom low adherent 96-well plates in full media and with 100 nM of BGJ398 or vehicle DMSO control. **A.** Spheroids were imaged with high content microscope after 72 hours of treatment and representative images are shown for each cell line. Representative images from 3 biological replicates. **B.** The largest cross-section area of each spheroid was calculated with imageJ. The dotted line represents the average area of WT$_L$ FGFR3 spheroids. Statistical analysis was performed with one-way ANOVA test to compare spheroid area of each cell line against the WT$_L$ control. *** p-value< 0.001. **C.** Spheroid area (continuation of figure legend on following page)

(continuation of legend of Figure 6.1) was calculated for BGJ398 treated cells and plotted against the DMSO results for each cell line shown in B. Two-way ANOVA was employed to assess the statistical significance between paired DMSO and BGJ398 treated cells. ** p-value< 0.01, *** p-value< 0.001. **B-C.** Spheroid area was calculated with imageJ. (n= 3 biological replicates).

To assess the dynamic growth rate of these spheroids, I undertook a temporal analysis of the spheroid area over the course of 9 days under DMSO conditions or a treatment with the small molecule inhibitors BGJ398 and dasatinib as single or combined agents. The data demonstrates that compared to WT FGFR3 and EV cells, all of the extracellular domain cysteine mutants showed an increase in spheroid growth with time reinforcing the concept that the presence of cysteine mutations is capable of inducing growth under non-adherent conditions (Figure 6.2). Given that I previously showed that Src is an important signalling pathway downstream of mutant FGFR3, I sought to establish if spheroid growth was dependent on this pathway by treating the cells with dasatinib (Figure 6.2). My experiments find that unlike treatment with BGJ398, spheroid growth was not affected by the presence of dasatinib, suggesting that the Src pathway is not a key driver of anchorage independent growth in FGFR3 mutant expressing cells. Treatment with the combined agent shows spheroid growth impairment similar to the effect of BGJ398 alone.

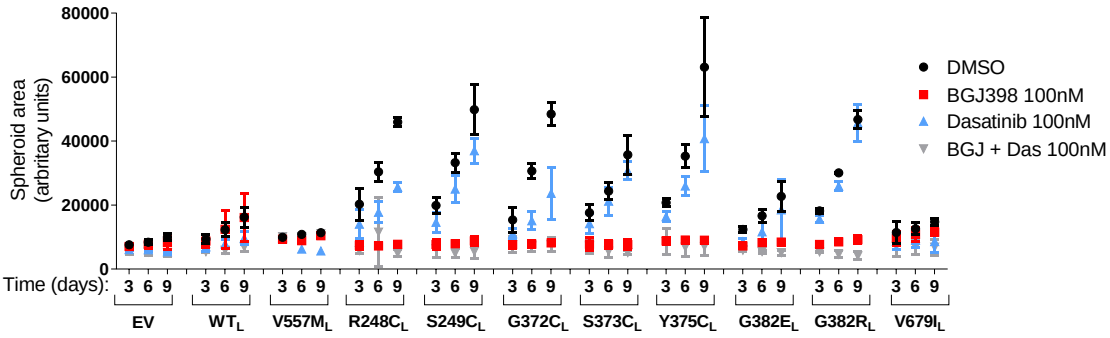

Figure 6.2 – Temporal analysis of spheroid growth of cancer-associated FGFR3 mutants. Spheroids were kept in culture for a total of 9 days after treatment with the indicated inhibitors at the indicated concentrations and imaged at 3 day intervals. The combined arm was used in a 1:1 ratio for a total concentration of 100 nM. Spheroid images were acquired with high content microscope at day 3, 6 and 9 after treatment. Spheroid area was calculated with imageJ. (n= 3 biological replicates).

6.2 - FGFR3 cysteine mutants form constitutive dimers

It has previously been shown that FGFR3 cysteine mutants are capable of forming disulphide bonds in the absence of ligand stimulation (Avis et al., 1998; Miyake et al., 2010; Naski et al., 1996). These disulphide bonds are thought to drive ligand-independent receptor dimerisation and constitutive receptor activation (Gallo et al., 2015). To confirm this observation in my NIH-3T3 cell line model, I assessed the entire cell line panel for FGFR3 expression in non-reducing gels. Upon immunoblotting for FGFR3, I sought to identify FGFR3 dimer at a MW of ~250 kDa (Figure 6.3). All cysteine mutations within the extracellular domain of FGFR3 (R248C, S249C, G372C, S373C and Y375C) were able to form dimers with the R248C and S249C forming more prominent dimers compared to G372C, S373C and Y375C. Dimerisation was also identified in the cell line expressing the fusion RT112Fus which has been described previously (Nelson et al., 2016). Taken together, my data suggests that FGFR3 cysteine mutations form constitutive dimers which may result in increased oncogenic activity and consequently increase spheroid cell growth.

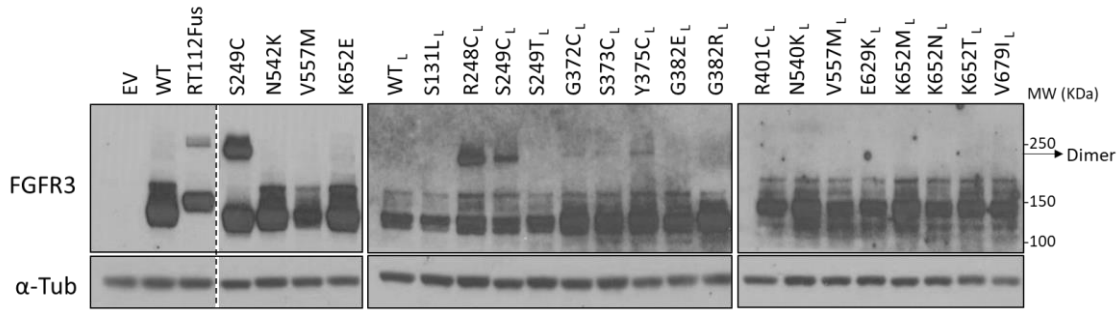

Figure 6.3 – Ligand-independent dimer formation of cancer-associated FGFR3 mutations. Cells were seeded in full media and lysed after 48 hours. Protein extracts were prepared in native conditions in the absence of β-mercaptoethanol and resolved by SDS-PAGE for immunoblotting with FGFR3. The MW for the indicated protein is indicated in KDa. The MW at which the dimer FGFR3 can be observed is indicated by the arrow. Tubulin was used as a loading control. This blot is a representative image from 2 biological replicates.

6.3 - FGFR3 cysteine mutations rescue PC9 sensitivity to gefitinib

To further evaluate the oncogenic potential of the FGFR3 cysteine mutants, I sought to assess the ability of these receptors to rescue the sensitivity of an EGFR dependent cell line to an EGFR inhibitor. It has previously been shown that ectopic FGFR1 or FGFR2 expression are capable of inducing EGFR inhibitor resistance in the PC9 cell line (Sharifnia et al., 2014). PC9 is a NSCLC cell line that expresses an EGFR-mutant (deletion E746-A750) which is a well-established model for sensitivity to EGFR TKIs such as erlotinib or gefitinib. The concept that a genetic modifier, such as an FGFR3 mutation for example, can overcome dependency of this cell line to EGFR signalling would indicate the potential of these mutants to induce the activation of compensatory pathways required for maintaining cancer cell survival in the presence of an EGFR inhibitor.

The FGFR3 cysteine mutations along with the controls EV, WT FGFR3, gatekeeper V557M and the non-cysteine negative control S249T were all transduced into the PC9 cells. S249T was chosen as a negative control to demonstrate that mutation to a cysteine residue (in S249C) is required for disulphide bond formation and not a threonine residue (in S249T), providing evidence that the cysteine residue is the key driver for any observed phenotype. Cells were selected with hygromycin to produce stable cell lines, and expression of mutant FGFR3 confirmed by western blotting (Figure 6.4A). FGFR3 expression was shown to be consistent across all transduced mutants. Cells were then subjected to viability assays in the presence of gefitinib to test the potential of FGFR3 mutants to rescue the sensitivity of PC9 cells to this drug (Figure 6.4B, C). Dose response curves demonstrate that the cells expressing the FGFR3 cysteine mutants were resistant to gefitinib treatment compared to the controls, including PC9-S249T (Figure 6.4B, C). This effect was driven exclusively by the presence of the cysteine residue as the variant S249T, unlike the S249C mutant, was unable to induce resistance in the PC9 cells with an IC_{50} closer to the parental and PC9-EV cell line.

Overall, data showed that cysteine variants could rescue PC9 oncogene dependency to EGFR signalling, demonstrating their increased oncogenic potential compared to other FGFR3 mutations.

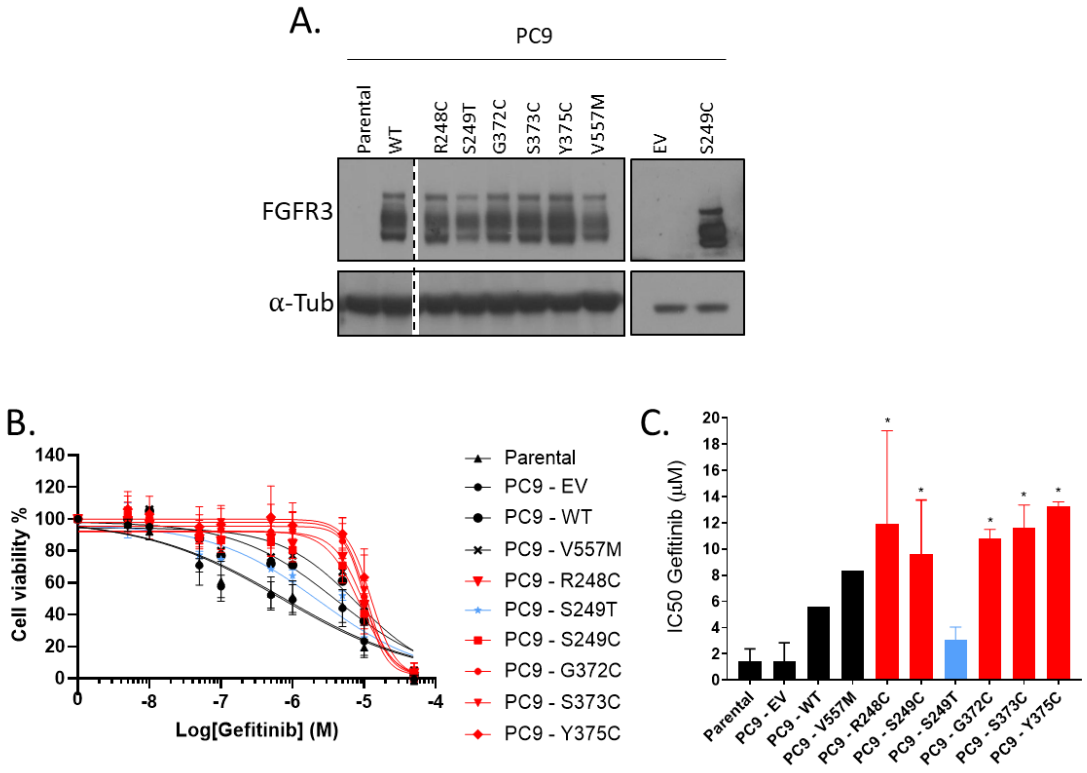

Figure 6.4 – Rescue of PC9 gefitinib sensitive cell line by the expression of FGFR3 cysteine mutations. A. PC9 cell lines were transduced with FGFR3 cysteine mutants and controls. Stable cell lines were lysed and proteins resolved on an SDS-PAGE for immunoblotting of FGFR3 protein. Samples were blotted along with the parental PC9 cell line and the EV control for comparison. Tubulin was used as a loading control. **B.** PC9 cells expressing mutant or WT FGFR3 were seeded (3000 cells/well) in 96-well plates for 24 hours and treated with a range of gefitinib doses. Viability was measured at 72 hours after treatment and data was normalised to the vehicle DMSO control of each cell line and fitted with a four-parameter non-linear regression on GraphPad Prism. **C.** IC_{50} values were calculated from the data points of each individual regression in B for independent replicates. One-way ANOVA statistical analysis was performed against the PC9-EV control. * p-value< 0.05. **B, C.** Results are the average of 3 technical replicates for 1 biological replicate for PC9-WT and PC9-V557M cells, 3 biological replicates for the parental cell line, PC9-EV and PC9-S249C and, 2 biological replicates for the remaining cell lines.

6.4 - Constitutive dimerisation and growth phenotype observed in FGFR3 cysteine mutant expressing cells is the consequence of cysteine point mutations

To investigate the role of the cysteine residue in driving constitutive receptor dimerisation and spheroid growth, the cysteine residues were substituted by SDM to an alanine in positions S249, G372, S373 and Y375. For the R248C mutant, a glycine substitution was utilised instead as it was not possible to generate the alanine mutation by SDM despite several attempts. Moreover, to determine if the addition of multiple disulphide bonds could further influence the transforming and oncogenic potential of cells, combination compound mutations of double and triple cysteine residues were engineered. This included the R248C+S249C in the extracellular region of FGFR3 and G372C+S373C, G372C+Y375C, S373C+Y375C and G372C+S373C+Y375C in the JM region of the receptor (Table 6.1).

Table 6.1 – List of FGFR3 cysteine mutants and respective controls.

Type of mutant	FGFR3 cysteine mutation	FGFR3 non-cysteine control mutation
Single	R248C	R248G
Single	S249C	S249A
Single	G372C	G372A
Single	S373C	S373A
Single	Y375C	Y375A
Double	R248C+S249C	
Double	G372C+S373C	
Double	G372C+Y375C	
Double	S373C+Y375C	
Triple	G372C+S373C+Y375C	

Constructs were then transduced into NIH-3T3 cells for comparison. Cells were selected with hygromycin for stable transduction and FGFR3 expression was evaluated by western blotting (Figure 6.5). Expression levels were fairly similar across mutants and were comparable to the cysteine mutants previously generated, although it was slightly lower for $S373A_L$. Cells were then subjected to the spheroid growth assay to evaluate their ability to grow under anchorage-independent conditions and form spheroids after 72 hours in the presence of

BGJ398 and the DMSO vehicle control. Spheroid area was calculated, and data plotted in Figure 6.6. As previously shown, all cysteine mutants examined formed larger spheroids under DMSO conditions while corresponding mutation to an alanine or glycine residue abolished this growth advantage, confirming that the cysteine residue was the key driver for the observed phenotype. Not all compound mutations conferred the ability for cells to grow under non-adherent conditions. When compared to the WT_L control, only the triple cysteine mutant (G372C+S373C+Y375C$_L$) and the S373C+Y375C$_L$ compound mutation were able to form larger spheroids. Notably, these two compound mutants did not display a higher growth potential compared to single cysteine mutations, suggesting that there is no additive effective when combining multiple cysteine residues. The abolishment of spheroid growth in the other 3 compound mutants suggests that localisation of compound cysteine residues (R248C+S249C, G372C+S373C and G372C+Y375C) may disrupt receptor activation and could be a reason why such compound mutations are not selected for in cancer.

To determine if constitutive dimer formation was abolished in the alanine and glycine mutants, a non-reducing western blot for total FGFR3 levels was performed (Figure 6.7). In this experiment, cells were either treated with DMSO or BGJ398 for 1 hour to determine if kinase activity is required for constitutive dimer formation in the FGFR3 cysteine mutants. Results confirmed that only the single FGFR3 cysteine mutants were able to form ligand-independent constitutive dimers and that BGJ398 did not have an impact on the levels of dimer formation. The data only showed that amongst the double and triple mutants, only the G372C+S373C$_L$ pair was able to induce dimer formation.

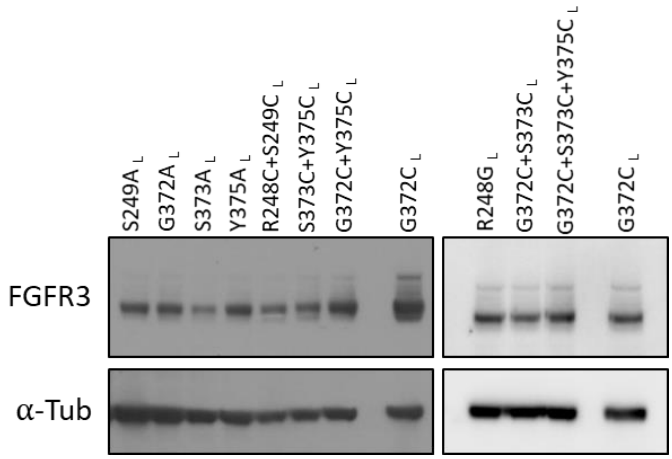

Figure 6.5 – Generation of NIH-3T3 cell line models with alanine and glycine mutations, as well as double and triple compound cysteine mutants. New FGFR3 mutant constructs were generated by SDM (Sanger sequencing results can be seen on Appendix Figure 8.1) and transduced into NIH-3T3 cells. Cell lines were selected with hygromycin for stable transduction. Cells were lysed and proteins resolved on an SDS-PAGE for immunoblotting of FGFR3 protein. $G372C_L$ is here used as a control to compare the expression of the previously generated FGFR3 mutants. Tubulin was used as a loading control.

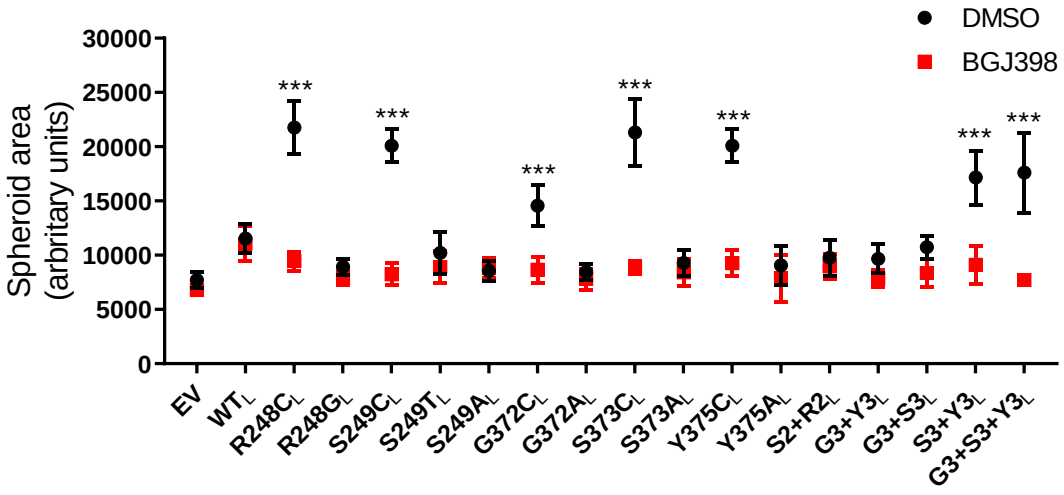

Figure 6.6 – Evaluation of spheroid growth in cysteine mutant FGFR3 expressing cell lines. Cells were seeded on round-bottom low adherent 96-well plates in full media for 24 hours and treated with 100 nM of BGJ398 or vehicle DMSO control. Spheroids were imaged with high content microscope after 72 hours of treatment. The largest cross-section area of each spheroid was calculated with imageJ. Two-way ANOVA tested the statistical significance between the pair DMSO and BGJ398 treated cells. Data shown for single cysteine mutations, WT and EV were previously shown (Figure 6.1C) and were used for comparison. *** p-value< 0.001. (n=3 biological replicates). *S2- S249C; R2- R248C; G3- G372C; S3- S373C; Y3- Y375C*.

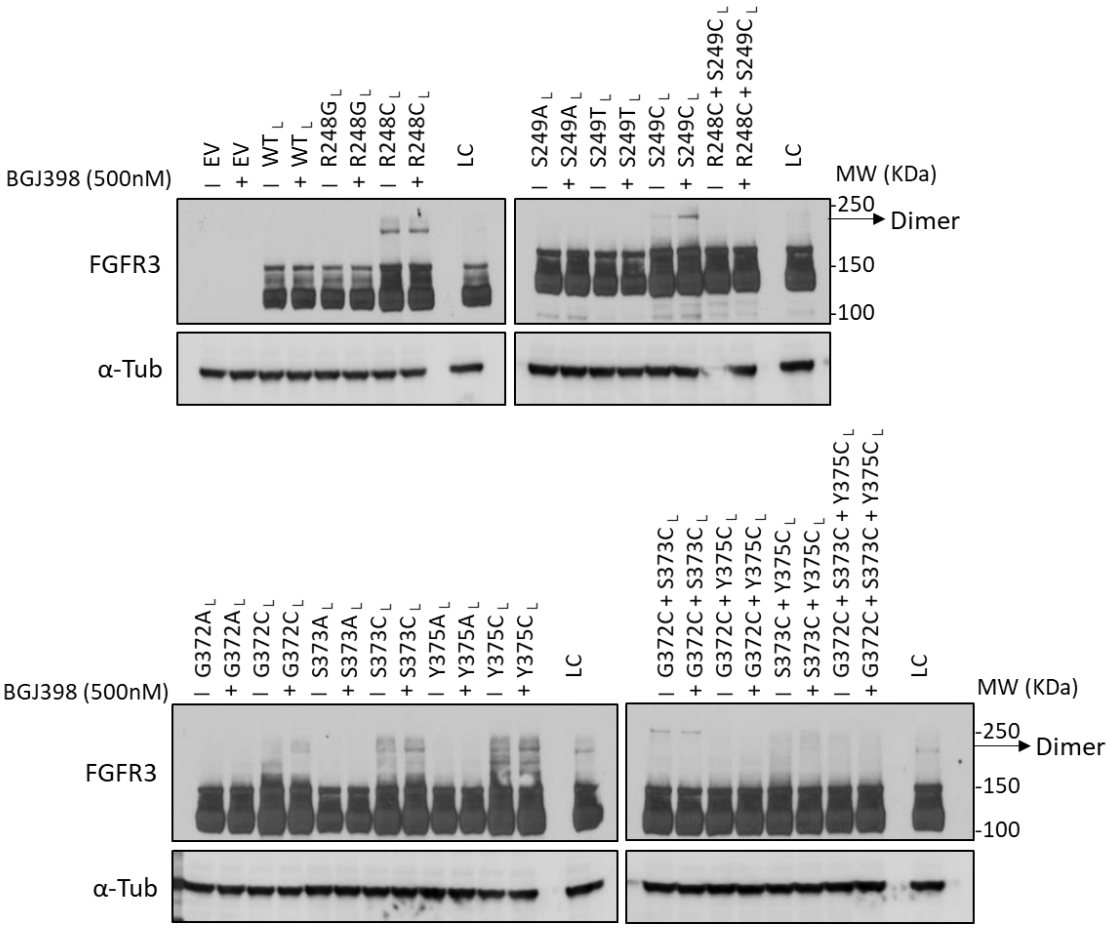

Figure 6.7 – Non reducing western blot analysis of constitutive dimer formation of FGFR3 cysteine mutants. Cells were seeded in full media for 48 hours and treated with 500 nM of BGJ398 (+) or vehicle control DMSO (-) for 1 hour. Protein extracts were prepared in native conditions in the absence of β-mercaptoethanol and resolved by SDS-PAGE for immunoblotting with FGFR3. The MW at which the dimer FGFR3 can be observed is indicated by the arrow. Tubulin was used as a loading control.

To investigate the cysteine-specific responses observed, the basal signalling levels of these cells and their controls were assessed by western blotting for the main downstream effectors of FGFR3 (Figure 6.8). Results demonstrated that when comparing to their individual controls, cysteine mutant cells showed increased pSTAT3 except for Y375C$_L$, whereas all alternative controls were found to have increased levels of Akt activation except for the position S249. The assay also showed an increased pSrc for S249C$_L$, G372C$_L$ and R248G$_L$, whereas pErk was only decreased for R248C$_L$ and S373C$_L$. Overall, it was challenging to establish a pattern between the basal activity of cysteine mutants and their controls that could explain the ability of all cysteine-specific mutants to grow bigger spheroids in culture.

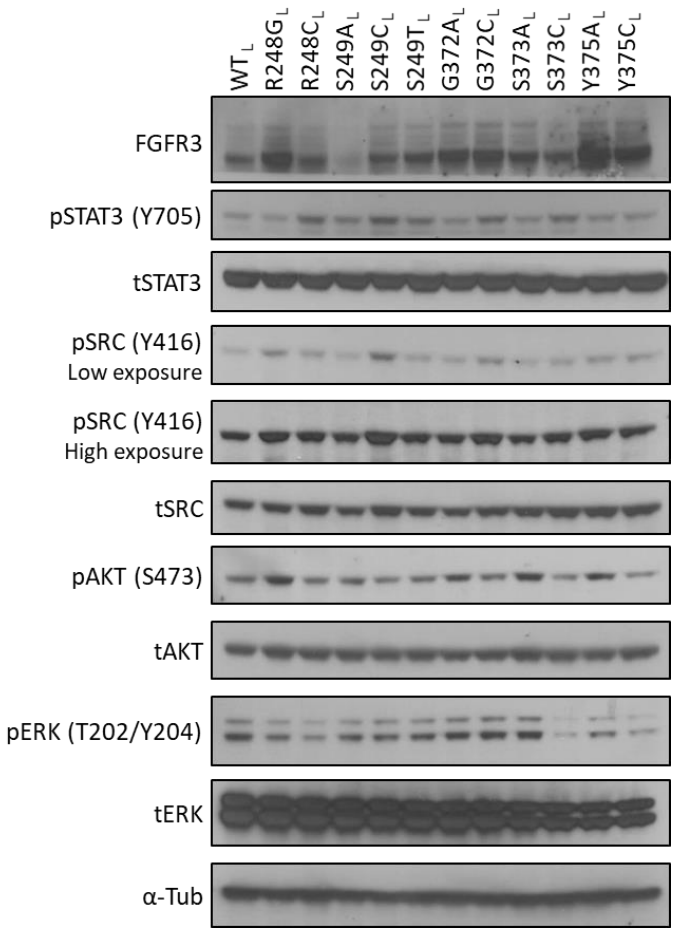

Figure 6.8 – Basal signalling pathways of FGFR3 cysteine mutants and their corresponding alanine and glycine mutant counterparts. Cells were seeded in full media and lysed after 48 hours in culture. Lysates were processed for protein extraction and samples resolved by SDS-PAGE for immunoblotting with the indicated proteins. Tubulin was used as a loading control.

6.5 - Dasatinib sensitises FGFR3 cysteine mutants to BGJ398 treatment

Based on the previous findings, S249C and fusion RT112Fus in NIH-3T3 cell lines along with RT112M (TACC3-FGFR3) and 639V (R248C) in bladder cancer cell lines, conferred a strong protective effect against dasatinib, but these were sensitive to the combination dasatinib plus BGJ398 in long-term assays. Here, all of the cysteine mutants and respective controls were next tested for their response towards BGJ398 and dasatinib as single or combined agents. This was set to understand whether there is a link between constitutive dimerisation and

dasatinib resistance, testing if only FGFR3 dimers activity can become modulated by Src signalling and also to test if dasatinib can sensitise cells to BGJ398. Thus, short-term 72 hours inhibitor response viability assays were performed (Figure 6.9). In the presence of BGJ398, results showed that cysteine mutants tended to be more sensitive than their respective controls, except S373C$_L$ and Y375C$_L$ that displayed a similar sensitivity to their controls (Figure 6.9). Regarding the response of these cells towards dasatinib there was a clear curve separation between cysteine FGFR3 mutant cells and respective controls, with cysteine mutant cell lines being significantly less sensitive to dasatinib than their control cells, except for S373C$_L$. Interestingly, in the presence of the combined treatment BGJ398 plus dasatinib, FGFR3 cysteine mutant cells S249C and S373C were found to be significantly more sensitive to some inhibitor doses than their controls S249A and S373A respectively.

To explore the response of these mutants in long-term assays, 14 days colony formation assays were also performed in the presence of the same inhibitors (Figure 6.10). Results showed that there was a trend for certain cysteine mutants to grow significantly better with dasatinib when comparing to their alanine controls, as it was the case for S249C$_L$ and G372C$_L$ (Figure 6.10B). On the other hand, crystal violet staining also showed that cysteine mutations are more sensitive to the combined agent BGJ398 and dasatinib than their controls, which was clear for all cell lines apart from cell lines with mutations on the residue G372 which displayed equal colony formation impairment (Figure 6.10A).

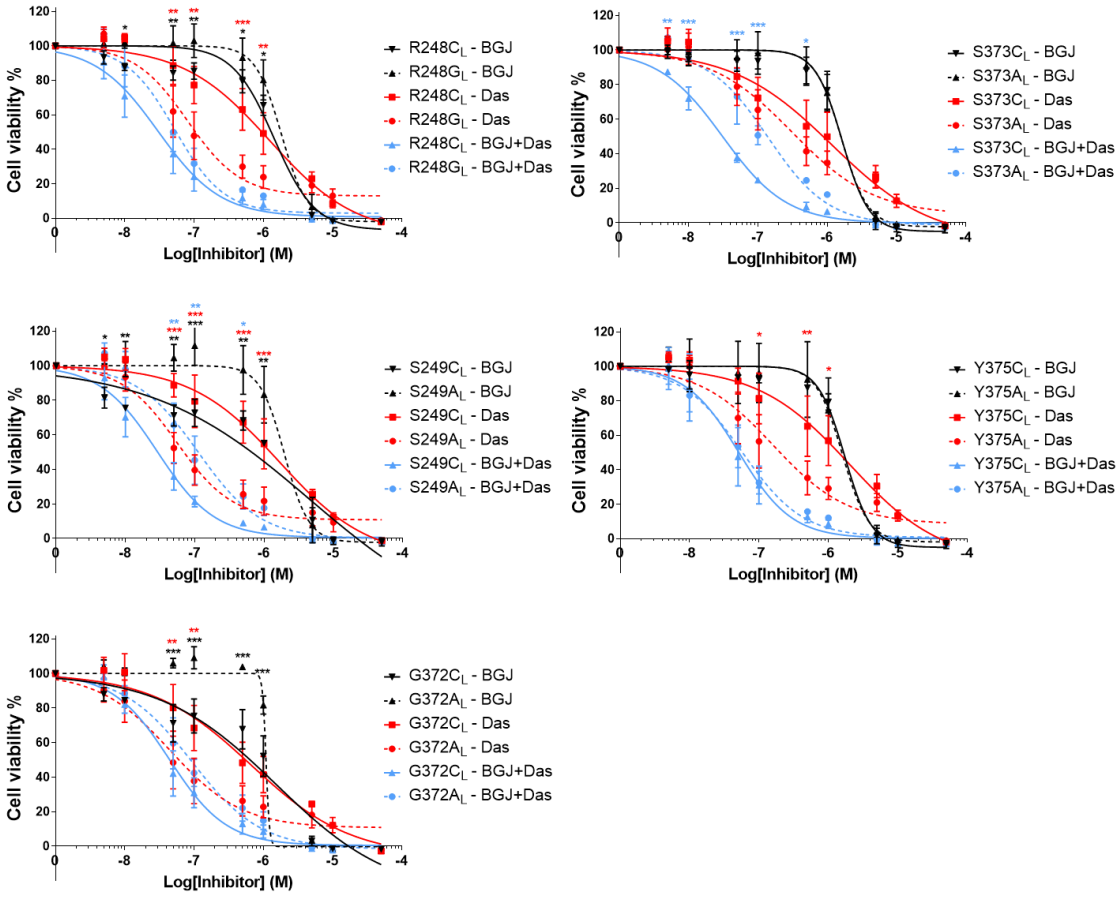

Figure 6.9 – Evaluation of dasatinib, BGJ398 and its combination effects on cell viability in the panel of FGFR3 cysteine mutant expressing cells. Cell viability was measured with CTG assay after 72 hours treatment with serial dilutions of the indicated inhibitors as single agent or in combination. The combination arm was added in a 1:1 ratio for each drug. Data was fitted with a four-parameter non-linear regression on GraphPad Prism. Statistical analysis was performed with two-way ANOVA for each individual inhibitor between the cysteine mutant and its corresponding alanine or glycine mutant counterpart. * p-value< 0.05, ** p-value< 0.01, *** p-value< 0.001. P-values represent the comparison between the cysteine mutant and its corresponding alanine or glycine mutant counterpart. Moreover p-values are represented by different colours, where black represents the p-value for BGJ398 treatment, red corresponds to dasatinib treatment and blue represents the p-value for the combination BGJ398+dasatinib treatment. (n=3 biological replicates). *BGJ- BGJ398; Das- dasatinib*.

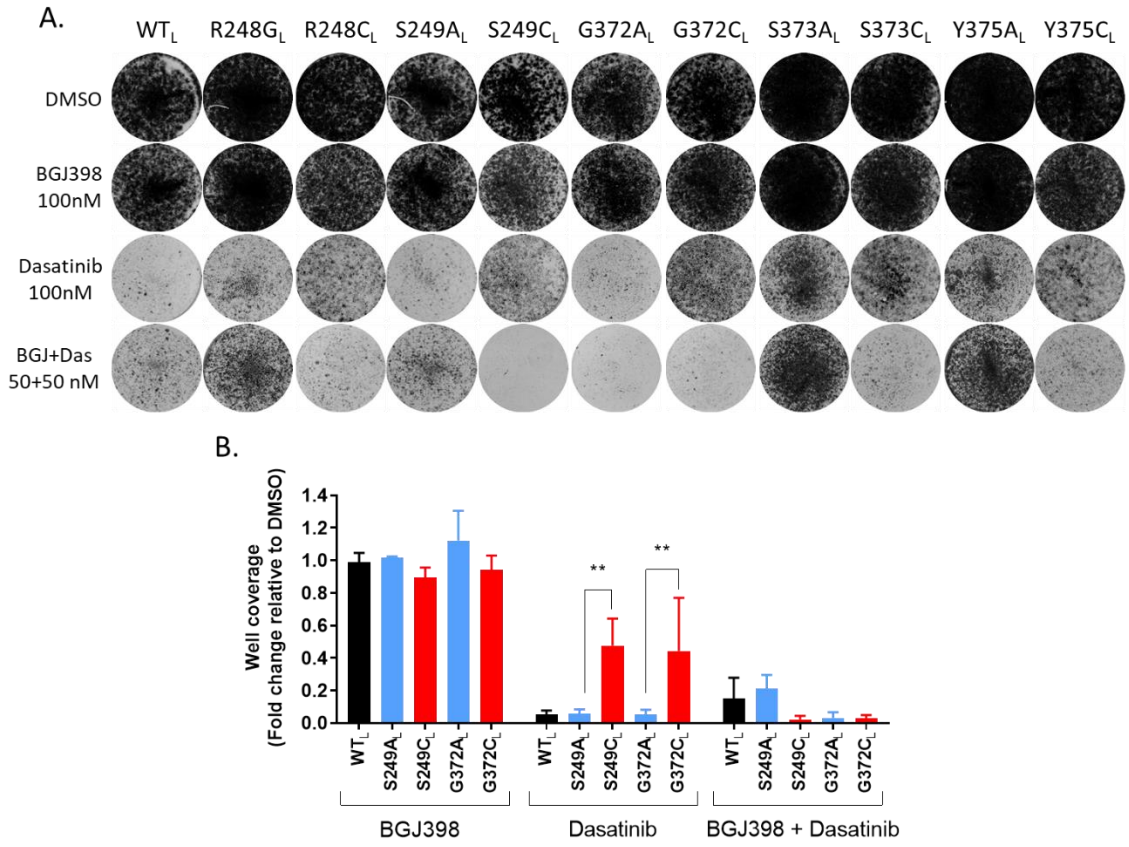

Figure 6.10 – Evaluation of FGFR3 cysteine mutant expressing cell lines in colony formation assays in the presence of dasatinib, BGJ398 as single agents and in combination. Cells were seeded to assess colony formation at low density (15,000 cells/well) in 6 well plates and treated with inhibitors at the indicated doses. **A.** Representative images of crystal violet staining of colonies at day 14. N=3 biological replicates for cell lines FGFR3 WT$_L$, S249C$_L$, S249A$_L$, G372C$_L$ and G372A$_L$; the remaining cell lines represent 1 biological replicate. **B.** The percentage of cells covering each well on the colony formation plates was calculated with imageJ for the indicated cell lines with 3 biological replicates and then normalised to the DMSO vehicle control. Statistical analysis used two-way ANOVA to compare the cysteine mutant and corresponding alanine or glycine mutant control for each inhibitor. ** p-value< 0.01. (n=3 biological replicates). *BGJ- BGJ398; Das- dasatinib*.

6.5 - Discussion

In this chapter, I investigated the importance of cancer-associated FGFR3 cysteine mutants in driving oncogenicity using the NIH-3T3 cell line as a model and assessed their sensitivity to BGJ398 and dasatinib as single agents and in combination. As controls, I engineered corresponding alanine or glycine counterparts to confirm that the functional effects observed are due to the presence of the cysteine residue.

Cell lines expressing FGFR3 extracellular domain cysteine mutants formed larger spheroids compared to other FGFR3 mutants in my panel of cells. I further showed that these cysteine mutants enhanced spheroid growth compared to their corresponding alanine or glycine counterparts, demonstrating that the increased proliferative potential was due to the presence of the cysteine mutation. Treatment with BGJ398 led to a reduction in spheroid size indicating that the increased proliferative potential of the cysteine mutations was due to FGFR3 kinase activity. Notably, in cell viability assays, FGFR3 cysteine mutant expressing cells were more sensitive to BGJ398 treatment compared to the alanine/glycine counterparts. Moreover, experiments in the PC9 model show that only the FGFR3 cysteine mutants were able to rescue drug sensitivity towards gefitinib, indicating their signalling potential as a genetic modifier to compensate for the inhibition of the EGFR oncogene. When downstream signalling pathways were evaluated by immunoblotting, the data shows that the majority of cysteine mutants examined (with the exception of Y375C) resulted in an upregulation of phosphorylated STAT3 compared to their alanine and glycine controls. Interestingly, I also show that these cysteine mutants appear to actively suppress the Akt pathways as mutation to an alanine or glycine led to an upregulation of Akt phosphorylation. Taken together, my data finds that cysteine mutations in the extracellular domain harbour increased oncogenic potential of FGFR3 in multiple cell line models.

It has previously been shown that the presence of unpaired cysteine residues in FGFR3 monomers leads to the formation of covalent disulphide bonds between monomers, resulting in ligand-independent receptor dimerisation (Gallo et al., 2015). I sought to investigate if this effect was also observed in the studied panel of cysteine FGFR3 mutants, and further engineered double and triple cysteine mutants to determine if the addition of more disulphide bonds would enhance dimerisation and oncogenic potential. Under non-reducing gel conditions, all the FGFR3 variants with extracellular cysteine mutants formed covalent dimers with the R248C and S249C expressing cells forming more prominent dimers compared to G372C, S373C and Y375C. As expected, mutation of the cysteine residue to alanine or glycine led to the loss of dimer formation. For the FGFR3 double and triple cysteine mutant expressing cells, only the G372C+S373C$_L$ cell

line was able to form dimers under the conditions studied. This data suggests that the addition of compound cysteine mutations does not necessarily lead to the formation of covalent dimers. Furthermore, the presence of compound cysteine mutations might account for structural constrains or alterations in the receptor that might influence its dimerisation capacity and receptor activity (Bocharov et al., 2013). Interestingly, across the double and triple cysteine mutant expressing cells, increased spheroid growth was only observed in the double mutant S373C+Y375C$_L$ and the triple mutant G372C+S373C+Y375C$_L$ cell lines which is not concordant with the assessment of dimerisation by non-reducing PAGE. One possible explanation for this result is that receptor dimerisation is not an important driver of oncogenic potential in these compound mutations and other mechanisms are at play. An alternative explanation is that compound cysteine mutants form dimers with different kinetics compared to single point mutants and further optimisation of experimental conditions are required to visualise these dimers in the non-reducing PAGE experiment. Finally, I show that treatment with BGJ398 did not have an impact on dimer formation confirming that kinase activity is not required for constitutive dimer formation in the FGFR3 cysteine mutants.

In addition to treatment with the FGFR inhibitors, I also assessed the effects of dasatinib on the FGFR3 cysteine mutants. The data demonstrates that the cysteine mutant cell lines were more resistant to this inhibitor when compared to their corresponding alanine and glycine controls in cell viability assays. In the long-term colony formation assays, only the S249C$_L$ and G372C$_L$ mutant cell lines are able to grow better in the presence of dasatinib compared to their corresponding alanine mutants. These two mutations have previously been reported to be the most activating mutants amongst the cysteine mutants in the extracellular domain of FGFR3 in NIH-3T3 cell lines (Avis et al., 1998) which may explain why these mutants are capable of providing survival signals to confer resistance to dasatinib treatment. In both the cell viability and colony formation assays, the dual inhibition with BGJ398 and dasatinib lead to a dramatic reduction in cell survival. Further work is necessary to determine the mechanisms by which this combination exerts its phenotypic effects on FGFR3 cysteine

mutants, including its effects on downstream cellular signalling, receptor localisation and kinase activity.

Collectively, my experiments have shown that FGFR3 cysteine mutants in the extracellular domain of the receptor form constitutive dimers which lead to enhanced proliferative potential and ability to rescue EGFR inhibitor resistance. Furthermore, I demonstrate that most of these mutants led to the modulation of downstream signalling including the upregulation of the STAT3 pathway and suppression of Akt phosphorylation. I further show that while these mutants are more sensitive to BGJ398 treatment and are resistant to dasatinib, the combined administration of these two drugs led to enhanced effectiveness in reducing cell viability and colony formation. These data reinforce the conclusions made in earlier chapters that this drug combination is an attractive strategy to overcome FGFR inhibitor resistance in cancers harbouring the most common FGFR3 mutations.

Chapter 7

Discussion

7.1 - FGFR3 mutations – one therapeutic target for many cancers

FGFR3 is one of the most commonly mutated FGFR isoforms found in cancer (Helsten et al., 2015). FGFR3 is frequently mutated in bladder cancer and is also known to account for the progression and development of several different cancers including prostate, colorectal, cervix, lung, MM and others (Kelleher et al., 2013; Wesche et al., 2011). In bladder cancer, FGFR3 mutations account for 40 % of cases and is associated with low grade urothelial carcinomas (Pandith et al., 2010). In lung cancer, FGFR3 mutations are present in 1.9 % of patients with lung squamous cell cancer (SCC) and accounts for one of the ten most frequent somatic mutations in this lung cancer subtype (Tao et al., 2016). FGFR3 mutations such as E322K, R401C and V679I have also been identified in colorectal cancer (Gallo et al., 2015; Jang et al., 2001). Analysis of 112 prostate cancer patient samples has revealed a prevalence of FGFR3 mutations in 8 % of the cases and was found to be associated with low-grade tumours (Hernández et al., 2009). However, there has been limited research in individual cancers bearing low-frequency FGFR3 mutations, and published work has mainly focused on the most common mutations found in bladder cancer due to its increased frequency (Helsten et al., 2015). Notably, point mutations are found across the entire length of the FGFR3 receptor and these are not exclusive to particular types of cancer, for instance the same mutation S249C is associated with different cancers, including bladder, prostate, lung and head and neck cancers (Gallo et al., 2015). Conversely the same cancer type may harbour different mutations, as for example S249C, Y375C and K652E mutations are all found in bladder cancers (Knowles, 2008).

As detailed in the introductory chapter, section 1.4, the value of FGFR3 as a therapeutic target has been established across different cancer types (Touat et al., 2015). In the context of FGFR3 mutation-driven lung SCC, the FGFR inhibitor BGJ398 was found to reduce tumour growth in xenograft mouse models expressing FGFR3 S249C and R248C mutations (Liao et al., 2013). In MM, the translocation t(4;14), which brings the FGFR3 and MMSET genes under the control of IgH locus promoter, increasing the expression of both genes, is a

primary event for oncogenesis (Trudel et al., 2004). However, studies have shown that FGFR3 activating mutations such as Y375C and K652E can also be acquired in t(4;14) MM (Chesi et al., 1997). In the context of t(4;14) MM with the FGFR3 mutation Y375C, the FGFR inhibitor PD173074 was found to delay tumour progression and increase survival of xenograft mouse models (Trudel et al., 2004). In bladder cancer, xenografts of established cell lines expressing FGFR3 S249C and Y375C (MGHU3 and UM-UC-14, respectively) (Lin et al., 1985; Sabichi et al., 2006), PD173074 suppressed tumour growth and induced apoptosis (Miyake et al., 2010). In metastatic bladder cancer, FGFR inhibition by erdafitinib, also confers a therapeutic advantage, being recently approved by the FDA for the treatment of patients with advanced or metastatic bladder cancer expressing FGFR2 or FGFR3 genetic alterations (Nadal and Bellmunt, 2019).

Overall, targeting FGFR3 is of clinical relevance for multiple cancer types and research in this field has the potential to impact a large number of patients (Hallinan et al., 2016). However, there is preclinical and clinical evidence which shows that not all FGFR3 alterations are equal and there are differential responses to distinct FGFR mutations (and tumours types) to FGFR inhibitors (Bahleda et al., 2019; Pal et al., 2018; Touat et al., 2015). Yet, the low frequency of certain mutations makes the design of targeted clinical trials aimed at rare FGFR3 mutations challenging and costly, as it would require the screening of a high number of patients for the selection of a representative cohort (Rouanne et al., 2016). While there is a drive to identify therapeutic strategies that can be employed to target both common and rare FGFR3 mutations in different cancer types, many of the past and ongoing clinical trials have studied the effects of FGFR inhibitors without discerning the specific FGFR3 aberration or mutation type (refer to table 1.5). Nevertheless, disease progression often occurs following the use of FGFR inhibitors, suggesting the need for more effective types of treatment to overcome drug resistance and achieve durable responses (Nogova et al., 2017).

7.1.1 - Discerning between passenger and driver mutations

Distinguishing between cancer-associated mutations that contribute to the initiation and progression of cancer, the 'driver mutations', and mutations that are biologically neutral and do not contribute to a growth advantage, the 'passenger mutations', have been addressed in different studies (Greenman et al., 2007; Merid et al., 2014). The distinction between these two types of mutations is particularly important to facilitate the development of personalised cancer therapies (Merid et al., 2014). Although high frequency or "hotspot" mutations commonly found in patient tumour samples have been associated with a higher likelihood to contribute to cancer progression, other studies have found that low frequency mutations can also act as 'drivers' (Wood et al., 2007). Therefore, preclinical methods that can systematically assess the functional relevance of different mutations observed in human tumour specimens in cell lines or *in vivo* models are essential to robustly discriminate between driver and passenger mutations (Carter et al., 2009). However, this effort becomes a challenge when there is a large number of candidate mutations either within the same gene or in the same tumour. There has been an intensive effort in the development of computational methods to predict driver mutations from sequencing data, but this is arguably still a developing field with few truly robust predictive algorithms (Bailey et al., 2018; Merid et al., 2014).

All of the FGFR3 mutant cell lines generated in this project have been reported to be found in cancer. However, for many of the mutations that I have investigated, there is no published information about their role in carcinogenesis, particularly for the rare FGFR3 mutants. Whereas some of the more common mutations are known for their ability to transform cells in culture, for instance S249C or K652E (Bernard-Pierrot et al., 2006; Ronchetti et al., 2001), others such as R401C that have been identified by large scale next generation sequencing studies have had no functional work performed thus far (Helsten et al., 2015).

The starting point of this project was to generate and characterise cell lines based on the NIH-3T3 model by expressing both common and rare FGFR3 mutations to study their potential as oncogenic drivers. A number of orthogonal assays were

used to evaluate oncogenic potential including spheroid growth under low adherent conditions and colony formation assays. My experiments demonstrate that while all known common activating mutations of FGFR3 (e.g. R248C, S249C, Y375C) led to an increase spheroid growth compared to the WT control, some poorly characterised FGFR3 mutants such as G382R and the rare K652M also formed larger spheroids in this assay. In contrast, non-cysteine mutations on the most common cancer associated FGFR3 residue (such as S249T) failed to confer a growth advantage compared to the WT FGFR3 expressing cells. My studies show that while the majority of hotspot mutations in FGFR3 are oncogenic drivers, there are exceptions to this rule (e.g. S249T). Furthermore, low frequency rare FGFR3 mutants should not be ignored given that a proportion of them harbour significant oncogenic potential. While predictive algorithms based on mutational frequency and structural information are useful for identifying candidate driver mutations *in silico*, my data demonstrates that functional characterisation in preclinical models is still necessary to ultimately prove that these FGFR3 mutants are oncogenic.

There are multiple mechanisms by which these oncogenic FGFR3 mutants drive anchorage independent growth. These include constitutive kinase activation through the stabilisation of the active conformation of the KD, ligand-independent receptor dimerisation, aberrant receptor localisation and differential activation of downstream signalling pathways. One of the limitations of my studies is the lack of in-depth biochemical, cell biology and structural assessment of individual mutants to identify which mechanisms are responsible for the observed cellular phenotypes. Future work will require the use of a multimodal strategy to elucidate the mechanisms driving the oncogenic properties of these mutations, in particular the rare poorly characterised oncogenic FGFR3 mutants identified in my studies.

7.2 - The need for effective therapies to achieve durable responses.

There are different treatment modalities under clinical investigation for mutant FGFR3-driven cancers, based on their promising results in the preclinical setting.

Most of these candidate agents are small molecule selective kinase inhibitors, followed by multi-targeted kinase inhibitors and antibody-based therapies (Katoh, 2019). However, only a small proportion of mutant FGFR3 patients respond to these drugs. Furthermore, one of the major problems of kinase inhibitor therapy is the inability to achieve long-term durable responses in patients harbouring mutant FGFR3 cancers (Nogova et al., 2017) due to the plasticity of tumour cells (Camidge et al., 2014). Most patients who initially respond to this class of drugs will almost inevitably acquire drug resistance and disease relapse with prolonged treatment with kinase inhibitors. The work presented in this thesis show that in long-term colony formation assays, the efficacy of FGFR3 inhibitors (BGJ398 and PD173074) is sub-optimal indicating that alternative strategies are required to establish durable responses with these drugs. Unlike other RTKs including EGFR and ALK where the majority of acquired resistance mechanisms have been attributed to drug resistant mutations such as EGFR T790M and C797S (Ma et al., 2011; Thress et al., 2015), such mutations are not commonly found in FGFR isoforms (Chell et al., 2013). Instead published studies have determined that some of the mechanisms responsible for FGFR3 inhibitor resistance are driven by the activation of PI3K/Akt pathways as well as co-opting the EGFR signalling pathway (Datta et al., 2017; Gavine et al., 2012; Herrera-Abreu et al., 2013).

One of the most common ways to overcome or prevent resistance is the use of combination therapies that abrogate emergent compensatory survival mechanisms. To date there are no clinical trials investigating the effects of a combination EGFR inhibitor with FGFR inhibition in mutant FGFR3-driven cancers. However, a phase I clinical trial has been carried out to explore the benefit of combining BGJ398 with the PI3K inhibitor BYL719 (NCT01928459). In this trial, the safety, tolerability and preliminary activity of the drug combination was assessed in patients with advanced solid tumours harbouring PI3K catalytic subunit (PIK3CA) mutations with or without FGFR alterations (Hyman et al., 2016). The maximum tolerated dose was calculated based on a total of 62 patients enrolled. During the expansion phase 24 patients (divided into 3 arms: PIK3CA-mutant; PIK3CA-mutant + FGFR-altered; PIK3CA-mutant + FGFR-altered in breast cancer) were enrolled. Of these patients, 8 had a partial response, with 4 cases comprised of urothelial, melanoma, anal and head and

neck cancers. Notably, 1 patient with FGFR3-TACC3 fusion positive urothelial carcinoma achieved a complete response lasting for 4 months with this combination (Hyman et al., 2016). However, this report did not specify which of the three arms the 8 partial responders came from and thus it is not possible to attribute the effects of this combination with FGFR3 alterations, furthermore, the benefit of the combination treatment over single agent was not investigated.

In addition to combinations of targeted therapies, there are currently several ongoing phase I clinical trials evaluating the combined use of FGFR inhibitors with immune checkpoint inhibitors (ICI) in bladder cancer (NCT03473743, NCT03123055 and NCT03473756) (Tony et al., 2019). Retrospective analysis of patients treated with ICIs has found that FGFR3-altered urothelial carcinoma patients respond worse to these drugs as the levels of immune infiltrate in the tumour are low (cold immune environment) (Robertson et al., 2017; Sweis et al., 2017). Given the lack of immune infiltrate in these tumours, it remains to be seen if the combination of FGFR inhibitors with ICI will be effective as a treatment strategy in FGFR3-mutant bladder cancer.

Although combination therapies as a means to overcome FGFR inhibitor resistance and achieve durable responses have proven beneficial in preclinical experiments, clinical investigation in patients who harbour FGFR3 mutations are still in its early stages. Furthermore, the large proportion of FGFR3 alterations assessed in these preclinical studies comprise of the common FGFR3 point mutations and not the rare variants. There thus remains a need to consider new treatment strategies either by way of drug combinations or dose scheduling to tackle kinase inhibitor resistance across pan-FGFR3 mutations in order to improve long-term patient outcomes.

7.2.1 - The role of Src in mutant FGFR3 driven cancers

In this thesis I show that Src phosphorylation is increased when FGFR3 mutants and RT112Fus are expressed in NIH-3T3 cells. Src is known to mediate the downstream signalling dynamics of the FGFR family of receptors (Li et al., 2004). Our understanding of the role of Src signalling in the FGFR receptor family has

been most well-studied in the prototypical member FGFR1. Src activation by FGFR1 and its adaptor FRS2 is important for phosphorylation of SPRY which is a negative regulator of MAPK signalling, highlighting the crucial role of Src in regulating signal attenuation after RTK activation (Li et al., 2004). Subsequent studies in MEF cells expressing endogenous FGFR1 show that Src is activated by FGFR1 but active Src is also reciprocally required for full activation of the receptor. Following receptor activation by FGF2, Src was shown to colocalise with FGFR1 at the cell membrane where Src activates FGFR1 leading to receptor internalisation (Sandilands et al., 2007). In addition, the same authors report that expressing a Src dominant negative kinase dead mutant failed to activate FGFR1 upon ligand stimulation. Furthermore, a constitutively active mutant of Src activates FGFR1 in the absence of ligand, demonstrating a reciprocal activation of Src by FGFR1 and vice versa. Although there are no studies specifically investigating the role of Src in FGFR3 signalling, my data demonstrating that multiple FGFR3 mutants activate Src phosphorylation, as well as prior studies in FGFR1 described above suggest that this pathway is important for propagating FGFR oncogenic signalling and may be a suitable candidate to be exploited for targeted therapy.

7.2.2 - Dasatinib in combination with FGFR inhibitors as a new strategy for treating FGFR3 mutant cancers

This thesis presents data that demonstrates that in the context of cell line models harbouring FGFR3 mutants such as the cysteine mutants and the translocation fusion RT112, the kinase inhibitor dasatinib is capable of overcoming resistance to the FGFR inhibitor BGJ398. Dasatinib is currently approved by the FDA for the treatment of ALL and CML with resistance to other therapies including the tyrosine kinase inhibitor imatinib (Kantarjian et al., 2006). It is a multi-kinase inhibitor that potently targets the Src and Abl kinases, along with c-KIT, PDGFR-β and other members of the SFK including Yes, Lck and Fyn (Kantarjian et al., 2006). In addition to ALL and CML, this drug has also been evaluated in preclinical studies across a wide range of cancer types including lung, MM, prostate and colorectal cancers (Gallo et al., 2015). For instance, in lung SCC,

studies have shown that dasatinib is an effective agent in patients that harbour DDR2 mutations (Pitini et al., 2013). Dasatinib treatment has also been shown to elicit an anti-tumour response in colorectal cancer KRAS mutant patient-derived xenograft mouse models, which was associated with an increased baseline of Src and FAK gene expression levels (Scott et al., 2017). Studies investigating the use of dasatinib for the treatment of FGFR3-driven cancers as single agent have shown that dasatinib treatment has the potential to reduce tumour growth and cell invasion in RT112 xenograft mouse models, but only if these cells are not resistant to the therapy regimen with gemcitabine (Vallo et al., 2016). However to date, there are no published studies investigating the benefit of using dasatinib in combination with FGFR3 inhibitors for FGFR3-driven cancers.

Given the increase in Src signalling observed upon the expression of FGFR3 mutants in the NIH-3T3 models, I investigated the use of dasatinib as a means to suppress this pathway in FGFR3 mutant expressing cell lines. While dasatinib was able to downregulate the phosphorylation of Src across the panel of cell lines, the FGFR3 cysteine mutants and RT112 fusion paradoxically conferred resistance to dasatinib treatment alone in both the NIH-3T3 and cancer cell line models, suggesting that dasatinib as a single agent is likely to be ineffective in FGFR3 mutant cancers. Mechanistic work in an expanded panel of extracellular domain cysteine mutants demonstrates that this resistance is due to the substitution of the cysteine residue, as corresponding glycine/alanine controls were sensitive to this drug. However, the addition of dasatinib was highly effective in sensitising the FGFR cysteine mutation or RT112 fusion bearing cells to BGJ398. This effect is synergistic and it is tempting to speculate a mechanism whereby the addition of dasatinib alone has no effect on FGFR3 cysteine mutations, but the addition of the FGFR inhibitor induces a new dependency to the Src pathway leading to vulnerability to co-treatment with dasatinib. The precise mechanisms that are operating to drive this synergistic interaction are unknown but my data provides evidence that this combination strategy is likely to be effective for some of the most oncogenic and difficult-to-treat FGFR3 mutant cancers.

The use of dasatinib to overcome resistance to RTK targeted agents has previously been shown in the context of EGFR driven cancers. In NCI-H226 lung

cancer cell lines, acquired resistance to cetuximab (an anti-EGFR antibody) is associated with an increase in the expression of the Src protein (Wheeler et al., 2009). Treatment with dasatinib is able to re-sensitise cells to cetuximab with the combined treatment leading to an augmentation of growth inhibition and decrease in pAkt survival pathways (Wheeler et al., 2009). In clinical trials, dasatinib in combination with erlotinib (an EGFR inhibitor) had a disease control rate of 63 % in a cohort of 34 patients with advanced NSCLC, compared to a disease control rate of 51% observed in a phase II study for erlotinib alone (Haura et al., 2010), demonstrating the clinical activity of such combination therapies involving dasatinib.

Future work will seek to extend these *in vitro* findings into *in vivo* xenograft mouse models using FGFR3 mutant bladder cancer cell lines RT112M, MGHU3 and 639V. If the combination of BGJ398 and dasatinib is able to induce a significant reduction in tumour growth and development, with an acceptable *in vivo* toxicity profile, then a clinical trial could be designed. The clinical trial would be aimed at investigating the clinical activity and safety of the combination of these two drugs. Although the safety of dasatinib treatment in bladder cancer patients was shown to be generally well tolerated (NCT00706641), toxicity remains a major concern (Hahn et al., 2016). Treatment related side-effects include amongst others supraventricular tachycardia, enteric fistula and pulmonary embolism (Hahn et al., 2016), which can progress into pleural effusions (Light, 2001). In addition, dasatinib in combination with erlotinib in the treatment of NSCLC patients was also reported to induce pleural effusions along with gastrointestinal intolerance, rash, anaemia, and fatigue (Haura et al., 2010). Therefore, toxicity is also likely to occur in patients treated with the combination of dasatinib and BGJ398. Hopefully early detection and management of side-effects such as pleural effusions can reduce morbidity and sustain the clinical benefit of dasatinib and FGFR inhibitor combinations (Cortes et al., 2017).

7.2.2 - Understanding the signalling dependencies driven by FGFR3 cysteine mutants

The most common cancer-associated point mutations in FGFR3 are the extracellular cysteine mutations (Di Martino et al., 2016). Data presented in this thesis shows that this class of mutations is consistently more oncogenic with a higher potential to grow under anchorage independent conditions compared to WT FGFR3 or other cancer-associated FGFR3 mutants. In the NIH-3T3 cell line model, these cysteine mutants formed covalently bound constitutive dimers in the absence of ligand and were resistant to dasatinib treatment as a single agent. As indicated in the previous section, durable response to BGJ398 in a colony formation assay could be augmented by the co-administration of dasatinib. A similar phenotype was also observed in the human bladder cancer cell lines. The combination of BGJ398 plus dasatinib was found to simultaneously abrogate Erk and Src phosphorylation in the cell lines harbouring endogenous FGFR3 mutations (MGHU3 and 639V) resulting in durable efficacy in long-term colony formation assays.

Other signalling pathway and RTK dependencies have been reported in the bladder cancer cell lines (harbouring FGFR cysteine mutants) that were used in my studies. For instance, MGHU3 is more dependent on the Akt pathway due to a mutation in the *AKT1* gene (E17K). This mutation induces PI3K/Akt pathway activation and a combination of the FGFR inhibitor AZD4547 together with the PI3K inhibitor BKM120 or the Akt inhibitor AZD5363 was synergistic in reducing cell viability (Davies et al., 2015; Wang et al., 2017). In addition, the 639V and MGHU3 cell lines have been shown to only be partially dependent on FGFR3 signalling, with EGFR playing an important role in maintaining cell survival in the presence of an FGFR inhibitor. These studies highlight the importance of a combination strategy in eliminating cancer cells harbouring FGFR3 cysteine mutant alterations by dual blockade of FGFR3 signalling and downstream signalling pathways such as PI3K/Akt or other RTKs such as EGFR. My studies show that the co-targeting of FGFR3 and the Src pathway can be exploited in a similar manner for cancer therapy in this class of FGFR3 mutants. It remains unclear if the PI3K/Akt, EGFR and Src signalling pathways intersect in the

bladder cancer cell line models featured in this thesis. Preliminary work presented in chapter 5 suggests that treatment with the EGFR inhibitor gefitinib does not reduce the phosphorylation levels of Src indicating that Src signalling in these cells is a parallel pathway that is not dependent on upstream EGFR activation. Future work will seek to unravel the likely complex pathway interactions that dictate signalling dependencies observed in mutant FGFR3 driven bladder cancer.

7.4 - Concluding remarks and future directions

FGFR3 mutations account for the development and progression of many different cancer types, and therefore FGFR3 inhibition has been investigated as a potential treatment option. Although preclinical assays show the ability for FGFR kinase inhibitors to supress tumour growth and survival, clinical trials show a lack of durable responses with this class of drugs and reinforce the need for more efficacious treatment strategies.

At the beginning of this project, there was a limited understanding about the role of different FGFR3 mutations in mediating oncogenesis. Moreover, most published studies focused on the most common mutations, for instance S249C in bladder cancer whereas little was known about the poorly characterised rare FGFR3 mutants. I conducted a systematic assessment of the phenotypic effects of a broad range of FGFR3 mutations in the NIH-3T3 model system. While this model has its limitations, it allowed for the robust assessment of the oncogenic potential of distinct FGFR3 mutants in the same genetic background. Response to the FGFR inhibitor BGJ398 was dependent on mutant FGFR3 expression levels and largely mediated through the downregulation of the MAPK pathway. Furthermore, while Src phosphorylation was increased in cells expressing FGFR3 activating mutations, a small molecule inhibitor screen showed that cell lines bearing FGFR3 cysteine mutations and the RT112 fusion were not dependent on this pathway for growth and survival. As elaborated in earlier sections, the combination of FGFR and Src inhibitors appears to be an effective mean to achieve durable responses in mutant FGFR3 bearing cell lines in my

preclinical experiments. While effectively, given the clinical experience with kinase inhibitor and the inevitability of resistance in this class of drugs, it is unlikely that this combination strategy will indefinitely overcome acquired resistance, and the challenge moving forward is to anticipate and predict what new mechanisms of resistance could arise as a result of this combination therapy.

Several outstanding questions remain. The role of Src signalling downstream of FGFR3 is currently unknown and therefore the mechanisms by which Src inhibition sensitises FGFR3 inhibition in a synergistic manner is poorly understood. From a clinical perspective, it is known that the combination of dasatinib with other kinase inhibitors such as erlotinib is toxic and may not be tolerable in patients. One possible strategy is to evaluate if other more selective (and therefore less toxic) Src inhibitors are similarly capable of achieving durable responses in FGFR3 mutant expressing cells. More work is also required to investigate the efficacy of the FGFR and Src inhibitors combination beyond FGFR3 cysteine mutations in order to expand its utility to patients harbouring other FGFR3 mutations. This thesis did not investigate the paradigm of acquired resistance to FGFR inhibitors. It would be interesting to generate BGJ398-resistant *in vitro* by exposing bladder cancer cell lines to long-term escalating dose treatment with FGFR inhibitors and establish that the blockade of the Src pathway is able to re-sensitise cells in this context. Finally, our preliminary studies show that FGFR cysteine mutations is likely to be a useful biomarker to select for patients who will benefit from FGFR and Src inhibitors combination therapy, whether this alone is sufficient or further biomarker optimisation is required must be ascertain in future *in vivo* experiments and clinical trials.

Chapter 8

Appendix

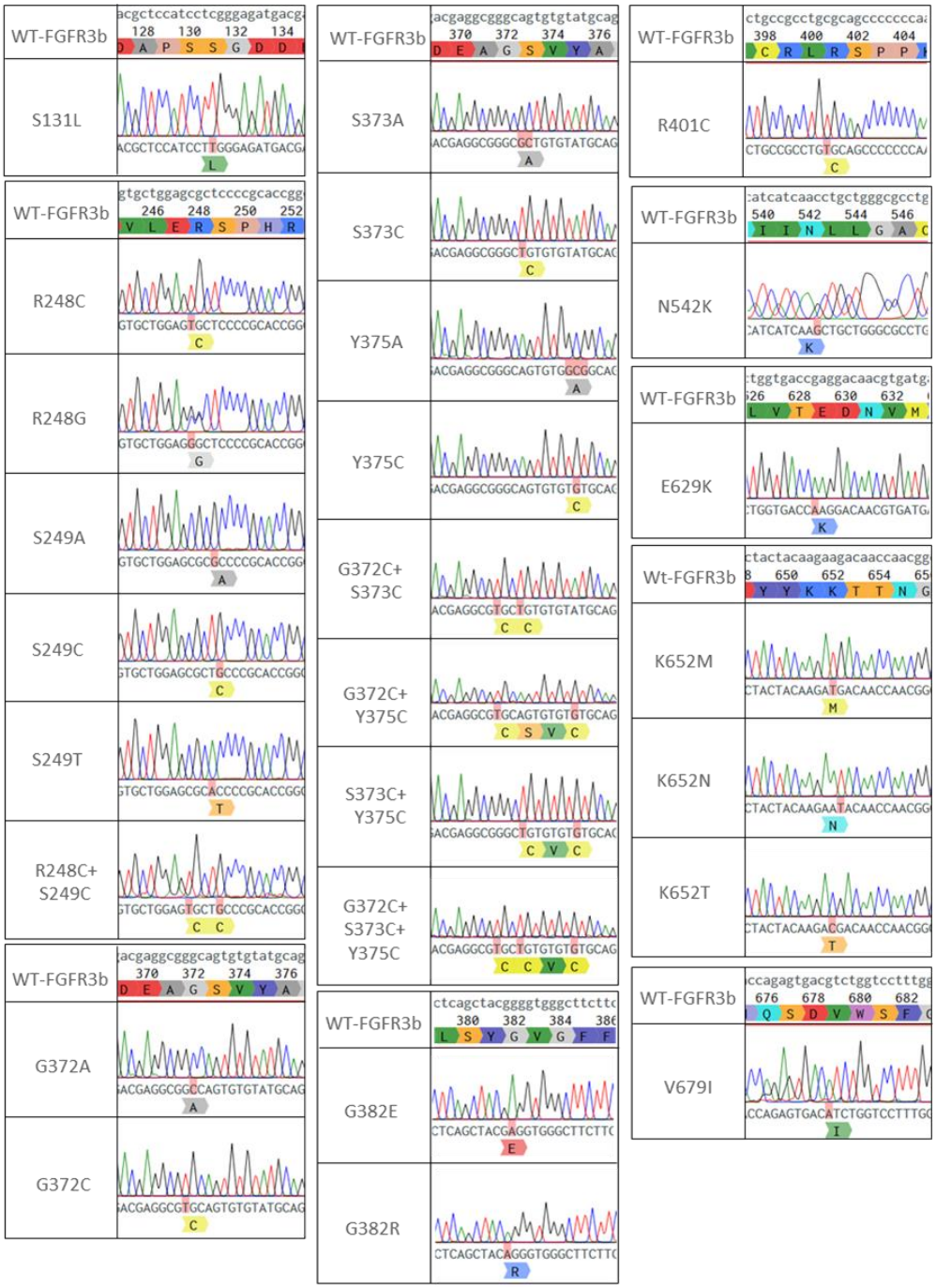

Figure 8.1 – Sanger sequencing of FGFR3 mutants. Sanger sequencing was performed for all generated pFB-FGFR3b mutants to confirm the presence of the mutation of interest for posterior cell transduction. Results were aligned to the WT-FGFR3b sequence for comparison. Altered nucleotides are highlighted in red and mutated amino acid residues are shown immediately below. The corresponding amino acid number is indicated on the WT-FGFR3b row. Note that V557M is not included as it was a gift from Prof. Matilda Katan (UCL).

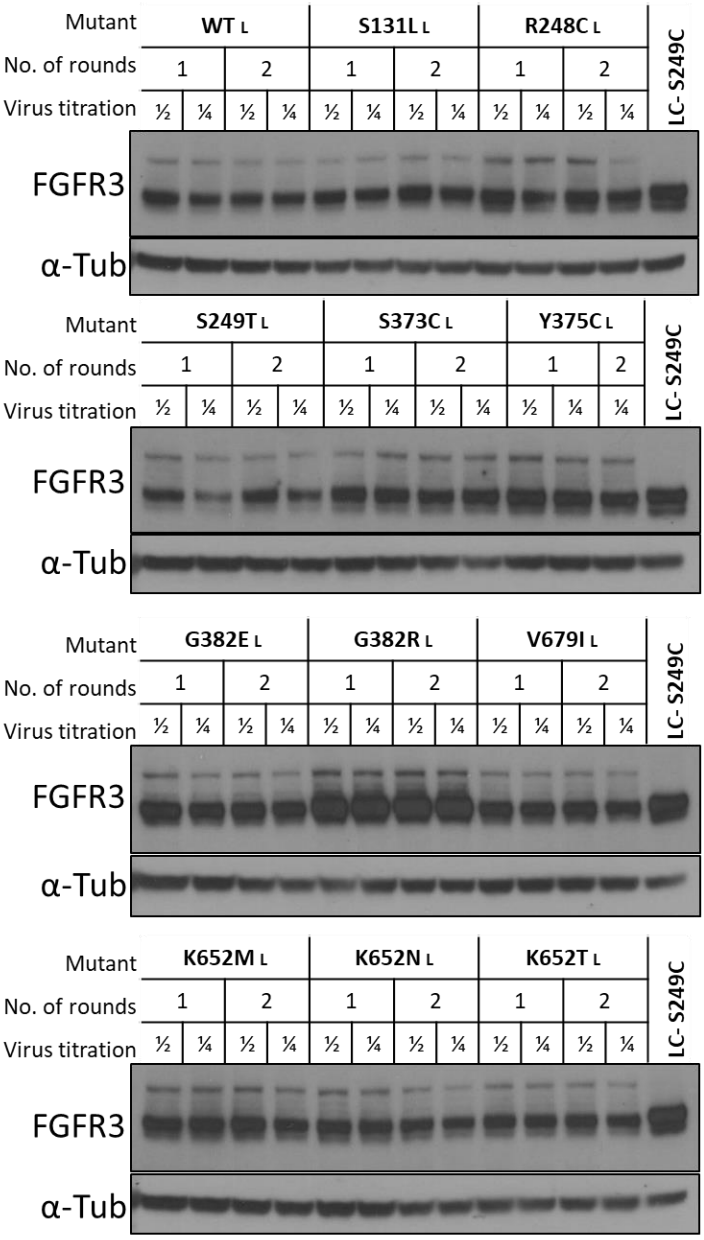

Figure 8.2 – Effect of virus titration and number of infections on FGFR3 mutant expression levels in NIH-3T3 cell lines. Transduction of FGFR3 mutants after virus production with HEK293 cells. One and two rounds of infection and different virus titrations were utilised to infect NIH-3T3 cells. Stable cells were collected and protein lysates isolated for western blotting with the indicated proteins.

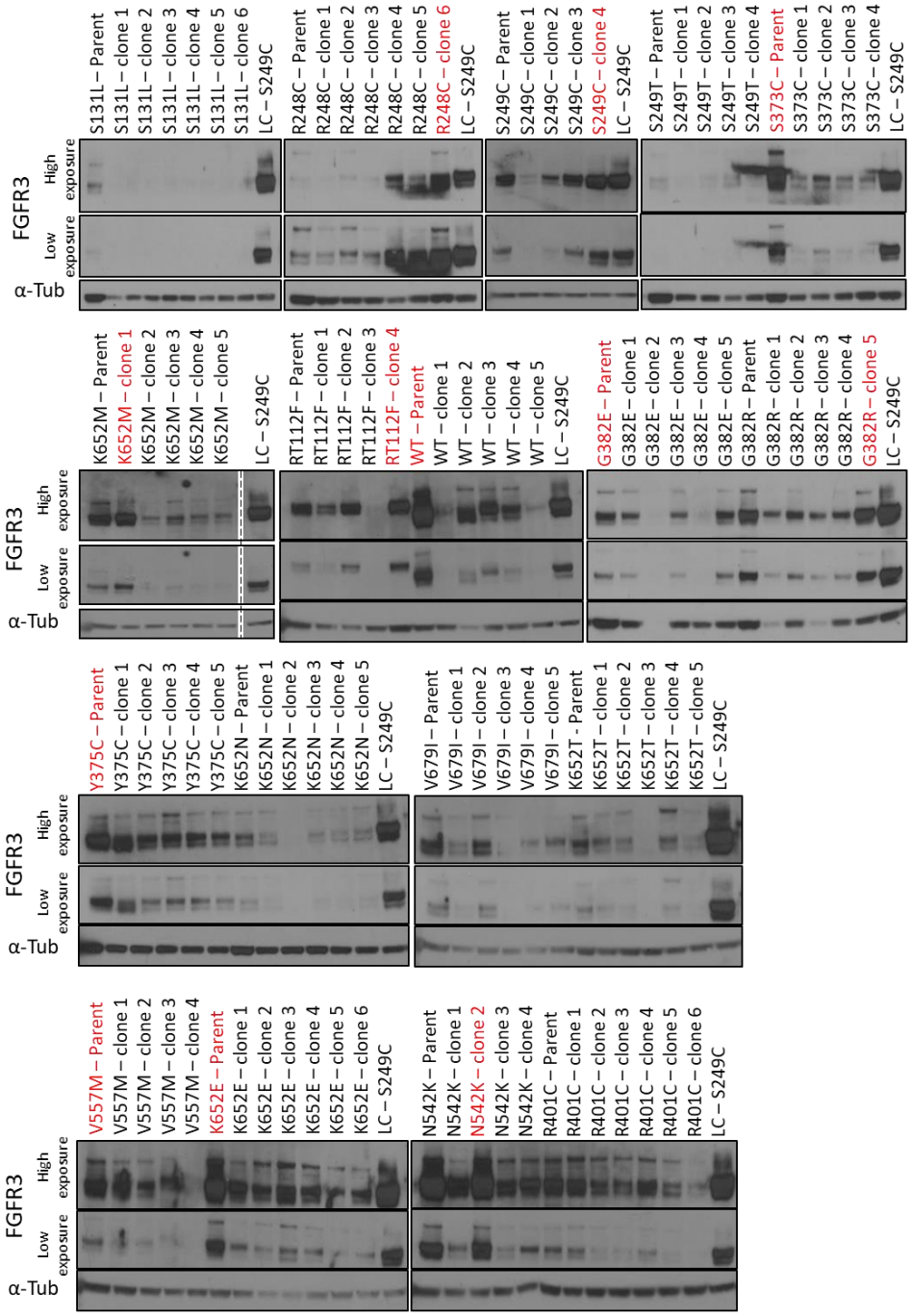

Figure 8.3 – FGFR3 expression levels in NIH-3T3 cell lines upon single cell clone generation. Collection of FGFR3 mutants and parental cell lines generated after single cell clone sorting and growth. Clones are numbered according to the originated clone number. WT, RT112Fus, S249C, N542K, V557M and K652E from UCL were used as parental cell lines to obtain lower levels of FGFR3 expression. The remaining cell lines used the in-house generated cell lines to obtain higher FGFR3 expression levels. Cell lines indicated in red were selected as having similar FGFR3 expression levels across all cell lines. Loading control (LC) was used to compare results with the high expression S249C mutant from UCL.

Bibliography

Acquaviva, J., He, S., Zhang, C., Jimenez, J.-P., Nagai, M., Sang, J., Sequeira, M., Smith, D.L., Ogawa, L.S., Inoue, T., Tatsuta, N., Knowles, M.A., Bates, R.C., Proia, D.A., 2014. FGFR3 Translocations in Bladder Cancer: Differential Sensitivity to HSP90 Inhibition Based on Drug Metabolism. Mol. Cancer Res. 12, 1042–1054.

Adar, R., Monsonego-ornan, E., David, P., Yayon, A., 2002. Differential Activation of Cysteine-Substitution Mutants of Fibroblast Growth Factor Receptor 3 Is Determined by Cysteine Localization. J. bone Miner. Res. 17.

Agazie, Y.M., Movilla, N., Ischenko, I., Hayman, M.J., 2003. The phosphotyrosine phosphatase SHP2 is a critical mediator of transformation induced by the oncogenic fibroblast growth factor receptor 3 6909–6918.

Aggarwal C, Redman MW, Lara PN Jr, Borghaei H, Hoffman P, Bradley JD, Newman AJ 3rd, Feldman MJ, Minichiello K, Miao J, Mack PC3, Papadimitrakopoulou VA, Herbst RS, Kelly K, G.D., 2019. Brief Report: SWOG S1400D (NCT02965378), a Phase II Study of the Fibroblast Growth Factor Receptor Inhibitor AZD4547 in Previously-treated Patients with Fibroblast Growth Factor Pathway-Activated Stage IV Squamous Cell Lung Cancer (Lung-MAP Sub-Study). J. Thorac. Oncol.

Ahmad, I., Iwata, T., Leung, H.Y., 2012. Mechanisms of FGFR-mediated carcinogenesis. Biochim. Biophys. Acta - Mol. Cell Res. 1823, 850–860.

Ahmed, Z., George, R., Lin, C., Man, K., Levitt, J.A., Suhling, K., Ladbury, J.E., 2010. Direct binding of Grb2 SH3 domain to FGFR2 regulates SHP2 function. Cell. Signal. 22, 23–33.

Alsmadi, O., Meyer, B.F., Alkuraya, F., Wakil, S., Alkayal, F., Al-Saud, H., Ramzan, K., Al-Sayed, M.A., 2009. Syndromic congenital sensorineural deafness, microtia and microdontia resulting from a novel homoallelic mutation in fibroblast growth factor 3 (FGF3). Eur. J. Hum. Genet. 17, 14–21.

Alvarez, A., Barisone, G.A., Diaz, E., 2014. Focus Formation: A Cell-based Assay to Determine the Oncogenic Potential of a Gene. J. Vis. Exp. 1–6.

Andersen, J., Burns, H.D., Enriquez-Harris, P., Wilkie, A.O.M., Heath, J.K., 1998. Apert syndrome mutations in fibroblast growth factor receptor 2 exhibit increased affinity for FGF ligand. Hum. Mol. Genet. 7, 1475–1483.

Andl, C.D., Rustgi, A.K., 2005. No one-way street: Cross-talk between E-cadherin and receptor tyrosine kinase (RTK) signaling: A mechanism to regulate RTK activity. Cancer Biol. Ther. 4, 28–31.

Andreadi, C., Noble, C., Patel, B., Jin, H., Hernandez, M.M.A., Balmanno, K., Cook, S.J.J., Pritchard, C., Aguilar Hernandez, M.M., Balmanno, K., Cook,

S.J.J., Pritchard, C., 2012. Regulation of MEK/ERK pathway output by subcellular localization of B-Raf. Biochem. Soc. Trans. 40, 67–72.

Arkin, I.T., 2002. Structural aspects of oligomerization taking place between the transmembrane α-helices of bitopic membrane proteins. Biochim. Biophys. Acta - Biomembr. 1565, 347–363.

Auciello, G., Cunningham, D.L., Tatar, T., Heath, J.K., Rappoport, J.Z., 2013. Regulation of fibroblast growth factor receptor signalling and trafficking by Src and Eps8. J. Cell Sci. 126, 613–624.

Avis, Y., Meyer, N., Webster, K., Robertson, C., Bardwell, M., Donoghue, D.J., 1998. Constitutive Activation of Fibroblast Growth Factor 3 by Mutations Responsible for the Lethal Skeletal Dysplasia Thanatophoric Dysplasia Receptor. Cell Growth Differ. 9, 71–78.

Babina, I.S., Turner, N.C., 2017. Advances and challenges in targeting FGFR signalling in cancer. Nat. Publ. Gr. 17, 318–332.

Bae, J.H., Schlessinger, J., 2010. Asymmetric Tyrosine Kinase Arrangements in Activation or Autophosphorylation of Receptor Tyrosine Kinases. Mol. Cells 29, 443–448.

Baertschi, S., Zhuang, L., Trueb, B., 2007. Mice with a targeted disruption of the Fgfrl1 gene die at birth due to alterations in the diaphragm. FEBS J. 274, 6241–6253.

Bahleda, R., Italiano, A., Hierro, C., Mita, A.C., Cervantes, A., Chan, N., Awad, M.M., Calvo, E., Moreno, V., Govindan, R., Spira, A.I., Gonzalez, M.D., Zhong, B., Santiago-Walker, A.E., Poggesi, I., Parekh, T., Xie, H., Infante, J.R., Tabernero, J., 2019. Multicenter Phase I Study of Erdafitinib (JNJ-42756493), Oral Pan-Fibroblast Growth Factor Receptor Inhibitor, in Patients with Advanced or Refractory Solid Tumors. Clin. Cancer Res. 25, 4888–4897.

Bailey, M.H., Tokheim, C., Porta-Pardo, E., Sengupta, S., Bertrand, D., Weerasinghe, A., Colaprico, A., Wendl, M.C., Kim, J., Reardon, B., Ng, P.K.S., Jeong, K.J., Cao, S., Wang, Z., Gao, J., Gao, Q., Wang, F., Liu, E.M., Mularoni, L., Rubio-Perez, C., Nagarajan, N., Cortés-Ciriano, I., Zhou, D.C., Liang, W.W., Hess, J.M., Yellapantula, V.D., Tamborero, D., Gonzalez-Perez, A., Suphavilai, C., Ko, J.Y., Khurana, E., Park, P.J., Van Allen, E.M., Liang, H., Caesar-Johnson, S.J., Demchok, J.A., Felau, I., Kasapi, M., Ferguson, M.L., Hutter, C.M., Sofia, H.J., Tarnuzzer, R., Yang, L., Zenklusen, J.C., Zhang, J. (Julia), Chudamani, S., Liu, J., Lolla, L., Naresh, R., Pihl, T., Sun, Q., Wan, Y., Wu, Y., Cho, J., DeFreitas, T., Frazer, S., Gehlenborg, N., Getz, G., Heiman, D.I., Lawrence, M.S., Lin, P., Meier, S., Noble, M.S., Saksena, G., Voet, D., Zhang, H., Bernard, B., Chambwe, N., Dhankani, V., Knijnenburg, T., Kramer, R., Leinonen, K., Liu, Y., Miller, M., Reynolds, S., Shmulevich, I., Thorsson, V., Zhang, W., Akbani, R., Broom, B.M., Hegde, A.M., Ju, Z., Kanchi, R.S., Korkut, A., Li, J., Ling, S., Liu, W., Lu, Y., Mills, G.B., Ng, K.S., Rao, A., Ryan, M., Wang, J., Weinstein, J.N., Zhang, J., Abeshouse, A., Armenia, J., Chakravarty, D.,

Chatila, W.K., de Bruijn, I., Gross, B.E., Heins, Z.J., Kundra, R., La, K., Ladanyi, M., Luna, A., Nissan, M.G., Ochoa, A., Phillips, S.M., Reznik, E., Sanchez-Vega, F., Sander, C., Schultz, N., Sheridan, R., Sumer, S.O., Sun, Y., Taylor, B.S., Anur, P., Peto, M., Spellman, P., Benz, C., Stuart, J.M., Wong, C.K., Yau, C., Hayes, D.N., Parker, J.S., Wilkerson, M.D., Ally, A., Balasundaram, M., Bowlby, R., Brooks, D., Carlsen, R., Chuah, E., Dhalla, N., Holt, R., Jones, S.J.M., Kasaian, K., Lee, D., Ma, Y., Marra, M.A., Mayo, M., Moore, R.A., Mungall, A.J., Mungall, K., Robertson, A.G., Sadeghi, S., Schein, J.E., Sipahimalani, P., Tam, A., Thiessen, N., Tse, K., Wong, T., Berger, A.C., Beroukhim, R., Cherniack, A.D., Cibulskis, C., Gabriel, S.B., Gao, G.F., Ha, G., Meyerson, M., Schumacher, S.E., Shih, J., Kucherlapati, M.H., Kucherlapati, R.S., Baylin, S., Cope, L., Danilova, L., Bootwalla, M.S., Lai, P.H., Maglinte, D.T., Van Den Berg, D.J., Weisenberger, D.J., Auman, J.T., Balu, S., Bodenheimer, T., Fan, C., Hoadley, K.A., Hoyle, A.P., Jefferys, S.R., Jones, C.D., Meng, S., Mieczkowski, P.A., Mose, L.E., Perou, A.H., Perou, C.M., Roach, J., Shi, Y., Simons, J. V., Skelly, T., Soloway, M.G., Tan, D., Veluvolu, U., Fan, H., Hinoue, T., Laird, P.W., Shen, H., Zhou, W., Bellair, M., Chang, K., Covington, K., Creighton, C.J., Dinh, H., Doddapaneni, H.V., Donehower, L.A., Drummond, J., Gibbs, R.A., Glenn, R., Hale, W., Han, Y., Hu, J., Korchina, V., Lee, S., Lewis, L., Li, W., Liu, X., Morgan, M., Morton, D., Muzny, D., Santibanez, J., Sheth, M., Shinbrot, E., Wang, L., Wang, M., Wheeler, D.A., Xi, L., Zhao, F., Hess, J., Appelbaum, E.L., Bailey, M., Cordes, M.G., Ding, L., Fronick, C.C., Fulton, L.A., Fulton, R.S., Kandoth, C., Mardis, E.R., McLellan, M.D., Miller, C.A., Schmidt, H.K., Wilson, R.K., Crain, D., Curley, E., Gardner, J., Lau, K., Mallery, D., Morris, S., Paulauskis, J., Penny, R., Shelton, C., Shelton, T., Sherman, M., Thompson, E., Yena, P., Bowen, J., Gastier-Foster, J.M., Gerken, M., Leraas, K.M., Lichtenberg, T.M., Ramirez, N.C., Wise, L., Zmuda, E., Corcoran, N., Costello, T., Hovens, C., Carvalho, A.L., de Carvalho, A.C., Fregnani, J.H., Longatto-Filho, A., Reis, R.M., Scapulatempo-Neto, C., Silveira, H.C.S., Vidal, D.O., Burnette, A., Eschbacher, J., Hermes, B., Noss, A., Singh, R., Anderson, M.L., Castro, P.D., Ittmann, M., Huntsman, D., Kohl, B., Le, X., Thorp, R., Andry, C., Duffy, E.R., Lyadov, V., Paklina, O., Setdikova, G., Shabunin, A., Tavobilov, M., McPherson, C., Warnick, R., Berkowitz, R., Cramer, D., Feltmate, C., Horowitz, N., Kibel, A., Muto, M., Raut, C.P., Malykh, A., Barnholtz-Sloan, J.S., Barrett, W., Devine, K., Fulop, J., Ostrom, Q.T., Shimmel, K., Wolinsky, Y., Sloan, A.E., De Rose, A., Giuliante, F., Goodman, M., Karlan, B.Y., Hagedorn, C.H., Eckman, J., Harr, J., Myers, J., Tucker, K., Zach, L.A., Deyarmin, B., Hu, H., Kvecher, L., Larson, C., Mural, R.J., Somiari, S., Vicha, A., Zelinka, T., Bennett, J., Iacocca, M., Rabeno, B., Swanson, P., Latour, M., Lacombe, L., Têtu, B., Bergeron, A., McGraw, M., Staugaitis, S.M., Chabot, J., Hibshoosh, H., Sepulveda, A., Su, T., Wang, T., Potapova, O., Voronina, O., Desjardins, L., Mariani, O., Roman-Roman, S., Sastre, X., Stern, M.H., Cheng, F., Signoretti, S., Berchuck, A., Bigner, D., Lipp, E., Marks, J., McCall, S., McLendon, R., Secord, A., Sharp, A., Behera, M., Brat, D.J., Chen, A., Delman, K., Force, S., Khuri, F., Magliocca, K., Maithel, S., Olson, J.J., Owonikoko, T., Pickens, A., Ramalingam, S., Shin, D.M., Sica, G., Van Meir, E.G., Eijckenboom, W., Gillis, A., Korpershoek, E., Looijenga, L.,

Oosterhuis, W., Stoop, H., van Kessel, K.E., Zwarthoff, E.C., Calatozzolo, C., Cuppini, L., Cuzzubbo, S., DiMeco, F., Finocchiaro, G., Mattei, L., Perin, A., Pollo, B., Chen, C., Houck, J., Lohavanichbutr, P., Hartmann, A., Stoehr, C., Stoehr, R., Taubert, H., Wach, S., Wullich, B., Kycler, W., Murawa, D., Wiznerowicz, M., Chung, K., Edenfield, W.J., Martin, J., Baudin, E., Bubley, G., Bueno, R., De Rienzo, A., Richards, W.G., Kalkanis, S., Mikkelsen, T., Noushmehr, H., Scarpace, L., Girard, N., Aymerich, M., Campo, E., Giné, E., Guillermo, A.L., Van Bang, N., Hanh, P.T., Phu, B.D., Tang, Y., Colman, H., Evason, K., Dottino, P.R., Martignetti, J.A., Gabra, H., Juhl, H., Akeredolu, T., Stepa, S., Hoon, D., Ahn, K., Kang, K.J., Beuschlein, F., Breggia, A., Birrer, M., Bell, D., Borad, M., Bryce, A.H., Castle, E., Chandan, V., Cheville, J., Copland, J.A., Farnell, M., Flotte, T., Giama, N., Ho, T., Kendrick, M., Kocher, J.P., Kopp, K., Moser, C., Nagorney, D., O'Brien, D., O'Neill, B.P., Patel, T., Petersen, G., Que, F., Rivera, M., Roberts, L., Smallridge, R., Smyrk, T., Stanton, M., Thompson, R.H., Torbenson, M., Yang, J.D., Zhang, L., Brimo, F., Ajani, J.A., Gonzalez, A.M.A., Behrens, C., Bondaruk, J., Broaddus, R., Czerniak, B., Esmaeli, B., Fujimoto, J., Gershenwald, J., Guo, C., Lazar, A.J., Logothetis, C., Meric-Bernstam, F., Moran, C., Ramondetta, L., Rice, D., Sood, A., Tamboli, P., Thompson, T., Troncoso, P., Tsao, A., Wistuba, I., Carter, C., Haydu, L., Hersey, P., Jakrot, V., Kakavand, H., Kefford, R., Lee, K., Long, G., Mann, G., Quinn, M., Saw, R., Scolyer, R., Shannon, K., Spillane, A., Stretch, J., Synott, M., Thompson, J., Wilmott, J., Al-Ahmadie, H., Chan, T.A., Ghossein, R., Gopalan, A., Levine, D.A., Reuter, V., Singer, S., Singh, B., Tien, N.V., Broudy, T., Mirsaidi, C., Nair, P., Drwiega, P., Miller, J., Smith, J., Zaren, H., Park, J.W., Hung, N.P., Kebebew, E., Linehan, W.M., Metwalli, A.R., Pacak, K., Pinto, P.A., Schiffman, M., Schmidt, L.S., Vocke, C.D., Wentzensen, N., Worrell, R., Yang, H., Moncrieff, M., Goparaju, C., Melamed, J., Pass, H., Botnariuc, N., Caraman, I., Cernat, M., Chemencedji, I., Clipca, A., Doruc, S., Gorincioi, G., Mura, S., Pirtac, M., Stancul, I., Tcaciuc, D., Albert, M., Alexopoulou, I., Arnaout, A., Bartlett, J., Engel, J., Gilbert, S., Parfitt, J., Sekhon, H., Thomas, G., Rassl, D.M., Rintoul, R.C., Bifulco, C., Tamakawa, R., Urba, W., Hayward, N., Timmers, H., Antenucci, A., Facciolo, F., Grazi, G., Marino, M., Merola, R., de Krijger, R., Gimenez-Roqueplo, A.P., Piché, A., Chevalier, S., McKercher, G., Birsoy, K., Barnett, G., Brewer, C., Farver, C., Naska, T., Pennell, N.A., Raymond, D., Schilero, C., Smolenski, K., Williams, F., Morrison, C., Borgia, J.A., Liptay, M.J., Pool, M., Seder, C.W., Junker, K., Omberg, L., Dinkin, M., Manikhas, G., Alvaro, D., Bragazzi, M.C., Cardinale, V., Carpino, G., Gaudio, E., Chesla, D., Cottingham, S., Dubina, M., Moiseenko, F., Dhanasekaran, R., Becker, K.F., Janssen, K.P., Slotta-Huspenina, J., Abdel-Rahman, M.H., Aziz, D., Bell, S., Cebulla, C.M., Davis, A., Duell, R., Elder, J.B., Hilty, J., Kumar, B., Lang, J., Lehman, N.L., Mandt, R., Nguyen, P., Pilarski, R., Rai, K., Schoenfield, L., Senecal, K., Wakely, P., Hansen, P., Lechan, R., Powers, J., Tischler, A., Grizzle, W.E., Sexton, K.C., Kastl, A., Henderson, J., Porten, S., Waldmann, J., Fassnacht, M., Asa, S.L., Schadendorf, D., Couce, M., Graefen, M., Huland, H., Sauter, G., Schlomm, T., Simon, R., Tennstedt, P., Olabode, O., Nelson, M., Bathe, O., Carroll, P.R., Chan, J.M., Disaia, P., Glenn, P., Kelley, R.K., Landen, C.N., Phillips, J., Prados, M., Simko, J.,

Smith-McCune, K., VandenBerg, S., Roggin, K., Fehrenbach, A., Kendler, A., Sifri, S., Steele, R., Jimeno, A., Carey, F., Forgie, I., Mannelli, M., Carney, M., Hernandez, B., Campos, B., Herold-Mende, C., Jungk, C., Unterberg, A., von Deimling, A., Bossler, A., Galbraith, J., Jacobus, L., Knudson, M., Knutson, T., Ma, D., Milhem, M., Sigmund, R., Godwin, A.K., Madan, R., Rosenthal, H.G., Adebamowo, C., Adebamowo, S.N., Boussioutas, A., Beer, D., Giordano, T., Mes-Masson, A.M., Saad, F., Bocklage, T., Landrum, L., Mannel, R., Moore, K., Moxley, K., Postier, R., Walker, J., Zuna, R., Feldman, M., Valdivieso, F., Dhir, R., Luketich, J., Pinero, E.M.M., Quintero-Aguilo, M., Carlotti, C.G., Dos Santos, J.S., Kemp, R., Sankarankuty, A., Tirapelli, D., Catto, J., Agnew, K., Swisher, E., Creaney, J., Robinson, B., Shelley, C.S., Godwin, E.M., Kendall, S., Shipman, C., Bradford, C., Carey, T., Haddad, A., Moyer, J., Peterson, L., Prince, M., Rozek, L., Wolf, G., Bowman, R., Fong, K.M., Yang, I., Korst, R., Rathmell, W.K., Fantacone-Campbell, J.L., Hooke, J.A., Kovatich, A.J., Shriver, C.D., DiPersio, J., Drake, B., Govindan, R., Heath, S., Ley, T., Van Tine, B., Westervelt, P., Rubin, M.A., Lee, J. Il, Aredes, N.D., Mariamidze, A., Godzik, A., Lopez-Bigas, N., Stuart, J., Wheeler, D., Chen, K., Karchin, R., 2018. Comprehensive Characterization of Cancer Driver Genes and Mutations. Cell 173, 371–385.e18.

Beenken, A., Mohammadi, M., 2009. The FGF family: Biology, pathophysiology and therapy. Nat. Rev. Drug Discov. 8, 235–253.

Bellus, G.A., Spector, E.B., Speiser, P.W., Weaver, C.A., Garber, A.T., Bryke, C.R., Israel, J., Rosengren, S.S., Webster, M.K., Donoghue, D.J., Francomano, C.A., 2000. Distinct Missense Mutations of the FGFR3 Lys650 Codon Modulate Receptor Kinase Activation and the Severity of the Skeletal Dysplasia Phenotype. Am J Hum Genet 67, 1411–1421.

Belov, A.A., Mohammadi, M., 2013. Molecular mechanisms of fibroblast growth factor signaling in physiology and pathology. Cold Spring Harb. Perspect. Biol. 5, 1–24.

Bernard-Pierrot, I., Brams, A., Dunois-Lardé, C., Caillault, A., Diez de Medina, S.G., Cappellen, D., Graff, G., Thiery, J.P., Chopin, D., Ricol, D., Radvanyi, F., 2006. Oncogenic properties of the mutated forms of fibroblast growth factor receptor 3b. Carcinogenesis 27, 740–747.

Bhullar, K.S., Lagarón, N.O., McGowan, E.M., Parmar, I., Jha, A., Hubbard, B.P., Rupasinghe, H.P.V., 2018. Kinase-targeted cancer therapies: progress, challenges and future directions. Mol. Cancer 17, 48.

Bocharov, E. V., Lesovoy, D.M., Goncharuk, S.A., Goncharuk, M. V., Hristova, K., Arseniev, A.S., 2013. Structure of FGFR3 Transmembrane Domain Dimer: Implications for Signaling and Human Pathologies. Structure 21, 2087–2093.

Bodoor, K., Ghabkari, A., Jaradat, Z., Alkhateeb, A., Jaradat, S., 2010. FGFR3 mutational status and protein expression in patients with bladder cancer in a Jordanian population. Cancer Epidemiol. 34, 724–732.

Bonaventure, J., Gibbs, L., Horne, W.C., Baron, R., 2007. The localization of FGFR3 mutations causing thanatophoric dysplasia type I differentially affects phosphorylation , processing and ubiquitylation of the receptor 274, 3078–3093.

Borowicz, S., Van Scoyk, M., Avasarala, S., Karuppusamy Rathinam, M.K., Tauler, J., Bikkavilli, R.K., Winn, R.A., 2014. The Soft Agar Colony Formation Assay. J. Vis. Exp. 1–6.

Bos, M., Gardizi, M., Schildhaus, H., 2013. Activated RET and ROS: two new driver mutations in lung adenocarcinoma. Transl. Lung Cancer Res. 2, 112–121.

Bradshaw, R.A., Chalkley, R.J., Biarc, J., Burlingame, A.L., 2013. Receptor tyrosine kinase signaling mechanisms: Devolving TrkA responses with phosphoproteomics. Adv. Biol. Regul. 53, 87–96.

Brown, W.S., Tan, L., Smith, A., Gray, N.S., Wendt, M.K., 2016. Covalent Targeting of Fibroblast Growth Factor Receptor Inhibits Metastatic Breast Cancer. Mol. Cancer Ther. 15, 2096–2106.

Byron, S. a, Chen, H., Wortmann, A., Loch, D., Gartside, M.G., Dehkhoda, F., Blais, S.P., Neubert, T. a, Mohammadi, M., Pollock, P.M., 2013. The N550K/H Mutations in FGFR2 Confer Differential Resistance to PD173074, Dovitinib, and Ponatinib ATP-Competitive Inhibitors. Neoplasia 15, 975–988.

Camidge, D.R., Pao, W., Sequist, L. V., 2014. Acquired resistance to TKIs in solid tumours: Learning from lung cancer. Nat. Rev. Clin. Oncol. 11, 473–481.

Cappellen, D., Oliveira, C. De, Ricol, D., Medina, S.G.D. de, Bourdin, J., Sastre-Garau, X., Chopin, D., Radvanyi, J.P.T.& F.R., 1999. Frequent activating mutations of FGFR3 in human bladder. Nat. Genet. 23, 18–20.

Cargnello, M., Roux, P.P., 2011. Activation and Function of the MAPKs and Their Substrates, the MAPK-Activated Protein Kinases. Microbiol. Mol. Biol. Rev. 75, 50–83.

Carter, E.P., Fearon, A.E., Grose, R.P., 2015. Careless talk costs lives: Fibroblast growth factor receptor signalling and the consequences of pathway malfunction. Trends Cell Biol. 25, 221–233.

Carter, H., Chen, S., Isik, L., Tyekucheva, S., Velculescu, V.E., Kinzler, K.W., Vogelstein, B., Karchin, R., 2009. Cancer-specific high-throughput annotation of somatic mutations: Computational prediction of driver missense mutations. Cancer Res. 69, 6660–6667.

Celestino, R., Sigstad, E., Løvf, M., Thomassen, G.O.S., Grøholt, K.K., Jørgensen, L.H., Berner, A., Castro, P., Lothe, R.A., Bjøro, T., Sobrinho-Simoes, M., Soares, P., Skotheim, R.I., 2012. Survey of 548 Oncogenic Fusion Transcripts in Thyroid Tumors Supports the Importance of the Already Established Thyroid Fusions Genes. Genes. Chromosomes

Cancer 51, 1154–1164.

Cerami, E., Gao, J., Dogrusoz, U., Gross, B.E., Sumer, S.O., Aksoy, B.A., Jacobsen, A., Byrne, C.J., Heuer, M.L., Larsson, E., Antipin, Y., Reva, B., Goldberg, A.P., Sander, C., Schultz, N., 2012. The cBio Cancer Genomics Portal: An open platform for exploring multidimensional cancer genomics data. Cancer Discov. 2, 401–404.

Chaffer, C.L., Brennan, J.P., Slavin, J.L., Blick, T., Thompson, E.W., Williams, E.D., 2006. Mesenchymal-to-epithelial transition facilitates bladder cancer metastasis: Role of fibroblast growth factor receptor-2. Cancer Res. 66, 11271–11278.

Chandarlapaty, S., 2012. Negative feedback and adaptive resistance to the targeted therapy of cancer. Cancer Discov. 2, 311–319.

Chang, C., Niu, Z., Gu, N., Zhao, W., Wang, G., Jia, Y., Li, D., Xu, C., 2015. Analysis of the ways and methods of signaling pathways in regulating cell cycle of NIH3T3 at transcriptional level. BMC Cell Biol. 16, 1–13.

Chell, V., Balmanno, K., Little, A.S., Wilson, M., Andrews, S., Blockley, L., Hampson, M., Gavine, P.R., Cook, S.J., 2013. Tumour cell responses to new fibroblast growth factor receptor tyrosine kinase inhibitors and identification of a gatekeeper mutation in FGFR3 as a mechanism of acquired resistance. Oncogene 32, 3059–3070.

Chen, H., Huang, Z., Dutta, K., Blais, S., Neubert, T.A., Li, X., Cowburn, D., Traaseth, N.J., Mohammadi, M., 2013. Cracking the Molecular Origin of Intrinsic Tyrosine Kinase Activity through Analysis of Pathogenic Gain-of-Function Mutations. CellReports 4, 376–384.

Chen, H., Ma, J., Li, W., Eliseenkova, A. V., Xu, C., Neubert, T. a., Miller, W. Todd, Mohammadi, M., 2007. A Molecular Brake in the Kinase Hinge Region Regulates the Activity of Receptor Tyrosine Kinases. Mol. Cell 27, 717–730.

Chen, H., Xu, C.-F., Ma, J., Eliseenkova, A. V, Li, W., Pollock, P.M., Pitteloud, N., Miller, W.T., Neubert, T. a, Mohammadi, M., 2008. A crystallographic snapshot of tyrosine trans-phosphorylation in action. PNAS 105, 19660–5.

Chen, J., Williams, I.R., Lee, B.H., Duclos, N., Huntly, B.J.P., Donoghue, D.J., Gilliland, D.G., 2005. Constitutively activated FGFR3 mutants signal through PLCγ-dependent and -independent pathways for hematopoietic transformation. Blood 106, 328–337.

Chesi, M., Nardini, E., Brents, L.A., Schrock, E., Ried, T., Kuehl, W.M., Bergsagel, P.L., 1997. Frequent translocation t(4;14)(p16.3;q32.3) in multiple myeloma is associated with increased expression and activating mutations of fibroblast growth factor receptor 3. Nat. Genet. 16, 260–264.

Chou, T.C., 2010. Drug combination studies and their synergy quantification using the chou-talalay method. Cancer Res. 70, 440–446.

Choudhary, C., Mann, M., 2010. Decoding signalling networks by mass spectrometry-based proteomics. Nat. Rev. Mol. Cell Biol. 11, 427–439.

Citores, L., Wesche, J., Kolpakova, E., Olsnes, S., 1999. Uptake and Intracellular Transport of Acidic Fibroblast Growth Factor : Evidence for Free and Cytoskeleton-anchored Fibroblast Growth. Mol. Biol. Cell 10, 3835–3848.

Comps-Agrar, L., Dunshee, D.R., Eaton, D.L., Sonoda, J., 2015. Unliganded fibroblast growth factor receptor 1 forms density-independent dimers. J. Biol. Chem. 290, 24166–24177.

Cortes, J.E., Jimenez, C.A., Mauro, M.J., Geyer, A., Pinilla-Ibarz, J., Smith, B.D., 2017. Pleural Effusion in Dasatinib-Treated Patients With Chronic Myeloid Leukemia in Chronic Phase: Identification and Management. Clin. Lymphoma, Myeloma Leuk. 17, 78–82.

Costa, R., Carneiro, B.A., Taxter, T., Tavora, F.A., Kalyan, A., Pai, S.A., Chae, Y.K., Giles, F.J., 2016. FGFR3-TACC3 fusion in solid tumors : mini review 7.

Criscitiello, C., Esposito, A., Curigliano, G., 2017. Targeting FGFR pathway in breast cancer. Breast Cancer Innov. Res. Manag. 37, 819–822.

Daly, C., Castanaro, C., Zhang, W., Zhang, Q., Wei, Y., Ni, M., Young, T., Zhang, L., Burova, E., Thurston, G., 2016. FGFR3-TACC3 fusion proteins act as naturally occurring drivers of tumor resistance by functionally substituting for EGFR/ERK signaling. Oncogene 471–481.

Dar, A.C., Shokat, K.M., 2011. The Evolution of Protein Kinase Inhibitors from Antagonists to Agonists of Cellular Signaling. Annu. Rev. Biochem. 80, 769–795.

Datta, J., Damodaran, S., Parks, H., Ocrainiciuc, C., Miya, J., Yu, L., Gardner, E.P., Samorodnitsky, E., Wing, M.R., Bhatt, D., Hays, J., Reeser, J.W., Roychowdhury, S., 2017. Akt Activation Mediates Acquired Resistance to Fibroblast Growth Factor Receptor Inhibitor BGJ398. Mol. Cancer Ther. 16, 614–624.

Davies, B.R., Guan, N., Logie, A., Crafter, C., Hanson, L., Jacobs, V., James, N., Dudley, P., Jacques, K., Ladd, B., D'Cruz, C.M., Zinda, M., Lindemann, J., Kodaira, M., Tamura, K., Jenkins, E.L., 2015. Tumors with AKT1E17K mutations are rational targets for single agent or combination therapy with AKT inhibitors. Mol. Cancer Ther. 14, 2441–2451.

De Moerlooze, L., Spencer-Dene, B., Revest, J.M., Hajihosseini, M., Rosewell, I., Dickson, C., 2000. An important role for the IIIb isoform of fibroblast growth factor receptor 2 (FGFR2) in mesenchymal-epithelial signalling during mouse organogenesis. Development 127, 483–492.

Del Piccolo, N., Placone, J., Hristova, K., 2015. Effect of thanatophoric dysplasia type I mutations on FGFR3 dimerization. Biophys. J. 108, 272–278.

Di Martino, E., L'Hote, C.G., Kennedy, W., Tomlinson, D.C., Knowles, M.A., 2009. Mutant fibroblast growth factor receptor 3 induces intracellular signaling and cellular transformation in a cell type-and mutation-specific manner. Oncogene 28, 4306–4316.

Di Martino, E., Tomlinson, D.C., Williams, S. V., Knowles, M.A., 2016. A place for precision medicine in bladder cancer: Targeting the FGFRs. Futur. Oncol. 12, 2243–2263.

Dieci, M.V., Arnedos, M., Andre, F., Soria, J.C., 2013. Fibroblast Growth Factor Receptor Inhibitors as a Cancer Treatment: From a Biologic Rationale to Medical Perspectives. Cancer Discov. 3, 264–279.

Dienstmann, R., Rodon, J., Prat, a., Perez-Garcia, J., Adamo, B., Felip, E., Cortes, J., Iafrate, a. J., Nuciforo, P., Tabernero, J., 2014. Genomic aberrations in the FGFR pathway: Opportunities for targeted therapies in solid tumors. Ann. Oncol. 25, 552–563.

Disanza, A., Frittoli, E., Palamidessi, A., Scita, G., Istituto, F., Molecolare, O., Adamello, V., 2009. Endocytosis and spatial restriction of cell signaling. Mol. Oncol. 3, 280–296.

Dougherty, M.K., Müller, J., Ritt, D.A., Zhou, M., Zhou, X.Z., Copeland, T.D., Conrads, T.P., Veenstra, T.D., Lu, K.P., Morrison, D.K., 2005. Regulation of Raf-1 by direct feedback phosphorylation. Mol. Cell 17, 215–224.

Druker, B.J., Tamura, S., Burchdunger, E., Ohno, S., Segal, G.M., Fanning, S., Zimmermann, J., Lydon, N.B., 1996. Effects of a selective inhibitor of the Abl tyrosine kinase on the growth of Bcr-Abl positive cells. Nat. Publ. Gr. 2, 561–566.

Du, Z., Lovly, C.M., 2018. Mechanisms of receptor tyrosine kinase activation in cancer. Mol. Cancer 17, 1–13.

Easton, D.F., Pooley, K.A., Dunning, A.M., Pharoah, P.D.P., Thompson, D., Ballinger, D.G., Struewing, J.P., Morrison, J., Field, H., Luben, R., Wareham, N., Ahmed, S., Healey, C.S., Bowman, R., Meyer, K.B., Haiman, C.A., Kolonel, L.K., Henderson, B.E., Le Marchand, L., Brennan, P., Sangrajrang, S., Gaborieau, V., Odefrey, F., Shen, C.Y., Wu, P.E., Wang, H.C., Eccles, D., Evans, D.G., Peto, J., Fletcher, O., Johnson, N., Seal, S., Stratton, M.R., Rahman, N., Chenevix-Trench, G., Bojesen, S.E., Nordestgaard, B.G., Axelsson, C.K., Garcia-Closas, M., Brinton, L., Chanock, S., Lissowska, J., Peplonska, B., Nevanlinna, H., Fagerholm, R., Eerola, H., Kang, D., Yoo, K.Y., Noh, D.Y., Ahn, S.H., Hunter, D.J., Hankinson, S.E., Cox, D.G., Hall, P., Wedren, S., Liu, J., Low, Y.L., Bogdanova, N., Schürmann, P., Dörk, T., Tollenaar, R.A.E.M., Jacobi, C.E., Devilee, P., Klijn, J.G.M., Sigurdson, A.J., Doody, M.M., Alexander, B.H., Zhang, J., Cox, A., Brock, I.W., MacPherson, G., Reed, M.W.R., Couch, F.J., Goode, E.L., Olson, J.E., Meijers-Heijboer, H., Van Den Ouweland, A., Uitterlinden, A., Rivadeneira, F., Milne, R.L., Ribas, G., Gonzalez-Neira, A., Benitez, J., Hopper, J.L., McCredie, M., Southey, M., Giles, G., Schroen, C., Justenhoven, C., Brauch, H., Hamann, U., Ko, Y.D., Spurdle, A.B.,

Beesley, J., Chen, X., Mannermaa, A., Kosma, V.M., Kataja, V., Hartikainen, J., Day, N.E., Cox, D.R., Ponder, B.A.J., Luccarini, C., Conroy, D., Shah, M., Munday, H., Jordan, C., Perkins, B., West, J., Redman, K., Driver, K., Aghmesheh, M., Amor, D., Andrews, L., Antill, Y., Armes, J., Armitage, S., Arnold, L., Balleine, R., Begley, G., Beilby, J., Bennett, I., Bennett, B., Berry, G., Blackburn, A., Brennan, M., Brown, M., Buckley, M., Burke, J., Butow, P., Byron, K., Callen, D., Campbell, I., Clarke, C., Colley, A., Cotton, D., Cui, J., Culling, B., Cummings, M., Dawson, S.J., Dixon, J., Dobrovic, A., Dudding, T., Edkins, T., Eisenbruch, M., Farshid, G., Fawcett, S., Field, M., Firgaira, F., Fleming, J., Forbes, J., Friedlander, M., Gaff, C., Gardner, M., Gattas, M., George, P., Gill, G., Gill, G., Goldblatt, J., Greening, S., Haan, E., Haan, E., Harris, M., Hart, S., Hayward, N., Hopper, J., Humphrey, E., Jenkins, M., Kefford, R., Kefford, R., Kirk, J., Kollias, J., Kovalenko, S., Lakhani, S., Leary, J., Lim, J., Lindeman, G., Lipton, L., Lobb, L., Maclurcan, M., Marsh, D., Marsh, D., McKay, M., Anne McLachlan, S., Milne, R., Mitchell, G., Mitchell, G., Newman, B., O'Loughlin, I., Osborne, R., Peters, L., Price, M., Price, M., Reeve, J., Reeve, T., Richards, R., Rinehart, G., Robinson, B., Rudzki, B., Salisbury, E., Saunders, C., Saunders, C., Scott, E., Scott, E., Seshadri, R., Shelling, A., Shelling, A., Suthers, G., Suthers, G., Taylor, D., Tennant, C., Townshend, S., Townshend, S., Tyler, J., Venter, D., Venter, D., Visvader, J., Walpole, I., Ward, R., Warner, B., Warner, B., Warren, G., Watson, E., Williams, R., Wilson, J., Winship, I., Young, M.A., Bowtell, D., DeFazio, A., DeFazio, A., Gertig, D., Webb, P., 2007. Genome-wide association study identifies novel breast cancer susceptibility loci. Nature 447, 1087–1093.

Eguchi, Y., Moriya, H., Makanae, K., Hasunuma, T., Ishibashi, Y., Kito, K., 2018. Estimating the protein burden limit of yeast cells by measuring the expression limits of glycolytic proteins. Elife 7, 1–23.

Elliott, A.Y., Bronson, D.L., Cervenka, J., Stein, N., Fraley, E.E., 1977. Properties of Cell Lines Established from Transitional Cell Cancers of the Human Urinary Tract. Cancer Res. 37, 1279--1289.

Erdem-Eraslan, L., Gao, Y., Kloosterhof, N.K., Atlasi, Y., Demmers, J., Sacchetti, A., Kros, J.M., Sillevis Smitt, P., Aerts, J., French, P.J., 2015. Mutation specific functions of EGFR result in a mutation-specific downstream pathway activation. Eur. J. Cancer 51, 893–903.

Eswarakumar, V.P., Lax, I., Schlessinger, J., 2005. Cellular signaling by fibroblast growth factor receptors. Cytokine Growth Factor Rev. 16, 139–149.

Faivre, S., Djelloul, S., Raymond, E., 2006. New Paradigms in Anticancer Therapy: Targeting Multiple Signaling Pathways With Kinase Inhibitors. Semin. Oncol. 33, 407–420.

Fan, Y., 2015. Tissue-Specific Gain of RTK Signalling Uncovers Selective Cell Vulnerability during Embryogenesis. PLoS Genet. 11, 1–17.

Ferrara, N., Gerber, H.P., LeCouter, J., 2003. The biology of VEGF and its receptors. Nat. Med. 9, 669–676.

Fracchiolla, N.S., Luminari, S., Baldini, L., Lombardi, L., Maiolo, A.T., Neri, A., 1998. FGFR3 Gene Mutations Associated With Human Skeletal Disorders Occur Rarely in Multiple Myeloma. Blood 5, 2987–2990.

Furdui, C.M., Lew, E.D., Schlessinger, J., Anderson, K.S., 2006. Autophosphorylation of FGFR1 Kinase Is Mediated by a Sequential and Precisely Ordered Reaction Short Article. Mol. Cell 21, 711–717.

Gallo, L.H., Nelson, K.N., Meyer, A.N., Donoghue, D.J., 2015. Functions of Fibroblast Growth Factor Receptors in cancer defined by novel translocations and mutations. Cytokine Growth Factor Rev. 26, 425–449.

Gao, J., Aksoy, B.A., Dogrusoz, U., Dresdner, G., Gross, B., Sumer, S.O., Sun, Y., Jacobsen, A., Sinha, R., Larsson, E., Cerami, E., Sander, C., Schultz, N., 2013. Integrative analysis of complex cancer genomics and clinical profiles using the cBioPortal. Sci. Signal. 6, 1–20.

Gavine, P.R., Mooney, L., Kilgour, E., Thomas, A.P., Al-Kadhimi, K., Beck, S., Rooney, C., Coleman, T., Baker, D., Mellor, M.J., Brooks, A.N., Klinowska, T., 2012. AZD4547: An orally bioavailable, potent, and selective inhibitor of the fibroblast growth factor receptor tyrosine kinase family. Cancer Res. 72, 2045–2056.

Gazdar, A.F., 2010. Activating and resistance mutations of EGFR in non-small cell lung cancer: role in clinical response to EGFR tyrosine kinase inhibitors. Oncogene 28, 1–14.

Gibbs, L., Legeai-Mallet, L., 2007. FGFR3 intracellular mutations induce tyrosine phosphorylation in the Golgi and defective glycosylation. Biochim. Biophys. Acta - Mol. Cell Res. 1773, 502–512.

Giordano, S., Petrelli, A., 2008. From Single- to Multi-Target Drugs in Cancer Therapy: When Aspecificity Becomes an Advantage. Curr. Med. Chem. 15, 422–432.

Goetz, R., Beenken, A., Ibrahimi, O.A., Kalinina, J., Olsen, S.K., Eliseenkova, A. V., Xu, C., Neubert, T.A., Zhang, F., Linhardt, R.J., Yu, X., White, K.E., Inagaki, T., Kliewer, S.A., Yamamoto, M., Kurosu, H., Ogawa, Y., Kuro-o, M., Lanske, B., Razzaque, M.S., Mohammadi, M., 2007. Molecular Insights into the Klotho-Dependent, Endocrine Mode of Action of Fibroblast Growth Factor 19 Subfamily Members. Mol. Cell. Biol. 27, 3417–3428.

Goldfarb, M., Schoorlemmer, J., Williams, A., Diwakar, S., Wang, Q., Huang, X., Giza, J., Tchetchik, D., Kelley, K., Vega, A., Matthews, G., Rossi, P., Ornitz, D.M., D'Angelo, E., 2007. Fibroblast Growth Factor Homologous Factors Control Neuronal Excitability through Modulation of Voltage-Gated Sodium Channels. Neuron 55, 449–463.

Gospodarowicz, D., Cheng, J., 1986. Heparin Protects Basic and Acidic FGF From Inactivation. J. Cell. Physiol. 128, 475–484.

Gozgit, J.M., Wong, M.J., Moran, L., Wardwell, S., Mohemmad, Q.K., Narasimhan, N.I., Shakespeare, W.C., Wang, F., Clackson, T., Rivera,

V.M., 2012. Ponatinib (AP24534), a Multitargeted Pan-FGFR Inhibitor with Activity in Multiple FGFR-Amplified or Mutated Cancer Models. Mol. Cancer Ther. 11, 690–699.

Grand, E.K., Chase, A.J., Heath, C., Rahemtulla, A., Cross, N.C.P., 2004. Targeting FGFR3 in multiple myeloma: Inhibition of t(4;14)-positive cells by SU5402 and PD173074. Leukemia 18, 962–966.

Green, T.P., Fennell, M., Whittaker, R., Curwen, J., Jacobs, V., Allen, J., Logie, A., Hargreaves, J., Hickinson, D.M., Wilkinson, R.W., Elvin, P., Boyer, B., Carragher, N., Plé, P.A., Bermingham, A., Holdgate, G.A., Ward, W.H.J., Hennequin, L.F., Davies, B.R., Costello, G.F., 2009. Preclinical anticancer activity of the potent, oral Src inhibitor AZD0530. Mol. Oncol. 3, 248–261.

Greenman, C., Stephens, P., Smith, R., Dalgliesh, G.L., Hunter, C., Bignell, G., Davies, H., Teague, J., Butler, A., Stevens, C., Edkins, S., O'Meara, S., Vastrik, I., Schmidt, E.E., Avis, T., Barthorpe, S., Bhamra, G., Buck, G., Choudhury, B., Clements, J., Cole, J., Dicks, E., Forbes, S., Gray, K., Halliday, K., Harrison, R., Hills, K., Hinton, J., Jenkinson, A., Jones, D., Menzies, A., Mironenko, T., Perry, J., Raine, K., Richardson, D., Shepherd, R., Small, A., Tofts, C., Varian, J., Webb, T., West, S., Widaa, S., Yates, A., Cahill, D.P., Louis, D.N., Goldstraw, P., Nicholson, A.G., Brasseur, F., Looijenga, L., Weber, B.L., Chiew, Y.E., DeFazio, A., Greaves, M.F., Green, A.R., Campbell, P., Birney, E., Easton, D.F., Chenevix-Trench, G., Tan, M.H., Khoo, S.K., Teh, B.T., Yuen, S.T., Leung, S.Y., Wooster, R., Futreal, P.A., Stratton, M.R., 2007. Patterns of somatic mutation in human cancer genomes. Nature 446, 153–158.

Greulich, H., Pollock, P.M., 2011. Targeting mutant fibroblast growth factor receptors in cancer. Trends Mol. Med. 17, 283–92.

Gross, I., Bassit, B., Benezra, M., Licht, J.D., 2001. Mammalian Sprouty Proteins Inhibit Cell Growth and Differentiation by Preventing Ras Activation. J. Biol. Chem. 276, 46460–46468.

Grubera, D.F., Pieriboneb, V.A., Portona, B., Kao, H.-T., 2008. Strict Regulation of Gene Expression from a High-Copy Plasmid Utilizing a Dual Vector System. Protein Expr Purif. 60, 53–57.

Guagnano, V., Furet, P., Spanka, C., Bordas, V., Le Douget, M., Stamm, C., Brueggen, J., Jensen, M.R., Schnell, C., Schmid, H., Wartmann, M., Berghausen, J., Drueckes, P., Zimmerlin, A., Bussiere, D., Murray, J., Graus Porta, D., 2011. Discovery of 3-(2,6-dichloro-3,5-dimethoxy-phenyl)-1-{6-[4-(4-ethyl-piperazin-1-yl)-phenylamino]-pyrimidin-4-yl}-1-methyl-urea (NVP-BGJ398), a potent and selective inhibitor of the fibroblast growth factor receptor family of receptor tyrosine kinase. J. Med. Chem. 54, 7066–83.

Guagnano, V., Kauffmann, A., Wöhrle, S., Stamm, C., Ito, M., Barys, L., Pornon, A., Yao, Y., Li, F., Zhang, Y., Chen, Z., Wilson, C.J., Bordas, V., Douget, M. Le, Gaither, L.A., Borawski, J., Monahan, J.E., Venkatesan, K., Brümmendorf, T., Thomas, D.M., Garcia-Echeverria, C., Hofmann, F.,

Sellers, W.R., Graus-porta, D., Li, F., Brummendorf, T., Garcia-Echeverria, C., Borawski, J., Wilson, C.J., Guagnano, V., Ito, M., Venkatesan, K., Thomas, D.M., Kauffmann, A., Yao, Y., Bordas, V., Stamm, C., Le Douget, M., Monahan, J.E., Barys, L., Zhang, Y., Hofmann, F., Wohrle, S., Pornon, A., Sellers, W.R., Gaither, L.A., 2012. FGFR Genetic Alterations Predict for Sensitivity to NVP-BGJ398, a Selective Pan-FGFR Inhibitor. Cancer Discov. 2, 1118–1133.

Gurdon, J.B., Bourillot, P.Y., 2001. Morphogen gradient interpretation. Nature 413, 797–803.

Ha, S.Y., Lee, J., Kang, S.Y., Do, I.G., Ahn, S., Park, J.O., Kang, W.K., Choi, M.G., Sohn, T.S., Bae, J.M., Kim, S., Kim, M., Kim, S., Park, C.K., Ignatius Ou, S.H., Kim, K.M., 2013. MET overexpression assessed by new interpretation method predicts gene amplification and poor survival in advanced gastric carcinomas. Mod. Pathol. 26, 1632–1641.

Hadari, Y.R., Gotoh, N., Kouhara, H., Lax, I., Schlessinger, J., Agg, T., J, A.-J.T., 2001. Critical role for the docking-protein FRS2a in FGF receptor-mediated signal transduction pathways. PNAS 98, 8578–8583.

Hahn, N.M., Bivalacqua, T.J., Ross, A.E., Netto, G.J., Baras, A., Park, J.C., Chapman, C., Masterson, T.A., Koch, M.O., Bihrle, R., Foster, R.S., Gardner, T.A., Cheng, L., Jones, D.R., McElyea, K., Sandusky, G.E., Breen, T., Liu, Z., Albany, C., Moore, M.L., Loman, R.L., Reed, A., Turner, S.A., De Abreu, F.B., Gallagher, T., Tsongalis, G.J., Plimack, E.R., Greenberg, R.E., Geynisman, D.M., 2017. A phase II trial of dovitinib in BCG-unresponsive urothelial carcinoma with FGFR3 mutations or overexpression: Hoosier Cancer Research Network trial HCRN 12-157. Clin. Cancer Res. 23, 3003–3011.

Hahn, N.M., Knudsen, B.S., Daneshmand, S., Koch, M.O., Bihrle, R., Foster, R.S., Gardner, T.A., Cheng, L., Liu, Z., Breen, T., Fleming, M.T., Lance, R., Corless, C.L., Alva, A.S., Shen, S.S., Huang, F., Gertych, A., Gallick, G.E., Mallick, J., Ryan, C., Galsky, M.D., Lerner, S.P., Posadas, E.M., Sonpavde, G., 2016. Neoadjuvant dasatinib for muscle-invasive bladder cancer with tissue analysis of biologic activity. Urol. Oncol. Semin. Orig. Investig. 34, 4.e11-4.e17.

Hallinan, N., Finn, S., Cuffe, S., Rafee, S., O'Byrne, K., Gately, K., 2016. Targeting the fibroblast growth factor receptor family in cancer. Cancer Treat. Rev. 46, 51–62.

Hanafusa, H., Torii, S., Yasunaga, T., Nishida, E., 2002. Sprouty1 and Sprouty2 provide a control mechanism for the Ras / MAPK signalling pathway. Nat. Cell Biol. 4, 850–8.

Hanks, S.K., 2003. Genomic analysis of the eukaryotic protein kinase superfamily: a perspective. Genome Biol. 4.

Hanks, S.K., 1991. Eukaryotic protein kinases. Curr. Opin. Struct. Biol. 1, 369–383.

Hänze, J., Henrici, M., Hegele, A., Hofmann, R., Olbert, P.J., 2013. Epithelial mesenchymal transition status is associated with anti-cancer responses towards receptor tyrosine-kinase inhibition by dovitinib in human bladder cancer cells. BMC Cancer 13.

Harbinski, F., Craig, V.J., Sanghavi, S., Jeffery, D., Liu, L., Sheppard, K.A., Wagner, S., Stamm, C., Buness, A., Chatenay-Rivauday, C., Yao, Y., He, F., Lu, C.X., Guagnano, V., Metz, T., Finan, P.M., Hofmann, F., Sellers, W.R., Porter, J.A., Myer, V.E., Graus-Porta, D., Wilson, C.J., Buckler, A., Tiedt, R., 2012. Rescue screens with secreted proteins reveal compensatory potential of receptor tyrosine kinases in driving cancer growth. Cancer Discov. 2, 948–959.

Harding, T.C., Long, L., Palencia, S., Zhang, H., Sadra, A., Hestir, K., Patil, N., Levin, A., Hsu, A.W., Charych, D., Brennan, T., Zanghi, J., Halenbeck, R., Marshall, S.A., Qin, M., Doberstein, S.K., Hollenbaugh, D., Kavanaugh, W.M., Williams, L.T., Baker, K.P., 2013. Blockade of nonhormonal fibroblast growth factors by FP-1039 inhibits growth of multiple types of cancer. Sci. Transl. Med. 5, 1–10.

Harmer, N.J., Pellegrini, L., Chirgadze, D., Fernandez-recio, J., Blundell, T.L., 2004. The Crystal Structure of Fibroblast Growth Factor (FGF) 19 Reveals Novel Features of the FGF Family and Offers a Structural Basis for Its Unusual Receptor. Biochemistry 43, 629–640.

Hart, K.C., Robertson, S.C., Donoghue, D.J., 2001. Identification of Tyrosine Residues in Constitutively Activated Fibroblast Growth Factor Receptor 3 Involved in Mitogenesis , Stat Activation , and Phosphatidylinositol 3-Kinase Activation. Mol. Biol. Cell 12, 931–942.

Hart, K.C., Robertson, S.C., Kanemitsu, M.Y., Meyer, A.N., Tynan, J.A., Donoghue, D.J., 2000. Transformation and Stat activation by derivatives of FGFR1, FGFR3, and FGFR4. Oncogene 19, 3309–3320.

Haugsten, E.M., Małecki, J., Bjørklund, S.M.S., Olsnes, S., Wesche, J., 2008. Ubiquitination of Fibroblast Growth Factor Receptor 1 Is Required for Its Intracellular Sorting but Not for Its Endocytosis. Mol. Biol. Cell 19, 3390–3403.

Haugsten, E.M., Wiedlocha, A., Olsnes, S., Wesche, J., 2010. Roles of Fibroblast Growth Factor Receptors in Carcinogenesis. Mol. Cancer Res. 8, 1439–1452.

Haugsten, E.M., Zakrzewska, M., Brech, A., Pust, S., Sandvig, K., Wesche, J., 2011. Clathrin- and Dynamin-Independent Endocytosis of FGFR3 – Implications for Signalling. PLoS One 6.

Haura, E.B., Tanvetyanon, T., Chiappori, A., Williams, C., Simon, G., Antonia, S., Gray, J., Litschauer, S., Tetteh, L., Neuger, A., Song, L., Rawal, B., Schell, M.J., Bepler, G., 2010. Phase I/II study of the Src inhibitor dasatinib in combination with erlotinib in advanced non-small-cell lung cancer. J. Clin. Oncol. 28, 1387–1394.

Helsten, T., Elkin, S., Arthur, E., Tomson, B.N., Carter, J., Kurzrock, R., 2015. The FGFR landscape in cancer: Analysis of 4,853 tumors by next-generation sequencing. Clin. Cancer Res. 22, 259–267.

Hernández, S., De Muga, S., Agell, L., Juanpere, N., Esgueva, R., Lorente, J.A., Mojal, S., Serrano, S., Lloreta, J., 2009. FGFR3 mutations in prostate cancer: Association with low-grade tumors. Mod. Pathol. 22, 848–856.

Herrera-Abreu, M.T., Pearson, A., Campbell, J., Shnyder, S.D., Knowles, M.A., Ashworth, A., Turner, N.C., 2013. Parallel RNA interference screens identify EGFR activation as an escape mechanism in FGFR3-mutant cancer. Cancer Discov. 3, 1058–1071.

Hirschhaeuser, F., Menne, H., Dittfeld, C., West, J., Mueller-Klieser, W., Kunz-Schughart, L.A., 2010. Multicellular tumor spheroids: An underestimated tool is catching up again. J. Biotechnol. 148, 3–15.

Huang, J., Mohammadi, M., Rodrigues, G.A., Schlessinger, J., 1995. Reduced activation of Raf-1 and MAP kinase by a fibroblast growth factor receptor mutant deficient in stimulation of phosphatidylinositol hydrolysis. J. Biol. Chem. 270, 5065-5072.

Huang, Z., Chen, H., Blais, S., Neubert, T.A., Li, X., Mohammadi, M., 2013. Structural Mimicry of A-Loop Tyrosine Phosphorylation by a Pathogenic FGF Receptor 3 Mutation. Struct. Des. 21, 1889–1896.

Hubbard, S.R., Till, J.H., 2000. Protein Tyrosine Kinase Structure and Function. Annu. Rev. Biochem. 69, 373–98.

Hyman, D.M., Tran, B., Corral Jaime, J., Garralda, E., Machiels, J.-P.H., Schellens, J.H.M., Bedard, P., Campone, M., Cassier, P., Sarantopoulos, J., Vaishampayan, U.N., Chugh, R., Mahipal, A., Lockhart, A.C., Sessa, C., Zander, T., Ng, M., Curigliano, G., Bendiske, J., Perez-Garcia, J.M., 2016. Phase Ib study of BGJ398 in combination with BYL719 in patients (pts) with select advanced solid tumors. J. Clin. Oncol. 34, 2500.

Iqbal, N., Iqbal, N., 2014. Human Epidermal Growth Factor Receptor 2 (HER2) in Cancers: Overexpression and Therapeutic Implications. Mol. Biol. Int. 2014, 1–9.

Irby, R.B., Yeatman, T.J., 2000. Role of Src expression and activation in human cancer. Oncogene 19, 5636–5642.

Itoh, N., Ornitz, D.M., 2010. Fibroblast growth factors: From molecular evolution to roles in development, metabolism and disease. J. Biochem. 149, 121–130.

Itoh, N., Ornitz, D.M., 2004. Evolution of the Fgf and Fgfr gene families. Trends Genet. 20, 563–569.

Ivanov, D.P., Parker, T.L., Walker, D.A., Alexander, C., Ashford, M.B., Gellert, P.R., Garnett, M.C., 2014. Multiplexing Spheroid Volume , Resazurin and Acid Phosphatase Viability Assays for High-Throughput Screening of

Tumour Spheroids and Stem Cell Neurospheres. PLoS One 9, 1–14.

Jang, J.H., Shin, K.H., Park, J.G., 2001. Mutations in fibroblast growth factor receptor 2 and fibroblast growth factor receptor 3 genes associated with human gastric and colorectal cancers. Cancer Res. 61, 3541–3543.

Jänne, P.A., Gray, N., Settleman, J., 2009. Factors underlying sensitivity of cancers to small-molecule kinase inhibitors. Nat. Rev. Drug Discov. 8, 709–723.

Javle, M., Lowery, M., Shroff, R.T., Weiss, K.H., Springfeld, C., Borad, M.J., Ramanathan, R.K., Goyal, L., Sadeghi, S., Macarulla, T., El-khoueiry, A., Kate, R., Borbath, I., Choo, S.P., Oh, D., Philip, P.A., Chen, L., Reungwetwattana, T., Cutsem, E. Van, Yeh, K., Ciombor, K., Finn, R.S., Patel, A., Sen, S., Porter, D., Isaacs, R., Zhu, A.X., Abou-alfa, G.K., Bekaii-saab, T., 2018. Phase II Study of BGJ398 in Patients With FGFR-Altered Advanced Cholangiocarcinoma. J. Clin. Oncol. 35.

Johnson, D.E., Williams, L.T., 1992. Structural and functional diversity in the fgf receptor multigene family. Adv. Cancer Res. 60, 1–41.

Kalff, A., Spencer, A., 2012. The t(4;14) translocation and FGFR3 overexpression in multiple myeloma: Prognostic implications and current clinical strategies. Blood Cancer J. 2.

Kalinina, J., Ilghari, D., Beenken, A., Goetz, R., Eliseenkova, A. V., Mohammadi, M., Dutta, K., Cowburn, D., 2012. The alternatively spliced acid box region plays a key role in FGF receptor autoinhibition. Structure 20, 77–88.

Kang, S., Elf, S., Dong, S., Hitosugi, T., Lythgoe, K., Guo, A., Ruan, H., Lonial, S., Khoury, H.J., Williams, I.R., Lee, B.H., Roesel, J.L., Karsenty, G., Hanauer, A., Taunton, J., Boggon, T.J., Gu, T.-L., Chen, J., 2009. Fibroblast Growth Factor Receptor 3 Associates with and Tyrosine Phosphorylates p90 RSK2, Leading to RSK2 Activation That Mediates Hematopoietic Transformation. Mol. Cell. Biol. 29, 2105–2117.

Kantarjian, H., Jabbour, E., Grimley, J., Kirkpatrick, P., 2006. Dasatinib 5, 717–718.

Kataoka, Y., Mukohara, T., Tomioka, H., Funakoshi, Y., Kiyota, N., Fujiwara, Y., Yashiro, M., Hirakawa, K., Hirai, M., Minami, H., 2012. Foretinib (GSK1363089), a multi-kinase inhibitor of MET and VEGFRs, inhibits growth of gastric cancer cell lines by blocking inter-receptor tyrosine kinase networks. Invest. New Drugs 30, 1352–1360.

Katoh, M., 2019. Fibroblast growth factor receptors as treatment targets in clinical oncology. Nat. Rev. Clin. Oncol. 16, 105–22.

Katoh, M., 2016. FGFR inhibitors: Effects on cancer cells, tumor microenvironment and whole-body homeostasis (Review). Int. J. Mol. Med. 38, 3–15.

Kelleher, F.C., O'Sullivan, H., Smyth, E., McDermott, R., Viterbo, A., 2013. Fibroblast growth factor receptors, developmental corruption and malignant disease. Carcinogenesis 34, 2198–2205.

Kholodenko, B.N., 2006. Cell Signalling Dynamics in Time and Space. Nat Rev Mol Cell Biol 7, 165–176.

Kholodenko, B.N., Hancock, J.F., Kolch, W., 2010. Signalling ballet in space and time. Nat. Rev. Mol. Cell Biol. 11, 414–426.

Kim, E., Lee, S., Mian, M.F., Yun, S.U., Song, M., Yi, K.S., Ryu, S.H., Suh, P.G., 2006. Crosstalk between Src and major vault protein in epidermal growth factor-dependent cell signalling. FEBS J. 273, 793–804.

Kimelman, D., Kirschner, M., 1987. Synergistic induction of mesoderm by FGF and TGF-β and the identification of an mRNA coding for FGF in the early xenopus embryo. Cell 51, 869–877.

Klint, P., Claesson-welsh, L., 1999. Signal transduction by fibroblast growth factor receptors. Front. Biosci. 4, 165–177.

Knowles, M.A., 2008. Novel therapeutic targets in bladder cancer: Mutation and expression of FGF receptors. Futur. Oncol. 4, 71–83.

Kong, M., Wang, C.S., Donoghue, D.J., 2002. Interaction of Fibroblast Growth Factor Receptor 3 and the Adapter Protein SH2-B. J. Biol. Chem. 277, 15962–15970. 0

Konig, H., Copland, M., Chu, S., Jove, R., Holyoake, T.L., Bhatia, R., 2008. Effects of Dasatinib on Src Kinase Activity and Downstream Intracellular Signaling in Primitive Chronic Myelogenous Leukemia Hematopoietic Cells. Cancer Res. 68, 9624–9633.

Korc, M., Friesel, R., 2009. The Role of Fibroblast Growth Factors in Tumor Growth. Curr. Cancer Drug Targets 9, 639–651.

Kouhara, H., Hadari, Y.R., Schilling, J., 1997. A Lipid-Anchored Grb2-Binding Protein That Links FGF-Receptor Activation to the Ras / MAPK Signaling Pathway. Cell 89, 693–702.

Kovalenko, D., Yang, X., Nadeau, R.J., Harkins, L.K., Friesel, R., 2003. Sef inhibits fibroblast growth factor signaling by inhibiting FGFR1 tyrosine phosphorylation and subsequent ERK activation. J. Biol. Chem. 278, 14087–14091.

Krause, D.S., Etten, R.A. Van, 2005. Tyrosine Kinases as Targets for Cancer Therapy. N. Engl. J. Med. 353, 172–187.

Krause, D.S., Etten, R.A. Van, Van Etten, R.A., 2005. Tyrosine Kinases as Targets for Cancer Therapy. N. Engl. J. Med. 353, 172–187.

Kurosu, H., Ogawa, Y., Miyoshi, M., Yamamoto, M., Nandi, A., Rosenblatt, K.P., Baum, M.G., Schiavi, S., Hu, M.C., Moe, O.W., Kuro-o, M., 2006. Regulation of fibroblast growth factor-23 signaling by Klotho. J. Biol. Chem.

281, 6120–6123.

Kwabi-Addo, B., Ropiquet, F., Giri, D., Ittmann, M., 2001. Alternative splicing of fibroblast growth factor receptors in human prostate cancer. Prostate 46, 163–172.

Kwarcinski, F.E., Brandvold, K.R., Phadke, S., Beleh, O.M., Johnson, T.K., Meagher, J.L., Seeliger, M.A., Stuckey, J.A., Soellner, M.B., 2016. Conformation-Selective Analogues of Dasatinib Reveal Insight into Kinase Inhibitor Binding and Selectivity. ACS Chem. Biol. 11, 1296–1304.

Lai, R., Ingham, R.J., 2013. The pathobiology of the oncogenic tyrosine kinase NPM-ALK: A brief update. Ther. Adv. Hematol. 4, 119–131.

Lamont, F.R., Tomlinson, D.C., Cooper, P.A., Shnyder, S.D., Chester, J.D., Knowles, M.A., 2011. Small molecule FGF receptor inhibitors block FGFR-dependent urothelial carcinoma growth in vitro and in vivo. Br. J. Cancer 104, 75–82.

Lax, I., Wong, A., Lamothe, B., Lee, A., Frost, A., Hawes, J., Schlessinger, J., Haven, N., 2002. The Docking Protein FRS2a Controls a MAP Kinase-Mediated Negative Feedback Mechanism for Signaling by FGF Receptors. Mol. Cell 10, 709–719.

Lecker, S.H., Goldberg, A.L., Mitch, W.E., 2006. Protein Degradation by the Ubiquitin–Proteasome Pathway in Normal and Disease States. J. Am. Soc. Nephrol. 17, 1807–1819.

Ledda, F., Paratcha, G., 2007. Negative Regulation of Receptor Tyrosine Kinase (RTK) Signaling: A Developing Field. Biomark. Insights 2, 45–58.

Lemmon, M.A., Schlessinger, J., 2010. Cell signaling by receptor tyrosine kinases. Cell 141, 1117–1134.

Levitt, J.M., Yamashita, H., Jian, W., Lerner, S.P., Sonpavde, G., 2010. Dasatinib Is Preclinically Active against Src-Overexpressing Human Transitional Cell Carcinoma of the Urothelium with Activated Src Signaling. Mol. Cancer Ther. 9, 1128–1135.

Levitzki, A., Mishani, E., 2006. Tyrphostins and Other Tyrosine Kinase Inhibitors. Annu. Rev. Biochem. 75, 93–109.

Li, X., Brunton, V.G., Burgar, H.R., Wheldon, L.M., Heath, J.K., 2004. FRS2-dependent SRC activation is required for fibroblast growth factor receptor-induced phosphorylation of Sprouty and suppression of ERK activity. J. Cell Sci. 117, 6007–6017.

Liao, R.G., Jung, J., Tchaicha, J., Wilkerson, M.D., Sivachenko, a., Beauchamp, E.M., Liu, Q., Pugh, T.J., Pedamallu, C.S., Hayes, D.N., Gray, N.S., Getz, G., Wong, K.-K., Haddad, R.I., Meyerson, M., Hammerman, P.S., 2013. Inhibitor-Sensitive FGFR2 and FGFR3 Mutations in Lung Squamous Cell Carcinoma. Cancer Res. 73, 5195–5205.

Light, R.W., 2001. Pleural effusion due to pulmonary emboli. Curr Opin Pulm

Med 7, 198–201.

Lin, C.W., Lin, J.C., Prout, G.R., 1985. Establishment and Characterization of Four Human Bladder Tumor Cell Lines and Sublines with Different Degrees of Malignancy. Cancer Res. 45, 5070–5079.

Lombardi, B., Ashford, P., Moya-Garcia, A.A., Rust, A., Crawford, M., Williams, S. V., Knowles, M.A., Katan, M., Orengo, C., Godovac-Zimmermann, J., 2017. Unique signalling connectivity of FGFR3-TACC3 oncoprotein revealed by quantitative phosphoproteomics and differential network analysis. Oncotarget 8, 102898–102911.

Loriot, Y., Necchi, A., Park, S.H., Garcia-Donas, J., Huddart, R., Burgess, E., Fleming, M., Rezazadeh, A., Mellado, B., Varlamov, S., Joshi, M., Duran, I., Tagawa, S.T., Zakharia, Y., Zhong, B., Stuyckens, K., Santiago-Walker, A., De Porre, P., O'Hagan, A., Avadhani, A., Siefker-Radtke, A.O., 2019. Erdafitinib in Locally Advanced or Metastatic Urothelial Carcinoma. N. Engl. J. Med. 381, 338–348.

Ma, C., Wei, S., Song, Y., 2011. T790M and acquired resistance of EGFR TKI: A literature review of clinical reports. J. Thorac. Dis. 3, 10–18.

Makarenkova, H.P., Hoffman, M.P., Beenken, A., Eliseenkova, A. V., Meech, R., Tsau, C., Patel, V.N., Lang, R.A., Mohammadi, M., 2009. Differential interactions of FGFs with heparan sulfate control gradient formation and branching morphogenesis. Sci. Signal. 2, 1–21.

Manning, G., Whyte, D.B., Martinez, R., Hunter, T., 2002. The Protein Kinase Complement of the Human Genome. Science 298.

Manstein, V., Yang, C., Richter, D., Delis, N., Vafaizadeh, V., Groner, B., 2014. Resistance of Cancer Cells to Targeted Therapies Through the Activation of Compensating Signaling Loops. Curr. Signal Transduct. Ther. 8, 193–202.

Markham, A., 2019. Erdafitinib: First Global Approval. Drugs 77, 2057–2062.

Marshall, C.J., 1995. Specificity of receptor tyrosine kinase signaling: Transient versus sustained extracellular signal-regulated kinase activation. Cell 80, 179–185.

Martínez, N., García-Domínguez, C.A., Domingo, B., Luis, J., Zarich, N., Sánchez, A., Gutiérrez-Eisman, S., Llopis, J., Rojas, J.M., Oliva, J.L., Zarich, N., Sánchez, A., Gutiérrez-Eisman, S., Llopis, J., Rojas, J.M., 2007. Sprouty2 binds Grb2 at two different proline-rich regions, and the mechanism of ERK inhibition is independent of this interaction. Cell. Signal. 19, 2277–2285.

Mason, J.M., Morrison, D.J., Basson, M.A., Licht, J.D., 2006. Sprouty proteins: Multifaceted negative-feedback regulators of receptor tyrosine kinase signaling. Trends Cell Biol. 16, 45–54.

Matsuo, I., Kimura-Yoshida, C., 2013. Extracellular modulation of Fibroblast

Growth Factor signaling through heparan sulfate proteoglycans in mammalian development. Curr. Opin. Genet. Dev. 23, 399–407.

Mazzola, C.R., Siddiqui, K.M., Billia, M., Chin, J., 2014. Dovitinib: rationale, preclinical and early clinical data in urothelial carcinoma of the bladder. Expert Opin. Investig. Drugs 23, 1553–1562.

McDonell, L.M., Kernohan, K.D., Boycott, K.M., Sawyer, S.L., 2015. Receptor tyrosine kinase mutations in developmental syndromes and cancer: Two sides of the same coin. Hum. Mol. Genet. 24, R60–R66.

Merid, S.K., Goranskaya, D., Alexeyenko, A., 2014. Distinguishing between driver and passenger mutations in individual cancer genomes by network enrichment analysis. BMC Bioinformatics 15, 1–21.

Mertins, P., Eberl, H.C., Renkawitz, J., Olsen, J. V., Tremblay, M.L., Mann, M., Ullricht, A., Daubt, H., 2008. Investigation of protein-tyrosine phosphatase 1B function by quantitative proteomics. Mol. Cell. Proteomics 7, 1763–1777.

Meyer, K.B., Maia, A.T., O'Reilly, M., Teschendorff, A.E., Chin, S.F., Caldas, C., Ponder, B.A.J., 2008. Allele-specific up-regulation of FGFR2 increases susceptibility to breast cancer. PLoS Biol. 6, 1098–1103.

Miaczynska, M., 2013. Effects of membrane trafficking on signaling by receptor tyrosine kinases. Cold Spring Harb. Perspect. Biol. 5, 1–20.

Michelle C. Mendoza, E. Emrah Er, and J.B., 2011. The Ras-ERK and PI3K-mTOR Pathways: Cross-talk and Compensation. Trends Biochem. Sci. 36, 320–328.

Miyake, M., Ishii, M., Koyama, N., Kawashima, K., Kodama, T., Anai, S., Fujimoto, K., Hirao, Y., Sugano, K., 2010. 1-tert-Butyl-3-[6-(3,5-dimethoxy-phenyl)-2-(4-diethylamino- butylamino)-pyrido[2,3-d]pyrimidin-7-yl]-urea (PD173074), a Selective Tyrosine Kinase Inhibitor of Fibroblast Growth Factor Receptor-3 (FGFR3), Inhibits Cell Proliferation of Bladder Cancer Carry. J. Pharmacol. Exp. Ther. 332, 795–802.

Mohammadi, M., Dikic, I., Sorokin, A., Burgess, W.H., Jaye, M., 1996. Identification of Six Novel Autophosphorylation Sites on Fibroblast Growth Factor Receptor 1 and Elucidation of Their Importance in Receptor Activation and Signal Transduction. Mol. Cell. Biol. 16, 977–989.

Mohammadi, M., Honegger, A.M., Rotin, D., Fischer, R., Bellot, F., Li, W., Dionne, C.A., Jaye, M., Rubinstein, M., Schlessinger, J., 1991. A Tyrosine-Phosphorylated Carboxy-Terminal Peptide of the Fibroblast Growth Factor Receptor (Flg) Is a Binding Site for the SH2 Domain of Phospholipase C-y1. Mol. Cell. Biol. 11, 5068–5078.

Mohammadi, M., Olsen, S.K., Ibrahimi, O.A., 2005. Structural basis for fibroblast growth factor receptor activation. Cytokine Growth Factor Rev. 16, 107–137.

Mohammadi, M., Schlessinger, J., Hubbard, S.R., 1996. Structure of the FGF Receptor Tyrosine Kinase Domain Reveals a Novel Autoinhibitory Mechanism. Cell 86, 577–587.

Monsonego-ornan, E., Adar, R., Rom, E., Yayon, A., 2002. FGF receptors ubiquitylation : dependence on tyrosine kinase activity and role in downregulation. FEBS Lett. 528, 83–89.

Morgenstern, J.P., Land, H., 1990. Advanced mammalian gene transfer: High titre retroviral vectors with multiple drug selection markers and a complementary helper-free packaging cell line. Nucleic Acids Res. 18, 3587–3596.

Nadal, R., Bellmunt, J., 2019. Management of metastatic bladder cancer. Cancer Treat. Rev. 76, 10–21.

Nakanishi, Y., Akiyama, N., Tsukaguchi, T., Fujii, T., Satoh, Y., Ishii, N., Aoki, M., 2015. Mechanism of Oncogenic Signal Activation by the Novel Fusion Kinase FGFR3-BAIAP2L1. Mol. Cancer Ther. 14, 704–712.

Narkis, G., Ofir, R., Manor, E., Landau, D., Elbedour, K., Birk, O.S., 2007. Lethal congenital contractural syndrome type 2 (LCCS2) is caused by a mutation in ERBB3 (Her3), a modulator of the phosphatidylinositol-3-kinase/akt pathway. Am. J. Hum. Genet. 81, 589–595.

Naski, M.C., Wang, Q., Xu, J., Ornitz, D.M., 1996. Graded activation of fibroblast growth factor receptor 3 by mutations causing achondroplasia and thanatophoric dysplasia. Nat. Publ. Gr. 13, 233–237.

Nelson, K.N., Meyer, A.N., Siari, A., Campos, A.R., Motamedchaboki, K., Donoghue, D.J., 2016. Oncogenic Gene Fusion FGFR3-TACC3 Is Regulated by Tyrosine Phosphorylation. Mol. Cancer Res. 14, 458–69.

Nelson, K.N., Meyer, A.N., Wang, C.G., Donoghue, D.J., 2018. Oncogenic driver FGFR3-TACC3 is dependent on membrane trafficking and ERK signaling. Oncotarget 9, 34306–34319.

Nogova, L., Sequist, L. V., Garcia, J.M.P., Andre, F., Delord, J.P., Hidalgo, M., Schellens, J.H.M., Cassier, P.A., Camidge, D.R., Schuler, M., Vaishampayan, U., Burris, H., Tian, G.G., Campone, M., Wainberg, Z.A., Lim, W.T., LoRusso, P., Shapiro, G.I., Parker, K., Chen, X., Choudhury, S., Ringeisen, F., Graus-Porta, D., Porter, D., Isaacs, R., Buettner, R., Wolf, J., 2017. Evaluation of BGJ398, a Fibroblast growth factor receptor 1-3 kinase inhibitor, in patientswith advanced solid tumors harboring genetic alterations in fibroblast growth factor receptors: Results of a global phase I, dose-escalation and dose-expansion stud. J. Clin. Oncol. 35, 157–165.

Olsen, S.K., Ibrahimi, O.A., Raucci, A., Zhang, F., Eliseenkova, A. V., Yayon, A., Basilico, C., Linhardt, R.J., Schlessinger, J., Mohammadi, M., 2004. Insights into the molecular basis for fibroblast growth factor receptor autoinhibition and ligand-binding promiscuity. Proc. Natl. Acad. Sci. 101, 935–940.

Ong, S.H., Guy, G.R., Hadari, Y.R., Laks, S., Gotoh, N., Schlessinger, J., 2000. FRS2 Proteins Recruit Intracellular Signaling Pathways by Binding to Diverse Targets on Fibroblast Growth Factor and Nerve Growth Factor Receptors. Mol. Cell. Biol. 20, 979–989.

Ori, A., 2008. The heparanome and regulation of cell function: structures, functions and challenges. Front. Biosci. 13, 4309–4338.

Ornitz, D.M., Itoh, N., 2015. The Fibroblast Growth Factor signaling pathway. Wiley Interdiscip. Rev. Dev. Biol. 4, 215–266.

Ornitz, D.M., Xu, J., Colvin, J.S., Mcewen, D.G., Macarthur, C.A., Gao, G., Goldfarb, M., 1996. Receptor Specificity of the Fibroblast Growth Factor Family. J. Biol. Chem. 271, 15292–15297.

Pal, S.K., Rosenberg, J.E., Hoffman-Censits, J.H., Berger, R., Quinn, D.I., Galsky, M.D., Wolf, J., Dittrich, C., Keam, B., Delord, J.P., Schellens, J.H.M., Gravis, G., Medioni, J., Maroto, P., Sriuranpong, V., Charoentum, C., Burris, H.A., Grünwald, V., Petrylak, D., Vaishampayan, U., Gez, E., De Giorgi, U., Lee, J.L., Voortman, J., Gupta, S., Sharma, S., Mortazavi, A., Vaughn, D.J., Isaacs, R., Parker, K., Chen, X., Yu, K., Porter, D., Porta, D.G., Bajorin, D.F., 2018. Efficacy of BGJ398, a fibroblast growth factor receptor 1–3 inhibitor, in patients with previously treated advanced urothelial carcinoma with FGFR3 alterations. Cancer Discov. 8, 812–821.

Pandith, A.A., Shah, Z.A., Siddiqi, M.A., 2010. Oncogenic role of fibroblast growth factor receptor 3 in tumorigenesis of urinary bladder cancer. Urol. Oncol. Semin. Orig. Investig. 31, 398–406.

Patani, H. et al, 2016. Landscape of activating cancer mutations in FGFR kinases and their differential responses to inhibitors in clinical use. Oncotarget 7, 1949–2553.

Paul A Bromann, H.K. and S.A.C., 2004. The interplay between Src family kinases and receptor tyrosine kinases. Oncogene 23, 7957–7968.

Pellegrino, M.J., Stork, P.J.S., 2006. Sustained activation of extracellular signal-regulated kinase by nerve growth factor regulates c-fos protein stabilization and transactivation in PC12 cells. J. Neurochem. 99, 1480–1493.

Perera, T.P.S., Jovcheva, E., Mevellec, L., Vialard, J., De Lange, D., Verhulst, T., Paulussen, C., Van De Ven, K., King, P., Freyne, E., Rees, D.C., Squires, M., Saxty, G., Page, M., Murray, C.W., Gilissen, R., Ward, G., Thompson, N.T., Newell, D.R., Cheng, N., Xie, L., Yang, J., Platero, S.J., Karkera, J.D., Moy, C., Angibaud, P., Laquerre, S., Lorenzi, M. V., 2017. Discovery & pharmacological characterization of JNJ-42756493 (Erdafitinib), a functionally selective small-molecule FGFR family inhibitor. Mol. Cancer Ther. 16, 1010–1020.

Perkins, N.D., 2012. The diverse and complex roles of NF-κB subunits in cancer. Nat. Rev. Cancer 12, 121–132.

Pérot, G., Soubeyran, I., Ribeiro, A., Bonhomme, B., Savagner, F., Boutet-

Bouzamondo, N., Hostein, I., Bonichon, F., Godbert, Y., Chibon, F., 2014. Identification of a recurrent STRN/ALK fusion in thyroid carcinomas. PLoS One 9, 1–9.

Pines, G., Köstler, W.J., Yarden, Y., 2010. Oncogenic mutant forms of EGFR: Lessons in signal transduction and targets for cancer therapy. FEBS Lett. 584, 2699–2706.

Pitini, V., Arrigo, C., Di Mirto, C., Mondello, P., Altavilla, G., 2013. Response to dasatinib in a patient with SQCC of the lung harboring a discoid-receptor-2 and synchronous chronic myelogenous leukemia. Lung Cancer 82, 171–172.

Plaza-Menacho, I., Barnouin, K., Goodman, K., Martínez-Torres, R.J., Borg, A., Murray-Rust, J., Mouilleron, S., Knowles, P., McDonald, N.Q., 2014. Oncogenic RET kinase domain mutations perturb the autophosphorylation trajectory by enhancing substrate presentation in trans. Mol. Cell 53, 738–751.

Porta, R., Borea, R., Coelho, A., Khan, S., Araújo, A., Reclusa, P., Franchina, T., Van Der Steen, N., Van Dam, P., Ferri, J., Sirera, R., Naing, A., Hong, D., Rolfo, C., 2017. FGFR a promising druggable target in cancer: Molecular biology and new drugs. Crit. Rev. Oncol. Hematol. 113, 256–267.

Qing, J., Du, X., Chen, Y., Chan, P., Li, H., Wu, P., Marsters, S., Stawicki, S., Tien, J., Totpal, K., Ross, S., Stinson, S., Dornan, D., French, D., Wang, Q.R., Stephan, J.P., Wu, Y., Wiesmann, C., Ashkenazi, A., 2009. Antibody-based targeting of FGFR3 in bladder carcinoma and t(4;14)-positive multiple myeloma in mice. J. Clin. Invest. 119, 1216–1229.

Raible, F., Brand, M., 2001. Tight transcriptional control of the ETS domain factors Erm and Pea3 by Fgf signaling during early zebrafish development. Mech. Dev. 107, 105–117.

Regad, T., 2015. Targeting RTK signaling pathways in cancer. Cancers (Basel). 7, 1758–1784.

Reintjes, N., Li, Y., Becker, A., Rohmann, E., Schmutzler, R., Wollnik, B., 2013. Activating Somatic FGFR2 Mutations in Breast Cancer. PLoS One 8, e60264.

Reis-Filho, J.S., Simpson, P.T., Turner, N.C., Lambros, M.B., Jones, C., Mackay, A., Grigoriadis, A., Sarrio, D., Savage, K., Dexter, T., Iravani, M., Fenwick, K., Weber, B., Hardisson, D., Schmitt, F.C., Palacios, J., Lakhani, S.R., Ashworth, A., 2006. FGFR1 emerges as a potential therapeutic target for lobular breast carcinomas. Clin. Cancer Res. 12, 6652–6662.

Rexer, B.N., Ham, A.J.L., Rinehart, C., Hill, S., De Matos Granja-Ingram, N., González-Angulo, A.M., Mills, G.B., Dave, B., Chang, J.C., Liebler, D.C., Arteaga, C.L., 2011. Phosphoproteomic mass spectrometry profiling links Src family kinases to escape from HER2 tyrosine kinase inhibition. Oncogene 30, 4163–4174.

Richelda, B.R., Ronchetti, D., Baldini, L., Cro, L., Viggiano, L., Marzella, R., Rocchi, M., Otsuki, T., Lombardi, L., Maiolo, A.T., Neri, A., 1997. A Novel Chromosomal Translocation t(4; 14)(p16.3; q32) in Multiple Myeloma Involves the Fibroblast Growth-Factor Receptor 3 Gene. Blood 90, 4062–4070.

Robertson, A.G., Kim, J., Al-Ahmadie, H., Bellmunt, J., Guo, G., Cherniack, A.D., Hinoue, T., Laird, P.W., Hoadley, K.A., Akbani, R., Castro, M.A.A., Gibb, E.A., Kanchi, R.S., Gordenin, D.A., Shukla, S.A., Sanchez-Vega, F., Hansel, D.E., Czerniak, B.A., Reuter, V.E., Su, X., de Sa Carvalho, B., Chagas, V.S., Mungall, K.L., Sadeghi, S., Pedamallu, C.S., Lu, Y., Klimczak, L.J., Zhang, J., Choo, C., Ojesina, A.I., Bullman, S., Leraas, K.M., Lichtenberg, T.M., Wu, C.J., Schultz, N., Getz, G., Meyerson, M., Mills, G.B., McConkey, D.J., Albert, M., Alexopoulou, I., Ally, A., Antic, T., Aron, M., Balasundaram, M., Bartlett, J., Baylin, S.B., Beaver, A., Birol, I., Boice, L., Bootwalla, M.S., Bowen, J., Bowlby, R., Brooks, D., Broom, B.M., Bshara, W., Burks, E., Cárcano, F.M., Carlsen, R., Carvalho, B.S., Carvalho, A.L., Castle, E.P., Castro, P., Catto, J.W., Chesla, D.W., Chuah, E., Chudamani, S., Cortessis, V.K., Cottingham, S.L., Crain, D., Curley, E., Daneshmand, S., Demchok, J.A., Dhalla, N., Djaladat, H., Eckman, J., Egea, S.C., Engel, J., Felau, I., Ferguson, M.L., Gardner, J., Gastier-Foster, J.M., Gerken, M., Gomez-Fernandez, C.R., Harr, J., Hartmann, A., Herbert, L.M., Ho, T.H., Holt, R.A., Hutter, C.M., Jones, S.J.M., Jorda, M., Kahnoski, R.J., Kasaian, K., Kwiatkowski, D.J., Lai, P.H., Lane, B.R., Lerner, S.P., Liu, J., Lolla, L., Lotan, Y., Lucchesi, F.R., Ma, Y., Machado, R.D., Maglinte, D.T., Mallery, D., Marra, M.A., Martin, S.E., Mayo, M., Meraney, A., Moinzadeh, A., Moore, R.A., Mora Pinero, E.M., Morris, S., Morrison, C., Mungall, A.J., Myers, J.B., Naresh, R., O'Donnell, P.H., Parekh, D.J., Parfitt, J., Paulauskis, J.D., Sekhar Pedamallu, C., Penny, R.J., Pihl, T., Porten, S., Quintero-Aguilo, M.E., Ramirez, N.C., Rathmell, W.K., Rieger-Christ, K., Saller, C., Salner, A., Sandusky, G., Scapulatempo-Neto, C., Schein, J.E., Schuckman, A.K., Shelton, C., Shelton, T., Simko, J., Singh, P., Sipahimalani, P., Smith, N.D., Sofia, H.J., Sorcini, A., Stanton, M.L., Steinberg, G.D., Stoehr, R., Su, X., Sullivan, T., Sun, Q., Tam, A., Tarnuzzer, R., Tarvin, K., Taubert, H., Thiessen, N., Thorne, L., Tse, K., Tucker, K., Van Den Berg, D.J., van Kessel, K.E., Wach, S., Wan, Y., Wang, Z., Weinstein, J.N., Weisenberger, D.J., Wise, L., Wong, T., Wu, Y., Yang, L., Zach, L.A., Zenklusen, J.C., Zhang, J. (Julia), Zmuda, E., Zwarthoff, E.C., 2017. Comprehensive Molecular Characterization of Muscle-Invasive Bladder Cancer. Cell 171, 540–556.

Robertson, S.C., Tynan, J.A., Donoghue, D.J., 2000. RTK mutations and human syndromes - When good receptors turn bad. Trends Genet. 16, 265–271.

Rodríguez-Antona, C., Pallares, J., Montero-Conde, C., Inglada-Pérez, L., Castelblanco, E., Landa, I., Leskelä, S., Leandro-García, L.J., López-Jiménez, E., Letón, R., Cascón, A., Lerma, E., Martin, M.C., Carralero, M.C., Mauricio, D., Cigudosa, J.C., Matias-Guiu, X., Robledo, M., 2010. Overexpression and activation of EGFR and VEGFR2 in medullary thyroid carcinomas is related to metastasis. Endocr. Relat. Cancer 17, 7–16.

Rodriguez-vida, A., Saggese, M., Hughes, S., Rudman, S., Chowdhury, S., Smith, N.R., Lawrence, P., Rooney, C., Dougherty, B., Landers, D., Kilgour, E., Arkenau, H., 2015. Complexity of FGFR signalling in metastatic urothelial cancer. J. Hematol. Oncol. 8.

Ronchetti, D., Greco, A., Compasso, S., Colombo, G., Dell'Era, P., Otsuki, T., Lombardi, L., Neri, A., 2001. Deregulated FGFR3 mutants in multiple myeloma cell lines with t(4;14): Comparative analysis of Y373C, K650E and the novel G384D mutations. Oncogene 20, 3553–3562.

Roskoski, R., 2015. Classification of small molecule protein kinase inhibitors based upon the structures of their drug-enzyme complexes. Pharmacol. Res. 103, 26–48.

Roskoski, R., 2012. ERK1/2 MAP kinases: Structure, function, and regulation. Pharmacol. Res. 66, 105–143.

Rouanne, M., Loriot, Y., Lebret, T., Soria, J.C., 2016. Novel therapeutic targets in advanced urothelial carcinoma. Crit. Rev. Oncol. Hematol. 98, 106–115.

Rousseau, F., El Ghouzzi, V., Delezoide, A.L., Legeai-Mallet, L., Le Merrer, M., Munnich, A., Bonaventure, J., Ghouzzi, V. El, Delezoide, A.L., Merrer, M. Le, Munnich, A., 1996. Missense FGFR3 mutations create cysteine residues in thanatophoric dwarfism type I (TD1). Hum. Mol. Genet. 5, 509–512.

Roy, C. Le, Wrana, J.L., 2005. Clathrin- and Non-Clathrin- Mediated Endocytic Regulation of Cell Signalling. Nature 6, 112–126.

Sabichi, A., Keyhani, A., Tanaka, N., Delacerda, J., Lee, I.L., Zou, C., Zhou, J.H., Benedict, W.F., Grossman, H.B., 2006. Characterization of a panel of cell lines derived from urothelial neoplasms: Genetic alterations, growth in vivo and the relationship of adenoviral mediated gene transfer to coxsackie adenovirus receptor expression. J. Urol. 175, 1133–1137.

Sahni, M., Ambrosetti, D., Mansukhani, A., Gertner, R., Levy, D., Basilico, C., 1999. FGF signaling inhibits chondrocyte proliferation and regulates bone development through the STAT-1 pathway. Genes Dev. 13, 1361–1366.

Saka, H., Kitagawa, C., Kogure, Y., Takahashi, Y., Fujikawa, K., Sagawa, T., Iwasa, S., Takahashi, N., Fukao, T., Tchinou, C., Landers, D., Yamada, Y., 2017. Safety, tolerability and pharmacokinetics of the fibroblast growth factor receptor inhibitor AZD4547 in Japanese patients with advanced solid tumours: a Phase I study. Invest. New Drugs 35, 451–462.

Saksela, O., Moscatelli, D., Sommer, A., Rifkin, D.B., 1988. Endothelial cell-derived heparan sulfate binds basic fibroblast growth factor and protects it from proteolytic degradation. J. Cell Biol. 107, 743–751.

Salazar, L., Kashiwada, T., Krejci, P., Meyer, A.N., Casale, M., Hallowell, M., Wilcox, W.R., Donoghue, D.J., Thompson, L.M., 2014. Fibroblast growth factor receptor 3 interacts with and activates TGFβ-activated kinase 1 tyrosine phosphorylation and NFκB signaling in multiple myeloma and

bladder cancer. PLoS One 9, e86470.

Salesse, S., Verfaillie, C.M., 2002. BCR/ABL: from molecular mechanisms of leukemia induction to treatment of chronic myelogenous leukemia. Oncogene 21, 8547–8559.

Sandilands, E., Akbarzadeh, S., Vecchione, A., Mcewan, D.G., Frame, M.C., Heath, J.K., 2007. Src kinase modulates the activation, transport and signalling dynamics of fibroblast growth factor receptors. EMBO Rep. 8.

Sarabipour, S., Hristova, K., 2016. Mechanism of FGF receptor dimerization and activation. Nat. Commun. 7, 1–12.

Sarkar, S., Ryan, E.L., Royle, S.J., Royle, S.J., 2017. FGFR3-TACC3 cancer gene fusions cause mitotic defects by removal of endogenous TACC3 from the mitotic spindle. Open Biol. 7.

Schlessinger, J., Shechter, Y., Cuatrecasas, P., Willingham, M.C., Pastan, I., 1978. Quantitative determination of the lateral diffusion coefficients of the hormone-receptor complexes of insulin and epidermal growth factor on the plasma membrane of cultured fibroblasts. Biochemistry 75, 5353–5357.

Schmidt, M., Scholz, C.J., Polednik, C., Roller, J., 2016. Spheroid-based 3-dimensional culture models: Gene expression and functionality in head and neck cancer. Oncol. Rep. 35, 2431–2440.

Schneider, L., Essmann, F., Kletke, A., Rio, P., Hanenberg, H., Wetzel, W., Schulze-Osthoff, K., Nürnberg, B., Piekorz, R.P., 2007. The transforming acidic coiled coil 3 protein is essential for spindle-dependent chromosome alignment and mitotic survival. J. Biol. Chem. 282, 29273–29283.

Scott, A.J., Song, E.K., Bagby, S., Purkey, A., McCarter, M., Gajdos, C., Quackenbush, K.S., Cross, B., Pitts, T.M., Tan, A.C., Eckhardt, S.G., Fenton, H., Arcaroli, J., Messersmith, W.A., 2017. Evaluation of the efficacy of dasatinib, a Src/Abl inhibitor, in colorectal cancer cell lines and explant mouse model. PLoS One 12, 1–14.

Ségaliny, A.I., Tellez-Gabriel, M., Heymann, M.F., Heymann, D., 2015. Receptor tyrosine kinases: Characterisation, mechanism of action and therapeutic interests for bone cancers. J. Bone Oncol. 4, 1–12.

Shah, D.R., Shah, R.R., Morganroth, J., 2013. Tyrosine kinase inhibitors: Their on-target toxicities as potential indicators of efficacy. Drug Saf. 36, 413–426.

Sharifnia, T., Rusu, V., Piccioni, F., Bagul, M., Imielinski, M., Cherniack, a D., Pedamallu, C.S., Wong, B., Wilson, F.H., Garraway, L. a, Altshuler, D., Golub, T.R., Root, D.E., Subramanian, A., Meyerson, M., 2014. Genetic modifiers of EGFR dependence in non-small cell lung cancer. PNAS 111, 18661–18666.

Shimokawa, K., Kimura-Yoshida, C., Nagai, N., Mukai, K., Matsubara, K., Watanabe, H., Matsuda, Y., Mochida, K., Matsuo, I., 2011. Cell Surface

Heparan Sulfate Chains Regulate Local Reception of FGF Signaling in the Mouse Embryo. Dev. Cell 21, 257–272.

Singh, D., Chan, J.M., Zoppoli, P., Niola, F., Sullivan, R., Castano, A., Liu, E.M., Reichel, J., Porrati, P., Pellegatta, S., Qiu, K., Gao, Z., Ceccarelli, M., Riccardi, R., Brat, D.J., Guha, A., Aldape, K., Golfinos, J.G., Zagzag, D., Mikkelsen, T., Finocchiaro, G., Lasorella, A., Rabadan, R., Iavarone, A., 2012. Transforming Fusions of FGFR and TACC Genes in Human Glioblastoma. Science 337, 1231–1235.

Soda, M., Choi, Y.L., Enomoto, M., Takada, S., Yamashita, Y., Ishikawa, S., Fujiwara, S.I., Watanabe, H., Kurashina, K., Hatanaka, H., Bando, M., Ohno, S., Ishikawa, Y., Aburatani, H., Niki, T., Sohara, Y., Sugiyama, Y., Mano, H., 2007. Identification of the transforming EML4-ALK fusion gene in non-small-cell lung cancer. Nature 448, 561–566.

Song, G., Ouyang, G., Bao, S., 2005. The activation of Akt/PKB signaling pathway and cell survival Apoptosis. J. Cell. Mol. Med. 9, 59–71.

Steven K. Hanks, T.H., 1995. The eukaryotic protein kinase superfamily: kinase (catalytic) domain structure and classification. FASEB J. 9, 576–596.

Stewart, S.A., Dykxhoorn, D.M., Palliser, D., Mizuno, H., Yu, E.Y., An, D.S., Sabatini, D.M., Chen, I.S.Y., Hahn, W.C., Sharp, P.A., Weinberg, R.A., Novina, C.D., 2003. Lentivirus-delivered stable gene silencing by RNAi in primary cells. RNA J. 9, 493–501.

Stover, E.H., Chen, J., Folens, C., Lee, B.H., Mentens, N., Marynen, P., Williams, I.R., Gilliland, D.G., Cools, J., 2006. Activation of FIP1L1-PDGFR requires disruption of the juxtamembrane domain of PDGFR and is FIP1L1-independent. Proc. Natl. Acad. Sci. 103, 8078–8083.

Stransky, N., Cerami, E., Schalm, S., Kim, J.L., Lengauer, C., 2014. The landscape of kinase fusions in cancer. Nat. Commun. 5, 1–10.

Sun, H., Charles, C.H., Lau, L.F., Tonks, N.K., 1993. MKP-1 (3CH134), an immediate early gene product, is a dual specificity phosphatase that dephosphorylates MAP kinase in vivo. Cell 75, 487–493.

Sutterluty, H., Mayer, C.-E., Setinek, U., Attems, J., Ovtcharov, S., Mikula, M., Mikulits, W., Micksche, M., Berger, W., 2007. Down-Regulation of Sprouty2 in Non-Small Cell Lung Cancer Contributes to Tumor Malignancy via Extracellular Signal-Regulated Kinase Pathway-Dependent and -Independent Mechanisms. Mol. Cancer Res. 5, 509–520.

Sweis, R.F., Spranger, S., Bao, R., Paner, G.P., Stadler, W.M., Steinberg, G., Gajewski, T.F., 2017. Molecular drivers of the non-T-cell- inflamed tumor microenvironment in urothelial bladder cancer. Physiol. Behav. 176, 139–148.

Tan, F.H., Putoczki, T.L., Stylli, S.S., Luwor, R.B., 2019. Ponatinib: A novel multi-tyrosine kinase inhibitor against human malignancies. Onco. Targets. Ther. 12, 635–645.

Tan, L., Wang, J., Tanizaki, J., Huang, Z., Aref, A.R., Rusan, M., Zhu, S.-J., Zhang, Y., Ercan, D., Liao, R.G., Capelletti, M., Zhou, W., Hur, W., Kim, N., Sim, T., Gaudet, S., Barbie, D. a., Yeh, J.-R.J., Yun, C.-H., Hammerman, P.S., Mohammadi, M., Jänne, P. a., Gray, N.S., 2014. Development of covalent inhibitors that can overcome resistance to first-generation FGFR kinase inhibitors. Proc. Natl. Acad. Sci. 111, E4869–E4877.

Tanner, Y., Grose, R.P., 2015. Dysregulated FGF signalling in neoplastic disorders. Semin. Cell Dev. Biol. 53, 126–135.

Tao, D., Han, X., Zhang, N., Lin, D., Wu, D., Zhu, X., Song, W., Shi, Y., 2016. Genetic alteration profiling of patients with resected squamous cell lung carcinomas. Oncotarget 7, 36590–36601.

Thomas, S., Overdevest, J.B., Nitz, M.D., Williams, P.D., Owens, C.R., Sanchez-Carbayo, M., Frierson, H.F., Schwartz, M.A., Theodorescu, D., 2011. Src and caveolin-1 reciprocally regulate metastasis via a common downstream signaling pathway in bladder cancer. Cancer Res. 71, 832–841.

Thress, K.S., Paweletz, C.P., Felip, E., Cho, B.C., Stetson, D., Dougherty, B., Lai, Z., Markovets, A., Vivancos, A., Kuang, Y., Ercan, D., Matthews, S., Cantarini, M., Barrett, J.C., Jänne, P.A., Oxnard, G.R., Author, N.M., 2015. Acquired EGFR C797S mediates resistance to AZD9291 in advanced non-small cell lung cancer harboring EGFR T790M HHS Public Access Author manuscript. Nat Med 21, 560–562.

Tiong, K.H., Mah, L.Y., Leong, C.-O., 2013. Functional roles of fibroblast growth factor receptors (FGFRs) signaling in human cancers. Apoptosis 18, 1447–68.

Tiseo, M., Gelsomino, F., Alfieri, R., Cavazzoni, A., Bozzetti, C., De Giorgi, A.M., Petronini, P.G., Ardizzoni, A., 2015. FGFR as potential target in the treatment of squamous non small cell lung cancer. Cancer Treat. Rev. 41, 527–539.

Tolcher, A.W., Papadopoulos, K.P., Patnaik, A., Wilson, K., Thayer, S., Zanghi, J., Gemo, A.T., Kavanaugh, W.M., Keer, H.N., LoRusso, P.M., 2016. A phase I, first in human study of FP-1039 (GSK3052230), a novel FGF ligand trap, in patients with advanced solid tumors. Ann. Oncol. 27, 526–532.

Tomlinson, D.C., Hurst, C.D., Knowles, M.A., 2007. Knockdown by shRNA identifies S249C mutant FGFR3 as a potential therapeutic target in bladder cancer. Oncogene 26, 5889–5899.

Tomlinson, D.C., L'Hôte, C.G., Kennedy, W., Pitt, E., Knowles, M.A., 2005. Alternative splicing of fibroblast growth factor receptor 3 produces a secreted isoform that inhibits fibroblast growth factor-induced proliferation and is repressed in urothelial carcinoma cell lines. Cancer Res. 65, 10441–10449.

Tony, I., Marco, G., Bahleda, R., Yohann, L., 2019. Clinical Development of

FGFR3 Inhibitors for the Treatment of Urothelial Cancer. Bl. Cancer 5, 87–102.

Touat, M., Ileana, E., Postel-Vinay, S., André, F., Soria, J.C., 2015. Targeting FGFR signaling in cancer. Clin. Cancer Res. 21, 2684–2694.

Trudel, S., Ely, S., Farooqi, Y., Affer, M., Robbiani, D.F., Chesi, M., Bergsagel, P.L., 2004. Inhibition of fibroblast growth factor receptor 3 induces differentiation and apoptosis in t(4;14) myeloma. Blood 103, 3521–3528.

Trueb, B., Zhuang, L., Taeschler, S., Wiedemann, M., 2003. Characterization of FGFRL1, a Novel Fibroblast Growth Factor (FGF) Receptor Preferentially Expressed in Skeletal Tissues. J. Biol. Chem. 278, 33857–33865.

Turner, N., Grose, R., 2010. Fibroblast growth factor signalling: from development to cancer. Nat. Rev. Cancer 10, 116–129.

Vallo, S., Michaelis, M., Gust, K.M., Black, P.C., Rothweiler, F., Kvasnicka, H.M., Blaheta, R.A., Brandt, M.P., Wezel, F., Haferkamp, A., Cinatl, J., 2016. Dasatinib enhances tumor growth in gemcitabine-resistant orthotopic bladder cancer xenografts. BMC Res. Notes 9, 1–8.

van Rhijn, B.W.G., van Tilborg, A.A.G., Lurkin, I., Bonaventure, J., de Vries, A., Thiery, J.P., van der Kwast, T.H., Zwarthoff, E.C., 2002. Novel fibroblast growth factor receptor 3 (FGFR3) mutations in bladder cancer previously identified in non-lethal skeletal disorders. Eur. J. Hum. Genet. 10, 819–824.

Visscher, M., Arkin, M.R., Dansen, T.B., Molecule, S., Francisco, S., 2017. Covalent targeting of acquired cysteines in cancer. Curr Opin Chem Biol 30, 61–67.

Volinsky, N., Kholodenko, B.N., 2013. Complexity of Receptor Tyrosine Kinase Signal Processing. Cold Spring Harb Perspect Biol 2013;5:a009043.

Von Kriegsheim, A., Baiocchi, D., Birtwistle, M., Sumpton, D., Bienvenut, W., Morrice, N., Yamada, K., Lamond, A., Kalna, G., Orton, R., Gilbert, D., Kolch, W., 2009. Cell fate decisions are specified by the dynamic ERK interactome. Nat. Cell Biol. 11, 1458–1464.

Wang, J., Mikse, O., Liao, R.G., Li, Y., Tan, L., Janne, P. a, Gray, N.S., Wong, K.-K., Hammerman, P.S., 2014. Ligand-associated ERBB2/3 activation confers acquired resistance to FGFR inhibition in FGFR3-dependent cancer cells. Oncogene 34, 2167–2177.

Wang, L., Sustic, T., Oliveira, R.L. de, Lieftink, C., Halonen, P., Ven, M. van de, Beijersbergen, R.L., Heuvel, M.M. van den, Bernards, R., Heijden, M.S. van der, 2017. A Functional Genetic Screen Identifies the Phosphoinositide 3-kinase Pathway as a Determinant of Resistance to Fibroblast Growth Factor Receptor Inhibitors in FGFR Mutant Urothelial Cell Carcinoma. Eur. Urol. 71, 858–862.

Webster, M.K., D'Avis, P.Y., Robertson, S.C., Donoghue, D.J., 1996. Profound ligand-independent kinase activation of fibroblast growth factor receptor 3

by the activation loop mutation responsible for a lethal skeletal dysplasia, thanatophoric dysplasia type II. Mol. Cell. Biol. 16, 4081–4087.

Werner, S., Duan, D.S., de Vries, C., Peters, K.G., Johnson, D.E., Williams, L.T., 1991. Differential splicing in the extracellular region of fibroblast growth factor receptor 1 generates receptor variants with different ligand-binding specificities. Mol. Cell. Biol. 12, 82–8.

Wesche, J., Haglund, K., Haugsten, E.M., 2011. Fibroblast growth factors and their receptors in cancer. Biochem. J. 437, 199–213.

Wheeler, D.L., Iida, M., Kruser, T.J., Nechrebecki, M.M., Dunn, E.F., Armstrong, E.A., Huang, S., Harari, P.M., 2009. Epidermal growth factor receptor cooperates with Src family kinases in acquired resistance to cetuximab. Cancer Biol. Ther. 8, 696–703.

Wiedemann, M., Trueb, B., 2000. Characterization of a novel protein (FGFRL1) from human cartilage related to FGF receptors. Genomics 69, 275–279.

Wilkie, A.O.M., 2005. Bad bones, absent smell, selfish testes: The pleiotropic consequences of human FGF receptor mutations. Cytokine Growth Factor Rev. 16, 187–203.

Williams, S. V., Hurst, C.D., Knowles, M. a., 2013. Oncogenic FGFR3 gene fusions in bladder cancer. Hum. Mol. Genet. 22, 795–803.

Wong, A., Lamothe, B., Lee, A., Schlessinger, J., Lax, I., 2002. FRS2a attenuates FGF receptor signaling by Grb2- mediated recruitment of the ubiquitin ligase Cbl. PNAS 99, 6684–6689.

Wood, L.D., Parsons, D.W., Jones, S., Lin, J., Sjöblom, T., Leary, R.J., Shen, D., Boca, S.M., Barber, T., Ptak, J., Silliman, N., Szabo, S., Dezso, Z., Ustyanksky, V., Nikolskaya, T., Nikolsky, Y., Karchin, R., Wilson, P.A., Kaminker, J.S., Zhang, Z., Croshaw, R., Willis, J., Dawson, D., Shipitsin, M., Willson, J.K.V., Sukumar, S., Polyak, K., Ben, H.P., Pethiyagoda, C.L., Pant, P.V.K., Ballinger, D.G., Sparks, A.B., Hartigan, J., Smith, D.R., Suh, E., Papadopoulos, N., Buckhaults, P., Markowitz, S.D., Parmigiani, G., Kinzler, K.W., Velculescu, V.E., Vogelstein, B., 2007. The genomic landscapes of human breast and colorectal cancers. Science. 318, 1108–1113.

Wu, Y.M., Su, F., Kalyana-Sundaram, S., Khazanov, N., Ateeq, B., Cao, X., Lonigro, R.J., Vats, P., Wang, R., Lin, S.F., Cheng, A.J., Kunju, L.P., Siddiqui, J., Tomlins, S.A., Wyngaard, P., Sadis, S., Roychowdhury, S., Hussain, M.H., Feng, F.Y., Zalupski, M.M., Talpaz, M., Pienta, K.J., Rhodes, D.R., Robinson, D.R., Chinnaiyan, A.M., 2013. Identification of targetable FGFR gene fusions in diverse cancers. Cancer Discov. 3, 636–647.

Xu, T., Wang, H., Huang, X., Li, W., Huang, Q., Yan, Y., Chen, J., 2018. Gene Fusion in Malignant Glioma: An Emerging Target for Next-Generation Personalized Treatment. Transl. Oncol. 11, 609–618.

Yagasaki, F., Wakao, D., Uchida, Y., Matsuda, A., Bessho, M., Yokoyama, Y., Kayano, H., Murohashi, I., Taniwaki, M., 2001. Fusion of ETV6 to fibroblast growth factor receptor 3 in peripheral T-cell lymphoma with a t(4;12)(p16;p13) chromosomal translocation. Cancer Res. 61, 8371–8374.

Yan, G., Fukabori, Y., McBride, G., Nikolaropolous, S., McKeehan, W.L., 1993. Exon switching and activation of stromal and embryonic fibroblast growth factor (FGF)-FGF receptor genes in prostate epithelial cells accompany stromal independence and malignancy. Mol. Cell. Biol. 13, 4513–4522.

Yang, X., Steinberg, F., Zhuang, L., Bessey, R., Trueb, B., 2016. Receptor FGFRL1 does not promote cell proliferation but induces cell adhesion. Int. J. Mol. Med. 38, 30–38.

Yang, Z., Allen, C.D.C., 2018. Expression of Exogenous Genes in Murine Primary B Cells and B Cell Lines Using Retroviral Vectors. Methods Mol Biol. 1707, 39–49.

Yeh, H.-H., Wu, C.-H., Giri, R., Kato, K., Kohno, K., Izumi, H., Chou, C.-Y., Su, W.-C., Liu, H.-S., 2008. Oncogenic Ras-Induced Morphologic Change Is through MEK/ERK Signaling Pathway to Downregulate Stat3 at a Posttranslational Level in NIH3T3 Cells. Neoplasia 10, 52–60.

Yusoff, P., Lao, D.H., Ong, S.H., Miin Wong, E.S., Lim, J., Lo, T.L., Leong, H.F., Fong, C.W., Guy, G.R., Sook, E., Wong, M., Lim, J., Lo, T.L., Leong, H.F., Fong, C.W., Guy, G.R., 2002. Sprouty2 inhibits the Ras/MAP kinase pathway by inhibiting the activation of Raf. J. Biol. Chem. 277, 3195–3201.

Zhang, J., Yang, P.L., Gray, N.S., 2009. Targeting cancer with small molecule kinase inhibitors. Nat. Rev. Cancer 9, 28–39.

Zhang, S., Yu, D., 2012. Targeting Src family kinases in anti-cancer therapies: Turning promise into triumph. Trends Pharmacol. Sci. 33, 122–128.

Zhang, S.Q., Yang, W., Kontaridis, M.I., Bivona, T.G., Wen, G., Araki, T., Luo, J., Thompson, J.A., Schraven, B.L., Philips, M.R., Neel, B.G., 2004. Shp2 Regulates Src Family Kinase Activity and Ras / Erk Activation by Controlling Csk Recruitment. Mol. Cell 13, 341–355.

Zhang, X., Ibrahimi, O.A., Olsen, S.K., Umemori, H., Mohammadi, M., Ornitz, D.M., 2006. Receptor specificity of the fibroblast growth factor family: The complete mammalian FGF family. J. Biol. Chem. 281, 15694–15700.

Zhang, X.H.F., Wang, Q., Gerald, W., Hudis, C.A., Norton, L., Smid, M., Foekens, J.A., Massagué, J., 2009. Latent Bone Metastasis in Breast Cancer Tied to Src-Dependent Survival Signals. Cancer Cell 16, 67–78.

Zhao, Q., Caballero, O.L., Davis, I.D., Jonasch, E., Tamboli, P., Yung, W.K.A., Weinstein, J.N., Shaw, K., Strausberg, R.L., Yao, J., 2013. Tumor-specific isoform switch of the fibroblast growth factor receptor 2 underlies the mesenchymal and malignant phenotypes of clear cell renal cell carcinomas. Clin. Cancer Res. 19, 2460–2472.

Zheng, J., 2013. Oncogenic chromosomal translocations and human cancer (Review). Oncol. Rep. 30, 2011–2019.